Synthesis, Characterization and Evaluation of Ionic liquids and Polymeric ionic liquids/functionalized multiwalled carbon nanotubes for Cr(VI) adsorption

Mzukisi MATANDABUZO

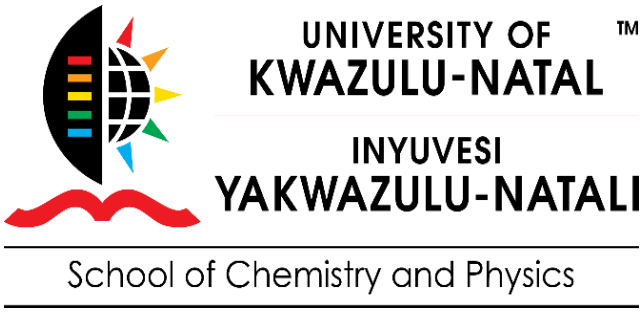

January 2019

Synthesis, Characterization and Evaluation of Ionic liquids and Polymeric ionic liquids/functionalized multiwalled carbon nanotubes for Cr(VI) adsorption

By

MZUKISI MATANDABUZO (217075347)

B. Sc., B. Sc. (Honours), M.Sc. Chemistry (UFH)

A thesis submitted to the College of Agriculture, Engineering and Science in fulfilment of the requirements for the award of the degree of

Doctor of Philosophy

of the

University of KwaZulu-Natal

Supervisor: Professor P. A. Ajibade

January 2019

DECLARATION BY CANDIDATE ON PLAGIARISM

I, Mzukisi Matandabuzo, declare that:

1. The research in this thesis, except where otherwise indicated, is my original research.
2. This thesis has not been submitted for any degree or examination at other university.
3. This thesis does not contain any other person data unless specifically acknowledged as being sourced from them.
4. This thesis does not contain any other persons' writing, unless specifically acknowledged as being sourced from other researchers. Where other written sources have been quoted, then:
    a. Their words have been re-written, but the general information attributed to them has been properly referenced.
    b. In all instances where the exact words of other authors have been used, then their writing has been placed in italics and inside quotation marks and referenced.
5. This thesis does not contain text or graphics from the internet copied and pasted, unless specifically acknowledged, and the source being detailed in the dissertation/thesis and in the references section.

10-09-2019

Date Mzukisi Matandabuzo

CERTIFICATION

This is to certify that this research is a record of original work carried out by Mzukisi Matandabuzo under my supervision in the Inorganic Materials Research laboratory of the School of Chemistry and Physics, University of KwaZulu-Natal in fulfilments of the requirements for the award of Doctor of Philosophy degree in Chemistry.

_____ _____

Date Supervisor

P. A. Ajibade
Professor of Inorganic Materials Chemistry
B. Sc (Hons), MSc (Ibadan);
PhD (UniZul); MRSC (London)

DEDICATION

I would like to dedicate this work to the following:

To my father, Mr. S Matandabuzo and my late mother, Mrs. NL Matandabuzo

ACKNOWLEDGEMENTS

First, I would like to thank God Almighty. All Praise and Glory belongs to Him, the Alpha and Omega. His pre-eminent grace has been enough for me throughout the study.

I am so grateful to my supervisor, Prof. P.A Ajibade, for his constant scholarly supervision, mentoring and everything he has done in support of my educational development and career. I am also grateful to have been given a privilege to work under him in his resourceful inorganic material research laboratory, where he provided clear background and understanding of inorganic materials chemistry. Indeed, he was not just an academic supervisor, but he has been a father and life coach to me.

Special appreciation also goes to the entire Inorganic Materials Chemistry research group. Their support, encouragements, fruitful and constructive criticisms were of paramount importance not only to my academic development, but also to my everyday life. I also acknowledge all academic and non-academic staff in the School of Chemistry and Physics, University of KwaZulu-Natal for their general help. I would like to acknowledge Mr. C. Grimmer for NMR analysis, Ms. N.C Matyumza and Ms. L Beukes for microscopic analyses.

I would also like to acknowledge and appreciate the support from my family; their endless love, and motivation. It has been a very challenging journey for all us but you all persevered with me

throughout my long years at the University. To the endless number of my friends and business partners, guys thank you so much. I profoundly appreciate the National Research Foundation (NRF) and Sasol for financial support throughout this study. Finally, I thank the University of KwaZulu-Natal for giving me the opportunity to come to study here and acquire more research and technical skills.

Table of Contents

LIST OF FIGURES

Figures ***Pages***

LIST OF TABLES

Tables ***Pages***

LIST OF SCHEMES

Schemes ***Pages***

ABBREVIATIONS AND SYMBOLS

ACN	Acetonitrile
AIBN	2, 2'-Azobis(2-methylpropoinitrile)
AMD	Acid mine drainage
ATRP	Atomic transfer radical polymerization
$TFSI^-$	Bis(trifluoromethanesulfonyl)imide ion
TF_2N^-	Bis(trifluoromethanesulfonyl)imide ion
CNTs	Carbon nanotubes
CBL	Carbaryl
CBF	Carbofuran
°C	Degrees Celsius
DMF	N, N-dimethyl formamide
DMSO	Dimethyl sulfoxide
DSC	Differential scanning calorimetry
PF_6^-	Hexafluorophosphate ion
Im+	Imidazolium cation
ILs	Ionic liquids
IL/MWCNT	Ionic liquids-functionalized multiwalled carbon nanotubes
Isop	Isopropyl
KeV	Kiloelectronvolt
MTC	Metocarb
MWCNTs	Multi-walled carbon nanotubes
ODA	Octadecylamine
PILs	Polymeric ionic liquids
PEUF	Polymer-enhanced ultrafiltration

PIL/MWCNT	Polymeric ionic liquids-functionalized multiwalled carbon nanotubes
PEO	Polyetheylene glycol
PVBCl	Poly(vinyl benzyl) chloride
Pyr^+	Pyridinium cation
RAFT	Reversible addition-fragmentation chain transfer
SMIP	Surface molecularly imprinted polymer
TGA	Thermogravimetric analyzer
VP	Vinyl pyridine
VB	Vinyl benzyl
XRD	X-ray diffraction

RESEARCH OUTPUTS

1. **Matandabuzo, M**.; Ajibade, P.A. Synthesis, characterization, and physicohemical properties of hydrophobic pyridinium-based ionic liquids with N-propyl and N-isopropyl. *Zeitschrift für anorganische und allgemeine Chemie (ZAAC). Z. Anorg. Allg. Chem*. 644 (2018) 489–495. **DOI:10.1002/zaac.201800006**.

2. **Matandabuzo, M**; Peter A. Ajibade, Synthesis and surface functionalization of multi-walled carbon nanotubes with imidazolium and pyridinium based ionic liquids: Thermal stability, dispersibility and hydrophobicity characteristics. *J. Mol. Liq*. 286 (2018) 248-293, **DOI:10.1016/j.molliq.2018.07.028.**

ABSTRACT

In this study, a series of imidazolium and pyridinium-based ionic liquids (ILs), polymeric ionic liquids (PILs), and their carbon nanotubes-functionalized composites were synthesized, characterized and applied as potential adsorbents for hexavalent Cr(VI). Polymeric ionic liquids of different polymerizable moieties (vinyl and styrenic moieties) were studied. Furthermore, multi-walled carbon nanotubes (MWCNTs) were synthesized, characterized and dispersed on both imidazolium and pyridinium-based ILs and PILs, respectively. Thermal studies revealed that vinyl pyridinium PILs possess good thermal stability than the vinyl imidazolium counterparts. The size of the counter-anions bromide (Br-), hexafluorophosphate (PF6-), and bis(trifluoromethanesulfonyl) imide (TFSI-) and the charge delocalization in cationic rings greatly influenced the glass transition temperatures of PILs. Expectedly, pyridinium and imidazolium-based PILs with hexafluorophosphate ions showed poor solubility in polar protic solvents (water, methanol) and good solubility in polar aprotic solvents (DMSO, DMF, THF) except acetone (a dipolar aprotic solvent).

The as-synthesized ILs/MWCNT composites were characterized using FTIR spectroscopy, scanning electron microscopy (SEM), energy dispersive X-ray spectroscopy (EDS), X-ray diffraction (XRD), and thermal analysis. The results obtained indicate that the pyridinium-based ILs exhibited higher decomposition temperatures (above 400 °C) compared to imidazolium-

based ILs counterparts (onset decomposition at 250 °C) with poor water-solubility and their glass transition temperatures were dependent on ion mobility. The effect of the alkyl lateral chain (propyl and isopropyl) at the first and third position of imidazolium and N-position of pyridinium cationic rings towards their thermal stability, conductivity, and solubility of the ionic liquids was investigated. Their solubilities in different polar and non-polar solvents were also investigated. Spectroscopic and microscopic analyses confirmed the formation of the ILs/MWCNT composites with new functionalities and unaltered surface morphology of carbon nanotubes. Pyridinium and imidazolium-based PILs/MWCNT composites were characterized by thermal, spectroscopic, and electron microscopy techniques. It was observed that the composites were thermally stable compared to the corresponding precursors and were insoluble in polar aprotic solvents.

For application, solid-liquid adsorption process was used in the adsorption of Cr(VI) from aqueous solution using the as-synthesized ILs/MWCNT and PILs/MWCNT composites as adsorbents. Under batch adsorption experiments, the effect of solution pH, contact time and initial concentration of Cr(VI) were investigated. It was established that the adsorption of Cr(VI) took place under acidic conditions (pH=2-3), thereby confirming significant adsorption of dichromate ($Cr_2O_7^-$) and hydrochromate ($HCrO_4^-$) anions. At lower pH values, the ionic and π-anionic electrostatic interactions between the positively-charged regions of the composites and

Cr(VI) were believed to have facilitated the adsorption of anionic ($Cr_2O_7^-$) and ($HCrO_4^-$). Adsorption results obtained based on contact time showed that increase in contact time gradually increases the adsorption of Cr(VI) within 2 h. However, further increase in experimental contact time above 2 h insignificantly affected the adsorption of Cr(VI) due to early or quick oversaturation of the surface active sites on the adsorbents.

The adsorption of Cr(VI) onto ILs/MWCNT and PILs/MWCNT composites fitted well into both Langmuir and Freundlich adsorption isotherms. However, the homogeneity/heterogeneity nature of the adsorbents relied on the diversified nature of the composites, which includes bulky pyridinium and imidazolium organic cations with delocalized charges, some large counter anions and the graphitic functional carbon groups. In order to understand the mechanisms of the adsorption of Cr(VI) onto ILs/MWCNT and PILs/MWCNT composites, pseudo-second-order kinetic model was employed. The results obtained showed that the calculated maximum adsorption capacities (q_{ecal}) and experimental maximum adsorption capacities ($q_{e.exp}$) depict high correlation co-efficiencies (R^2>0.99) confirming the applicability and feasibility of pseudo-second-order model on the adsorption of Cr(VI) in this study.

CHAPTER ONE

INTRODUCTION AND LITERATURE REVIEW ON IONIC LIQUIDS AND POLYMERIC IONIC LIQUIDS

Chapter 1

1.1 Introduction

The general increase of industrialization and urbanization have directly and/or indirectly contributed to high levels of surface and ground water contamination and existence of other toxic substances in potable water sources [1-2]. Almost all water contaminants are toxic towards both biotic and abiotic ecosystem [3]. Inorganic substances such as chromium, arsenic, cadmium, lead, mercury, and other organic contaminants continue to pollute both surface and underground water and render them unusable [4]. Several organic and inorganic pollutants are emitted from industrial operations such as mining and road construction [5]. Several quantities of solid inorganic waste or by-product materials are produced every year [5]. However, inorganic and/or some organic materials normally accumulate through metal production operations into the surface and underground water bodies [5-6]. A reliable and cost-effective method to remove the above-mentioned water-pollutants must be introduced and widely used to combat the growing negative effect of these pollutants.

Carbon nanotubes (CNTs) are one of the carbon-based materials that have been investigated in wastewater treatment, and they possess large surface area, high conductivity, low dispersibility

and limited solubility [7-8]. However, two main strategies being utilized to improve the characteristics of CNTs are: the non-covalent and covalent functionalization [8]. Covalent functionalization produces materials with surface structural defects and relatively stable materials [9]. Recently, ionic liquids and their polyelectrolyte derivatives have been utilized as innovative class of carbon material modifiers [10-11]. Li *et al*. [12] reported the wrapping of single-walled carbon nanotubes with PILs and the application of the resulting nanocomposites in chemiresistive CO_2 sensors. Free radical graft polymerization and non-covalent modification by direct mixing of PILs and CNTs using ultrasonication were reported as the leading methods to produce polymer-modified carbon materials [9, 13]. Functionalization with polymer materials increased thermal stability, surface area, dispersibility, and reduced water solubility of CNTs [14-17].

Ionic liquids (ILs) have been associated with green chemistry as substitutes for volatile and flammable organic solvents [18]. ILs, together with their polymerized derivatives have found applications in organic and polymer chemistry [18], catalysis [19], electrochemistry [20], analytical chemistry [21], nanotechnology [22], energy [23], CO_2 separation/sorption [24], and biotechnology [25]. ILs are also used as plasticizers, additives, components of polymer electrolytes, and porogenic agents to polymers [26]. However, there is a very limited literature

on the application of ionic liquids and polymeric ionic liquids (PILs) in wastewater treatment and as potential adsorbents for metal ions. Therefore, the use of carbon nanotubes-functionalized with the ionic liquids derivatives must be considered and thoroughly investigated.

1.2 Literature review on ionic liquids derivatives

Polymeric ionic liquids (PILs) are polyelectrolyte-forms of ionic liquids (ILs) produced by a direct and/or indirect polymerization of ionic liquids (ILs) monomers, or by modification of the existing polymers [27-28]. PILs are non-covalently bonded subclass of polyelectrolytes, comprised of organic cations such as imidazolium, pyrrolidinium, pyridinium, tetraalkylammonium, tetraalkyl-phosphonium, piperidinium, and quinolinium, and organic/ inorganic anions such as halide ions (Cl^-, Br^-), polyatomic inorganics such as tetrafluoroborate (BF_4^-), hexafluorophosphate (PF_6^-), and pure organic anions such as bis(trifluoromethanesulfonyl)imide ($TFSI^-$) and dicyanamide [$N(CN)_2^-$] [29]. Polymeric ionic liquids normally combine the special properties of ILs species in each of the repeating units with those of macromolecular architectures [28, 30-31]. The first discovery of polymeric ionic liquids was reported in 1970, wherein a monomer containing cationic-vinyl group was polymerized via free radical polymerization [28].

Polymerization of ionic liquids to prepare polymerized ionic liquid (PILs) is regarded as the earliest chemical transformation of ILs and have received a considerable interest from researchers. Polymeric ionic liquids usually combines the novel attributes of ILs monomers with well improved durability, processibility, enhanced mechanical and thermal stability, dynamic chains and spatial controllability of resultant PILs [32-36]. It has been reported that most synthesized PILs are solids at room or ambient temperature [30]. Numerous types of polymeric ionic liquids have been reported in the literature and varied with the position of the polymerizable units [33]. As presented in Fig. 1.1, some PILs are poly cations (polymerizable unit located on the cation), poly anions (polymerizable unit on the anion), copolymers (two or more monomers held together by either cationic or anionic backbone), and some are network polymers or polyzwitterion (both cation and anion parts of polymer backbone) [27, 34].

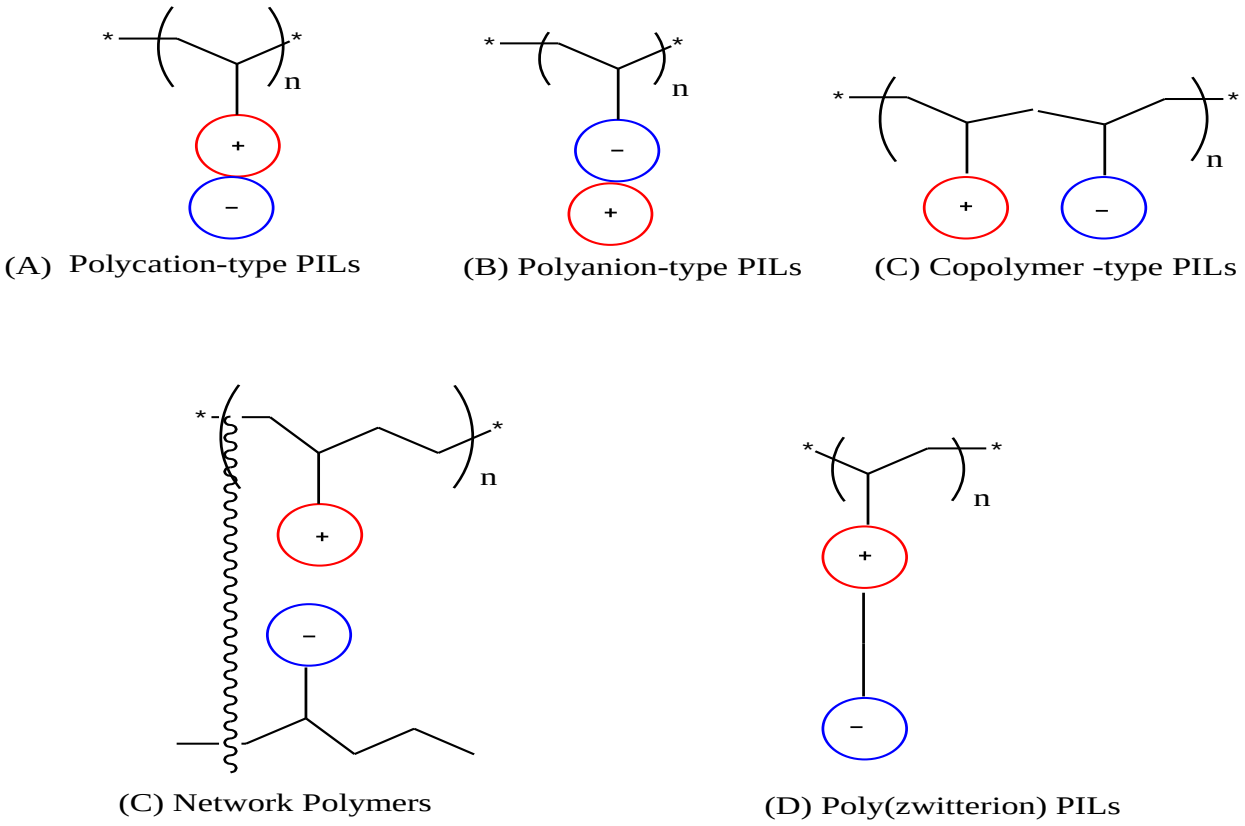

Figure 1.1 Different types of PILs [27, 34]

Polymerizable units used in polymerization processes includes vinyl, (meth)acryloyl, and vinyl benzyl (styrene) groups [27]. In most PILs, the polymerizable groups are normally attached to the cationic part of the ionic liquid monomer. Fig. 1.2 shows common polymerizable groups.

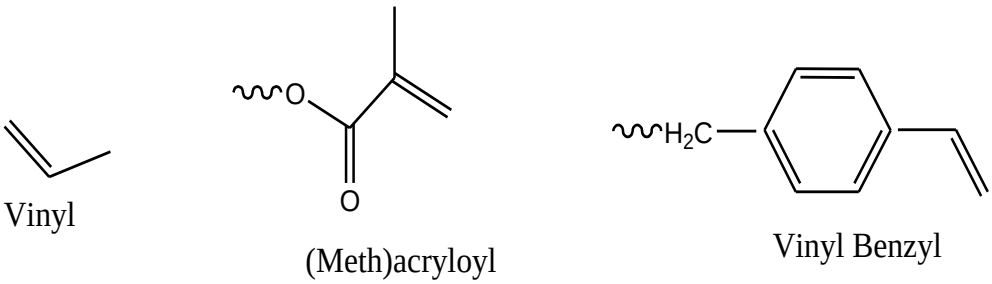

Figure 1.2 Common polymerizable groups [27]

Schemes 1.1 and 1.2 illustrates the synthesis of ILs monomers with vinyl benzyl (styrenic) and (meth)acryloyl polymerizable groups, respectively [27]. For example, 1-methylimidazole reacts with 4-vinylbenzyl chloride to form the polymerizable ILs monomer, 1-methyl-3-(4-vinylbenzyl) imidazolium chloride as shown (Scheme 1.1). In Scheme 1.2, 1-methylimidazole reacts with halide (meth)acrylate species to produce polymerizable ILs monomer with (meth)acrylate group [27].

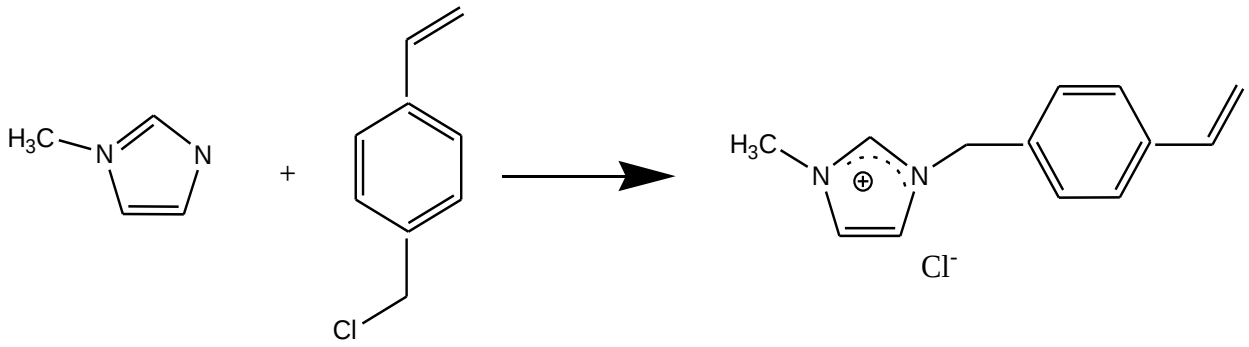

Scheme 1.1 Synthesis of 1-methy-3-(4-vinylbenzyl) imidazolium chloride with vinyl benzyl polymerizable group

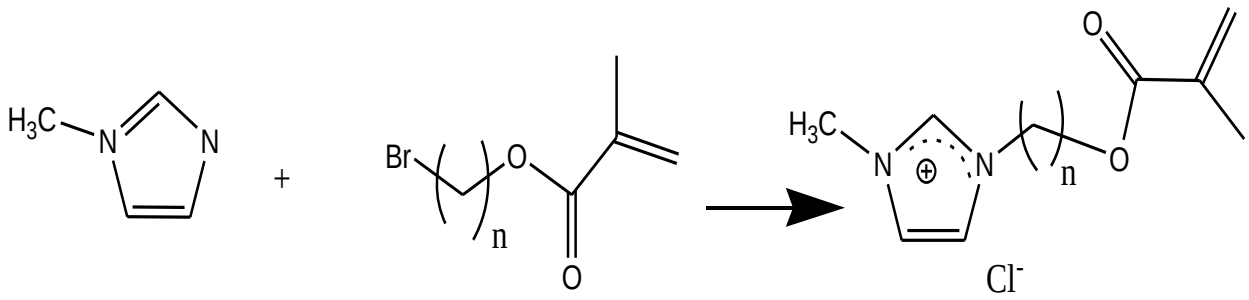

Scheme 1.2 Synthesis of methacrylate-containing polymerizable ILs monomer

1.2.1 Properties of PILs

Physicochemical properties of polymeric ionic liquids can be tuned by changing the ions involved [36-38]. Some PILs are normally soluble in water (imidazolium-based PILs with halides as counter anions), and some are only soluble in organic polar aprotic solvents such as dimethyl form amide (DMF), dimethyl sulfoxide (DMSO) and acetonitrile [30]. This is so because the properties of PILs depends on the types of counter anions and/or counter cations involved, the alkyl chain length, and the chemical architecture of the polymer backbone [39]. The most common PILs properties are: ionic conductivity, glass transition temperature and amphiphilic behaviour [39].

1.2.1.1 Ionic conductivity

The fundamental aspect of PILs in electrochemical science lies on the availability of mobile ions in the system and therefore the ion conductivity of PILs depends on the delocalization and movement of ions in it [39]. Eftekhari and Saito [40] reported that the ionic conductivity of PILs is greatly influenced by the mobility of cations if the polymer backbone is anionic (polyanion), and vice-versa. When the polymer backbone is the polycation, only anions are moving and impact the conductivity. The ion conductivity of polymeric ionic liquids is also influenced by the impurities, moisture, and environmental humidity [31, 39-40]. Thus, the ionic conductivity of

PILs will be smaller than that of their corresponding counter ILs [40]. This is due to the limited movement of ions in the polymer structure compared to ILs moieties. High thermal stability of PILs usually leads to strong ionic conductivities at high temperature [40-43]. Dynamic viscosity and glass transition temperature inversely impacts the ionic conductivity of PILs [41, 43-44].

1.2.1.2 Glass transition temperature (T_g)

This is a temperature region where polymer materials transitions from a hard, glassy materials to a soft, rubber-like materials [45-46]. T_g is the temperature below which a solid remain in glassy state and above which it becomes viscous liquid [45]. It has been observed that molecules or atoms at glassy state are subject only to vibrational and not transitional and rotational motions [45-49]. The process of solid melting (T_m) occurs at a temperature above T_g [50]. Polymers below T_g usually behave brittle, whereas above T_g they become more rubber-like material. Glass transition temperature of polymers can be affected by different factors such as molecular weight [49], molecular structure [50], length of side group(s) [50], double bond in polymer backbone [49-50], chemical cross-linked [51], backbone flexibility [52], branching [53], and alkyl chain length [54]. Glass transition temperature of PILs is effectively controlled by the structure of the polymer, the sizes of counter cations and counter anions used [41, 44].

Differential scanning calorimeter (DSC) can be used to determine glass transition temperature in polymer materials [45, 49-55]. Elabd and Ye [56] probed the effect of anion exchange on ionic conductivity, chemical and thermal stability of poly(1-[(2-methacryloxy)ethyl]-3-butylimidazolium-based poly(ionic liquid)s. The glass transition temperatures of the series of polymers they synthesized were investigated using DSC and decreases in the following trends based on the anions: $Br^->PF_6^->BF_4^->CF_3SO_3^->TFSI^-$ [83]. The trends showed approximately 95 °C difference from Br^- salt (T_g =102 °C) to the $TFSI^-$ salt with T_g = 7 °C. In the study done by Smith *et al*. [47], DSC was employed to determine glass transition temperatures of various salts of poly(1-ethyl-3-methyl-4-vinylimidazolium) and poly(3-ethyl-1-vinylimidazolium) with BF_4^-, PF_6^-, AsF_6^-, $CF_3SO_4^-$, $[CF_3SO_2]_2N^-$, and $C_2N_3^-$ as counter anions. Their intrinsic interest was on the comparison between the polymers of imidazolium with vinyl polymerizable group on the 1st and 4th-positions of the five-membered rings of imidazolium salts. Fig.1.3 shows the polymer structures of poly(1-ethyl-3-methyl-4-vinylimidazolium) and poly(3-ethyl-1-vinylimidazolium) salts studied by Smith *et al*. [47].

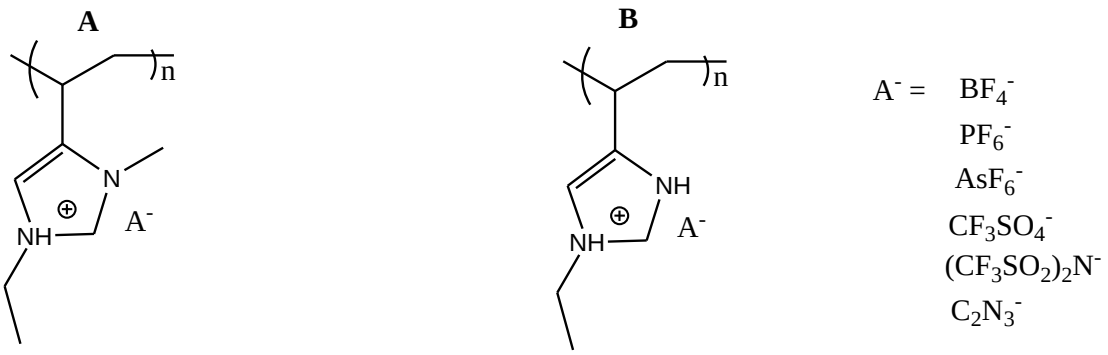

Poly(1-ethyl-3-methyl-4-vinylimidazolium) salts

Poly(3-ethy-1-vinylimidazolium) salts

Figure 1.3 Poly(1-ethyl-3methyl-4-vinylimidazolium) (A), poly(3-ethyl-1-vinylimidazolium) (B) salts [47]

1.2.1.3 Amphiphilic behaviour

The hydrophobicity-hydrophilicity of PILs can be controlled or reversibly switched by interchanging the polyanions involved [57-58]. This depends on the type of the polymer architecture required, potential application, and poly ions used [59]. Hydrophobic polymers comprising of hydrophobic anions such as hexafluorophosphate (PF_6^-) or bis(trifluoromethanesulfonyl)imide ($TFSI^-$) always precipitate in aqueous solution, without altering the chemical structure of the cationic polymer backbone [59-60]. These types of polymers are useful in water purification and gas separation [61]. Zhang and Yuan [62] reported the synthesis of 1-vinyl-1,2,4-triazolium PILs with PF_6^- and $TFSI^-$ as hydrophobic counter anions via radical polymerization of corresponding ILs monomers and anion metathesis of already existing polymers (Scheme 1.3).

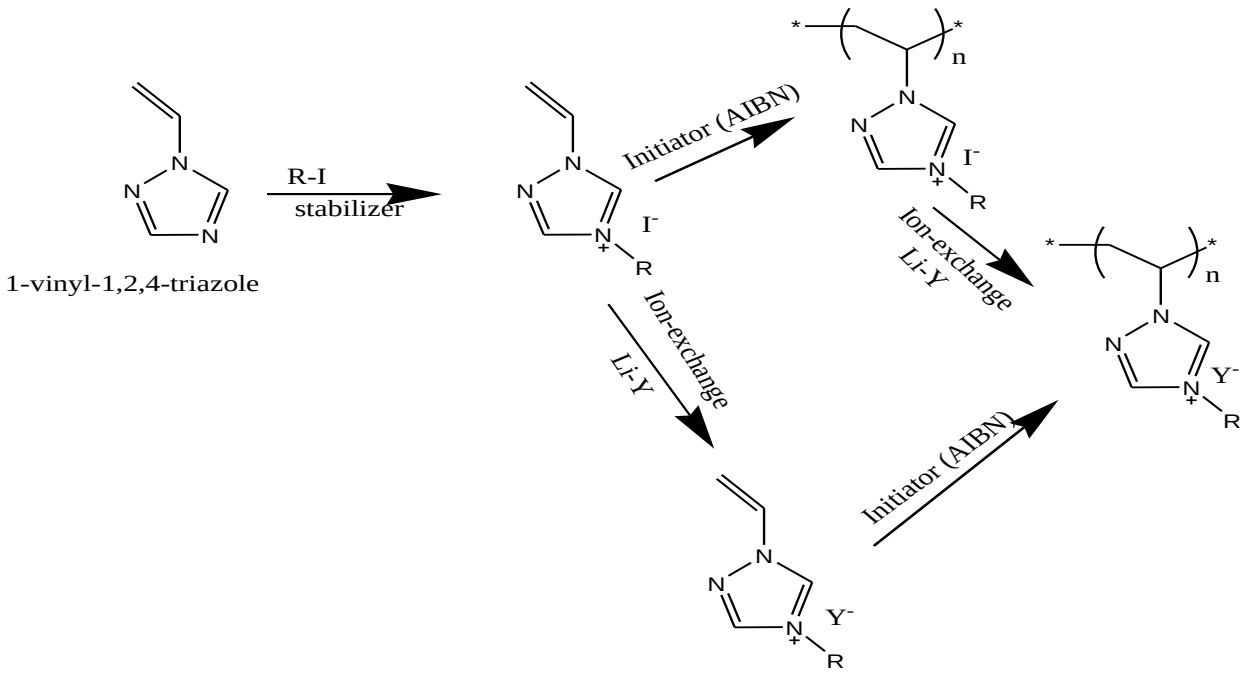

Scheme 1. 3 Synthesis of hydrophobic poly(4-alkyl-1-vinyl-1,2,4-triazolium) [62]

1.2.2 Synthesis of PILs

Synthesis of PILs depends on the required PILs structure, properties, and intended application(s) [28-29, 38, 58, 65-70]. Polymeric ionic liquids can be synthesized by either direct free radical polymerization of ILs monomers [33], and/or via modification of existing polymers [70-75]. The advantage of post-polymerization is the flexibility and specific reactivity of the synthesized PILs [76]. Kuzmicz *et al*. [77] discovered that the specific surface area (1000 m^2/g) of polymer materials can be obtained by copolymerization of PILs through cross-linking. This well-defined surface area is predominantly important for adsorption applications.

Nakabayashi *et al*. [78] reported the synthesis of poly(*N*-viny-1,2,4-triazolium bromide) polymers via RAFT polymerization. The synthesized polymers were utilized as polymer precursors to synthesize two series of 1,2,4-triazolium-amphiphilic block copolymers by RAFT polymerization. High ionic conductivities of 3.1 x 10^{-4} mS/cm at 90 °C, 1.1 x 10^{-4} mS/cm at 55 °C, and 3.4 x 10^{-5} mS/cm at 25 °C were obtained respectively. Isik *et al*. [59] also reported the synthesis of imidazolium–based PILs via RAFT polymerization of methacrylamido monomer with different alkyl chains such as ethyl, isopropyl, butyl, (1-phenyl ethyl), and dodecyl. The morphologies of the synthesized PILs were found to range from spherical to rod-like micelles. Scheme 1.4 illustrates the synthetic procedure for amphiphilic PILs via RAFT [36].

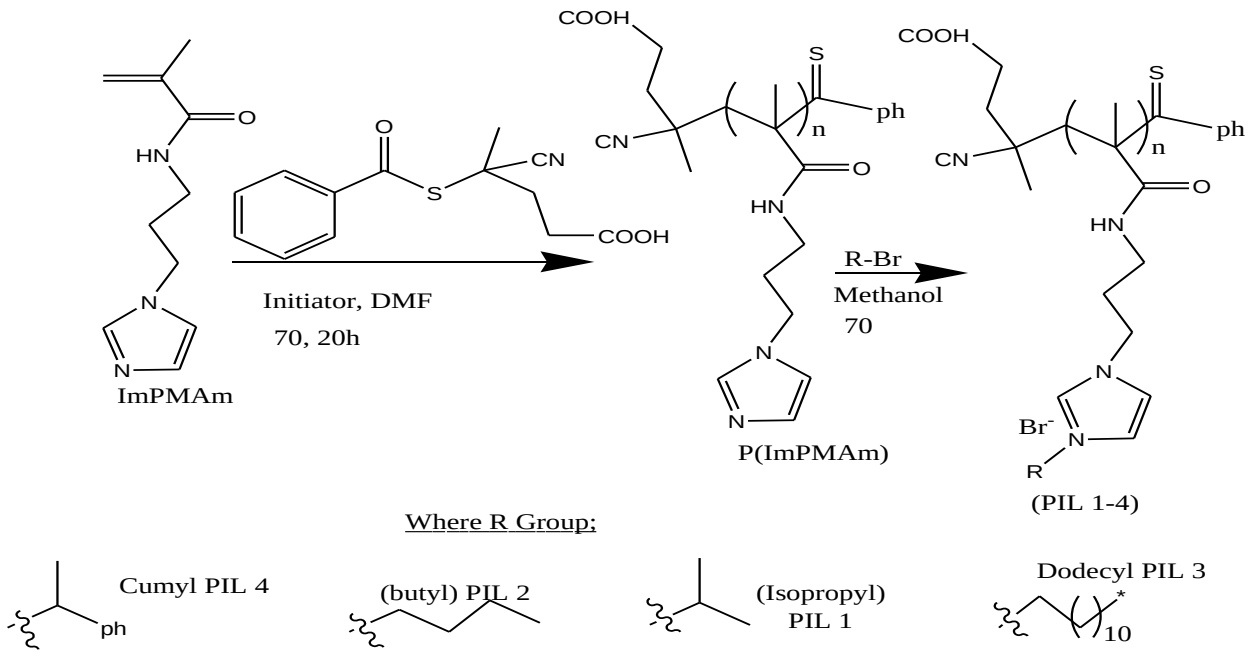

Scheme 1.4 Synthetic procedure for amphiphilic PILs via RAFT [36]

1.2.3 Applications of PILs

The present literature review paid specific focus on the application of polymer materials on the removal of metal ions, sometimes referred to as heavy metals from industrial and aqueous solution.

1.2.3.1 Polymer materials on metal ions removal

Fresh potable water is a basic requirement and necessity for the sustainability of humanity and wild-life on earth [81]. However, the continuously contamination of different water bodies by numerous water contaminants renders them unusable and non-reliable for supporting humanity and aquatic ecosystems. Different micro-to-nanopollutants and metal ions are found in almost all water bodies today, in both degradable and/or non-degradable forms. Therefore, the removal of such water pollutants together with metal ions has been at the centre of research today. As one of the most dominant and leading applicable method for the removal of water-pollutants, adsorption has been intensively studied and recommended. Among the key properties of the suitable and reliable adsorbents include low-cost production, easy to operate, recoverable and reusable. Several adsorbents having used so far includes silica [82], carbon materials [83], rice hush [84], natural adsorbents [85-86], activated carbon [87], polymers [88], and dendrimers [81, 89-91].

Shen and co-workers [92] studied the adsorption of Cr(III), Zn(II), and Cd(II) onto the surface of micelle-like aggregates of polymer-surfactant system made up of poly(dialldimethyl ammonium chloride)-poly(ethyleneimine) as cationic polymer and sodium dodecyl sulfate as a surfactant on the polymer backbone. It was established that the removal of all the multivalent species reached 99% efficiency at their respective optimum dosages during the first 20 minutes of contact interface time. The use of magnetoactive polymer networks and their applicability as adsorbents for U(VI) and Th(IV) radioactive metal ions removal have been reported and its gaining popularity [93, 94-95]. Al Hamouz *et al*. [96] reported the synthesis and the use of three novel cross-linked polymer hydrogels with amino and hydroxyl functional groups prepared via Mannich polycondensation reaction as adsorbents, as shown in Fig. 1.4.

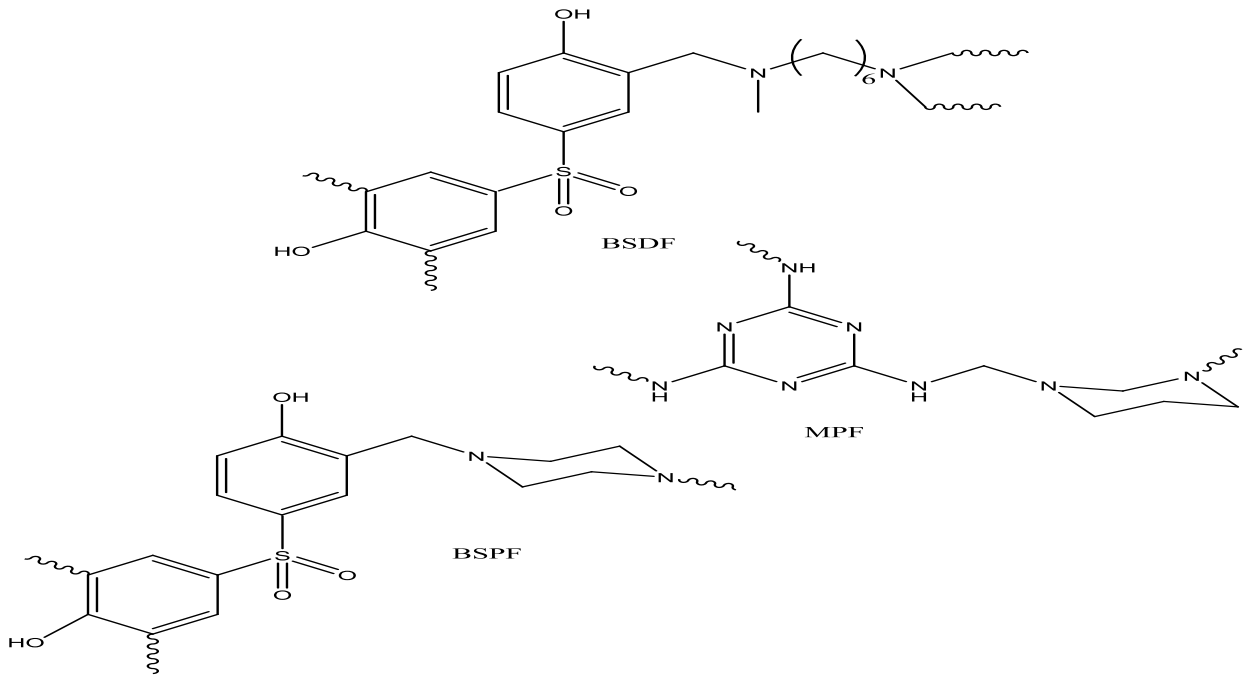

Figure 1.4 Bisophenol-S paraformaldehyde 1.6-diaminohexane polymer (BSDF), bisophenol-S paraforldehyde piperazine polymer (BSPF), and melamine paraformaldehyde piperazime cross-linked polymer (MPF) [96]

Ligand-carrying polymeric nanoparticles (LC-NPs) were investigated and tested against the absorption of various metal ions from aqueous solution in the form of Ni(II), Co(II), Cu(II), and Cr(VI) [97]. The metal ion removal, recovery and efficacy of the designed nanomaterials were also investigated. Chen and Huang [98] probed the *in situ* polymerization of 1-vinyl-3-octylimidazolium tetraborate (VOI) and the use of two cross-linkers, (divinylbenzene and *N*,*N*-methylene bisacrylamine). The as-synthesized PILs material (Fig. 1.5) was employed to co-

extract acidic (phenols), basic (aromatic amines), and parabens (neutral) analytes. The as-synthesized PILs materials were merged with stir cake sorptive extraction (SCSE) to produce SCSE/PIL as the potential adsorbent for acidic, basic, and neutral analytes.

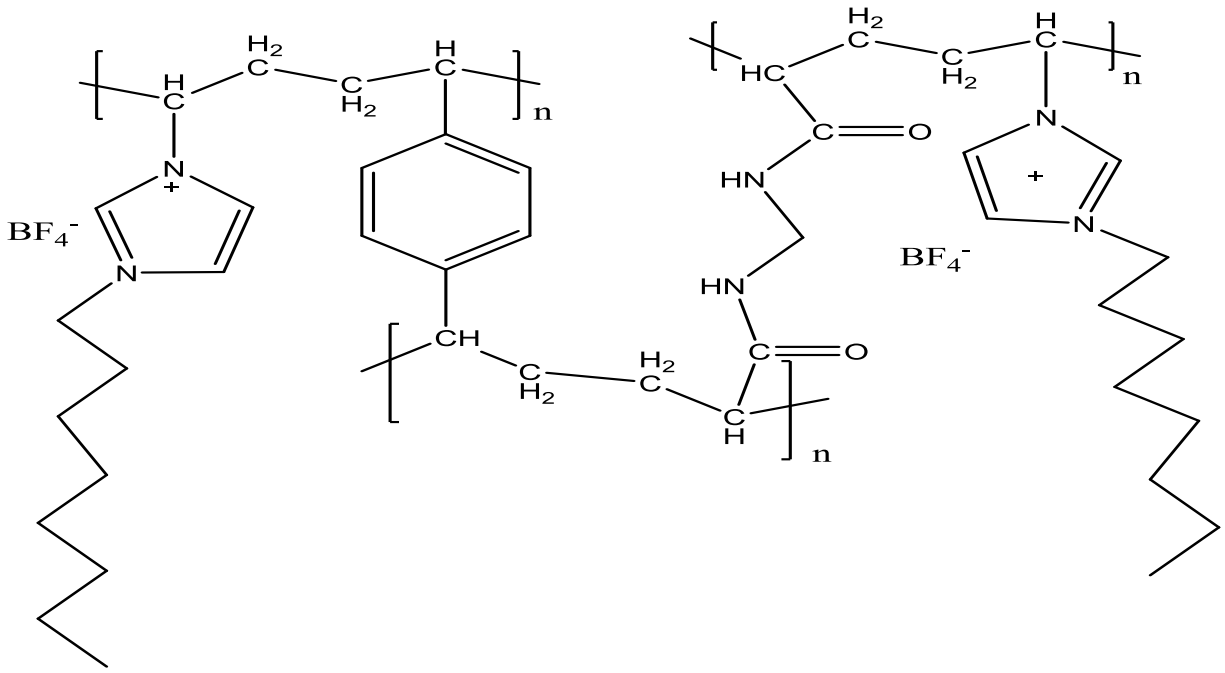

Figure 1.5 PIL material of 1-vinyl-3-octylimidazolium tetraborate (VOI) with two cross-linkers (Divinylbenzene and N,N-metheylene bisacrylamine) [98]

1.2.3.2 Natural polymers on metal ions removal

In one of the attempts to use natural and synthetic polymers, Lam *et al*. [99] reported the use of polymer-enhanced ultrafiltration (PEUF) made up of chitosan and carboxylmethyl cellulose (CMC). The PEUF system was designed to be used in urban or industrial wastewater treatment.

Among the important attributes of the system was its performance induced by the use of the natural polymers in different conditions, taking into account the effect of metal ion concentration, salt addition, and pH of the solution. The natural and synthetic polymers used by Lam and co-workers [99] are presented in Fig. 1.6. In another study, Huang and co-workers [100] probed the applicability of polyvinylamine (PVAm) as the chelating polymer agent for the removal of certain metal ions using ultrafiltration process. However, it was established that the coordination interactions between the polymer chelating agent and the metal ion relatively influenced the performance of the polymer-enhanced ultrafiltration (PEUF). The authors also concluded that due to the availability of $–NH_2$ binding sites, the PVAm can be successfully used in flocculation/coagulation processes as flocculant to bind and remove metal ions from wastewater plants.

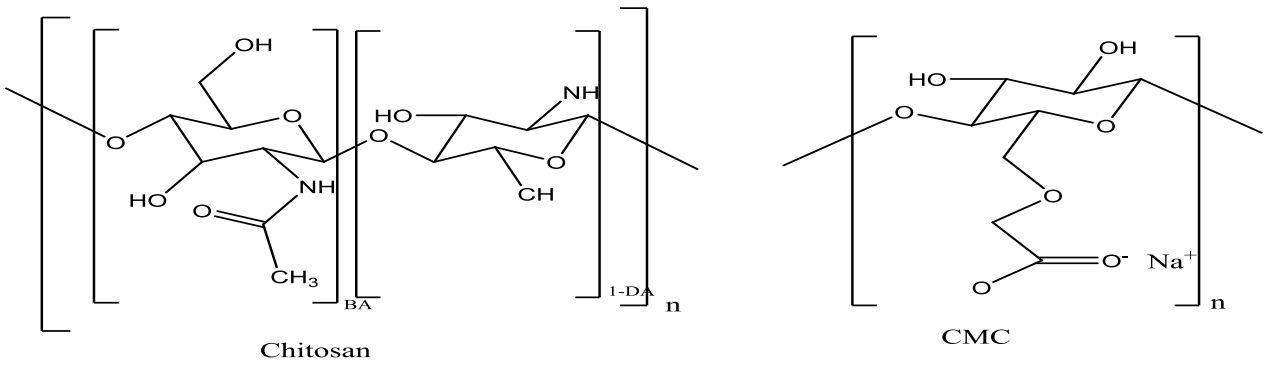

Figure 1.6 Natural polymer (chitosan), and synthetic polymer (carboxylmethyl cellulose) [99]

Another study on the use of natural polymers for the removal of metal ions was conducted by Siahkamari and co-workers [101]. In this study, the adsorption of Pb(II) by chitosan and chitin nano-sorbents was investigated and it was established that the adsorption process reached equilibrium at 60 minutes of contact time interface [101]. The adsorption mechanism of Pb(II) on chitosan nanoparticles is shown in Fig. 1.7. In an attempt to study the adsorption behavior of chitin derivatives, Cao and co-workers [102] reported the adsorption of methylene blue (MB) onto the porous chitin. They achieved a removal efficiency of 79.8%, thanks to the lower crystallinity and more porous structure of chitin sorbents (PChs). Their conclusion was derived based on adsorption mechanisms involved which include heterogeneous mass transfer with multiple diffusion processes such as diffusion of MB from the liquid state to the external surface of the adsorbent, diffusion of MB from outer surface to the inner surface of the adsorbent, and finally the diffusion of MB from one pore to another pore of the adsorbent.

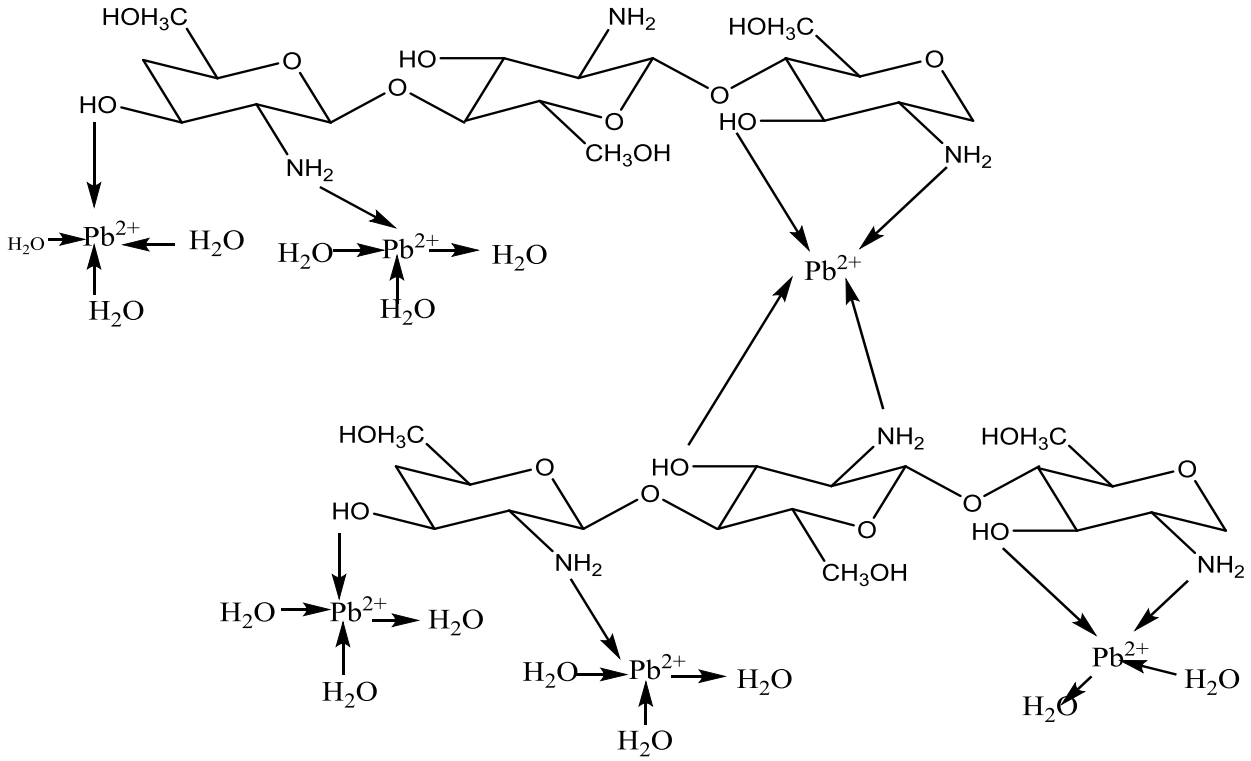

Figure 1.7 Adsorption mechanism of Pb(II) on Chitosan nanoparticles [101].

1.2.3.3 Synthetic polymers on metal ions removal

Ceglowski and Schroeder [103] prepared two new chelating polysiloxane-based polymers by grafting pyridine-pyrazole ligands onto poly(methyl hydrosiloxane) (PMHS) and used them in selective extraction of Cu(II), Cd(II), Cr(III), Ni(II), and Co(II). The structures of the polymers obtained by hydrosilylation reaction of poly(methylhydrosiloxane) with pyridine-pyrazole ligands are shown in Fig. 1.8. It was established that the length or the nature of the linker have influenced the metal ion uptake of the synthesized chelating polysiloxane-based polymers. For example, the polymer structure with the shorter linker was found to be more selective towards

Cu(II) ion, whereas the other one with longer linker exhibited more flexibility and multifunctional behavior towards metal ions uptake [103].

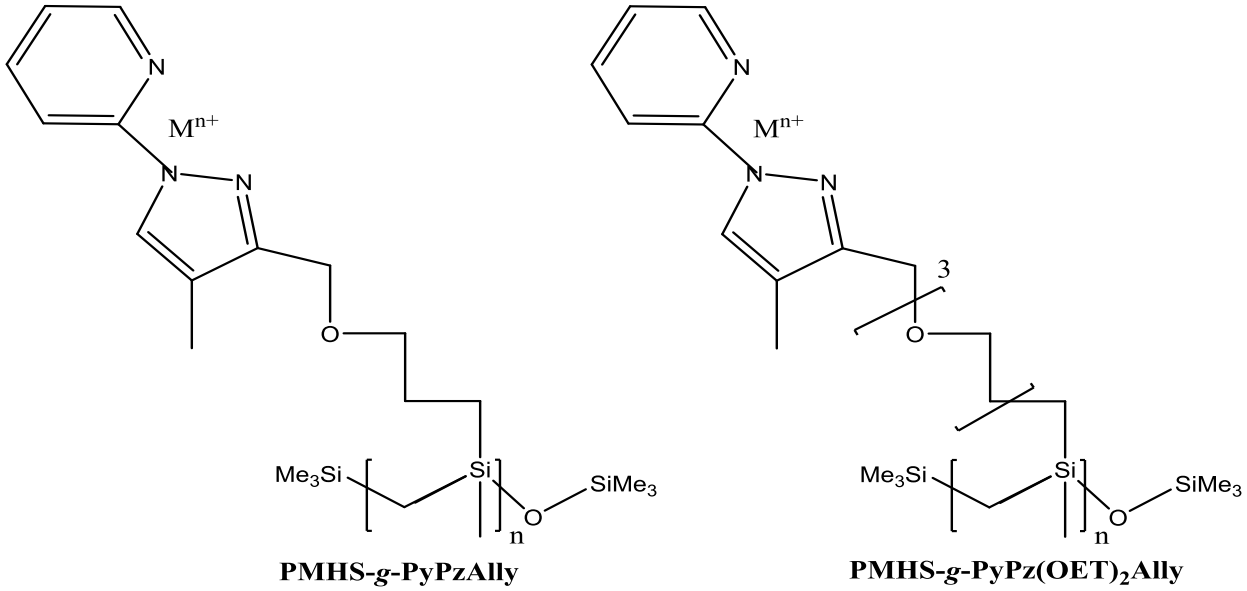

Figure 1.8 Structures of chelating polysiloxane-based polymers after adsorption of metal ions [103]

El-Said *et al*. [104] reported the synthesis of meso-sorbent silica polyaniline (MSNPs/MANI)) composite for the removal of chloridazon (n-CLZ) from aqueous solution. The polymeric composite was synthesized from mesoporous silica support together with polyaniline (*in situ* polymerization of polyaniline in MSNPs). The authors established that the removal of chloridazon increased sharply at low n-CLZ concentrations when using MSNPs/PANI meso-

sorbent. It was also observed that the adsorption of n-CLZ pesticide by MSNPs/PANI followed Freundlich isotherm (assuming multilayer adsorption onto the heterogeneous surface).

Hosseini *et al*. [105] reported the synthesis of polypyrrole via oxidative polymerization and the resultant available amine functional groups were used for selective co-ordination with Cu(II) ions. Both the ion-exchange property and porosity of the polypyrrole are believed to be the main properties that facilitated the interactions and possibly removal of Cu(II). The adsorption mechanism of Cu(II) by polypyrrole is shown in Fig. 1.9. Polyaniline (PANI), polypyrrole (PPY), and polythiophene (PT) conducting polymers have been synthesized and used in the removal of nitrate anions from water. Based on the properties of the polymeric chain, it was expected that the polymer chain fairly contributes to the reduction of nitrate without the use of a particular metal catalyst [106]. In PANI, the ion-exchange between Cl^- and SO_4^{2-} counter-ions and NO_3^- from water was considered as the possible interaction and mechanism behind the removal of nitrate.

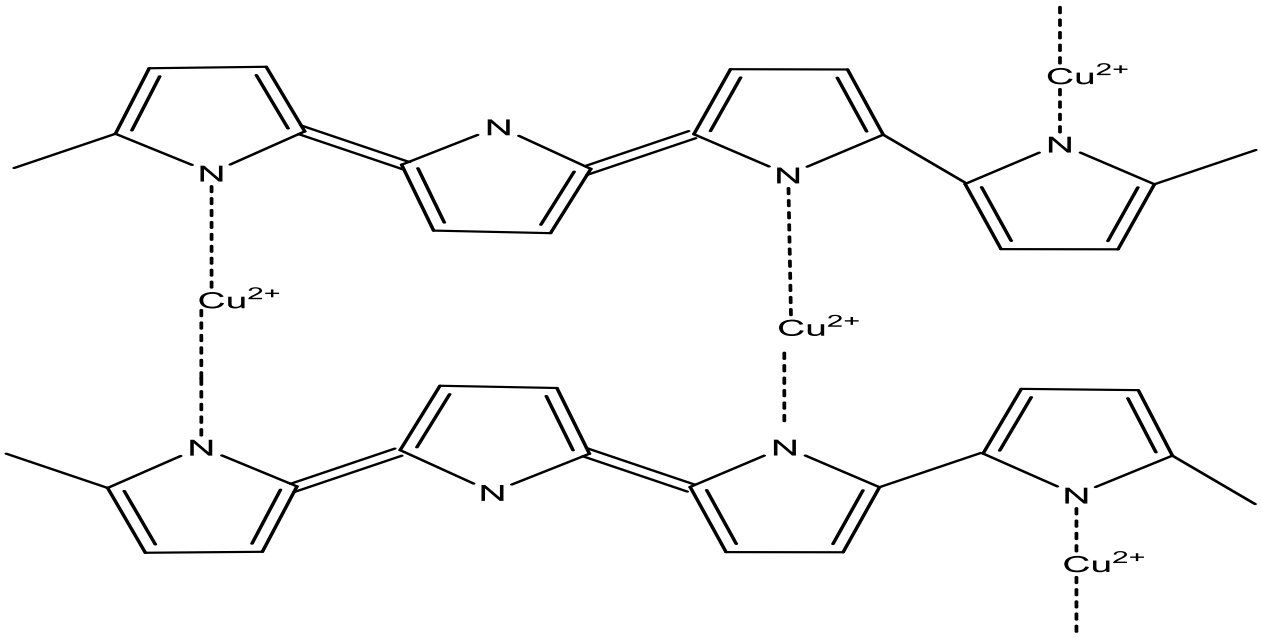

Figure 1.9 Adsorption of mechanism of cu(II) by polypyrrole [105]

The use of carbon-based materials grafted with polymers has been briefly investigated in metal ions removal. For example, Ko and co-workers [107] have recently reported the synthesis of disulfide-linked polymer grafted activated carbon (DiS-AC) (Fig. 1.10) and its applicability in heavy metals' removal from storm water runoff. Comparing the sorption affinities of Cd(II) removal using conventional sorbents, it was observed that the distribution coefficient of Cd(II) bonding using DiS-AC was 89.10^3 L/Kg at solution concentration of 0.35 mg/L.

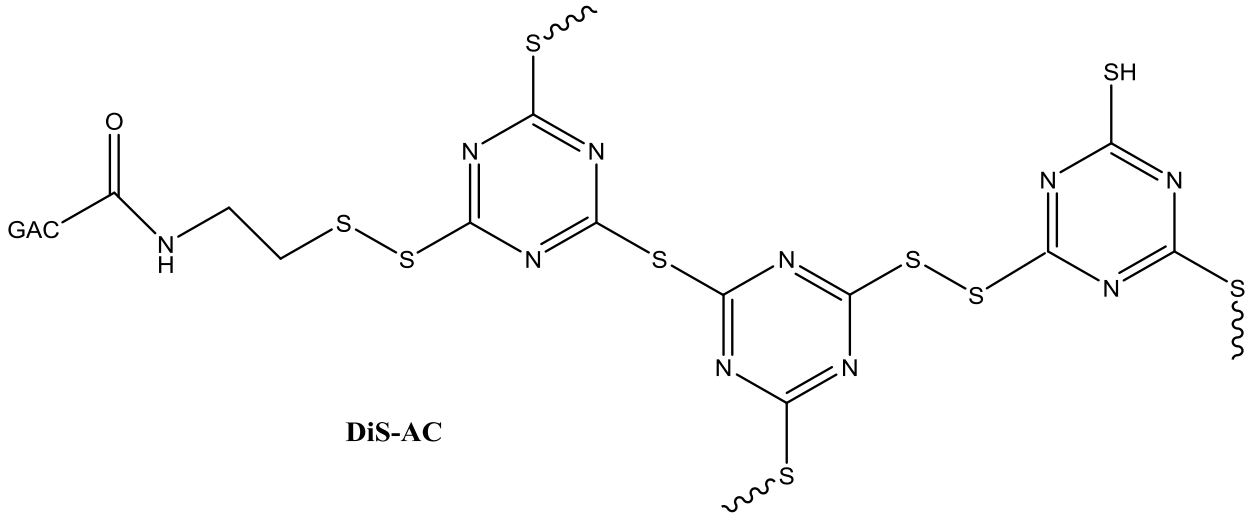

Figure 1.10 Structure of disulfide-linked polymer grafted activated carbon [107].

1.2.3.4 Ion-imprinted polymers on metal ions removal

The synthesis and study of magnetic ion-imprinted polymer systems (IIPs) have recently gained significant consideration in wastewater treatment and removal of metal ions. Yuan and co-workers [108] synthesized cobalt ion-imprinted polymer systems based on metal-organic frameworks and employed them on the removal of cobalt(II). It was seen that the adsorption capacity of the synthesized Co-IIP adsorbent was 175 mg/g and the experimental data fitted well into the pseudo-second-order kinetic model. Another study on the use of ion-imprinted polymer systems was reported by Liang and co-workers [109]. They synthesized novel magnetic Cr(VI) ion-imprinted polymer systems via sol-gel process for the removal or retention of Cr(VI). However, the resultant Cr(VI) ion-imprinted polymer materials yielded high adsorption capacity

of about 311.95 mg/g for hexavalent chromium at low pH (optimal pH of 2.0). At low pH levels, the adsorption of Cr(VI) was observed to be high due to the presence of protonated nitrogen groups in the pyridine structure. Furthermore, the desorption and reusability of the adsorbent were investigated and it was discovered that the Cr(VI) ion-imprinted polymer systems were stable and reusable up to five repeatable cycles with less than 5% loss of adsorption capacity. Owing to the conversion or transformation of Cr(VI) to less toxic Cr(III), authors also concluded that the desorption method used decreased or minimized the toxicity of chromium.

Xi *et al*. [110] reported a maximum adsorption capacity of 46.5 mg/g using cadmium imprinted polymers. Li and co-workers prepared inverse emulsion Cd(II) ion imprinted polymers (Cd(II)-IEIIPs) and evaluated them on the selective removal of Cd(II) from aqueous solution. Their study achieved adsorption capacity of about 86.7 mg/g. Taking into consideration the selectivity coefficients *k* obtained for Cd(II)/Pb(II), Cd(II)/Zn(II), and Cd(II)/Cu(II), which were 2.4998, 1.2437, and 4.6882, respectively, they concluded that the synthesized Cd(II) ion imprinted polymer system could be used to selectively remove Cd(II) from other wastewater bodies. For the first time, So and co-workers [111] reported the selective ability of surface molecularly imprinted polymer (SMIP) in removing carbaryl (CBL) in competitive adsorptions with carbofuran (CBF) and metolcarb (MTC). An adsorption capacity of 41.14 mg/g for CBL was

achieved in the competitive environment against 8.12 and 4.15 mg/g of CBF and MTMC, respectively.

He *et al*. [112] recently studied the surface modification of β-cyclodextrin (β-CD) by cross-linking it with rigid aromatic compound like tetrafluoroterephthalonitrile, resulting to a β-CD polymer with high surface area. The competitive adsorption capacity of β-CD polymer was evaluated against Pb(II), Cu(II), and Cd(II) and it was discovered that certain structural and chemical properties such as large surface area, the presence of negative charge and H^+ ions on hydroxyl groups played a significant role in facilitating and monitoring the adsorption of Pb(II), Cu(II), and Cd(II) onto the surface of β-CD polymer. Adsorption equilibrium was reached at 5 min time and adsorption capacities of 196.42, 164.45, and 136.43 mg/g at initial concentration of 200 mg/L for Pb(II), Cu(II), and Cd(II) were achieved, respectively.

Fallah *et al*. [113] reported the synthesis and evaluation of new highly selective molybdenum (VI) ion-imprinted polymer (Mo(VI)-IIP) on selective adsorption of Mo(VI) from aqueous solution. Maximum adsorption capacity of 131.75 mg/g was achieved. In addition to high selectivity behavior, the Mo(VI) imprinted polymer was found to be thermally stable and reusable up to six cycles without losing its adsorption capacity. Furthermore, a wide variety of

adsorption capacities of some polymer systems that have been recently studied and reported for the removal of certain metal ions are presented in Table 1.1.

Table 1.1 Adsorption capacities of some polymer materials.

Polymer system type	**Targeted species**	**Adsorption capacity (mg/g)**	**pH/ contact time (min)**	**Ref.**
Cd(II)-IIP	Cd(II)	46.5	5.0/20	[110]
Surface-grafted Cd(II)-IIP	Cd(II)	46.8	6.0/35	[114]
Cd(II)-IIP	Cd(II)	45		[115]
Cd(II)IP	Cd(II)	40		[116]
IEIIP	Cd(II)	86.7	7/80	[117]
IEIIP	Pb(II)	27.95	6.0/10	[118]
IIP	Cu(II)	84		[119]
SMIP	CBL	41.14	7/40	[111]
β-CD polymer	Pb, Cu, & Cd	196.42, 164.45, 136.43	7-11/5	[112]
Mo(II)-IIP	Mo(VI)	126.06	10/10	[113]
CSF/PDMAEMA	Cr(VI)	145	3/10	[120]
CS-Fe-SO_4 complex	dyes	249.22	4.6.5/10	[121]
Cu(II)-IIP	Cu(II)	48	-	[122]
Magnetic Hg(II)-MIIP	Hg(II)	78.3	6/5	[124]
Ni(II)-IIPs	Ni(II)	40	9/15	[124]
Cd(II)-IIP	Cd(II)	16.5	6.0/20	[125]
Ni(II)-IIPs/MWCNTs	Ni(II)	19.86	6/30	[126]
β-CD polymer	Cd(II)	107	7/80	[127]

: Ion-imprinted polymer (IIP), inverse emulsion ion-imprinted polymer (IEIIP), surface molecularly imprinted polymer (SMIP), corn stalk fibers/poly(dimethylaminoethyl methacrylate (CSF/PDMAEMA)), multi-walled carbon nanotubes (MWCNTs).

1.2.4 The effect of pH

The effect of solution pH on the removal of metal ions from aqueous solution plays crucial role in understanding adsorption mechanism. The protonation of functional groups on the adsorbent and the solution-chemistry properties of the metal ions are among the most influential pH attributes [128]. In the study of Kang *et al*. [128], the precipitation of $Co(OH)_2$ occurred at pH>7, signifying the increase of adsorption capacity of Co(II)-IIP and NIP for Co(II) with increasing pH of solution and decrease at low pH values (pH<6). Xu *et al*. [129] reported that sulfur-rich microporous polymer (SMP) exhibited excellent removal efficiency of greater than 98% on the removal of Hg(II) over a wide range of pH values (from acidic to alkaline conditions).

Sanchez *et al*. [130] investigated the effect of pH on the removal of hexavalent chromium species using poly(*N*,*N*-dimethylaminoethyl methacrylate) (PDMAEMA) in a polymer-enhanced ultrafiltration (PEUF). Their study showed that the retention of Cr(VI) reached maximum at pH=4 and 6, showing significant decrease around acidic medium (pH<4) and neutral to basic

conditions (pH>6). The fundamental reason behind the retention of Cr(VI) at such pH values is the fact that PDMAEMA is protonated and enabled to electrostatically interact with dichromate and hydrochromate anions.

In generally, the retention of chromium anions from aqueous solution depends on the degree of protonation of the adsorbent and the type of chromium species in solution [130]. It has been reported in the literature that the protonation of the nitrogen atom (or $-NH_2$) of the amino-containing polymer adsorbents usually facilitate the efficient removal of Cr(VI) in the form of dichromate ($Cr_2O_7^{2-}$) [131-134]. It was also established that the adsorption mechanisms were prompted by the ionic electrostatic interaction between the protonated polymer parts and the negatively charged dichromate anion [131, 135].

Literature have also reported that the adsorption of Cr(VI) reached equilibrium at low pH values (pH=2), and decreased at high pH values [131]. Poor electrostatic interactions (at high pH values due to the competition between CrO_4^{2-} and OH^-) and excellent electrostatic interactions (at low pH values due to the protonated adsorbent surface) are known to be the main attributes behind the adsorption of Cr(VI) [136-137]. Having mentioned the influence or existence of electrostatic interactions during the adsorption processes (i.e. the adsorption of Cr(VI)), it is also worthy to

mention the formation of electrostatic repulsion between the specific functional groups and certain species. When an adsorbent-functional group such as $-NH_2$ is protonated to $–NH_3^+$ at low pH values, electrostatic repulsions are experienced in the case of divalent metal ions adsorption [138]. Electrostatic repulsions significantly reduce the adsorption or removal efficiency.

Mishra and Verma [139] studied the binding affinity of Pb(II) with novel Pb(II) ion-imprinted /carbon nanofibers-grafted highly porous polymeric beads (CNF-IIP). High adsorption capacity (47.62 mg/g) was achieved at pH=6, and adsorption capacity decreased at high pH levels due to the precipitation of Pb(II) as hydroxides, i.e. $Pb(OH)^+$, or $Pb(OH)_3^-$. Table 1.2 presents the summary of some studies reported in the literature based on the effect of pH in the adsorption of come metal ions.

Table 1.2 Some literature findings on the effect of pH.

Polymer system	Target species	Adsorption capacity (mg/g)	pH	Ref.
CNF/Pb(II)-IIP	Pb(II)	47.02	6	[139]
PDMAEMA-PEUF	Cr(VI)	100	4-6	[130]
Co(II)-IIP	Co(II)	23.09	≥7	[128]
SMP	Hg(II)	RE>98.8%	Acidic to basic	[129]
CSMA-MO	Cu(II)	RE>100%	6-8	[140]
Poly(MAAcH)-*cl*-DVB	Cr(VI)	100	2.0	[131]
CTS-PVA/APT	Cu(II)	4.26	5.50-6.50	[141]
Poly(AN-*co*-AA)	Cd(II)	RE>90%	9	[142]
Poly(AN-*co*-AA)	Pb(II)	RE>98%	9	[142]
PAMA	Cr(VI)	192.2	4	[143]
PAMA	Ni(II)	243.2	6	[143]
L-IIPs	Pr, Nd, Sm, Eu, Gd	125.3, 126.5, 127.6, 128.2, 129.1	6	[144]

Carbon nanofibers (CNF), chitosan-poly(vinyl alcohol)/attapulgite (CTS-PVA/APT), poly(acrylonitrile-co-acrylic acid) [poly(AN-co-AA), poly(acrylonitrile co maleic acid) (PAMA).

1.2.5 Regeneration and reusability of polymer adsorbents

The ability to regenerate and reuse the adsorbents is the most fundamental characteristic of an ideal adsorbent. Regenerative and reusable adsorbents are the most desirable materials in separation technology [145]. Owing to excellent elution solution, adsorbents are normally regenerated and reused multiple times with promising results and performance [146]. Tolessa *et al*. [147] probed and reported the reusability of magnetic chitosan microspheres (MCMs). They

discovered that after the first use, the adsorbent (MCM) maintained extraction efficiency of 89.6%, then an average extraction efficiency of up to 77.2±22% after three consecutive cycles. Fe_3O_4 magnetic nanoparticles surface-modified with 2,4-diaminophenol and formaldehyde (DAPF) were investigated as potential adsorbent for anionic dyes [148]. The latter authors discovered that the adsorption-desorption efficiency of Fe_3O_4@DAPF was maintained up to three cycles. In the study of Sikdera *et al*. [149], the adsorption-desorption studies have been conducted and have proven the mechanically and chemically robustness of CS-β-CDP-CMβ-CD beads used in the removal of Cd(II) ions from aqueous solution. The latter material was reusable up to seven (7) times without exhibiting a loss in adsorption capacity [149].

Maity and Ray [150] studied the regeneration and reusability of Cs-PMA/HNT on the removal/adsorption of Pb(II) and Cd(II). Their results showed that the Cs-PMA/HNT can be reused up to 5 times with excellent adsorption capacities ranging from 60 to 98% recovery of both Pb(II) and Cd(II). The regeneration and reusability of adsorbents mainly depends on the number of parameters including, to mention the few, the interactions between the metal ion(s) and the adsorbent, the nature of the adsorbent sites, and the eluent used [151-152]. Ravi and Ahn [153] regenerated and tested IPOP-Ns adsorbent ten (10) consecutive times to determine its reusability and stability after so many adsorptions-desorption cycles. It was established that the

latter adsorbent was chemical and structural stable, producing similar sorption performance in all cycles. Taghizadeh and Hassanpour [154] also studied the use of magnetic multi-walled carbon nanotubes-ion imprinted polymers (mMWCNTs-IIPs) for the removal of Cr(VI). Regarding the reusability of the adsorbent, they discovered that the polymer-functionalized carbon nanotubes material could be regenerated and reused up to the fifth time with only less than 7% adsorption capacity loss. However, Table 1.3 shows some of the polymer-based materials that have been regenerated and reused in the literature recently.

Table 1.3 Some regenerated and reused polymer-based materials

Polymer adsorbent	Target species	Max. Adsorption capacity (%)	No. adsorption-desorption cycles	Ref.
Cs/WCGs	MET, ASA, ACE, CAF	>50	5	[155]
mMWCNTs@PIL	Cu, Zn-SOD	>60	5	[156]
Cu(II)-IIPs	Cu(II)	99.9	5	[157]
NFC-MAA-MA aerogel	Pb, Cd, Zn, Ni	>80	10	[158]
TSP-NS	Cu(II)	>90	5	[159]
CMC-g-PAM/MMT	Rb^+ & Cs^+	-	5	[160]
Jule/PAA gel	Cd(II) & Pb(II)	81 & 94	5	[161]

Poly(methacrylic acid-co-maleic acid) grafted nanofibrillated cellulose (NFC-MAA-MA), chitosan/waste coffe-grounds (Cs/WCGs), triazine and thiophene bifunctionalized task-specific porous organic polymer with N and S atoms (TSP/NS) , carboxymethylcellulose-g-poly(acrylamide)/montmorillonite (CMC-g-PAM/MMT), Jute/Polyacrylic acid (Jute/PAA).

1.3 Problem statement

The environmental concern posed by the existence of toxic metal ions in drinking water and acid mine drainage from either abandoned and active coal and/or gold mines in the mining regions has drawn a serious attention of researchers and government institutions world-wide. For example, acid mine drainage posed a very negative–ecological impact on the ecosystem. This water threat is facilitated by the combination of factors such as low rainfall and high evaporation (high evapotranspiration than precipitation), expanding economy, and overpopulation. On the other hand, hexavalent chromium is known to be 100-fold more toxic than the trivalent moiety, especially in oxidized states. Presently, there is a growing need for a reliable, eco-friendly, and cost-effective method to remove toxic metal ions in drinking water. However, quite number of conventional methods such as coagulation, precipitation, reverse osmosis, and membrane filtration has been applied, yet showed high cost of operation. Recently, adsorption processes have been gaining moment as a potential metal ion remedial action and the fabrication of green chemistry materials as adsorbents is of importance.

The use of ionic liquids, polymeric ionic liquids, and their carbon nanotubes-functionalized composites on metal ions adsorption still lacks in the literature and need to be thoroughly investigated. For example, the knowledge about the interactions between IL salts and metal ions

during liquid/liquid extraction is still in nascent stage in the literature. The reports on the synthesis and use of PILs from imidazolium-based IL monomers with halide anions and short–alkyl chains have dominated the literature, however, their carbon nanotubes-functionalized derivatives and evaluation on metal ions removal are hardly reported so far.

1.4 Rationale and motivation

Imidazolium and pyridinium-based ILs and PILs with tunable hydrophobic anions offer several advantages such as water immiscibility, high thermal stability, and very low vapour pressure. Functionalized carbon nanotubes with hydrophobic ILs and PILs offer high thermal stability, large surface area, and dispersibility and hydrophobicity characteristics. Availability of poorly-coordinated organic and/or inorganic ions in ILs and PILs derivatives may be favourable to Cr(VI) retention at variable pH levels. The synthesis and application of selected ILs and PILs with fluorinated anions such as hexafluorophosphate (PF_6^-) and bis(trifluoromethanesulfonyl) imide ($TFSI^-$) offers the advantage of water immiscibility, high thermal stability, and solid at high temperatures. Ionic liquids and polymeric ionic liquids with hydrophobic anions (PF_6^- and $TFSI^-$), aromatic cations and three or low-alkyl chain length substituents are hydrophobic and convenient for solid-liquid adsorption. For example, *N*-vinyl imidazolium–based ILs monomers with PF_6^- usually precipitate out of aqueous solution. Carbon nanotubes tend to agglomerate,

therefore functionalising or dispersing them in ionic liquids derivatives will be necessary for the proposed use as adsorbent of metal ion. Hybrids of ILs/CNT and PILs/CNT provide high adhesion between CNT and metal ion. Functionalized carbon nanotubes with hydrophobic ILs and PILs possess high dispersibility and hydrophobicity.

1.5 Aim and objectives

This study has two major aims:

Aim 1: To synthesize and characterize pyridinium and imidazolium based ionic liquids (ILs) and polymeric ionic liquids (PILs).

To achieve aim 1, the objectives are:

- To synthesize and characterize pyridinium and imidazolium based ILs with three carbons lateral chains.
- To synthesize and characterize pyridinium based polymeric ionic liquids with vinyl polymerizable moiety.
- To synthesize and characterize imidazolium based polymeric ionic liquids with vinyl and styrenic polymerizable moieties.

Aim 2: To synthesize and characterize ILs and PILs-functionalized MWCNT composites and apply on the adsorption of Cr(VI).

To achieve aim 2, the objectives are:

- To synthesize MWCNTs using facile chemical method.
- To characterize MWCNTs using Infrared spectroscopy, thermal analysis, XRD, solubility, SEM/EDS and TEM microscopic analysis.
- To synthesize and characterize ILs and PILs-modified MWCNT composites using direct mixing method.
- To evaluate the as-synthesized ILs and PILs-functionalized composites potential as adsorbent for Cr(VI).

CHAPTER TWO

SYNTHESIS AND CHARACTERIZATION OF IONIC LIQUIDS AND IONIC LIQUIDS/MULTIWALLED CARBON NANOTUBES COMPOSITES

Part of Chapter two has been published:

Matandabuzo, M.; Ajibade, P.A. Synthesis, characterization, and physicochemical properties of hydrophobic pyridinium-based ionic liquids with N-propyl and N-isopropyl. *Z. Anorg. Allg. Chem*. **2018**, *644*, 489–495.

Matandabuzo, M; Peter A. Ajibade, Synthesis and surface functionalization of multi-walled carbon nanotubes with imidazolium and pyridinium based ionic liquids: Thermal stability, dispersibility and hydrophobicity characteristics. *J. Mol. Liq.***2018**, *286*, 248-293.

Chapter 2

2.1 Synthesis of ILs and IL/MWCNT composites

2.1.1 Background into pyridinium and imidazolium-based ionic liquids

Ionic liquids (ILs) are salts (organic and/or inorganic), with melting point relatively lower than (<100 °C) and are liquid at room temperature [162-163]. They were first discovered in 1914, when Weldon reported the physical properties of ethyl ammonium nitrate $(C_2H_5NH_3)NO_3$ with melting point of 12 °C [163]. Ionic liquids consist of an organic cation with delocalized charge, and organic or inorganic counter-ion [164-165]. The tunability of ionic liquids to give specific properties for a particular application is the reason for being given nickname "designer solvents" [162-166]. Ionic liquid salts possess special properties such as relatively non-volatile [167], good thermally stability [168], low melting point [167, 169], and high density [170]. Some of the properties of ionic liquids largely depend on the chosen cation and/or alkyl chain, and anion [171-172].

Kubisa [166] reported that both the cation and anion contribute to the melting point of an ionic liquid. An ionic liquid salt has no measurable vapor pressure, which makes them good replacements for volatile organic solvents [173]. It has been reported that organic cation(s) with

low symmetry or branched chain relatively produce low melting point salts [149]. Hydrophobicity, viscosity, density, and solvation of ionic liquids can be changed or manipulated by changing the anion [175-176]. The most common procedure used to synthesize water-immiscible ILs involves the preparation of aqueous solution of the halide salt with desired cation such as 1-ethly-3-methylimmidazolium halide followed by the anion-exchange process [177-179]. The water solubility or miscibility of ionic liquids depends on the type of counter-ion used [176, 178]. A typical example is that of 1-butyl-3-methylimidazolium in which the ionic liquids of 1-butyl-3-methylimidazolium cation and PF_6^- anion are immiscible in water, whereas that of 1-butyl-3-methlyimmidazolium cation and BF_4^- is soluble [176]. The functionality of ionic liquids can be tune by functionalizing the organic cation and anion molecular structure [177, 180]. Ionic liquids are associated with green chemistry as substitutes for volatile and flammable solvents. However, these types of salts have recently drawn significant interests for application in organic and polymer chemistry, catalysis, electrochemistry, analytical chemistry, nanotechnology, energy, micellization, and biotechnology [181-183]. ILs are also used as plasticizers, additives, components of polymer electrolytes, and porogenic agents to polymers [193].

Papaiconomou *et al*. [184] synthesized and studied the physicochemical properties of four pyridinium-based ionic liquids namely: 1-butyl-4-methylpyridnium bis(trifluoromethylsulfonyl) imide $[MBPYR]^+[Tf_2N]^-$, 1-butyl-4-methylpyridnium trifluoromethyl sulfonate $[MBPYR]^+[TfO]^-$, 1-butyl-4-methylpyridnium nonafluorobutyl sulfonate $[MBPYR]^+[NfO]^-$, and 1-butyl-4-methylpyridnium dicyanamide $[MBPYR]^+[N(CN)_2^-]$, respectively. They discovered that two of the four pyridinium-based ionic liquids, $[MBPYR]^+[N(CN)_2^-]$ and $[MBPYR]^+[NfO]^-$ were solid at room temperature, while $[MBPYR]^+[Tf_2N]^-$ and $[MBPYR]^+[TfO]^-$ were found to have densities higher than that of water at ambient temperature, which were 1.35 and 1.17 $g{\cdot}mL^{-1}$, respectively. Again, $[MBPYR]^+[NfO]^-$ and $[MBPYR]^+[Tf_2N]^-$ were found to be insoluble in water at 25 °C. Their melting points increases as follows: $[MBPYR]^+[N(CN)_2^-]$> $[MBPYR]^+[NfO]^-$> $[MBPYR]^+[TfO]^-$>> $[MBPYR]^+[Tf_2N]^-$. They concluded that ionic liquids containing 1-butyl-4-methylpyridinium cations have considerable high melting points, high densities, but lower solubility's in water than their imidazolium cation counterparts [184-186].

Dzyuba [186] reported the synthesis of N-substituted pyridinium bromide ionic liquids. Although research into the synthesis of pyridinium-based ionic liquids has received considerable attention in recent years, the wide applicability of imidazolium–based ionic liquids makes the pyridinium-based ionic liquids less attractive. N-substituted pyridinium halides are known to be solids,

which is in agreement with the findings of Papaiconomou and co-workers [184]. Dyzuba [186] also reported the novel synthesis of dicationic salts containing both pyridinium and ammonium cations.

2.1.2 Background into pyridinium and imidazolium-based ILs/functionalized carbon nanotubes

The incorporation and/or coating of carbon nanotubes with different salts, nanoparticles, polymers, and ionic liquids produces composites with enhanced physical, chemical and mechanical stability that can be easily processed and hydrophobic [187]. The formation of bulky gels is known as the first discovery of ionic liquids/carbon nanotubes composites [188-196]. However, due to the presence of highly polarizable π electrons in ionic liquids, the interactions between the carbon-based π-systems and ionic liquids are very complex [193]. Espejo *et al*. [197] reported the dispersion of multi-walled carbon nanotubes (MWCNTs) in imidazolium-based ILs to produce stable and homogeneous dispersions with relatively new and unique properties. It was also reported that dispersion of CNTs in ILs produces composites with enhanced surface area [197]. Yang *et al*. [198] reported the functionalization of MWCNTs with 2,2'-(ethylendioxy)-diethylamine, 1,8-diaminoctane, and pristine. They observed that MWCNTs functionalized with 2,2'-(ethylendioxy)-diethylamine were individually integrated into the epoxy

matrix, whereas MWCNTs with 1,8-diaminoctane were poorly dispersed with notable weak interface adhesion. Salam & Burk [199] reported the synthesis and functionalization of multi-walled carbon nanotubes by octadecylamine (ODA) and polyethylene glycol (PEO). Their results revealed that only 16% (wt) of MWCNTs was covered by PEG, while 39% (wt) was covered by ODA. The dispersion of MWCNTs in polymer composites was reported by Pereira *et al*. [200], in their preliminary study of MWCNTs in poly(vinilydene fluoride), MWCNT/PVDF/ZrO_2. Spectra studies of the synthesized nanocomposites confirmed the incorporation of the MWCNTs into poly(vinilydene fluoride) matrix [200].

Ohba and Chaban [201] reported the structure and dynamics of imidazolium-based ILs confined inside carbon nanotubes. França [194] reported that CNTs covalently modified with imidazolium-based ILs are dispersible only in water when they contain Cl^- or Br^- counter ions. Further studies indicate that fluorine-based anions such as BF_4^-, PF_6^-, and Tf_2N^- permit the dispersion of imidazolium-modified CNTs only in organic solvents ($CHCl_3$), forming black homogeneous solutions. In other study, Chaban and Prezhdo [202] suggested that highly viscous liquid composed of asymmetrical cations and small anions can penetrate inside the apolar CNTs at ambient pressure and high temperatures. Recently, Taherkhani and Minofar [203] studied the effect of impurity and radius of CNT on glass transition and electrical conductivity of 1-ethyl-3-

methylimidazolium hexafluorophosphate [EMIM][PF_6] encapsulated in CNT, using molecular dynamic simulations (MDS). Their findings indicate that the electrical conductivity of [EMIM][PF_6]/CNT increases with increasing radius of CNT, whereas the electrical conductivity of [EMIM][PF_6] decreases significantly when encapsulated in zigzag CNT.

Chen *et al*. [204] reported the encapsulation of 1-butyl-3-methylimidazolium hexafluorophosphate in MWCNTs, and they observed that ILs coated in the hollow interior of MWCNTs produces ILs/MWCNT composites with high thermal stability due to the presence of *van der Waals* and hydrogen-bonding interactions. Ohba *et al*. [205] reported that cations adhere weakly to the sidewalls of CNTs, while anions move freely inside the interior of CNTs. Studies on the mechanisms of interactions between carbon nanotubes (CNTs) and ionic liquids suggested that ILs interact with CNTs via π-cation and/or π-π interactions [204, 206-207]. In other studies, weak *van der Waals* or electrostatic forces inferred as basic interactions behind the formation of CNTs-ILs composites [209-211]. For instance, Fileti and Chaban [211] conducted a study where they concluded that fullerene-ionic liquid binding forces were not exclusively of the *van der Waals* interactions. In this chapter, the synthesis, characterization, and physicochemical properties of some hydrophilic and hydrophobic pyridinium and imidazolium–based ionic liquids 3-carbons isomeric alkyl chain lateral are presented.

2.1.3 Materials

All chemicals were purchased from Sigma-Aldrich and BDH chemicals Ltd, and were used as received without further purification unless stated otherwise. Chemicals used to synthesize ionic liquids: 1-methylimidazole (≥99%, purified by redistillation), pyridine (ACS reagent, ≥99.0%), 1-bromopropane (99%), 2-bromopropane (99%), and potassium hexafluorophosphate (≥99%, solid). Chemicals used to synthesize polymeric ionic liquids: 4-vinylpyridine (containing 100 ppm hydroquinone as inhibitor, 95%), bromoethane (98%), potassium persulfate (≤98%), 1-vinylimidazole (≥99%), 4-vinyl benzyl chloride (90%), bis(trifluoromethanesulfonyl)imide lithium salt (99.95% trace metals basis), and *2,2*'-Azobis(2-methypropionitrile) solution (AIBN, 0.2 M in toluene). Solvents and other materials: Dimethyl sulfoxide (ACS, ≥99.9% for analysis), dichloromethane (ACS reagent, ISO, ≥99.9%, GC), *N*, *N*-Dimethyl formamide (DMF, ≥99.8%), diethyl ether (99%), acetone (≥99.8%), acetonitrile (≥99.9%, gradient analysis), methanol (ACS, ISO, reag. Ph Eur for analysis), ethanol (≥99.5%, A.R), graphite powder (<μm, synthetic, Switzerland), sulphuric acid (95-99%, A.R), nitric acid (70%, A.R), sodium nitrate (>98%, ex NO_3), and potassium dichromate ($K_2Cr_2O_7$).

2.1.4 Characterization techniques

Infrared spectroscopic measurements were obtained from Fourier transform Infrared (Perkin-Elmer, Universal ATR sampling Accessory 4000-600 cm^{-1}). ^{1}H, ^{13}C, ^{31}P, and ^{19}F-nuclear magnetic resonance (NMR) spectra were obtained on a Bruker Avance III 400 at frequencies 500 MHz or 400 MHz (^{1}H). The mass spectrometry (MS) was recorded on a Waters Micro-mass LCT Premier spectrometer. Thermal stability of ILs, PILs, MWCNTs, and PILs-functionalized hybrids was determined by Thermogravimetric analyzer (Perkin-Elmer TGA 4000), with sample (10-30 mg) weight placed in a ceramic sample pan and heated above a temperature range of 50-900 °C at a heating rate of 40 °C /min under nitrogen flow. Scanning electron microscopy (SEM) micrographs were obtained using Zeiss Evols 15 Scanning electron microscopy combined with energy dispersive X-ray spectroscopy (EDS). Samples were coated with gold before imagining. Transmission electron microscopy (TEM) images were obtained using JOEL JEM-1400 transmission electron microscopy with Gatal microscopy Suit Software. 827 pH Lab Metrohm (Swiss made) pH meter was used for solution pH measurements. The crystallinity of all carbon containing samples was determined by Philips PW1710 X-ray diffraction spectrometer X-ray diffractometer (XRD) equipped with secondary monochromatized radiation source of Cu-Kα of 1.79290Å. All samples were scanned in the range of 5 to 90° 2θ with a step size of 0.008° and step time of 8.25 Sec at room temperature (25 °C).

2.2 Experimental procedure for the synthesis of ionic liquids

2.2.1 Synthesis of pyridinium-based ILs

2.2.1.1 Synthesis of N-alkylpyridinium bromide

Into a vigorously stirred solution of pyridine (4.21 mL, 52.10 mmol) and (20 mL) toluene at 0 °C, 1-bromopropane (4.09 mL, 45.0 mmol) or 2-bromopropane (4.91 mL, 45.0 mmol) was added slowly in three-neck round bottom flask. The mixture was heated to reflux at 100 °C for 24 h. Toluene was decanted and the remaining brown to gold viscous liquid was re-crystallized in dichloromethane (20 mL x 2). Dichloromethane was evaporated using vacuum rotary evaporator and the product was dried for 10 h to further remove any solvent residue. The product obtained was either *N*-propylpyridinium bromide [*N*-propylPyr]$^{+}$[Br]$^{-}$, or *N*-isopropyl pyridinium bromide [*N*-isopropylPyr]$^{+}$[Br]$^{-}$.

[N-propylPyr]$^{+}$: Anal. Calcd for $C_8H_{12}N^{+}$ (122.19): C, 78.64%; H, 9.90; N, 11.46%. ***[N-isopropylPyr]***$^{+}$: Anal. Calcd for $C_8H_{12}N^{+}$ (122.19): C, 78.64%; H, 9.90; N, 11.46%.

[N-propylPyr]$^{+}$***[Br]***$^{-}$: **^{1}H NMR** (400 MHz, ppm, DMSO-d^6, δ): 9.27 (2H, d, pyr-CHo), 8.19 (2H, t, pyr-CH_m), 8.66 (1H, t, pyr-CH_p), 4.69 (2H, d, CH_2), 1.95 (2H, m, CH_2), 0.83 (3H, t, CH_3). **FT-IR** (υ/cm^{-1}): 3348 (=C-H, w), 2870 (C-H_{sp}^3, s), 1591 (C=C_{pyr}, s), 1417 (C=N_{pyr}, m), 1145 (C-N, m).

[N-isopropylPyr]$^{+}$***[Br]***$^{-}$: **^{1}H NMR** (400 MHz, ppm, DMSO-d^6): 9.21 (2H, d, pyr-CH_o), 8.62 (1H, m, pyr-CH_p), 8.17 (2H, t, pyr-CH_m), 5.08 (1H, m, CH), 1. 62 (6H, d, CH_3x2). **FT-IR** (υ/cm^{-1}): 3374 (=C-H, s), 3150-3109 (C-H_{sp}^2, s), 3091-2978 (C-H_{sp}^3, s), 1635 (C=C_{pyr}, m), 1456 (C=N_{pyr}, m), 1157-1110 (C-N, m).

2.2.1.2 Synthesis of N-alkylpyridinium hexafluorophosphate

Viscous liquid of either [*N*-propylPyr]$^{+}$[Br]$^{-}$ or [*N*-isopropylPyr]$^{+}$[Br]$^{-}$ (1.0 mL), and 2.02 g (11 mmol) of potassium hexafluorophosphate salt were mixed in a 100-mL round-bottomed flask containing water (10 mL) and stirred for 12 h at 50 °C. The resultant product was re-crystallized from dichloromethane (10 mL x 2) and dried with anhydrous magnesium sulphate to remove water residue. The solvent was evaporated by vacuum rotary evaporator at 40 °C. Light brown to gold and white solid products were obtained and further dried for 2 h. It was observed that the obtained products have a tendency to melt and become liquids when stored in an oven, although when stored in a fume hood at room temperature they tend to crystallized immediately.

[N-propylPyr]$^{+}$[PF$_6$]$^{-}$: **^{1}H NMR** (400 MHz, ppm, DMSO-*d*^{6}, *δ*): 9.07 (2H, d, pyr-CHo), 8.62 (1H, t, pyr-CH$_p$), 8.17 (2H, t, pyr-CH$_m$), 4.58 (2H, t, CH$_2$), 1.99 (2H, m, CH$_2$), 0.90 (3H, t, CH$_3$). **^{31}P NMR** (DMSO-*d*^{6}, *δ*): -144.179 ppm (m, PF_6^-, $^{1}J_{p\text{-}f}$ = 709.24 Hz). **^{19}F NMR** (DMSO-*d*^{6}, *δ*): -69.240 to -71.129 ppm (d, PF_6^-). **FT-IR** (υ/cm^{-1}): 3348 (=C-H$_{pyr}$, m), 3104 (C-H$_{sp}^{2}$, s), 2978-2885 (C-H$_{sp}^{3}$, s), 1640 (C=C$_{pyr}$, m), 1566-1409 (C=N$_{pyr}$, s), 1179 (C-N, s).

[N-isopropylPyr]$^{+}$[PF$_6$]$^{-}$: **^{1}H NMR** (400 MHz, ppm, DMSO-*d*^{6}, *δ*): 9.17 (2H, d, pyr-CH$_o$), 8.61 (1H, m, pyr-CH$_p$), 8.17 (2H, t, pyr-CH$_m$), 5.03 (1H, m, CH), 1.62 (6H, d, CH$_3$x2). **^{31}P NMR** (DMSO-*d*^{6}, *δ*): -131.54 ppm (m, PF_6^-, $^{1}J_{p\text{-}f}$ = 713.09 Hz). **^{19}F NMR** (DMSO-*d*^{6}, *δ*): -69.25 ppm (d, PF_6^-). **FT-IR** (υ/cm^{-1}): 3336 (=C-H$_{pyr}$, m), 3150-3109 (C-H$_{sp}^{2}$, m), 2907 (C-H$_{sp}^{3}$, m), 1635 (C=C$_{pyr}$, s), 1486 (C=N$_{pyr}$, s), 1156 (C-N).

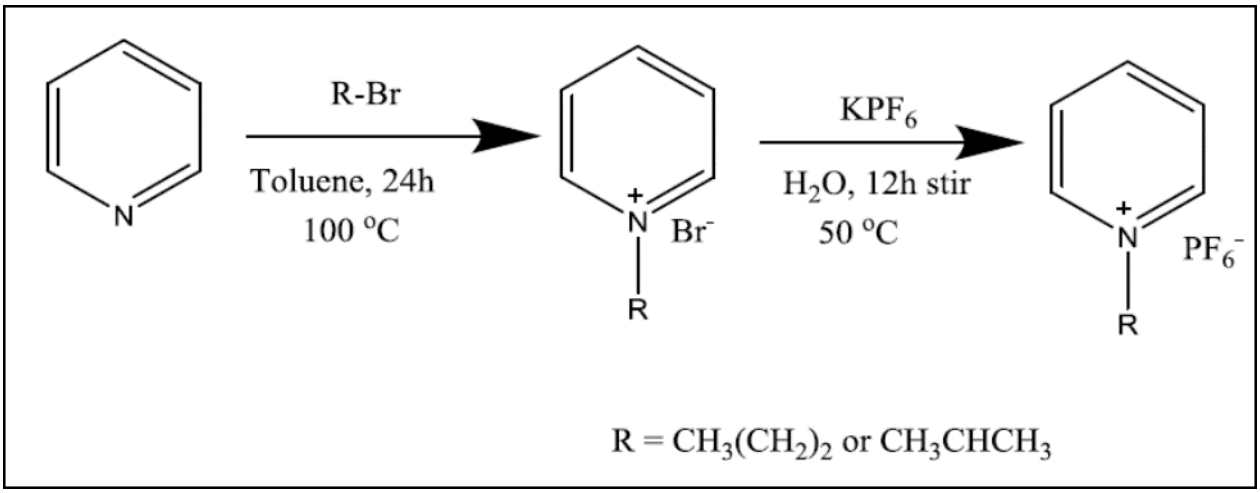

Scheme 2.1 Synthetic route of pyridinium-based ILs

2.2.1 Synthesis of imidazolium-based ILs

2.2.1.1 Synthesis of 3-methyl-1-propylimidazolium bromide [MPIm$^+$][Br$^-$]

Into a two-neck round bottom flask fitted with reflux condenser, 5 mL of 1-methylimidazole, 2 mL of 1-bromopropane and acetonitrile (10 mL) were added. The mixture was heated to reflux for 12 h at 80-100 °C with stirring until the formation of two organic phases. The top layer which contained unreacted materials was discarded, and the colorless viscous lower layer was dissolved in two portions of 20 mL dichloromethane. Thereafter, the solvents were removed under vacuum. Colorless viscous liquid was obtained and dried for 5 h (Scheme 2.2A).

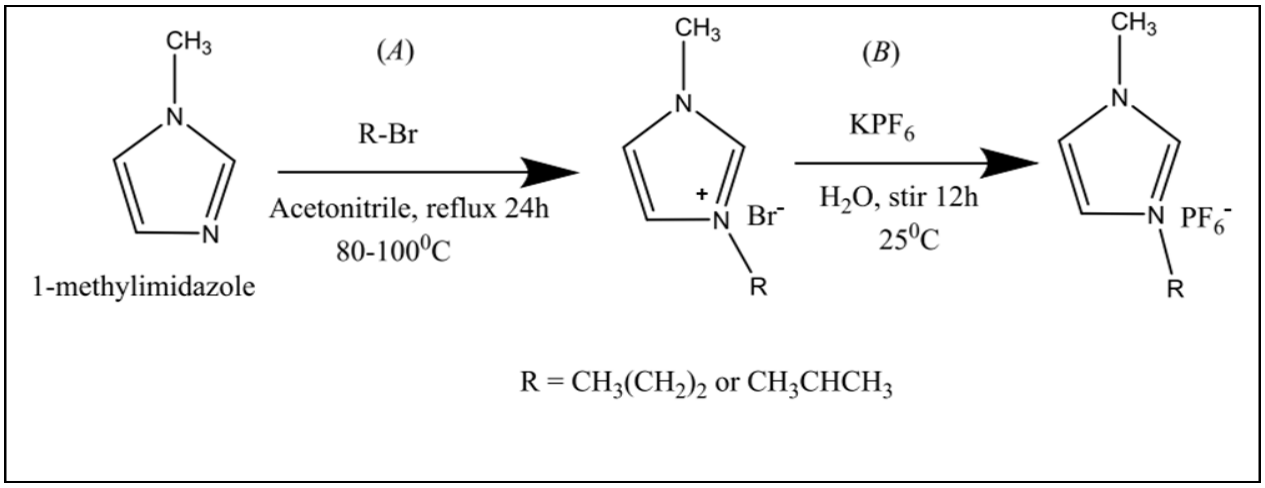

Scheme 2.1 Synthetic route of imidazolium-based ILs

[MPIm$^+$][Br$^-$] **^{1}H NMR (400 MHz, ppm, DMSO-*d*^{6}, *δ*):** 7.185 (1H, s, Im-H*f*), 7.061 (1H, s, Im-H*g*), 4.239 (2H*c*, t, CH_2), 3.963 (3H*d*, s, CH_3), 3.775 (1H, s, Im-H*e*), 1.992 (2H*b*, m, CH_2), 0.999 (3H*a*, t, CH_3). **^{13}C NMR (400 MHz, ppm, D_2O-*d*^{6}, *δ*):** 10.05 (C1), 22.94 (C2), 39.00

(C5), 51.34 (C3), 122.26 (C4), 123.55 (C7), 127.56 (C6). **FT-IR (υ/cm^{-1}):** 3289-3110 (=C-H, & C-H$_{sp}^{2}$, m), 2854 (C-H$_{sp}^{3}$, m), 1648 (C=C, m), 1132 & 989 (C-N, s).

2.2.1.2 Synthesis of 1-isopropyl-3-methylimidazolium bromide [IsopropylMIm^{+}][Br^{-}]

Into a two-neck round bottom flask fitted with reflux condenser, 5 mL of 1-methylimidazole, 2 mL of 2-bromopropane, and acetonitrile (10 mL) were added (Scheme 2.2A). The mixture was refluxed for 12 h at 80-100 °C while stirring until the formation of two organic phases. The top layer which contained unreacted materials was discarded, and the golden viscous lower layer was dissolved in two portions of 20 mL dichloromethane. Thereafter, the solvents were removed by vacuum.

[IsopropylMIm^{+}][Br^{-}] **^{1}H NMR (400 MHz, ppm, DMSO-*d*^{6}, *δ*):** 9.4798 (1H, s, Im-H), 7.9426 (2H, t, 2Im-H), 4.3490 (2H, t, CH_2), 4.0512 (3H, s, CH_3), 1.9333 (2H, m, CH_2), 0.9101 (3H, t, CH_3). **^{13}C NMR (400 MHz, ppm, D_2O-*d*^{6}, *δ*):** 22.06 (C1, 2), 33.32 (C5), 35.92 (C3), 52.98 (C4), 123.46 (C7), 127.55 (C6). **FT-IR** (υ/cm^{-1}): 3391-3150 (=C-H, & C-H$_{sp}^{2}$), 2891 (C-H$_{sp}^{3}$, m), 1561 (C=C, s), 1101-998 (C-N,s).

2.2.1.3 Synthesis of 1-isopropyl-3-methylimidazolium hexafluorophosphate [IsopropylMIm+][PF6-]

3.0 mL of [IsopropylMIm$^+$][Br$^-$] and 3.0 g of potassium hexafluorophosphate were mixed in a 50 mL round bottom flask with 10 mL of distilled water (Scheme 2.2B). The reaction mixture was stirred for 12 h at room temperature. Then the resultant product was rinsed with several portions of water and dissolved in 20 mL dichloromethane and dried in anhydrous magnesium sulphate ($MgSO_4$). The solvent was then removed by vacuum. The resultant golden liquid was dried for 12 h under vacuum.

[IsopropylMIm$^+$][PF$_6^-$] **^{1}H NMR (400 MHz, ppm, DMSO-*d*^{6}, *δ*):** 9.1536 (1H, s, Im-H), 7.8594 (1H, t, Im-H), 7.7003 (1H, t, Im-H), 4.6473 (1H, m, CH), 3.8344 (3H, s, CH_3), 1.4761 (6H, d, CH_3X2). **^{13}C NMR (400 MHz, ppm, DMSO-*d*^{6}, *δ*):** 22.79 (C1, 2), 36.19 (C5), 40.04 (C3), 52.62 (C4), 120.92 (C7), 124.15 (C6). **^{31}P NMR** (DMSO-*d*^{6}, *δ*): -130.94 ppm (m, PF_6^-, $^1J_{p\text{-}f}$ = 715.09 Hz). **^{19}F NMR** (DMSO-*d*^{6}, *δ*): -69.35 ppm (d, PF_6^-). **FT-IR (υ/cm^{-1}):** 3361 (=C-H, m), 3091 (C-H_{sp}^2, s), 2872 (C-H_{sp}^3, m), 1591 (C=C, m), 1150-1110 (C-N, s).

2.2.2 Synthesis of CNTs and MWCNTs

2.2.2.1 Synthesis of carbon nanotubes (CNTs)

Carbon nanotubes were synthesized using a chemical method according to Leo and Seo [212]. Briefly, a solution of graphite powder (5 g) in water (5 mL) and solution of nitric acid (25

mL)/sulphuric acid (50 mL) were prepared separately at low temperature (ice-bath) under constant stirring. The two solutions were mixed followed by the addition of sodium nitrate (25 g) at 0 °C. The mixture was stirred for 36 h at ambient temperature, and further refluxed for 12 h at 90 °C. Thereafter, the mixture was centrifuged, neutralized with sodium hydroxide solution, and filtered to obtain the CNTs.

2.2.2.2 Synthesis of MWCNTs

MWCNTs were synthesized from as-synthesized CNTs, wherein 0.317 g of CNTs was ultrasonicated for 5 minutes in a mixture of concentrated sulphuric acid 15 mL (H_2SO_4, 65%)/5 mL nitric acid (HNO_3, 98%), 3:1 by volume. The solution was refluxed for 5h at 60 °C, and then washed with distilled water to neutralize acid residue, dried in air vacuum at 70 °C to obtain the MWCNTs.

2.2.3 Synthesis of IL/MWCNTs composites

ILs/MWCNT composites were synthesized according to the reported methods with minor modifications [171, 179, 188]. Briefly, a solution of 5 mg of MWCNTs and 10 mg of each ILs in 10 mL of *N*, *N*-dimethylformamide (DMF) was ultrasonicated for 20 minutes. The mixture was

then vigorously stirred for 24 h at 50 °C. The unreacted MWCNTs residues were removed by centrifugation. Thereafter, ILs/MWCNT composites were filtered, thoroughly washed with DMF, ethanol, and water, respectively.

2.3 Results and Discussion

2.3.1 Nuclear magnetic resonance (NMR) spectroscopic studies

2.3.1.1 NMR analyses of pyridinium-based ILs

Pyridinium-based ionic liquids were synthesized as shown in Scheme 2.1. The synthesized ionic liquids comprise of pyridinium cation and a counter anion (halide or hexafluorophosphate). These ionic liquids were synthesized via two-step metathesis method that involves the quaternization of pyridine with three-carbon alkyl bromide (propyl and isopropyl bromides) followed by ion exchange with potassium hexafluorophosphate (KPF6). ^{1}H, ^{13}C, ^{31}P and ^{19}F-NMR spectroscopy were used to characterize the as-synthesized pyridinium and imidazolium-based ionic liquids. The ^{1}H-NMR spectrum of [*N*-propylPyr]$^{+}$[Br]$^{-}$ showed signals at 9.27, 8.19, and 8.66 ppm due to the protons resonance at *ortho*-, *meta*-, and *para*-positions of pyridinium ring (APX 2-1). Protons signals at 4.94-4.66 and 1.95 ppm were assigned to the two -CH_2 groups of the propyl lateral chain, while the protons signals at 0.83-0.78 ppm were assigned to the methyl (-CH_3) group of the propyl functionality. Relatively similar but less deshielded ^{1}H-

NMR signals were obtained for [*N*-propylPyr]$^{+}$[PF_6]$^{-}$. For isopropyl-featuring ionic liquids, [*N*-isopropylPyr]$^{+}$[Br]$^{-}$, ^{1}H-NMR signals responsible for proton resonances at *ortho*-, *para*-, and *meta*-positions were observed at 9.22-9.21, 8.62-8.58, and 8.17-8.13 ppm, respectively (APX 2-2). The multiplet at 5.08-5.04 ppm was assigned to the single-proton of the isopropyl carbon close to pyridinium-nitrogen atom. The doublet at 1.62-1.59 ppm was due to the six-protons of the two methyl groups (CH_3x2) of isopropyl. The hydrophobic moiety, [*N*-isopropylPyr]$^{+}$[PF_6]$^{-}$, shows similar but comparable less deshielded proton signals. The presence of bromide ion in hydrophilic ionic liquids have resulted in some proton resonances being deshielded. The electron density of substituents in a compound usually affects signal position in the ^{1}H-NMR [220]. However, due to high electronegative behavior of the halogen, protons close or associated with halides are normally deshielded and appear at downfield.

The hydrophobic [*N*-propylPyr]$^{+}$[PF_6]$^{-}$ and [*N*-isopropylPyr]$^{+}$[PF_6]$^{-}$ ionic liquids were further studied using ^{31}P and ^{19}F NMR spectroscopy (APX 2-3 and APX 2-4), respectively. For [*N*-propylPyr]$^{+}$[PF_6]$^{-}$, ^{31}P was found to have a multiplet (m) around -144.179 ppm, which confirmed the presence of phosphorous atom coupled with six fluorine atoms. ^{19}F was found to have a doublet (d) around -169.25 to -71.13 ppm, confirming the coupling of six fluorine atoms with one phosphorous atom. The coupling distances between the peaks in both ^{31}P and ^{19}F NMR

spectra were found to be approximately the same and constituted the coupling constant of ${}^{1}J_{p\text{-}f}$ = 709.24 Hz. For [*N*-isopropylPyr]$^{+}$[PF_6]$^{-}$, ^{31}P was found to have multiplet peaks around -131.54 ppm, while ^{19}F was found to have doublet around -69.25 to -71.13 ppm and with coupling constant of ${}^{1}J_{p\text{-}f}$ = 713.09 Hz. Both ^{31}P and ^{19}F NMR confirmed the presence of fluorine and phosphorous atoms coupled together in the form of PF_6^- in the as-synthesized ionic liquids. The close range of the obtained coupling constants for both hydrophobic ionic liquids is the clearest indication of the presence of counter anion.

2.3.1.2 NMR analyses of imidazolium-based ILs

The ^{1}H-NMR spectra of imidazolium-based ionic liquids showed large frequency downshift and overlapping of three protons chemical shifts around the imidazole ring (APX 2-6 to APX 2-10). The protons at positions 4 and 5 were found to resonate or deshielded (downfield signal) around low field due to the presence of bromide ion in halide-containing ILs. However, after anion-exchange, the protons at positions 4 and 5 show less deshielding due to the absence of the bromide ion. The ^{13}C-NMR spectra of the ILs obtained showed direct information about the carbon skeleton and the number of equivalents/non-equivalents carbons in the ILs. The electronegative atoms and π-bonds tend to cause downfield chemical shifts. For example, C4, C6, and C7 of the imidazolium rings are deshielded (shifted downfield) due to the presence of

the π-electron systems in the imidazolium ring and the influence of the attached electronegative bromide counter-ion. As it was expected, C1 and C2 in all isopropyl-containing ILs are chemically equivalent and are assigned to one signal. However, the appearance of the peak at 40.041 ppm corresponds to the overlap of the C3 carbon of the isopropyl group and the DMSO solvent. ^{19}F NMR spectra were found to contain doublets (d) between -69 to -71.0 ppm that confirmed the coupling of six fluorine atoms with one phosphorous atom. On the other hand, the ^{31}P NMR spectra of both hydrophobic ILs were found to have multiplet (m) between -130 to -159 ppm confirming the presence of the phosphorous atom coupled with six fluorine atoms. In addition to the ^{1}H, ^{13}C, ^{19}F, and ^{31}P-NMR studies, single mass analysis data of the synthesized ILs compounds based on C, H, and N confirmed the accurate mass values (125.1075, 122.0966, and 122.0973 m/z for methyl-propyl imidazolium, isopropyl-methyl imidazolium, isopropyl pyridinium and propyl pyridinium, respectively). The results agree with the calculated masses based on their respective molecular formulas (APX 2-12 to 2-15).

2.3.2 Fourier Transform Infrared (FTIR) spectroscopy of ILs

2.3.2.1 FTIR spectra of pyridinium-based ILs

The FTIR spectrum of pyridinium-based ionic liquids, [*N*-propylPyr]$^{+}$[Br]$^{-}$ shows the presence of a weak vibrational band around 3348 cm^{-1} attributed to =C-H stretch in *ortho*, *meta*, and *para*

positions on the pyridinium ring (APX 2-16). Strong vibrational bands at 2870 and 1579 cm^{-1} can be assigned to the C-H_{sp}^3 of propyl group, and C=C of pyridine, respectively. Medium absorption bands at 1417 and 1145 cm^{-1} are assigned to the C=N of pyridinium cation and C-N bonding between the nitrogen atom of pyridinium and first carbon of propyl, respectively. In the FTIR spectrum of [*N*-isopropylPyr]$^+$[Br]$^-$, similar vibrational bands to that of [N-propylPyr]$^+$[Br]$^-$ were observed. For ionic liquids containing PF_6^-, vibrational bands were found to be similar to those obtained for ionic liquids containing bromide [204-205]. These results confirmed that ion-exchange was carried out successfully and the cationic components of the ionic liquids remained unaltered.

2.3.2.2 FTIR Spectra of imidazolium-based ILs

The FTIR spectrum of [MPIm$^+$][Br$^-$] shows well pronounced absorption bands in the range 3390-3150 cm^{-1} assigned to the =C-H stretch and C-H_{sp}^2 stretching vibrations. The shifts in the absorption bands could be attributed to the presence of halide counter ions and the bromide-hydrogen interionic bonding. The absorption bands at 2891 and 1561 cm^{-1} are assigned to the C-H_{sp}^3 stretching vibrations of propyl and C=C of the imidazolium ring, respectively. The strong vibrational bands in the range 1101-998 cm^{-1} are due to the presence of the C-N functional group between the imidazolium ring and alkyl groups. The FTIR spectrum of hexafluorophosphate-

containing ILs, [*N*-isopropylMIm$^+$][PF_6^-], showed similar vibrational bands compared to that of [MPIm$^+$][Br^-] but shifted slightly due to the absence of the halide. The stretching vibrations of C-H_{sp}^3 of propyl and isopropyl were observed in relatively similar region [179].

2.3.3 Thermogravimetric analyses (TGA) of ILs

2.3.3.1 TGA analyses of pyridinium-based ILs

Thermogravimetric analysis was used to obtain information about the thermal stability of the synthesized ILs. Pyridinium-based ionic liquids with halide counter anion, [*N*-propylPyr]$^+$[Br^-] and [*N*-isopropylPyr]$^+$[Br^-] displayed minor weight losses less than 5% within 100 °C, which were due to the loss of moisture from the ILs indicating that they were slightly hygroscopic (Fig. 2.1). Considerable weight loss between 18-35% was observed at temperatures above 290 °C for both pyridinium ionic liquids with halide due to the decomposition of the ionic liquid salts. [*N*-propylPyr]$^+$[Br^-] and [*N*-isopropylPyr]$^+$[Br^-] were seen to be thermally stable below 400 °C and their total decompositions were recorded at 356 °C and 342 °C, respectively, showing unimodal decomposition character.

The compounds, [*N*-propylPyr]$^+$[PF_6]$^-$ and [*N*-isopropylPyr]$^+$[PF_6]$^-$, which are the hydrophobic pyridinium-based ILs with PF_6^- counter anion were observed to be thermally stable up to 400 °C. No moisture weight loss was observed for both hydrophobic ionic liquids. Significant

decomposition between 400-550 °C was observed for both hydrophobic ionic liquids. Interestingly, hydrophobic ionic liquids showed multimodal decomposition characteristics, due to the degradation of pyridinium-organic material followed by the inorganic counterion. Carbon loss for both [*N*-propylPyr]$^{+}$[PF_6]$^{-}$ and [*N*-isopropylPyr]$^{+}$[PF_6]$^{-}$ were also observed at 721°C and 552 °C, respectively.

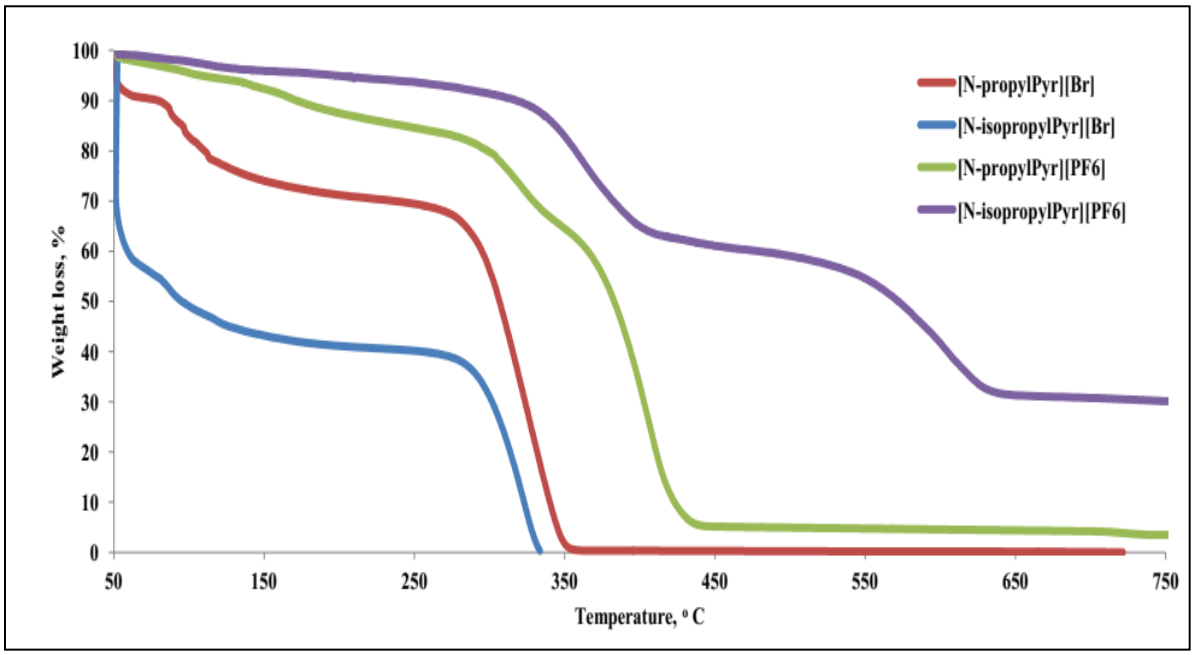

Figure 2.1 TGA profiles of pyridinium-based ILs

It can therefore be concluded that ionic liquids with hydrophobic counter anion such as PF_6^{-} are more thermally stable than those with halide counter anion (hydrophilic). Papaiconomou *et al.* [184] in their study discovered that thermal stability of ionic liquids is related to the nature of the

counteranion involved. For the ionic liquids investigated in this study, it was evident that ILs with pyridinium cation containing isopropyl group on the N-position of pyridinium were more thermally stable than those with propyl counterpart in the following order: [*N*-IsopropylPyr]$^{+}$[Br]$^{-}$> [*N*-propylPyr]$^{+}$[Br]$^{-}$, while [*N*-isopropylPyr]$^{+}$[PF_6]$^{-}$> [*N*-propylPyr]$^{+}$[PF_6]$^{-}$. Thus, the thermal stabilities of ionic liquids in this study are dependent on the counter anions involved and the isomeric alkyl groups on the N-position of pyridinium in the following order: [*N*-isopropylPyr][PF_6]> [*N*-propylPyr][PF_6]> [*N*-IsopropylPyr][Br]> [*N*-propylPyr][Br].

2.3.3.2 TGA analyses of imidazolium-based ILs

Thermogravimetric analyses of the imidazolium-based ILs (Fig.2.2) exhibit weight loss at different temperatures. For instance, [MPIm^{+}][Br^{-}] showed a weight loss of T_d, <30% with onset of decomposition at 250 °C and complete second decomposition around 400 °C. The imidazolium-based ILs with hexafluorophosphate anion, [isopropylMIm^{+}][PF_6^{-}] shows a considerable thermal stability with weight degradation recorded to be less than 15% at 400 °C. However, at 450 °C, a complete decomposition of [isopropylMIm^{+}][PF_6^{-}] ILs was observed.

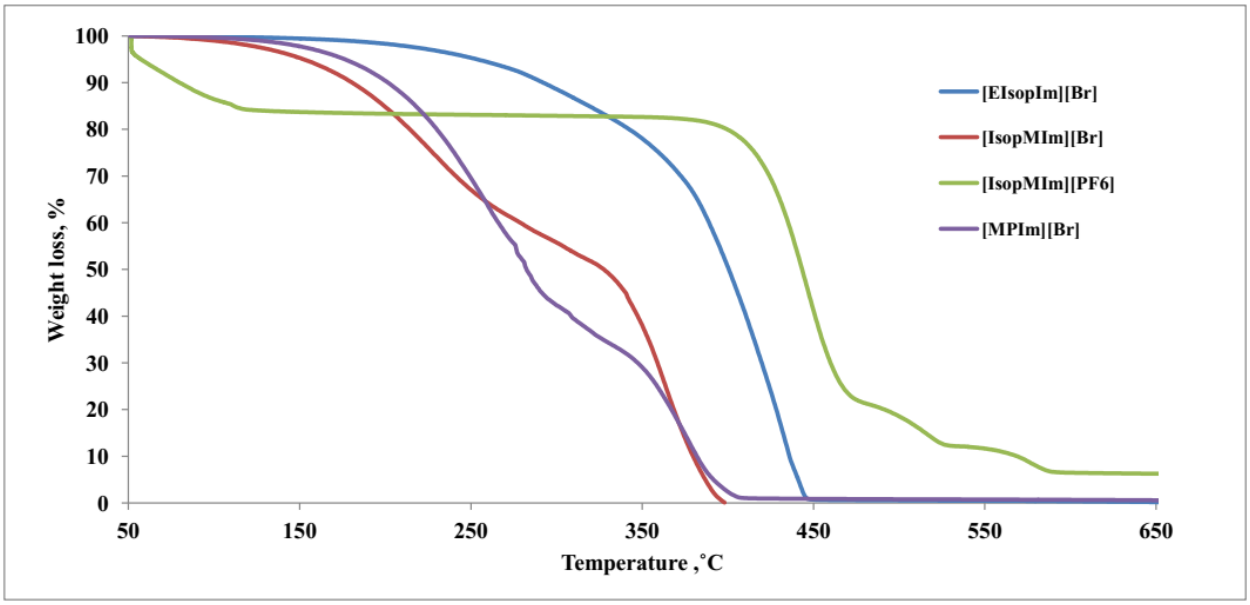

Figure 2.2 TGA profiles of imidazolium-based ionic liquids.

2.3.4 Glass transition temperatures and melting points of pyridinium and imidazolium-ILs

Melting and glass transition temperatures of ILs were obtained using differential scanning calorimetry (DSC). Table 2.1 shows the melting point ($T_{m)}$, glass transition (T_g), and decomposition (T_d) temperatures in degrees Celsius (°C) at given temperatures. As presented in Table 2.1, the glass transition T_g of [*N*-propylPyr]Br] was found to be 28 °C and that of [*N*-isopropylPyr][Br] to be 25 °C, which are the inflation point (endothermic direction) between the first peak onset temperature and offset temperature, respectively. Glass transitions of hydrophobic [*N*-propylPyr][PF_6] and [*N*-isopropylPyr][PF_6] ILs were observed to be slightly smaller in comparison to other corresponding pyridinium-ionic liquids containing halide ions.

Eftakhari and Saito [191] once concluded that larger counter anions lower the T_g due to their bulkiness and distributed charges. As presented in Table 2.1, pyridinium ionic liquids with hexafluorophosphate counter anion exhibit high melting temperature than their halide counterparts in this study. These results are in agreement with the results obtained from the thermogravimetric analyses, which indicates that pyridinium ILs with hydrophobic counter anion are more thermally stable than those with halide counter anion.

Table 2.1 Melting (Tm), glass transition (Tg) and decomposition (Td) temperatures (°C)

Ionic liquids	T_g	T_m	T_d
[*N*-propylPyr][Br]	28	67	291
[*N*-IsopropylPyr][Br]	25	59	293
[*N*-propylPyr][PF_6]	26	92	289
[*N*-isopropylPyr][PF_6]	24	89	543
[MPIm][Br]	26	42	180
[EIsopropylIm][Br]	28	37	215
[IsopropylMIm][Br]	27	52	204
[IsopropylMIm][PF_6]	25	68	399

2.3.5 Solubility studies of ILs

2.3.5.1 Solubility of pyridinium-based ILs

The solubility of the as-synthesized pyridinium-based ILs was determined by dissolving equal amount of ILs in different aqueous and organic solvents. Owing to the type of counter anion,

and/or isomeric carbon lateral chain involved, these ILs showed varied solubility in different solvents. It has been established that a solvent or solute will only dissolve or be dissolved in a substance of similar polarity, respectively ("like dissolves likes"). However, [*N*-propylPyr]$^{+}$[Br]$^{-}$ was soluble in polar protic and non-polar solvents, and slightly insoluble in polar aprotic solvents. This behaviour can be correctly linked to the formation of hydrogen bonding (intermolecular forces) between the polar protic or non-polar solvents and ILs. On the other hand, [*N*-IsopropylPyr]$^{+}$[Br]$^{-}$ behaved differently and showed significant miscibility only in non-polar solvents. The hydrophilic character and the formation of hydrogen bonding are responsible for this latter ILs behaviour in aqueous and organic medium. One thing worthy to be mentioned which comparatively affected the solubility of ILs is the alkyl lateral chains. It is evident that pyridinium-ILs with straight-lateral alkyl chain (propyl) attached to pyridinium-nitrogen atom are more soluble in aqueous and organic medium than their corresponding isomeric counterparts. Hydrophobic [*N*-propylPyr]$^{+}$[PF_6]$^{-}$ and [*N*-isopropylPyr]$^{+}$[PF_6]$^{-}$ ionic liquids were observed to be insoluble in all polar protic and non-polar solvents, yet soluble in DMSO. The hydrophobicity of these ILs and large dielectric constant of DMSO played significantly role in the insolubility of the ILs in other solvents except DMSO.

Table 2.2 Solubility test of pyridinium-based ILs in different solvents

Ionic liquids	Polar protic		Non-polar		Polar aprotic	
	H_2O	**MeOH**	**HEX**	**$CHCl_3$**	**DMSO**	**DMF**
[*N*-propylPyr][Br]	S	S	S	N.S	N.S	N.S
[*N*-IsopropylPyr][Br]	P.S	P.S	N.S	N.S	S	S
[*N*-propylPyr][PF_6]	Suspended	N.S	N.S	N.S	P.S	P.S
[*N*-IsopropylPyr][PF_6]	N.S	N.S	N.S	N.S	S	S

:Soluble (S), Non-soluble (N.S) or Partial soluble (P.S) in polar protic, non-polar or polar aprotic solvents.

2.4 Characterization of MWCNTs and IL/MWCNT composites

2.4.1 Spectroscopic studies of MWCNTs and IL/MWCNT composites

The FTIR spectrum of MWCNTs shows stretching vibrational band at 1734 cm^{-1} corresponding to the carboxylic and graphite groups on the surface of pure nanotubes. A weak OH^- stretching vibration around 3598 cm^{-1} is assigned to the moisture content absorbed by the carbon materials and was also confirmed by the thermogravimetric analysis [205, 213]. Other important vibrational bands found at 2323 and 1239 cm^{-1} are attributed to CO_2, and C-O, respectively. After functionalization with ILs, the skeletal vibrational bands of graphitic and carboxylic groups at 1734 cm^{-1} corresponding to C=O disappeared in ILs/MWCNT composites spectra. The shift of the weak OH stretching vibration from 3619 cm^{-1} to 3789 cm^{-1} in the ILs/MWCNT composites with bromide ions indicates successful modification. The sharp peak at 3170 cm^{-1} is ascribed to

the stretching vibration of C-H_{sp}^2 of the ILs heterocyclic rings in the ILs/MWCNTs composites. The introduction of ionic liquids on the surface of carbon nanotubes does change the functional groups or morphology of the nanotubes. It can also be stated that the disappearance or less intense stretching vibrational bands of pure ILs signify the total incorporation of ILs with carbon nanotubes and the formation of new functional composites with completely different properties. The vibrational bands around 798 and 788 cm^{-1} are ascribed to P-F bond stretching in hydrophobic ILs. The results obtained from the FTIR spectra studies indicate that the interactions between the ILs with MWCNTs occur via non-covalent interactions after functionalization.

2.4.2 TGA analyses of MWCNTs and ILs/MWCNTs composites

Pure MWCNTs TGA thermograms showed multi-step degradations, even though the weight loss is insignificant (onset of decomposition at T_d, 5% around 250 °C, and final decomposition at T_d, 10% around 750 °C). The TGA results obtained for the MWCNTs are in agreement with the findings from other studies [193]. Comparison of the TGA curves of pure ILs, MWCNTs, and their ILs-functionalized composites clearly shows that ILs/MWCNT composites are more thermally stable with two major weight losses. The first small weight loss could be attributed to the degradation of ILs on the surface of nanotubes and the second decomposition corresponds to CNTs fragments. It can thus be concluded that composites of ILs/MWCNT are effectively thermally stable in comparison to pure ILs and/or pristine MWCNTs [204]. The degree of

thermal stability of ILs/MWCNT hybrids can be associated with non-covalent (ionic-interactions or exchange), and strong *van der Waals* interactions between the ILs and MWCNTs. Another potential contributing factor to the stability of ILs/MWCNT hybrids could be differences in polarity of both the dispersing molecule (ILs) and the solute (MWCNTs). However, other studies suggested that the thermal stability of CNT-ILs depends on the type of the ILs counter-ions [199].

2.4.3 Solubility study of MWCNTs and ILs/MWCNTs composites

Solubility studies of the MWCNTs and ILs/MWCNT were carried out in nine solvents (polar to non-polar) namely: water (H_2O), ethanol (EtOH), acetonitrile (ACN), dimethyl sulfoxide (DMSO), acetone (Ace), tetrahydrofuran (THF), diethyl ether (DEE), toluene (TOL), and hexane (HEX). The results shows that some MWCNTs and/or ILs/MWCNT composites were not soluble (N.S), whilst some were partially soluble (P.S), and others were completely soluble (S) in different solvents depending on their polarities. Pure MWCNTs were completely insoluble in polar solvents such as water and ethanol, yet suspendable in other polar solvents (acetonitrile, dimethyl sulfoxide, acetone, and tetrahydrofuran). On the other hand, MWCNTs were insoluble in non-polar solvents (diethyl ether, toluene, and hexane). The solubility characteristics of MWCNTs can be attributed to its hydrophobicity character (non-polar substance). Another

important observation is the relative insolubility of MWCNTs in more non-polar solvents such as toluene and hexane. This indicates that differences in polarity between MWCNTs and other non-polar solvents played an essential role.

Furthermore, the solubility study of ILs/MWCNT composites was also conducted in different solvents. The solubility of [*N*-isopropylPyr$^+$][PF_6^-]/MWCNT showed that the composite is insoluble in all solvents. On the other hand, the composite of MWCNTs with hydrophilic pyridinium-based ILs such as [*N*-propylPyr$^+$][Br^-]/MWCNT shows different solubility behavior. [*N*-propylPyr$^+$][Br^-]/MWCNT showed wide-ranging solubility profiles from insoluble to slightly soluble in polar solvents with varied polarity index, while showing better solubility in most non-polar solvents. This suggests that non-polar and hydrophobicity character of the solute was maintained after functionalization. Solubility studies of the MWCNT composites with imidazolium-based ILs indicates that the solute was insoluble in water (a strong polar solvent), but soluble in ethanol (another strong polar solvent). Secondly, the same composite was soluble or partially suspended in non-polar solvents except hexane.

However, the poor solubility of this composite in water and hexane brings the discussion of polarity level between the composite and the solvent. In this instance, strong polar solvent (water) molecules cannot be detached by relatively non-polar substance, and also strong non-

polar solvent (hexane) cannot detach MWCNT (non-polar) molecules. This observation is in agreement with the study of Salam and Burk [199]. On the other hand, [isopropylPyr^{+}][PF_6^{-}]/ MWCNT composite was soluble in hexane and not in water. This latter behavior confirmed the hydrophobicity of the synthesized material. Based on the solubility study conducted, it can be concluded that when the polarity of both the solvent and the compound are similar, then the solute and the solvent definitely separate (detach) each other leading to increase in solubility.

2.4.4 Surface morphologies of MWCNTs and ILs/functionalized composites

The surface morphology of MWCNTs and the ILs/functionalized composites (Fig. 2.3) showed highly twisted or tangled tubes of MWCNTs. Carbon nanotubes showed clustered or fused morphologies with limited surface area. However, ILs/functionalized MWCNT composites show different morphological orientations, well dispersed with uniformly structured and increased surface area. Some areas of the MWCNTs are restacked together inside ionic liquids producing flake-layers orientations [213]. It is also worth noting that the morphology of the MWCNTs is unaltered but shows improved dispersion (Fig. 2.4). Energy-dispersive X-ray spectroscopy (EDS) results confirmed the presence of (C, O, and S) in MWCNTs and ILs/MWCNT (C, O, N, Br, F, and P) composites (Figs. 2.3 C-D and 2.5). The intensity of the carbon peak (Fig. 2.4C-D) confirmed the presence of carbon material in the sample produced [205]. The presence of

bromide (Br), phosphorous (P) and fluorine (F) (Fig. 2.5 A-D) confirms the successfully dispersion of MWCNTs in hydrophilic and hydrophobic ILs [204].

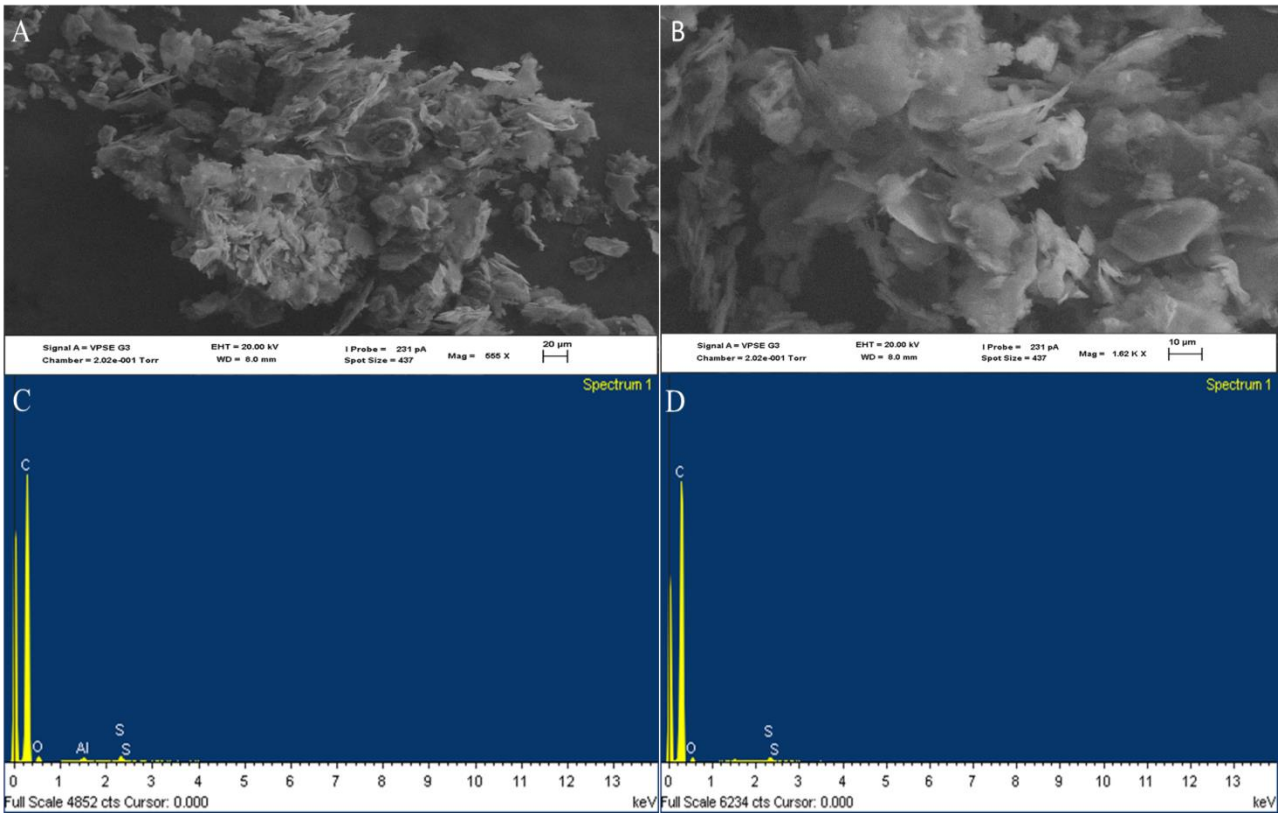

Figure 2.3 SEM (A &B) images and EDS (C &D) spectra of MWCNTS.

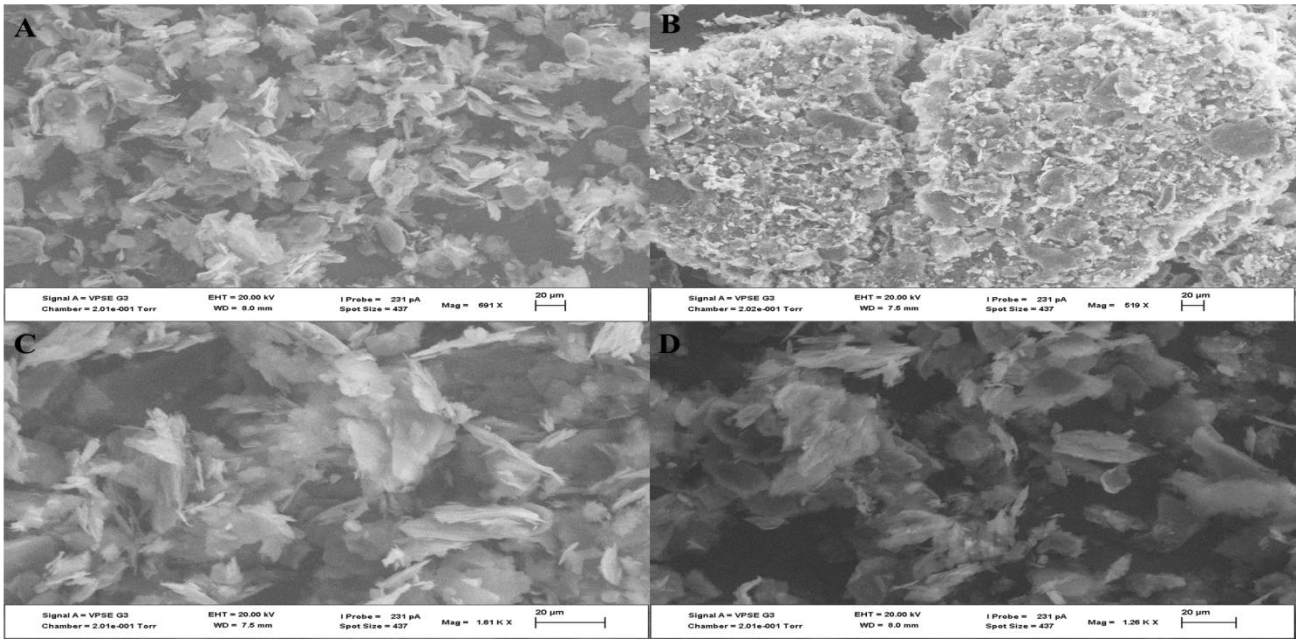

Figure 2.4 SEM images of some ILs/MWCNT composites. [N-propylPyrBr]/MWCNT (A), [N-IsopropylPyrPF6]/MWCNT (B), [MPIm-Br]/MWCNT (C), and [IsopMIm-PF6]/MWCNT (D).

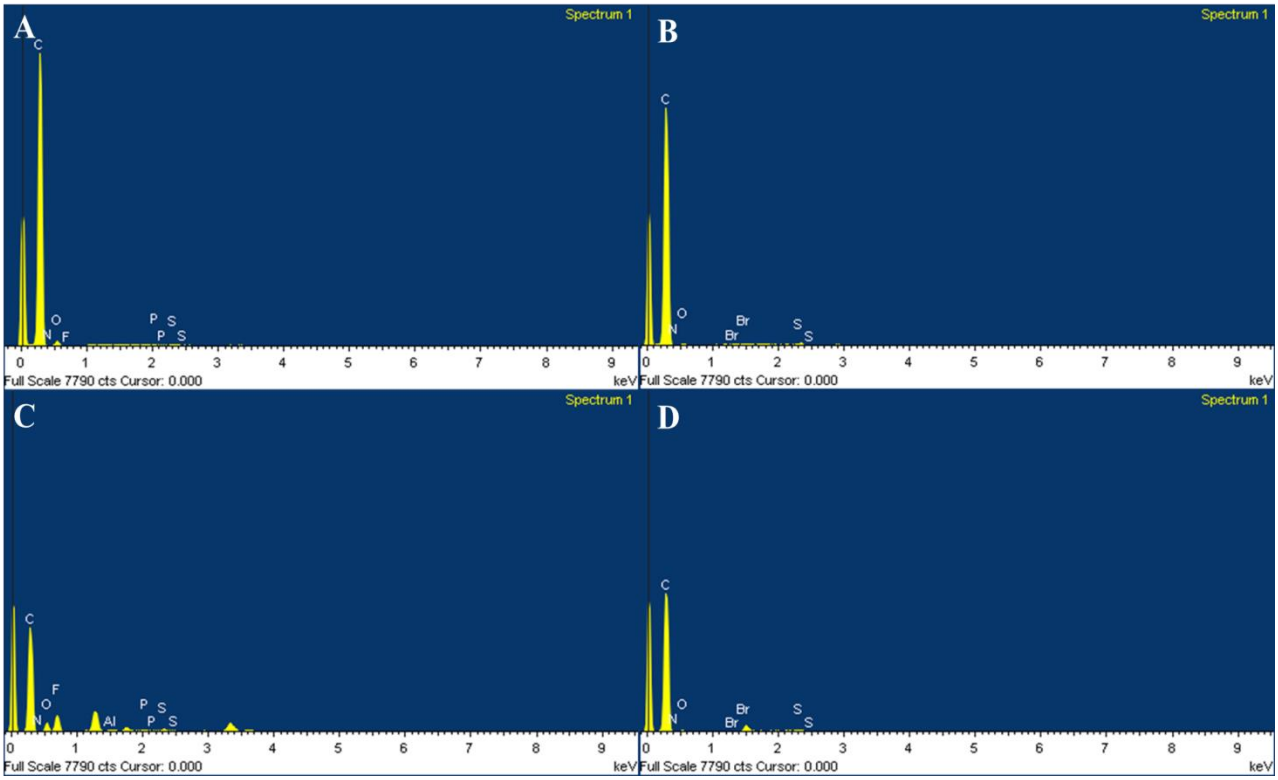

Figure 2.5 EDS mappings of ILs/MWCNT composites. [IsopMIm-PF6]/MWCNT (A), [MPIm-Br]/MWCNT (B), [N-IsopPyrPF6]/MWCNT (C), and [N-propylPyrBr]/MWCNT (D).

2.4.5 Powder X-ray Diffraction studies of MWCNTs and ILs/MWCNTs

The changes in the crystalline structure of the pristine MWCNTs upon functionalization with ionic liquids were carefully investigated with the aid of microscopic and spectroscopic techniques. However, the crystallinity phase and identification of MWCNTs and ILs/MWCNT samples were studied by powder X-ray diffraction (XRD). Fig. 2.6 showed the XRD patterns of pristine MWCNTs and some of the pyridinium and imidazolium-based ILs/MWCNTs composites. Generally, it can be observed that pristine MWCNTs exhibited two prominent peaks: One around 31.05° (002 in plane) confirming the highly graphitic structure of carbon nanotubes and the other broad and weak peak around 64.62° (100 in plane), corresponding to the interplanar *d*-spacing of 3.34408Å and 1.67610Å, respectively. The crystalline size of MWCNTs was found to be 12.537 nm, calculated from the Scherer equation (equation 2.1) [199], with the full width of diffraction peak at half maximum (FWHM) intensities, β=0.1338 and 0.960, respectively.

$$D = \frac{k\lambda}{\beta Cos\theta} \qquad \text{Equation 2.1 [199]}$$

Where *k* is a constant ~0.9, λ is wavelength of X-ray (1.79290Å), β is a full width of diffraction peak at half maximum (FWHM) intensity, and θ is the Bragg angle (n°/2).

In this study, the XRD patterns of all ILs/MWCNTs composites (Fig. 2.6) showed diffraction peaks with varied intensities around 2θ values 30.9079-30.9148° (002 in plane) ascribed to the graphitic structure from MWCNTs, and a broad and weak characteristic peak around 64.8765° (100 in plane) ascribed to the semi-crystalline structure of the ILs derivatives, with interplanar *d*-spacing of 3.35938, 3.35864, 3.36977, and 3.35622Å, respectively. However, the new diffraction peaks can be attributed to the formation of new crystalline functionalities between ILs and carbon materials after functionalization. The crystalline size of most ILs/MWCNTs studied was found to range between 6.7049-9.66 nm, suggesting a decrease in MWCNTs size due to encapsulation with ILs. Moreover, the XRD studies confirmed that the side-wall functionalization (non-covalent) of MWCNTs with ILs did not alter the crystallographic character of the MWCNTs [199].

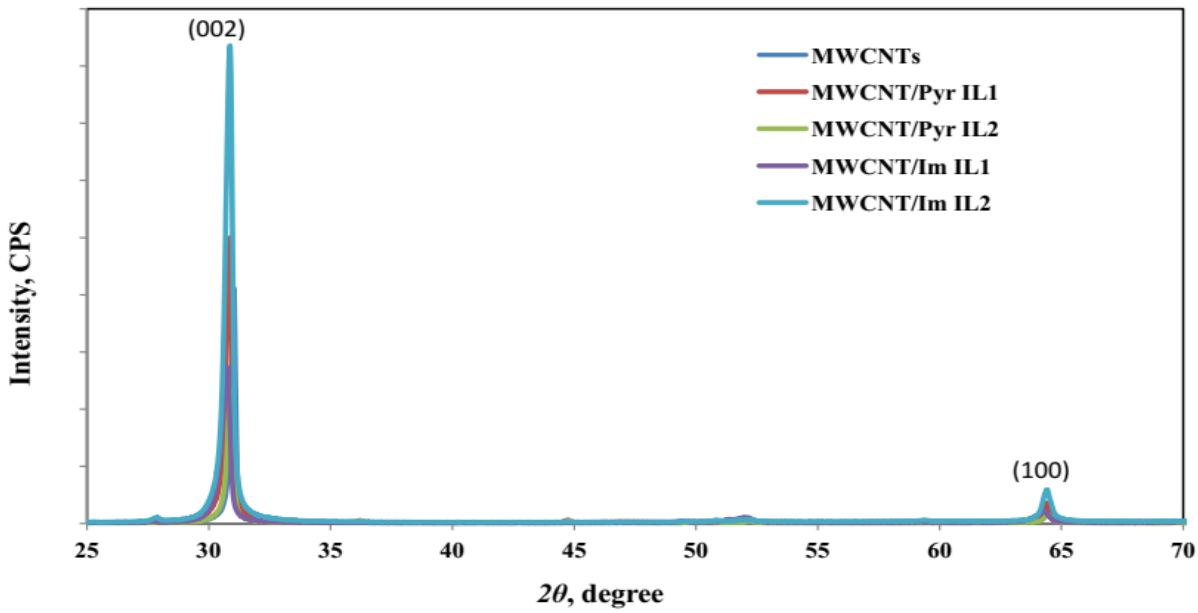

Figure 2.6 XRD patterns of pristine MWCNTs and some pyridinium and imidazolium-based IL/MWCNTs composites.

2.5 Chapter summary

In this chapter, imidazolium and pyridinium-based ionic liquids (ILs) were successfully synthesized and characterized by FTIR, ^{1}H, ^{19}F, and ^{31}P-NMR spectroscopy, and mass spectrometry. The effects of the alkyl lateral chain (propyl and isopropyl) at the first and third positions of imidazolium and N-position of pyridinium cations on the thermal stability, conductivity, and solubility of ionic liquids were investigated. The results obtained confirmed that the ionic liquids based on pyridinium cations exhibit higher decomposition temperature, low melting points, and poor water solubility. Furthermore, multi-walled carbon nanotubes

(MWCNTs) were synthesized by simple chemical method, and dispersed using imidazolium and pyridinium-based ionic liquids (ILs).

The structures of the as-synthesized ILs/MWCNT composites were studied using FTIR spectroscopy, scanning electron microscopy (SEM), energy dispersive X-ray spectroscopy (EDS), thermogravimetric analysis (TGA) and solubility in different polar and non-polar solvents. Spectroscopic analyses confirmed graphitic and carboxylic groups in the pure MWCNTs and the formation of the ILs/MWCNT composites with new functionalities. On the other hand, SEM and TEM of MWCNTs showed entangled bundles, while ILs/MWCNTs showed debundled composites with increased diameter and unaltered MWCNTs morphology. TGA showed that the MWCNTs are thermally stable, owing to the *van der Waals* and non-covalent interactions within the composites matrices. Solubility studies indicate that ILs/MWCNT composites are hydrophobic and insoluble in water and other polar solvents.

CHAPTER THREE

SYNTHESIS, CHARACTERIZATION, AND PHYSICOCHEMICAL PROPERTIES OF PYRIDINIUM-BASED POLYMERIC IONIC LIQUIDS (PILS) WITH VINYL MOIETY: FUNCTIONALIZED CARBON NANOTUBES

Chapter 3

3.1 Synthesis of pyridinium-based PILs and PILs/MWCNT composites

3.1.1 Background into pyridinium-based PILs

Polymeric ionic liquids (PILs) are the polyelectrolytic-forms of ionic liquids (ILs) or electrolytes produced by a direct and/or indirect polymerization of ionic liquid (IL) monomers, or modification of the existing polymers [214-215]. PILs are non-covalently bonded subclass of polyelectrolytes, consisting of organic cations namely: imidazolium, pyrrolidinium, pyridinium, tetraalkylammonium, tetraalkyl-phosphonium, piperidinium, and quinolinium, and organic or inorganic anions such as halide ions (Cl^-, Br^-), polyatomic inorganics such as tetrafluoroborate (BF_4^-), hexafluorophosphate (PF_6^-), and pure organic anions including bis(trifluoromethanesulfonyl)imide ($TFSI^-$) and dicyanamide [$N(CN)_2^-$] [216-218].

Physicochemical properties of polymeric ionic liquids can be tuned by changing the ions involved [218-225]. Some PILs, depending on the type of polycation or polyanion involved are relatively soluble in water (e.g. imidazolium-based PILs with halides as counter anions), and some are only soluble in organic polar solvents such as dimethyl form amide (DMF), dimethyl sulfoxide (DMSO), and acetonitrile [217]. Polymeric ionic liquids are normally synthesized with

intended application and desired properties in place [221-222]. Henceforth, the polymer structure, size, amphiphilic behaviour, durability, and glass transition temperature are always optimized and monitored during synthesis.

The application of PILs on removal and/or retention of chromium ions have recently gained significant attention from academia and industries. Industrial activities are the leading sources of chromium moiety-pollutions [227-228]. A numerous number of conventional methods have been developed and utilized to remove hexavalent chromium from industrial effluents. However, several demerits such as high operation cost, chemical sludge, and low output have prohibited and hindered the applicability of these conventional methods. On the other hand, adsorption process has been the subject of research and gained popularity due to its effectiveness, ease of generation and responsiveness economically [229]. Recently, the use of polymer materials as adsorbents to remediate metal ions from wastewater has been the subject of intense research. Kumar *et al*. [9-10] reported the use of polyaniline and aniline-formaldehyde condensation polymers to remove hexavalent chromium from wastewater. They discovered that the removal of chromium species from wastewater was due to the electrostatic interactions between the chromate species and protonated polymer systems via the reduction of Cr(VI) to Cr(III).

Tavengwa *et al*. [11] probed the use of *N*-propyl quaternized magnetic poly(4-vinylpyridine) to selectively remove hexavalent chromium from aqueous solution. They studied the effect of pH (4), time (40 min), and amount of the adsorbent (20 and 65 mg) and initial concentration (5 mgL^{-1}) on removal efficiency. In order to effectively probe the reusability of the adsorbent, Tavengwa *et al*. [11] also performed six adsorption-desorption cycles and they discovered that their magnetic polymers were still stable and able to attract chromium up to the sixth cycle with adsorption capacity of 98.5% and 89% for magnetic ion imprinted polymers and non-imprinted polymers, respectively. In a similar studied, Hara [216] probed the behaviuor of poly(4-vinylpyridine) *N*-alkyl quaternized with short alkyl lateral chains (C_2-C_4) in water/chloroform interface. It was evident from the investigation that the polyelectrolyte systems prepared were soluble in water and inappropriate for adsorption processes. Moreover, poly(4-vinylpyridine) *N*-alkyl quaternized polyelectrolyte systems with longer alkyl chains including hexyl, octyl, and decyl have been reported and are insoluble in water [212-216].

Some poly(4-vinylpyridine) *N*-alkyl quaternized polyelectrolyte systems with shorter alkyl chain length have been reported and are water-soluble and inappropriate for metal ion removal. However, the current study proposes further investigation on the synthesis, physicochemical properties, and evaluation of poly(4-vinylpyridine) *N*-alkyl quaternized polymers with short

alkyl lateral chains (ethyl, propyl, and isopropyl) and hydrophobic counter ions for metal ions removal. Thus, the current work focuses on the synthesis of water-insoluble polyelectrolyte polymers of poly(4-vinylpyridine) with short alkyl chains.

3.1.2 Synthesis of pyridinium-based PILs with vinyl moiety

The starting material (monomer, 4-vinylpyridine) was distilled prior use at 65 °C to remove the hydroquinone (the inhibitor). Following the distillation of the starting material, the actual synthesis of hydrophilic and hydrophobic pyridinium-based PILs involved three-steps method: (I) polymerization of 4-vinylpyridine, (II) quaternization of the polymer, and (III) anion-exchange with hydrophobic anion (hexafluorophosphate, PF_6^-) analogous to the method reported by Tavengwa *et al*. [11].

3.1.2.1 Polymerization of 4-vinylpyridine (4-VP)

4-vinylpyridine (15.0 mL, 110 mmol), and 50.0 mL distilled water were added into 100-mL three-necked flask equipped with a reflux condenser and nitrogen inlet. A solution of potassium persulfate (0.5 g, 1.8 mmol) in 5.0 mL distilled water was transferred into the flask, stirred and heated to 90 °C for 2 h. The resultant precipitate was filtered and washed with distilled water. The resultant plastic-like and sticky product was heated inside the oven and easily pulled out of

the reaction flask using a spatula and washed with several portions of DMF. The final polymer product, poly(4-vinylypyridine) (P4-VP) was dried at 40 °C under vacuum for 24 h.

3.1.2.2 Quaternization of poly(4-vinylpyridine) (P4-VP): Poly(N-alkyl-4-vinylpyridinium)

Poly(4-vinylpyridine) (3.00 g, 0.04 mol) and alkyl halide 0.07 mol (6.45 mL, 6.67 mL, and 5.29 mL 1-bromopropane, 2-bromopropane, and 1-bromoethane, respectively, in excess mole ratio) were dissolved in 20 mL DMF in a round-bottomed flask. The reaction mixtures were stirred at room temperature for 1h, and then refluxed under inert N_2 conditions at 50 °C for 5 h. The resultant solutions were added into diethyl ether to obtain solid polymer materials, rinsed with several portions of ether, dried under vacuum at room temperature to constant mass. The resultant polymer material(s), poly(*N*-alkyl-4-vinylpyridinium bromide) (PIL1-3) were stored in very tightly dark area (Scheme 3.1).

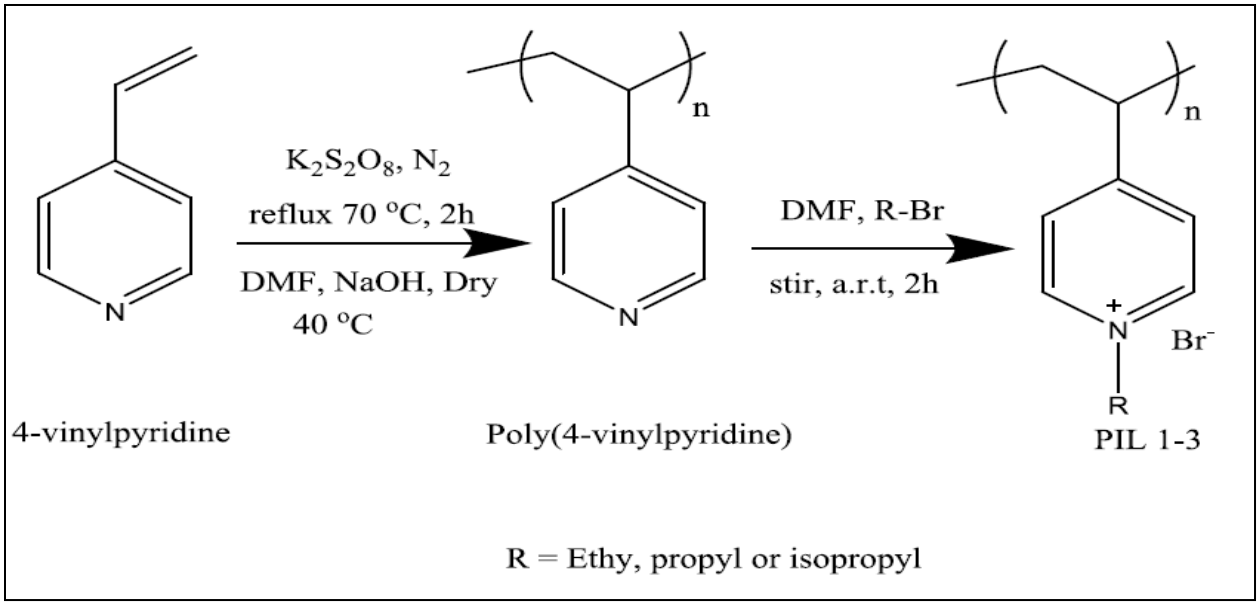

Scheme 3.1 Synthesis of hydrophilic pyridinium-based ILs

3.1.2.3 Anion-exchange with hexafluorophosphate (PF_6^-)

Final step involved the synthesis of water-insoluble (hydrophobic) PILs via the anion-exchange of bromide to hexafluorophosphate as presented in Scheme 3.2. Briefly, into 50 mL round-bottomed flask (1.0 g, repeating units) of polymeric materials (PIL1-3) were prepared in 10-mL ultra-pure water, and another solution of potassium hexafluorophosphate (2.0 g, 10.87 mmol) in 10 mL ultra-pure water were also prepared separately. The solution of the salt was added drop-wise to the polymer solution upon stirring to yield colorful (green to brownish) precipitate. The final mixtures were stirred for 20h at room temperature. Resultant precipitates were rinsed with several portions of ultra-pure and dried in an oven at 40 °C for 12 h.

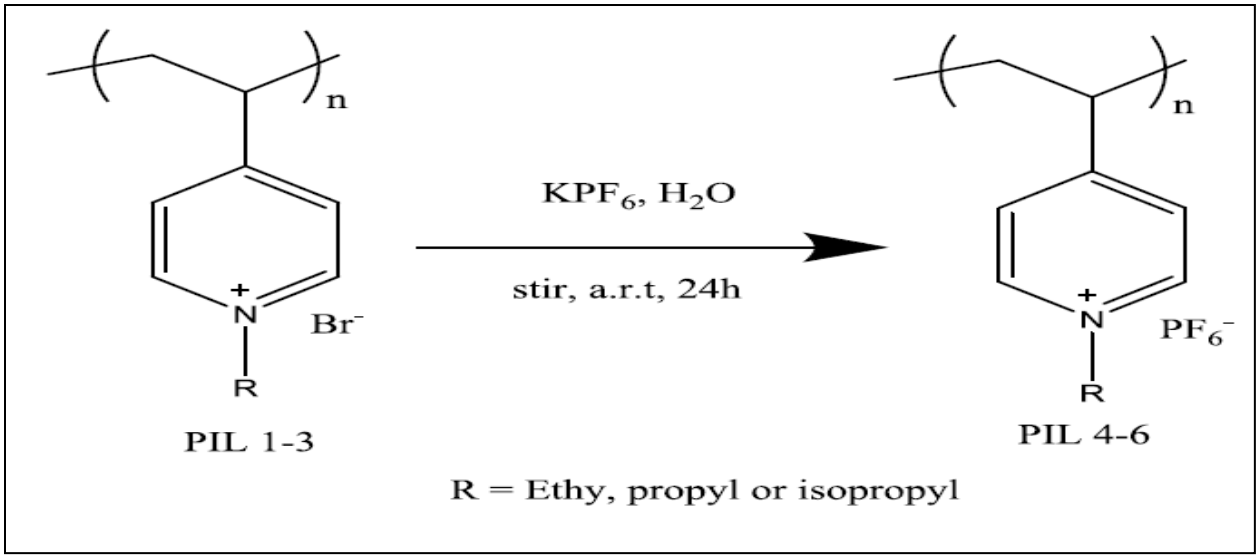

Scheme 3.2 Anion-exchange to prepare hydrophobic pyridinium-based PILs

3.1.3 Synthesis of PIL/MWCNT composites

PILs/MWCNT composites were synthesized according to previously reported work [237] with some minor modifications. Briefly, solution of 5.0 mg of MWCNTs in 17-mL DMF and 11.0 mg of each PIL in 10-mL DMF were placed into 100-mL round-bottomed flask. After ultrasonicating for 30 min at ambient temperature, the reaction mixture was vigorously stirred for 24h at 50 °C. The unreacted MWCNT residues were removed by centrifugation, and the resultant PIL/MWCNT composites were filtered, thoroughly washed with DMF, ethanol, and ultrapure water, respectively. The composites were then dried in an oven at 90 °C for 12h.

3.2 Results and Discussion

During the polymerization of 4-vinylpyridine with potassium persulfate, the initial formation of cream-white precipitate in less than 40 mins of the reaction was observed. The resultant poly(4-vinylpyridine) material was elastic. In order to remove it from the reaction flask it had to be heated and pulled out. When P4-VP was stored in an oven between 80-100 °C it behaved like a heated-plastic and elastic, while at room temperature it was like hard-plastic material. Upon addition of alky-quaternizing agents, the solution became light-green after 30 mins heating. During drying of the resultant hydrophobic PILs 4-6, huge amount of water was removed from each polymer systems.

As-synthesized PILs (PIL1-6):

Poly(*N*-ethyl-4-vinylpyridinium bromide) (**PIL1),** Poly(*N*-propyl-4-vinylpyridinium bromide) (**PIL2),** Poly(*N*-isopropyl-4-vinylpyridinium bromide) (**PIL3**),Poly(*N*-ethyl-4-vinylpyridinium hexafluorophosphate) (**PIL4*),*** Poly(*N*-propyl-4-vinylpyridinium hexafluorophosphate) (**PIL5**), Poly(*N*-isopropyl-4-vinylpyridinium hexafluorophosphate) (**PIL6**).

3.2.1 FTIR spectra studies of vinyl pyridinium-based PILs

P4-VP and quaternized samples (**PIL 1-3**) were studied using FTIR spectroscopy (APX 3-5). In **P4-VP** spectrum, the vibrational band at 3380 cm^{-1} was ascribed to the presence of hydroxyl group from water residue. Vibrational bands at 949 and 1418 cm^{-1} corresponds to the vibrations of the vinyl polymerizable moiety. The most significant band was that of C=N in pyridine, which

is usually found at 1600 cm^{-1} in non-quaternized pyridine materials. In this present case, it was exactly located at 1600 cm^{-1} before quaternization, which agrees with the literature findings [227, 232, 235, 222]. To ascertain the successful quaternization, the most important FTIR vibrational band (C=N) is slightly shifted to higher regions. For instance, the characteristic absorption bands of the quaternized pyridinium group shifted to 1651, 1654 and 1657 cm^{-1} in **PIL1**, **2** and **3**, respectively.

Esma *et al*. [221] and Briones *et al*. [222] reported the shifting at 1640 cm^{-1}, whereas Toral *et al*. [214] reported it at 1636 cm^{-1}. The presence of positively charged nitrogen atoms or pyridinyl ring in the polymers can be observed by vibration bands at 1558, 1500, and 1557 cm^{-1} in **PIL 1**, **2**, and **3**, respectively. The intensity of vibrations bands at 2934 cm^{-1} (**PIL1**), 2931 cm^{-1} (**PIL2**), and 2933 cm^{-1} (**PIL3**) can be ascribed to the valence oscillations of $C\text{-}H_{sp}^{3}$ in $–CH_2$- and CH_3 alkyl substituent's attached on the pyridine-N and polycation main chain. Consequently, the absence of $C\text{-}H_{sp}^{2}$ vibration band around 3024 cm^{-1} signifies a complete polymerization of vinyl group. The presence of strong O-H stretching vibration around 3450-3400 cm^{-1} in quaternized pyridine-materials is due to the protonated carbonyl-oxygen of *N*, *N*-dimethyl formamide (DMF) solvent. FTIR results obtained in this current work were consistent with those in literature [228, 235, and 222].

The FTIR spectra of the pyridinium PILs showed strong characteristic signals of the hexafluorophosphate species at 838, 822, and 821 cm^{-1} for **PIL 4-6** (APX 3-6), respectively. The lower frequency shifting and low intensity of vibration bands around 1650-1600 cm^{-1} is due to the exchange of halide (Br^-) to hydrophobic anion (PF_6^-). It has been discussed in the literature that halides normally shift the vibration bands towards higher regions of the FTIR. Therefore the low or backward shifting of the FTIR bands around 1650-1600 cm^{-1} in hydrophobic PILs compared to high-frequency shifting of the same bands around 1651-1657 cm^{-1} in hydrophilic PILs, confirms anion metathesis. The presence of the vibration band around 3350 cm^{-1} in hydrophobic PILs is due to the hydroxyl (O-H) of water used during synthesis.

3.2.2 Thermogravimetric analysis (TGA) of vinyl pyridinium-based PILs

TGA curves of **P4-VP**, **PIL1-3** are presented in Fig. 3.1. Poly(4-vinylpyridine) (P4-VP) exhibits unimodal (one-step) degradation [203, 215]. A weight loss at the beginning of the TGA curve (<10%) in **P4-VP** between 50-100 °C corresponds to the removal of moisture content from the hygroscopic polymer material and the final weight loss of 95% at 420 °C corresponds to the degradation of vinyl pyridine moiety. Quaternized derivatives of **P4-VP** (**PIL 1-3**) exhibited multimodal (multi-step) degradation [203]. **PIL 1-3** showed weight loss of about 30% between 50-150 °C, second weight loss between 150-300 °C due to the degradation of alkyl chain

connecting the pyridinium ring (ethyl, propyl, and isopropyl) groups during the cleavage of C-N^+ bonds, and finally the degradation (>80%) due to polymer backbone(s) beginning from 300 to 450 °C [214]. Poly(4-vinylpyridine) was observed to be far more thermally stable than all of its quaternized derivatives. The resultant polymer materials in this study showed thermal stability up to 150 °C.

TGA curves of hydrophobic pyridinium-based PILs presented in Fig. 3.2 showed that pyridinium-based PILs with hydrophobic counter anions are more thermally stable than their halide-containing analogous. All the hydrophobic pyridinium PILs (**PIL 4-6**) remain thermally stable up to 350 °C. A weight loss (<30%) observed between 50-100 °C can be attributed to the minor degradation of alkyl side chains and breaking of C-N^+ bonds in the polymer materials. The hydrophobic PILs appeared thermally stable in comparison to their halide-containing PILs counterparts in this study. This is attributed to the strong electrostatic interactions between pyridinium cation and hexafluorophosphate anions [222]. Briones *et al*. [222] in their recent study discovered that it was difficult to handle and characterize polymers with hexafluorophosphate counterion because of generated white vapours from the polymer materials. However, the results obtained in this study clearly confirmed the successful synthesis of poly(4-vinylpyridine) compounds.

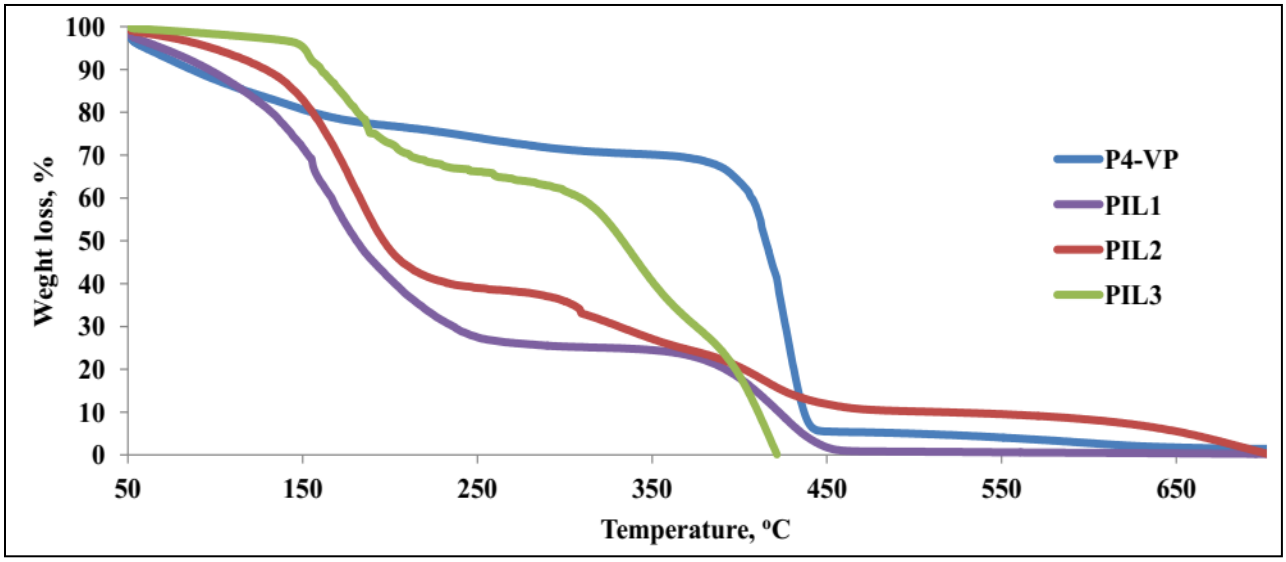

Figure 3.1 TGA profiles of poly(4-vinylpyridine) **P4-VP**, poly(N-ethyl-4-vinylpyridinium bromide) **PIL1**, poly(N-propyl-4-vinylpyridinium bromide) **PIL2**, and poly(N-isopropyl-4-vinylpyridinium bromide) **PIL3**

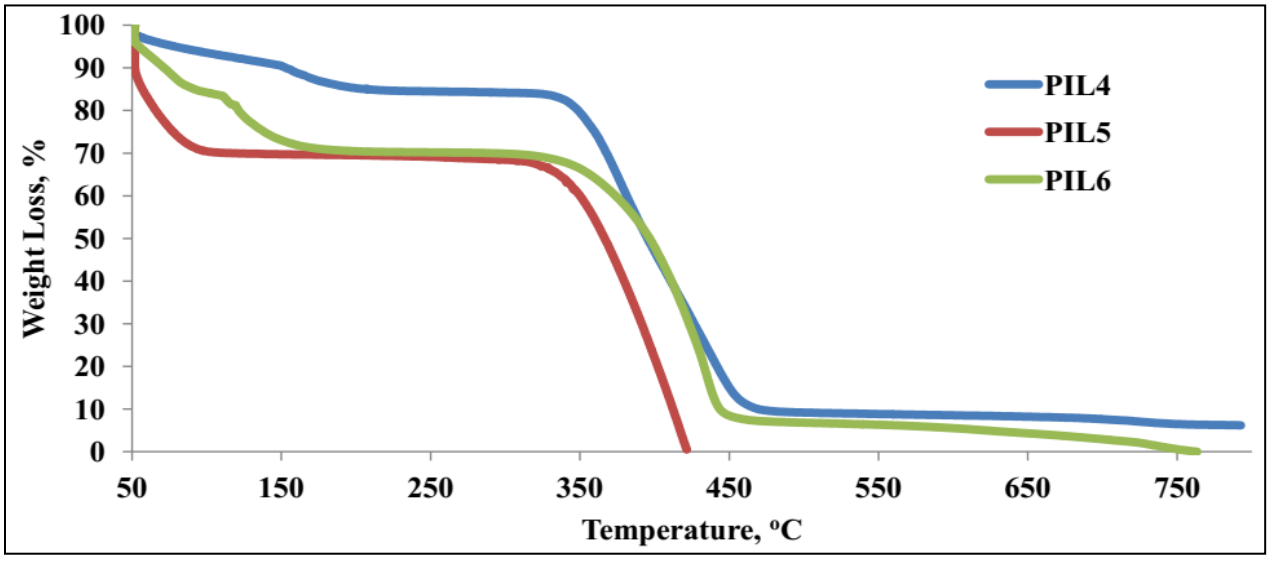

Figure 3.2 TGA profiles of hydrophobic poly(N-ethyl-4-vinylpyridinium hexafluorophosphate) **PIL4**, poly(N-propyl-4-vinylpyridinium hexafluorophosphate) **PIL5**, and poly(N-isopropyl-4-vinylpyridinium hexafluorophosphate) **PIL6.**

3.2.3 Differential scanning calorimetry analysis (DSC) of vinyl pyridinium-based PILs

Table 3.1 illustrates the glass transition temperature (T_g) values of P4-VP, PIL 1-6 discussed in this study. T_g of polymer materials usually depends on the size of the poly-anion and charge delocalization. Generally, an increase in counteranion size decreases the T_g of the polymer respectively [224]. The involvement of electrostatic interactions associated with hydrophobic anion tends to affect the movement of positively charged ions [239]. However, it has been reported that T_g values of polymer materials also varies with alkyl chain length involved [239]. In the present study, we discovered that polymers containing bromide ions showed high T_g values than their corresponding PF_6^- containing counterparts. This may be ascribed to less steric hindrance exhibited by the short alkyl chains towards the mobility of positively charged ions in the polymer backbone, which also affect the glass transition temperature in the polymers [239].

Table 3.1 Glass transition temperatures of poly(4-vinylpyridine) P4-VP and vinyl pyridinium PILs

Polymer material	**Anion**	**Alkyl group**	**T_g($^{\circ}$C)**
P4-VP	-	-	66
PIL 1	Br^-	ethyl	60
PIL 2	Br^-	propyl	30
PIL 3	Br^-	isopropyl	55
PIL 4	PF_6^-	ethyl	75
PIL 5	PF_6^-	propyl	57
PIL 6	PF_6^-	isopropyl	65

3.2.4 Solubility studies of vinyl pyridinium-based PILs

In order to test the hydrophobicity-hydrophilicity balance of the as-synthesized polymers, solubility studies were performed. Poly(N-ethyl-4-vinylpyridinium bromide) **PIL1,** poly(N-propyl-4-vinylpyridinium bromide) **PIL2, and** poly(N-isopropyl-4-vinylpyridinium bromide) **PIL3** were found to be soluble in most solvents including water, methanol, and acetone. On the other hand, polymer materials containing PF_6^- were only soluble in polar aprotic solvents such as dimethyl formamide (DMF), dimethyl sulfoxide (DMSO), and tetrahydrofuran (THF) including chloroform [239]. Thus, the successful anion-exchange resulted in hydrophobic polymers suitable for metal ion removal such as hexavalent chromium (Cr(VI)).

3.2.5 Nuclear Magnetic Resonance (NMR) vinyl pyridinium-based PILs

NMR was employed to study and confirm the purity and the successful synthesis of the PILs. ^{1}H-NMR spectra of poly(*N*-ethyl-4-vinylpyridinium bromide) **PIL1**, poly(*N*-propyl-4-vinylpyrinium bromide) **PIL2**, and poly(*N*-isopropyl-4-vinylpyrinium bromide) **PIL3** were obtained. Deshielded Signals at 7.6-8.0 ppm can be attributed to the protons of quaternized pyridine rings (3-6 numbering) [222]. Signals at 3.41-5.0 ppm were due to the protons of methylene groups close to the pyridinium-nitrogen atom (7). Signals at 2.78-3.01 ppm were due to the protons of the repeating methylene units of the main chain (1-2). Low field signals at 1.0-1.98 ppm and

0.87-0.97 ppm were due to (-CH_2-), and (-CH_3-) units of the alkyl chains located far from the pyridinium-nitrogen atom (8-9). The presence of bromide ion has resultant in some protons being deshielded in various PIL systems [221-222]. It has been reported that the electron density of substituents in a compound usually affects peak position. However, due to high electronegative behavior of halogens, protons close or associated with halides are normally deshielded and appear at downfield [222].

^{19}F and ^{1}H-NMR spectra of poly(poly(*N*-ethyl-4-vinylpyridinium hexafluorophosphate), poly(*N*-propyl-4-vinylpyridinium hexafluorophosphate), and poly(*N*-isopropyl-4-vinylpyridinium hexafluorophosphate) were collected and studied, respectively. One thing worthy to be mentioned is the fact that the protons are shielded in hydrophobic systems, confirming the absence of bromide ions [221]. The measured coupling constants (J_{Hz}) between the peaks of the ^{19}F- and ^{31}P-NMR in all polymer systems were 713.80, 703.99, and 708.14 Hz for **PIL 4**, **5**, and **6**, respectively.

3.3 Characterization of PIL/MWCNT composites

3.3.1 FTIR spectroscopy of vinyl pyridinium-based PILs/MWCNT composites

As-synthesized PIL/MWCNT composites:

Poly(N-isopropyl-4-vinylpyridinium bromide)/MWCNT (**PIL/MWCNT3**), Poly(N-propyl-4-vinylpyridinium hexafluorophosphate)/MWCNT (**PIL/MWCNT5**), Poly(N-isopropyl-4-vinylpyridinium hexafluorophosphate)/MWCNT (**PIL/MWCNT6**).

Generally, integrated PILs/MWCNT composites introduce new electronic properties emanating from morphological modifications and electronic interactions between the two materials via either π-π stacking or cation-π and anion-π electronic interactions. The FTIR spectroscopy was therefore used to elucidate the type of interactions in PILs/MWCNT composites. MWCNTs showed very weak vibrational bands. Vibrational band around 1751 cm^{-1} was ascribed to aromatic ring stretching vibration (C=C). Vibrational band around 1239 cm^{-1} was assigned to the presence of carboxylic group (-COOH) and graphitic moieties on the surface of MWCNT. The FTIR results obtained for MWCNTs agreed with those obtained in the literature [240]. On the other hand, new vibrational bands were observed in PIL/MWCNT composites. Stretching vibrations around 3043 to 3854 cm^{-1} were ascribed to (-CH_2-) rocking vibrations due to tail to tail addition in PILs and lateral alkyl chains (ethyl, propyl or isopropyl) attached on pyridinium-nitrogen atom. The FTIR bands at 1638, 1637, and 1628 cm^{-1} in PILs/MWCNT composites were due to C=N stretching vibration in pyridinium-ring of the PILs.

3.3.2 TGA of vinyl pyridinium-based PILs/MWCNT composites

Fig. 3.3 (A&B) showed the TGA thermograms of MWCNTs and PILs/MWCNT composites. A slight weight loss (<15%) around 120 °C for MWCNTs in both thermograms was due to the loss of moisture absorbed by MWCNTs [240]. A significant and common weight loss in both MWCNTs and its polymer-functionalized derivatives above 700 °C can be attributed to the decomposition of carbon materials released during temperature scan under airflow condition. A strong weight loss between 250 and 450 °C in polymer-functionalized MWCNTs was due to the decomposition of PILs moieties attached onto the surface of MWCNTs. For example, a weight loss of 65, 32, and 20% was observed for PIL3/MWCNT, PIL5/MWCNT, and PIL6/MWCNT, respectively.

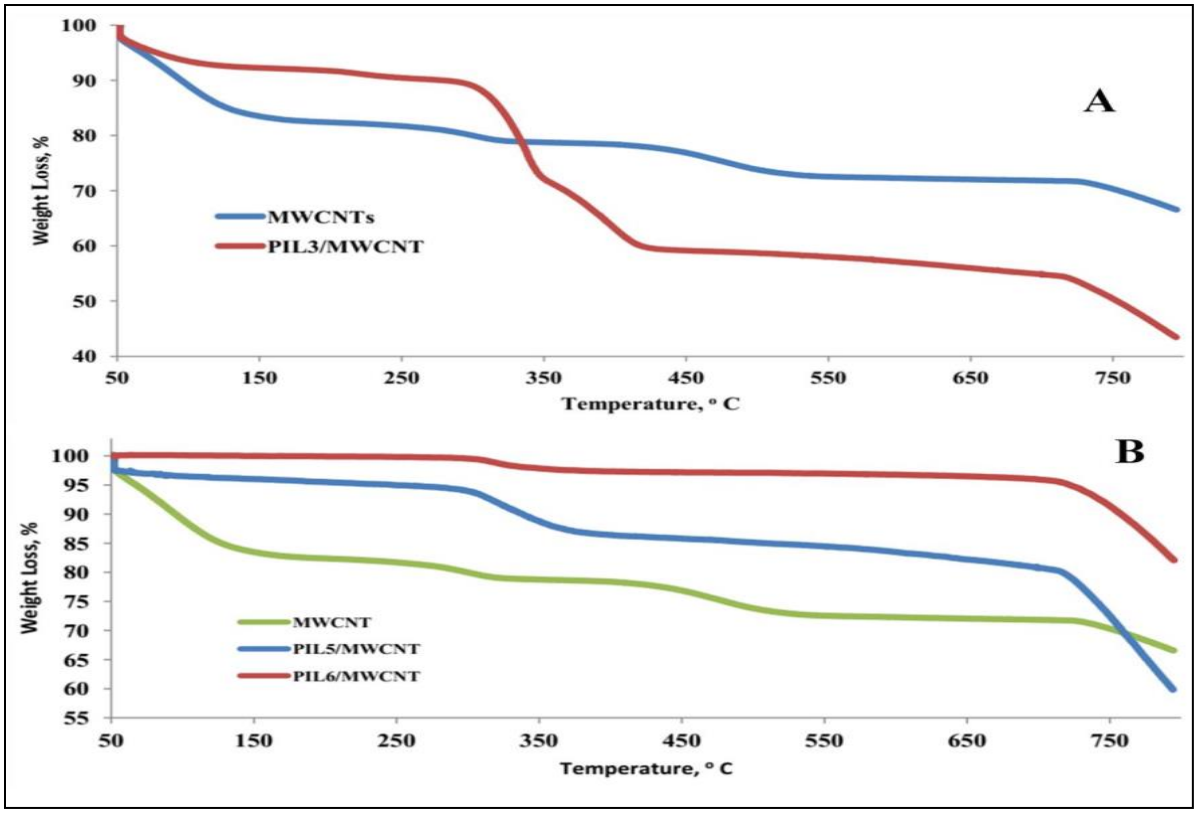

Figure 3.3 TGA curves of MWCNTs and PIL3/MWCNT (A), PIL5/MWCNT and PIL6/MWCNT (B) composites

3.3.3 Solubility of vinyl pyridinium-based PILs/MWCNT composites

It is evident that the surface-modification of MWCNTs with PILs has significant effect on the solubility and functionality of MWCNTs and its functionalized derivatives. Carbon nanotubes are known to have low intrinsic solubility in both organic and aqueous medium [240]. MWCNT and its polymer-functionalized derivatives were dissolved in organic and aqueous solvents to test their solubility character. Pristine MWCNTs showed poor or no solubility in polar protic solvents

such as water, methanol, and ethanol and in non-polar solvents which includes diethyl ether, toluene, and hexane. However, the same carbon-based materials showed good solubility in polar and dipolar aprotic solvents such as acetonitrile, dimethyl sulfoxide, acetone, and tetrahydrofuran.

On the other hand, polymer-functionalized MWCNT derivatives exhibited diversified solubility characteristics depending on the polymer systems involved. PIL3/MWCNT showed solubility in DMSO (polar aprotic), slight or suspended in water (polar protic). The slight suspension of the latter composites in water was due to the formation of hydrogen bond (intermolecular forces) between the composite and water molecules. It is also a clear indication of the presence of hydrophilic counterion (bromide) as part of the composite. Polar solvents are best to dissolve polar reactants, while non-polar solvents stand a good chance to dissolve non-polar materials ("like dissolves likes"). PIL5/MWCNT and PIL6/MWCNT composites are insoluble in all non-polar solvents and only slightly soluble in DMSO (large dielectric constant polar aprotic solvent). This therefore confirmed the hydrophobicity of the latter composites and their possible capability to precipitate out of water during adsorption applications.

3.3.4 SEM and TEM of vinyl pyridinium-based PILs/MWCNT composites

Scanning electron microscopy and energy-dispersive X-ray spectroscopy were used to study both the surface morphology and the composition of the nanocomposites synthesized. As presented in Fig. 2.3 (A-B), CNTs synthesized by chemical method showed curled and highly tangled tubes [241]. On the other hand, the EDS spectra (Figs. 3.4) showed high intensity carbon peak from the carbon material. In addition, SEM/EDS were also employed to further study the surface interaction between the amorphous polymer materials and MWCNTs. The structural size and shape of MWCNTs have been modified and re-structured by the functionalization [241]. It has also been reported in the literature that the stirring or contact time and the modification method can greatly affect the dispersion of CNTs into polymer [241]. However, the mechanism behind the dispersion process is very complex, owing to the primarily involved interactions which include *van der Waals* and electrostatic forces. The EDS spectra of the PIL/MWCNTs elucidated the appearance of elements such as N, Br, P, and F confirming the successful coating of amorphous polymers on the surface of CNTs. TEM analysis revealed that MWCNTs have relatively small diameter (≈18 nm) and long length (≈620.21 nm) (Fig. 3.5). After modification, it can be observed that the surface of MWCNTs was equally enveloped by the polymer materials resulting in an increase in surface area (Figs. 3.5 B-D) [240, 242]. TEM results complemented the SEM findings obtained and confirmed that the dispersion or functionalization method was facile and success.

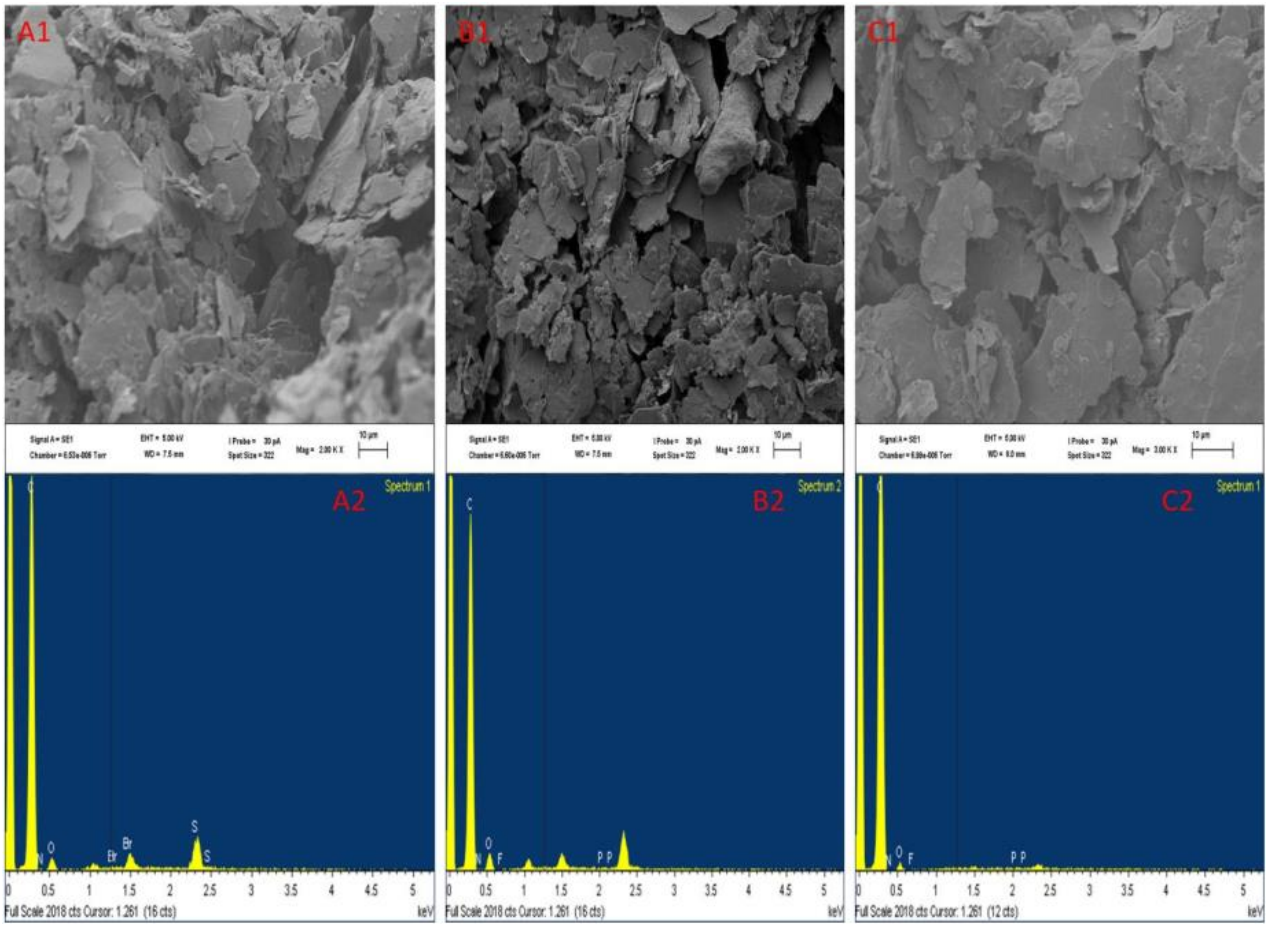

Figure 3.4 SEM images and EDS spectra of PIL3/MWCNT (A1-A2), PIL5/MWCNT (B1-B2), and PIL5/MWCNT (C1-C2) composites

.

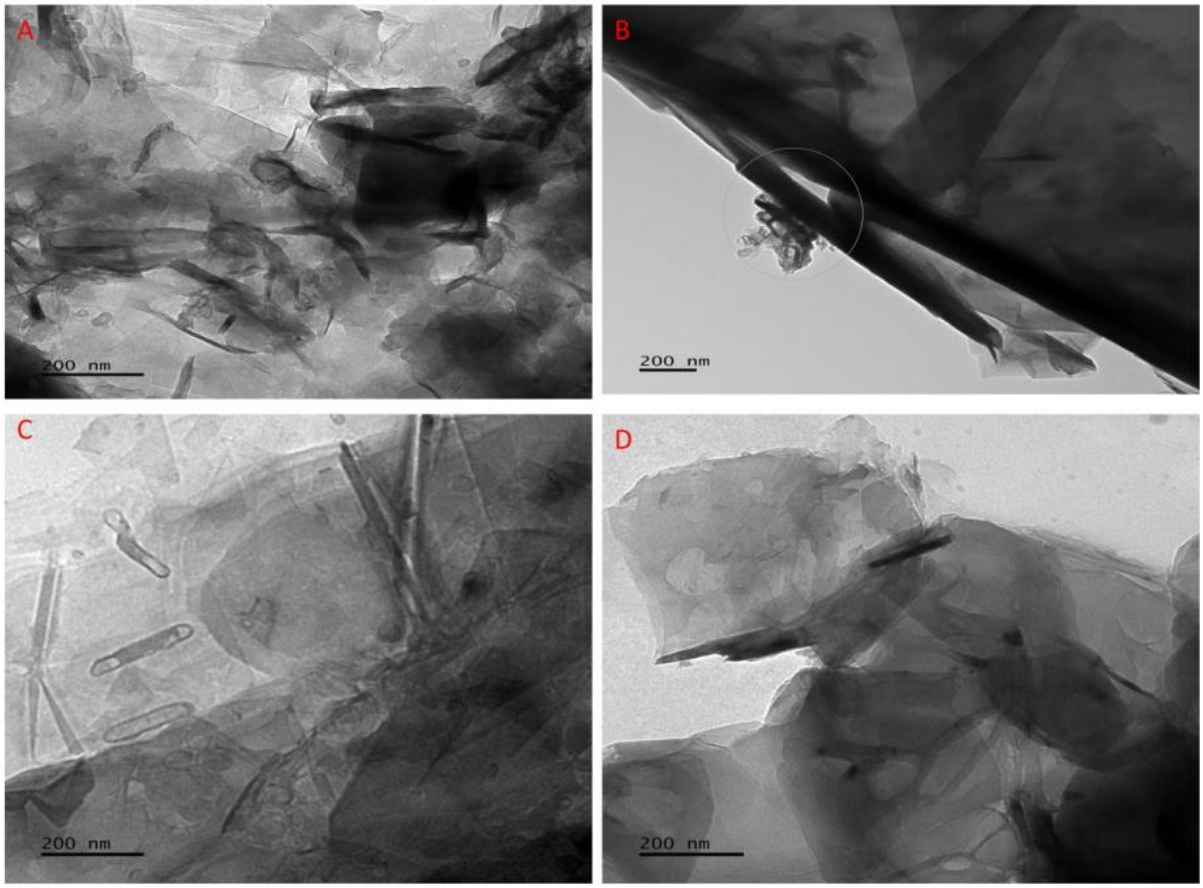

Figure 3.5 TEM micrographs of MWCNTs (A), PIL3/MWCNT (B), PIL5/MWCNT (C), and PIL6/MWCNT (D)

3.3.5 Power X-ray diffraction studies of PILs/MWCNT composite

All pyridinium-based PILs/MWCNTs composites studied under XRD showed diffraction peaks around 2θ values 30.9372-36.1092° (002 in plane) based on graphitic structure derived from carbon nanotubes with interplanar *d*-spacing of 3.353884, 2.99183, and 1.67580Å, respectively (Fig. 3.6). However, the broad and weak diffraction peak around 64.7864° (100 in plane) belongs to the amorphous structure of the PIL derivatives, respectively. The calculated crystalline size of

all PIL/MWCNTs composites ranges between 12.4572-22.0981 nm. Normally, the sharpness and intensity of the XRD peak signify high crystalline samples, while broad peaks show amorphous structure. CNTs are known to be crystalline materials and they produce crystalline peaks in polymer nanocomposites [199] but in this study, the XRD patterns of PILs/MWCNTs composites shows relatively low intensity peaks (amorphous) compared to high intensity crystalline peaks of carbon materials, with unaltered crystalline structure.

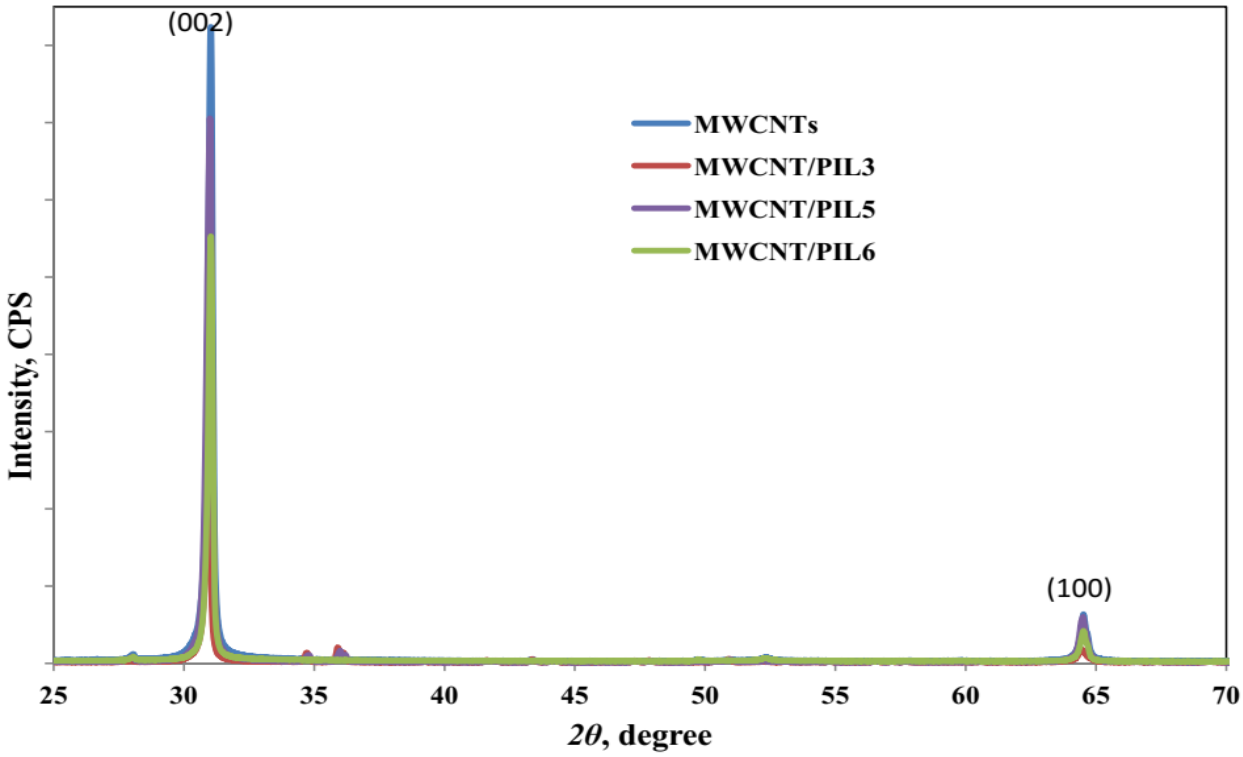

Figure 3.6 XRD patterns of pristine MWCNTs and some pyridinium-based PIL/MWCNTs composites

3.4 Chapter summary

In this chapter, the synthesis of vinyl pyridinium PILs via radical polymerization of ILs monomers using potassium persulfate has been discussed. Six sticky and highly plasticizing PIL materials and several PILs/MWCNT composites were synthesized and characterized with thermal, spectroscopic and microscopic characterization techniques. Spectroscopic studies were used to confirm the synthesis of PILs materials. The FTIR characteristic bands due to C=N functional group appeared at 1600 cm^{-1}, compared to 1640 and 1636 cm^{-1} reported in literature. Thermal studies have revealed that pyridinium-PILs containing hydrophobic counter anions (PF_6^-) are more thermally stable (>350 °C) than their halide-containing counterparts. High thermal stability values of PILs can be attributed to strong electrostatic interactions between pyridinium cations and hexafluorophosphate anions. The results shows that the delocalized charge in pyridinium cationic ring and the size of counter anions influenced the glass transition temperatures of PILs materials. Furthermore, the functionalization of carbon nanotubes with vinyl pyridinium-PILs resulted in 10-fold more thermally stable and relatively insoluble PILs/MWCNT composites, this characteristic is useful for solid-liquid adsorption process. SEM and TEM microscopic analyses confirmed the coating of PILs materials on the surface of carbon nanotubes and it can be concluded that the direct mixing-functionalization method did not alter the surface morphology of pristine carbon materials.

CHAPTER FOUR

SYNTHESIS, CHARACTERIZATION, AND PHYSICOCHEMICAL PROPERTIES OF IMIDAZOLIUM-BASED POLYMERIC IONIC LIQUIDS (PILS) WITH VINYL AND STYRENIC MOIETIES: FUNCTIONALIZED CARBON NANOTUBES

Chapter 4

4.1 Background into imidazolium-based PILs and PILs/MWCNT composites

The synthesis and the use of imidazolium-based PILs containing vinyl and/or vinyl benzyl (styrene) polymerizable moieties have since gained significant attention. Generally, vinyl-based imidazolium ILs monomer involves the quaternization of a starting material (1-vinyl imidazole) with an alkyl halide, followed by free radically polymerization [33]. However, the first and the earliest synthesis of vinyl ILs monomers and corresponding polymerized materials were reported in 1973 by Salamone *et al*. [243]. Many years later, Ohno's group intensified the research and the use of imidazolium PILs in ion conductive materials [244]. On the other hand, the synthesis and the application of vinyl benzyl-based imidazolium PILs were also reported by [243]. The authors discussed the series of imidazolium PILs involving poly[1-(4-vinylbenzyl)-3-butylimidazolium tetrafluoroborate (poly[$VBBIm^+$][BF_4^-]) and poly[1-(4-vinylbenzyl)-3-butylimidazolium hexafluorophosphate (poly[$VBBIm^+$][PF_6^-]).

Bacon *et al*. [245] reported the synthesis of imidazolium-based PILs for the absorption of n-butanol and other hydrophilic fermentation products. The influence of both the aliphatic N-alkyl side chain length (C8 to C16) and the counter anions on the absorption performance and selectivity were investigated. It was observed that PILs with long N-alkyl chain were insoluble in

water and possessed improved absorptive performance. Generally, owing to the counter anion used, 1,3-dialkyl imidazolium PILs are hydrophilic and high acidic [246]. Imidazolium-based PILs have a tendency to homogeneously disperse CNTs and graphene derivatives with or without an aid of a particular solvent [247-250]. Relevant improvements in electrical, mechanical, and thermal properties of CNT/imidazolium-based polymer composites have been reported [247, 251]. In another study, Meyer *et al*. [252] discussed an imidazolium end-functionalized poly($_L$-lactide) synthesized by ring-opening polymerization of $_L$-lactide.

4.2 Synthesis of imidazolium-based PILs

4.2.1 Synthesis of imidazolium-PILs with vinyl moiety

Vinyl imidazolium-based PILs were synthesized according to the method described by Green *et al*. [33], with some modifications. Generally, the procedure involves three-step processes as shown in Scheme 4.1. Unlike the other known procedures [33], herein the first step involve the quaternization of 1-vinylimidazole with active alkyl halides (1-bromopropane, and 2-bromopropane) followed by the polymerization of the vinyl polymerizable moiety using potassium persulfate ($K_2S_2O_8$) as a radical initiator. The final step involves the anion-exchange of bromide with hexafluorophosphate to produce hydrophobic PILs.

4.2.1.1 Quaternization of 1-vinylimidazole (1-VIm)

In a typical procedure, 44.16 mmol (4 mL) of 1-vinyl imidazole and 75.50 mmol (6.86, and 7.09 mL) of each of 1-bromopropane, and/or 2-bromopropane, respectively, were charged into a 100 mL round-bottom flask equipped with reflux condenser and 30 mL DMF. The reaction masses were heated to reflux at 85 °C for 20 h. To remove DMF from the sample, each sample was charged into a beaker with ice. When the ice has melted, diethyl ether was added and the mixture was charged into a separating funnel without shaking much (just gently swirl). The bottom-water layer was collected and further washed with ice-cold water. The resultant mixture was dried over sodium sulfate and concentrated using rotary evaporator, and then stored in an oven at 70 °C for 12 h. The monomers were 3-propyl-1-vinylimidazolium bromide (3P-VImBr) and 3-isopropyl-1-vinylimidazolium bromide (3Isop-VImBr) as shown in Scheme 4.1(A).

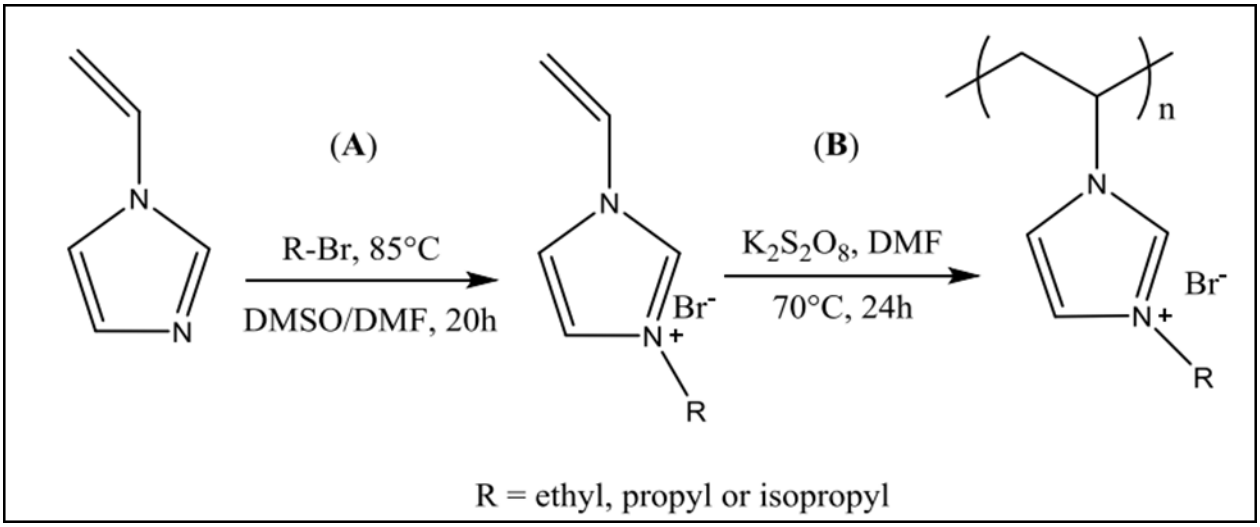

Scheme 4.1 Synthesis of hydrophilic imidazolium-based PILs

[3P-VImBr]: **^{1}H NMR** (400 MHz, ppm, D_2O, δ): 8.07 (1H, s, H*d*), 7.99 (1H, t, H*e*), 7.80 (1H, t, H*f*), 7.36 (1H, t, H*c*), 6.00 (1H, split doublets, H*a*), 5.58 (1H, split doublets, H*b*), 4.39 (2H, t, H*g*), 2.09 (2H, m, H*h*), 1.07 (3H, t, H*i*). ***FTIR*** (cm^{-1}): 3359 (=C-H 2-position, m), 3123-3098 (C-H_{sp}^2, m), 2976-2879 (C-H_{sp}^3, m), 1655 (C=C and C=N, s/m), 1415 (methyl, m), 1479 (methylene, s), 1102 (C-N, m).

[3Isop-VImBr]: **^{1}H NMR** (400 MHz, ppm, D_2O, δ): 9.16 (1H, s, H*d*), 7.86 (1H, t, H*f*), 7.76 (1H, t, H*e*), 7.31 (1H, m, H*g*), 5.90 (1H, d, H*a*), 5.87 (1H, d, H*b*), 5.54 (1H, m, H*c*), 1.65 (6H, d, H*h*, *i*). ***FTIR*** (cm^{-1}): 3410 (C-H, 2-position, m), 3078 (C-H_{sp}^2, m, vinyl), 2982 (C-H_{sp}^2, isopropyl), 1652 (C=C & C=N overlapped), 1084 (C-N).

4.2.1.2 Polymerization of N-alkyl-1-vinylimidazolium bromide monomers

Briefly, 6.0 mL of each monomer and a solution of 0.5 g (1.85 mol of $K_2S_2O_8$) in 6.7 mL distilled water were charged into a 100 mL round bottom flask equipped with a reflux condenser, N_2 gas inlet, and 40 mL of DMF. The mixture was refluxed for 24 h at 70 °C under N_2 flow. The polymer product was precipitated into acetone and filtered to obtain the solid product. Resultant product was further dried in an oven at 50 °C for 5 h to remove solvent and unreacted materials. The prepared polymers were poly(3-propyl-1-vinylimidazolium bromide) P[3P-VImBr] and poly(3-isopropyl-1-vinylimidazolium bromide) P[3Isop-VImBr] as shown in Scheme 4.1(B).

P*[3P-VImBr]*: **^{1}H NMR** (400 MHz, ppm, D_2O, δ): 9.10 (1H, s, H*c*), 7.84 (1H, s, H*d*), 7.64 (1H, s, H*c*), 5.89 (2H, split doublets, H*e*), 5.50 (2H, split doublets, H*d*), 4.28 (2H, t, H*f*), 2.79 (6H, m, H*a* & H*b*), 2.02-1.93 (2H, m, H*g*), 1.01-0.97 (3H, t, H*h*). ***FTIR*** (cm^{-1}): 3347 (=C-H 2-position, m), 2940-2878 (C-H_{sp}^3, m), 1654 (C=C & C=N, s), 1431 (methyl, m), 1039 (C-N, m).

P[3Isop-VimPF$_6$]: **^{1}H NMR** (400 MHz, ppm, DMSO, δ): 9.28 (1H, s, H*c*), 8.14 (1H, 2, H*d*), 8.00 (1H, s, H*e*), 4.64 (2H, s, H*a*), 3.55 (>3H, m, H*b*,*f*), 1.49 (>6H, m, H*h*,*g*). ***FTIR*** (cm^{-1}): 3426 (=C-H 2-position, m), 3136 (C-H_{sp}^2, imidazole ring), 2986 (C-H_{sp}^3, isopropyl), 1655 (C=N, s), 1099 (C-N, m), 839 (m, hexafluorophosphate species).

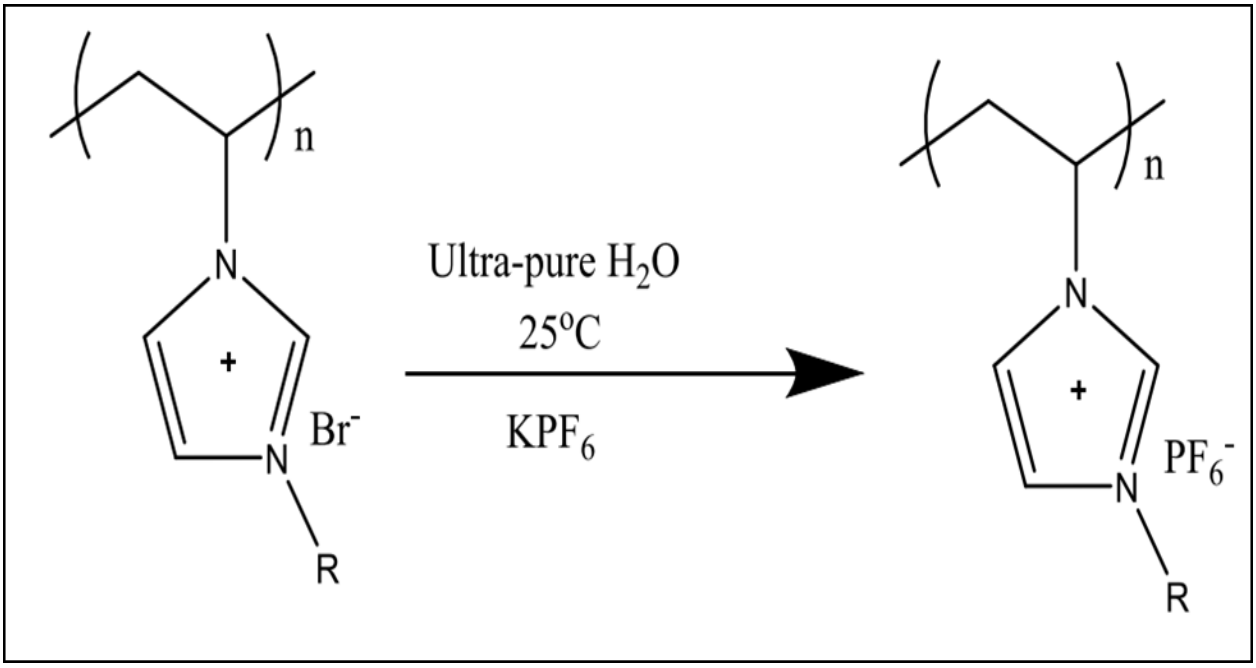

Scheme 4.2 Synthesis of hydrophobic PILs via anion-exchange

4.2.2 Synthesis of imidazolium-based PILs with styrenic moiety

4.2.2.1 Synthesis of IL-monomer

Imidazolium-based PILs with styrenic polymerizable group were synthesized according to the methods reported in the literature with some modifications [219-221]. Briefly, 1-methylimidazole (3607 mg, 43.94 mmol), 4-vinylbenzyl chloride (5959 mg, 39.05 mmol), and 30 mL acetonitrile were added into a 100 mL round-bottomed flask with stir bar. The resultant mixture was heated to reflux at 60 °C for 45 h under N_2 flow. The resultant viscous solution was concentrated in a vacuo to remove solvent and rinsed with acetone. Plastic-sticky material was produced with mouldable behaviour along the walls of the flask. Having rinsed with acetone several times, the monomer material was dried in a reduced pressure oven at 45 °C for 5 h (Scheme 4.3)**.** The product formed was 3-methyl-1-(4-vinylbenzyl) imidazolium chloride [MVBIm-Cl] with % yield (7550 mg, 82.15%).

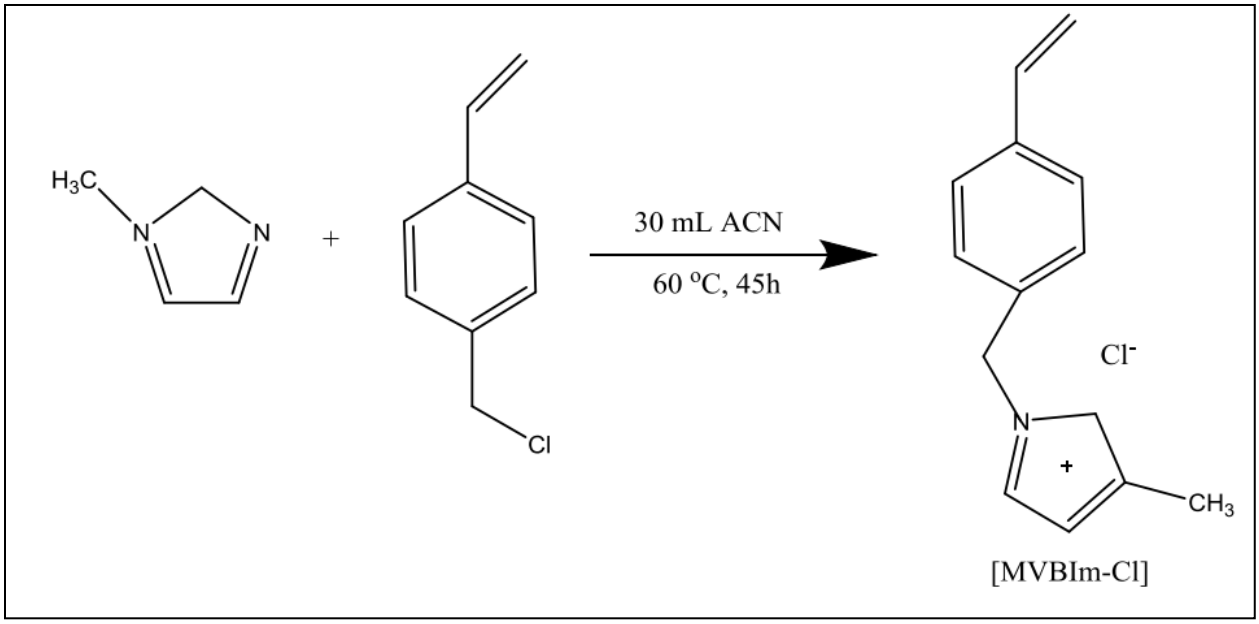

Scheme 4.3 Synthesis of ILs-monomer [MVBIm-Cl]

[MVBIm-Cl] **^{1}H NMR** (400 MHz, ppm, DMSO-d^6, δ): 9.458 (1H, s, N=CH-N), 7.851 (2H, d, N-CH=CH-N), 7.520 (2H, split doublets, -vinyl CH_2), 7.103 (1H, s, Ar-CH-vinyl), 6.874-6.778 (2H, split doublets, Ar-H_{ortho}), 6.74 (2H, split doublets, Ar-H_{meta}), 5.88 (2H, s, N-CH_2-Ar), 1.09 (3H, s, N-CH_3). **^{13}C NMR** (400 MHz, ppm, DMSO-d^6, δ): 138.30 (C4 &5), 136.44 (C8), 134.89 (C14), 129.24 (C13), 124.43 (C9 &10), 122.78 (C11 &12), 120.98 (C15), 115.72 (C2), 51.97 (C7), 36.34 (C2).

FT-IR (υ/cm^{-1}): 3371 (intermolecular H-bonding stretching vibration), 3054-3012 (=C-H_{sp^2}, aromatic & aliphatic), 2829 (N-$\underline{CH_3}_{sp^3}$), 1628-1408 (C=C &C=N), 1449-1333 (CH_2 & CH_3 bending vibrations in the fingerprint region), 1159-1017 (C-N bending vibration).

4.2.2.2 Polymer synthesis

[MVBIm-Cl] (3100 mg, 13.15 mmol), AIBN (4290 mg, 26.13 mmol), and 50/50 (v/v) solution of DMF/H_2O (50 mL) were discharged into a 100 mL round-bottomed flask. The reaction mixture was purged with N_2 gas for 20 mins and then heated to reflux at 60 °C for 24 h under continuous N_2 flow. Goldish-solution was produced, dissolved in ethyl acetate and precipitated out from acetone to get hard-sticky plastic like solid polymer product. After precipitation the polymer product was dried in air vacuum at 70 °C for 4 h for complete removal of acetone (Scheme 4.4). The product produced poly[3-methyl-1-(4-vinylbenzyl) imidazolium chloride] P[MVBIm-Cl] (2650 mg, 76%).

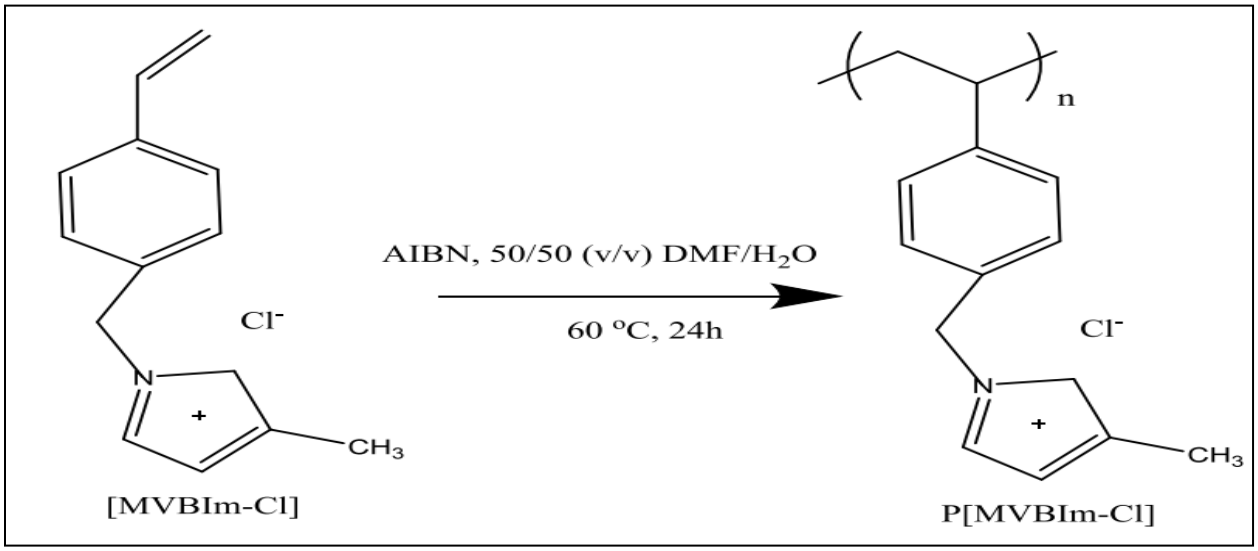

Scheme 4.4 Polymerization of ILs-monomers to prepare P[MVBIm-Cl]

P[MVBIm-Cl] **^{1}H NMR** (400 MHz, ppm, DMSO-d^6, δ): 9.93 (1H, s, N=CH-N), 7.77 (2H, d, N-C<u>H</u>=C<u>H</u>-N), 7.37 (2H, d, Ar-H_{ortho}), 6.42 (2H, d, Ar-H_{meta}), 5.55 (2H, s, N-C<u>H_2</u>-Ar), 3.83 (3H, s, N-CH_3), 1.97 (1H, d, Ar-C<u>H</u>-CH_2, polymerized vinyl), 1.42-1.14 (2H, m, CH_{2sp^3} polymerized vinyl). **FT-IR** (υ/cm^{-1}): 3385 (O-H^- for water residue), 3140 (=C-H_{sp^2}, aromatic & aliphatic), 2928 (N-<u>CH_{3sp^3}</u> & polymerized vinyl), 1658-1426 (C=C &C=N), 1409-1387 (CH_2 & CH_3 bending vibrations in the fingerprint region), 1160-1093 (C-N bending vibration).

4.2.2.3 Anion-metathesis with bis(trifluoromethanesulfonyl)imide lithium salt

Poly[MVBIm-Cl] (460 mg, 1.73 mmol) was dissolved in 10 mL of ultrapure water, and then two separate salt solutions of bis(trifluoromethanesulfonyl)imide lithium salt (LiTFSI 3000 mg, 10.45 mmol) and potassium hexafluorophosphate (KPF_6 3000 mg, 16.29 mmol) were also prepared in 10 mL ultrapure water aliquots. The resulting polymer solution was added drop-wise into each salt to yield a white precipitate. The reaction mixture was then stirred for 16 h at 25 °C and the white precipitate formed in each reaction flask was rinsed with several portions of distilled water until the filtrate was chloride free determined using a silver nitrate test (Scheme 4.5). The products formed were poly[3-methyl-1-(4-vinylbenzyl) imidazolium bis(trifluoromethane)sulfonamide] P[MVBIm-TFSI] (450 mg, 49.44%) and poly[3-methyl-1-(4-vinylbenzyl) imidazolium hexafluorophosphate] P[MVBIm-PF_6] (570 mg, 84.19%).

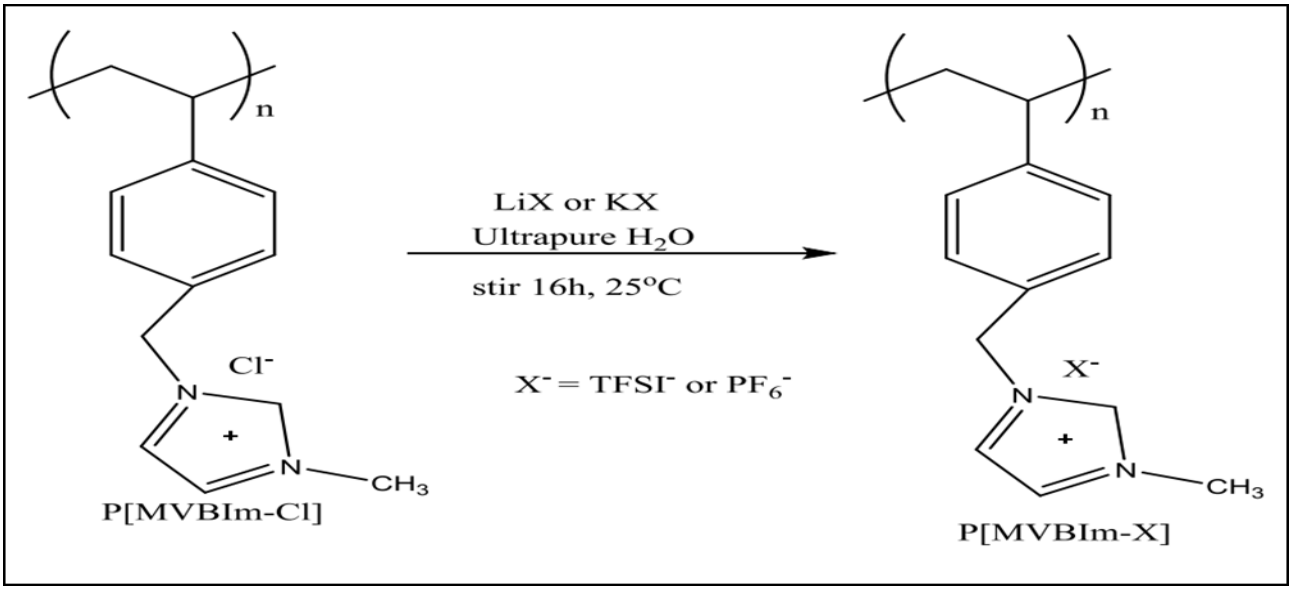

Scheme 4.5 Anion-exchange to prepare P[MVBIm-TFSI] and P[MVBIm-PF6]

P[MVBIm-TFSI] **^{1}H NMR (400 MHz, ppm, DMSO-*d*^{6}, *δ*)**: 9.15 (1H, N-CH=N), 7.68 (1H, N-C$\underline{H}^4$=CH-N), 7.54 (1H, N-CH=C$\underline{H}^5$-N), 6.98 (2H, Ar-H_{ortho}), 6.42 (2H, Ar-H_{meta}), 5.22 (2H, N-CH_2-Ar), 3.86 (1H, Ar-RC$\underline{H}$-CH_2), 1.44 (2H, Ar-RCH-C$\underline{H}_2$ & 3H, N-CH_3).

P[MVBIm-PF$_6$] **^{1}H NMR (400 MHz, ppm, DMSO-*d*^{6}, *δ*)**: 9.17 (1H, N-CH=N), 7.61 (1H, N-C$\underline{H}^4$=CH-N), 7.43 (1H, N-CH=C$\underline{H}^5$-N), 7.02 (2H, Ar-H_{ortho}), 6.43 (2H, Ar-H_{meta}), 5.40 (2H, N-CH_2-Ar), 3.86 (1H, Ar-RC$\underline{H}$-CH_2), 1.44 (2H, Ar-RCH-C$\underline{H}_2$ & 3H, N-CH_3).

4.2.2.4 Anion-exchange with hexafluorophosphate (PF_6^-)

Water insoluble (hydrophobic) PILs were prepared via an anion-exchange of bromide with hexafluorophosphate ion. Briefly, into 50 mL round-bottomed flasks (1.5 g of each repeating polymer units) were prepared in 15 mL ultra-pure water. Another solution of potassium hexafluorophosphate (2.0 g, 10.87 mmol) in 15 mL ultra-pure water was prepared separately. Thereafter the solution of the salt was added drop-wise to the polymer solution upon stirring, and then vigorously stirred for 20 h at room temperature. The resultant product was then rinsed with portions of ultra-pure water to remove all the unreacted species, and then dried in an oven at 40 °C for 5 h. The resulted hydrophobic polymeric materials were; poly(3-propyl-1-vinylimidazolium hexafluorophosphate) P[3P-VImPF_6]and poly(3-isopropyl-1-vinylimidazolium hexafluorophosphate) P[3Isop-VImPF_6].

[3Isop-VImPF$_6$]: **^{1}H NMR** (400 MHz, ppm, DMSO, δ): 9.49 (1H, t, H*d*), 8.19 (1H, t, H*f*), 8.0 (1H, t, H*e*), 7.22 (1H, q, H*c*), 5.97 and 5.44 (split doublets of H*a* & H*b*, respectively), 4.68 (1H, m, H*g*), 1.51 (7H, d, H*h*, *i*). ***FTIR*** (cm^{-1}): 3404 (C-H, 2-position), 3043 (C-H_{sp}^2 of imidazole), 2990-2783 (C-H_{sp}^3, isopropyl), 1653 (C=N), 1079 (C-N).

P[3P-VImPF$_6$]: **^{1}H NMR** (400 MHz, ppm, DMSO, δ): 8.97 (1H, s, H*c*), 7.86 (1H, t, H*d*), 7.52 (1H, t, H*e*), 4.10 (2H, t, H*f*), 3.33 (7H, m, H*a*, *b*), 1.82 (2H, m, H*g*), 0.98 (3H, t, H*b*). ***FTIR*** (cm^-

[1]): 3237 (=C-H 2-position, m), 2910-2818 (C-H_{sp}^3, m), 1564 (C=C & C=N, s), 1331 (methyl, m), 678 (C-N, m).

4.2.3 Synthesis of PILs/MWCNT composites: Functionalized with imidazolium-PILs

PILs/MWCNT composites were synthesized according to previously reported work with minor modifications [222-223]. Briefly, a solution of MWCNTs (200.0 mg) in 17.0 mL DMF and 100.0 mg of each of P[3P-VImBr^-], [3Isop-VImPF_6], P[3P-VImPF_6], or P[3Isop-VImPF_6] PILs in DMF (20 mL) were placed in 100 mL round-bottomed flask. After ultrasonicating for 30 mins at ambient temperature, the reaction mixture was vigorously stirred for 24 h at 50 °C. The unreacted MWCNT residues were removed by centrifugation, and the resultant PIL/MWCNT composites were filtered, thoroughly washed with DMF, ethanol, and ultrapure water, respectively. The composites were then dried in an oven at 90 °C for 12 h before characterization.

4.3 Results and discussion

The synthesis of PILs was carried out via a three-step process which involves the quaternization of 1-vinylimidazole first, polymerization of ILs monomer, and finally the metathesis. Specifically, 3-isopropyl-1-vinylimidazolium-containing PILs were polymerized after anion-

exchange. Resultant polymer systems in this study were very hard sticky-plastic and gel like materials.

4.3.1 Nuclear magnetic resonance of vinyl imidazolium PILs

It was observed that the three protons on the vinyl group were in different chemical environments, resulting in each other having split doublets from coupling with each other [224]. The proton at the second position of imidazolium ring was found to be more deshielded and appeared at downfield as singlet around 8.07 ppm. The presence of bromide halide anion was somewhat extent responsible for some deshielding of protons. It has been reported that bromide counterion normally cause a strong shifts to the ^{1}H atom at the 2-position of imidazolium ring [225]. The protons at the fourth and fifth positions also appeared at downfield as doublets around 7.99 and 7.79 ppm. The protons on the first carbon of the propyl chain appeared as triplet due to coupling with the nearby protons. Multiplets around 2.09-2.00 ppm corresponded to the protons on the second carbon of propyl alkyl chain. Protons on the last carbon of propyl appeared at upfield and shielded around 1.07 ppm. Sharp signals around 2.90-3.01 ppm may be assigned to the DMF residue, which was used as solvent during the synthesis. The ^{1}H NMR results obtained for [3-propyl-1-vinylimidazolium bromide] (APX 4-2) fully agreed with the results obtained by Yang [226].

The polymerized derivative of [3-propyl-1-vinylimidazolium bromide] showed similar but less shielded peaks and some extra-signals due to the absence of vinyl cone π-cloud after polymerization. The proton at the 2-position of imidazolium ring in the polymerized derivative have been deshielded to 9.09 ppm compared to 8.07 ppm of the same proton in the non-polymerized monomer. This 2-position proton was initially shielded by the cone of the π-cloud exhibited from vinyl group in the counter monomer. Owing to polymerization, second-position proton also produces another split doublets around 7.25-7.19 ppm. The individually protons at the fourth and fifth positions of imidazolium ring have triplets around 7.85-7.82 ppm and 7.66-7.63 ppm due to coupling with the proton on the second-position and each other. In addition, the fourth and fifth positions protons also produced extra-split doublets around 5.87-5.85 and 5.49-5.47 ppm, respectively due to polymerization. In the polymer materials, the protons on the first and second carbons of the attached propyl group appeared around 4.28-4.24 ppm as triplet and as multiplet around 2.01-1.92 ppm, respectively.

The important observation and prominent indication of the successful polymerization is the appearance of the polymerized vinyl protons upfield (shielded) around 1.00-0.96 ppm. Signal at 2.78 ppm may be due to the DMF residue. The ^{1}H NMR of hydrophobic poly(3-propyl-1-vinylimidazolium hexafluorophosphate) showed proton signals relatively similar but less

deshielded than those of halide-containing polymer counterpart in this study. For example, signal for the single proton at the 2-position of imidazolium was found at 8.97 ppm, slightly lower than 9.09 ppm observed in halide-containing polymer system. Single protons at 4-, and 5-position of imidazolium were found to have triplets around 7.86-7.84 and 7.52-7.49 ppm, coupled with second-position proton and each other, respectively. Signals corresponding to the two protons on the first propyl carbon were also observed to have triplet around 4.10-3.99 ppm due to coupling with two protons on the second carbon of propyl. Polymerized vinyl moiety protons appeared around 3.33-3.31 ppm due to the effect of aromaticity and deshielding exhibited by imidazolium-nitrogen atom [227]. The ^{19}F-NMR of poly(3-propyl-1-vinylimidazolium hexafluorophosphate) showed coupling constant of $^{1}J_{p\text{-}f}$ = 707.65 Hz (APX 4-4).

The ^{1}H-NMR of 3-isopropyl-1-vinylimidazolium bromide, poly(3-isopropyl-1-vinylimidazolium bromide), and poly(3-isopropyl-1-vinylimidazolium hexafluorophosphate) compounds were obtained and proton signals were assigned and justified. However, the peak at 2.81 ppm in 3-isopropyl-1-vinylimidazolium materials can be attributed to the DMF solvent residue. 3-isopropyl-1-vinylimidazolium materials undergone anion-exchange of bromide to hexafluorophosphate before polymerization and the ^{1}H-NMR of 3-isopropyl-1-vinylimidazolium hexafluorophosphate species and strange new single peak at 3.33 ppm was due to solvent

(DMSO-d_6) residual peak accordingly. Furthermore, the ^{1}H-, ^{19}F-NMR spectra of poly(3-isopropyl-1-vinylimidazolium hexafluorophosphate) were obtained and confirmed successful synthesis of the polymer material, respectively.

4.3.2 FTIR spectra studies of vinyl imidazolium PILs

The FTIR spectra of 3-propyl-1-vinylimidazolium bromide (3P-VImBr) and 3-isopropyl-1-vinylimidazolium bromide (3Isop-VImBr) (APX 4-9), showed medium to weak stretching vibrations around 3412-3359 cm^{-1} corresponding to the (=C-H) bond of imidazolium rings resulting from the Fermi resonance effect of the C-H vibrations with the in-plane ring deformations [227]. C-H_{sp}^{2} stretching vibrations between 3123-3098 cm^{-1} can be ascribed to vinyl group methylene. The stretching vibrations around 2976-2879 cm^{-1} were assigned to the (C-H_{sp}^{3}) of propyl and isopropyl groups' components. Methyl and methylene bending vibrations in the region 1455-1415 and 1499-1496 cm^{-1} were assigned to propyl, isopropyl and vinyl moieties, respectively. Strong to medium stretching vibrations in the region 1655-1546 cm^{-1} were ascribed to be (-C=C-, C-N, and -C=N-) bands which overlapped with each other. Other important and strong bending vibrations around the fingerprint region (1108-1102 cm^{-1}) can be ascribed to (C-N) and in-plane bending vibrations of (C-H) on the imidazolium ring [228].

On the other hand, poly(3-propyl-1-vinylimidazolium bromide) P[3P-VImBr] and poly(3-isopropyl-1-vinylimidazolium bromide) P[3Isop-VImBr] showed relatively similar bands compared to their corresponding non-polymerized monomers except for notable changes due to polymerization. For instance, well-pronounced C-H_{sp}^3 stretching vibrations around 2940-2878 cm^{-1} were ascribed to the propyl and isopropyl moieties and the polymerized vinyl group. Another important observation is the shifting of the (C-H) band at second-position to higher wavelength regions. In the polymer materials the (-C=C-) and (-C=N-) stretching vibration appeared to be stronger and sharp around 1655-1654 cm^{-1}, signifying the absence of vinyl π-bond. The disappearance of the stretching vibrations at 3098 cm^{-1} confirmed the polymerization and disappearance of π-bond in the vinyl group. In the hexafluorophosphate containing polymer materials, P[3P-VImPF_6] and P[3Isop-VImPF_6] shows relatively similar but lower-frequency shifted bands. Generally, the presence of bromide anion usually shifts the IR frequencies of functional groups towards the high region (away the fingerprint region). However, that shifting can be easily noticed on the bromide-containing imidazolium derivatives in this study. Moreover, after anion-exchange all the bands corresponding to P[3P-VImPF_6] and P[3Isop-VImPF_6] appeared in lower regions due to the absence of bromide anions. Hexafluorophosphate species in hydrophobic polymer systems appear around 839-847 cm^{-1}, signifying successful anion-metathesis.

4.3.3 Thermogravimetric analysis of vinyl imidazolium PILs

TGA curves of vinyl imidazolium-PILs are presented in Fig. 4.1. Generally, thermal and glass transition temperatures of polyelectrolytes were influenced by both the cationic substituents, counterion changes and the alkyl lateral chain [227]. However, imidazolium-based polyelectrolytes containing halides (Br^- or Cl^-) counter ions normally exhibited poor thermal stabilities compared to their hydrophobic counterion-containing analogues [245-246]. As shown in Fig. 4.1, bromide-containing PILs showed slight weight loss (<5%) below 100 °C which was due to the loss of moisture content from the hygroscopic PILs. However, beside the loss of moisture degradation, vinyl imidazolium-based PILs containing bromide counterion showed a unimodal degradation profile ranging from 300-350 °C. On the other hand, the hexafluorophosphate containing analogues showed onset of decomposition from 350-400 °C. To confirm the hydrophobicity and thermal stability of hexafluorophosphate analogues, no significant weight loss was observed below 100 °C [228] and all showed simple one-step degradation profile.

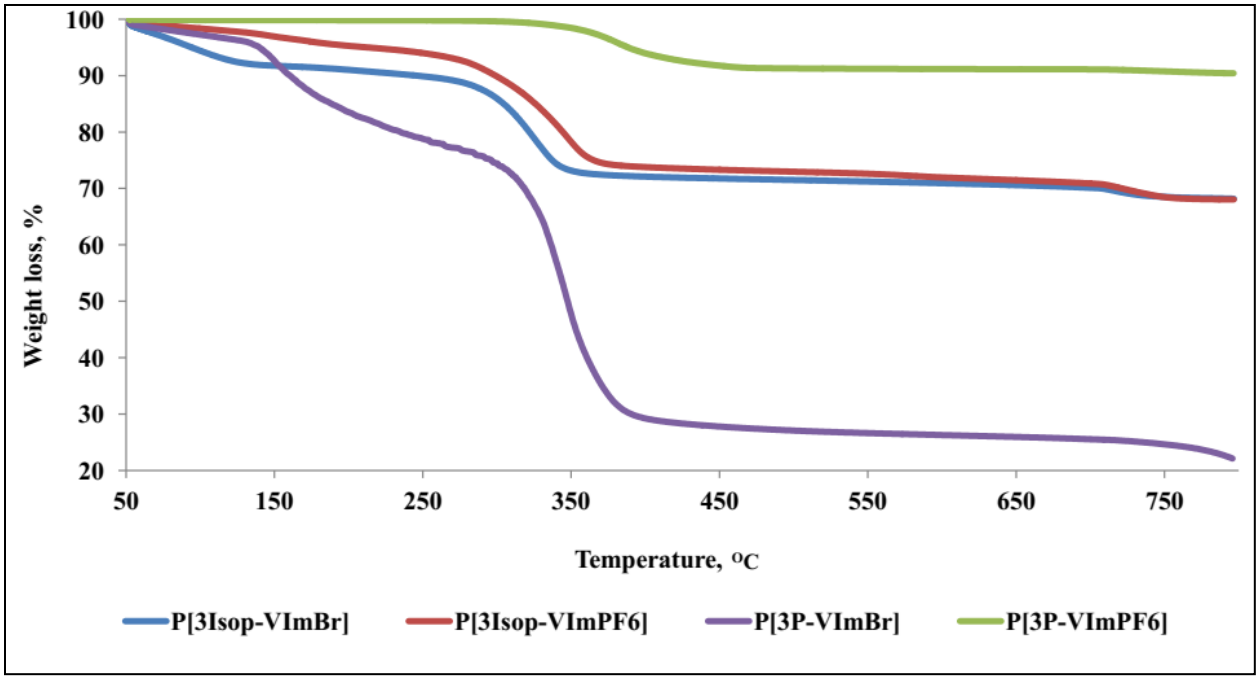

Figure 4.1 TGA profiles of vinyl imidazolium-based PILs

.

4.3.4 Characterization of styrenic imidazolium-PILs

The imidazolium-based PILs with styrenic polymerizable moiety were prepared via the free radical polymerization of the corresponding ILs-monomer. The method used involved three (3) steps: (I) synthesis of the corresponding imidazolium-based ILs monomer by the reaction of 1-alkylimidazole and vinyl benzyl chloride, (II) free radical polymerization of the resultant ILs-monomer bearing styrenic polymerizable group, and lastly the anion-metathesis reaction involving the replacement of chloride with the large bulky anions [bis(trifluoromethane)sulfonamide or hexafluorophosphate]. Hard sticky-plastic like polymer

P[MVBIm-Cl] was produced and showed poor solubility in most solvents except DMSO. When P[MVBIm-Cl] was heated it showed moulded or plasticity character. P[MVBIm-PF_6] and P[MVBIm-TFSI] were obtained by anion-exchange reaction at room temperature. The replacement of hydrophilic anion (Cl^-) with more hydrophobic anions (PF_6^- and $TFSI^-$) resulted in imidazolium-based homopolymers with relatively high hydrophobicity and increased water-insolubility.

4.3.4.1 FTIR spectra studies of styrenic imidazolium-PILs

In the FTIR spectrum of the ILs-monomer MVBIm-Cl, a broad stretching vibration at 3371 cm^{-1} was ascribed to the possible intermolecular hydrogen bonding between chlorine and hydrogen atom of the imidazole ring (C-H----Cl, known as chlorine-hydrogen interionic bonding) [229-230]. The vibrational bands in the region 3054-3012 cm^{-1} were ascribed to the unsaturated aromatic and alkene (=C-H_{sp}^2) on the imidazole and styrenic components. The stretching vibration at 2829 cm^{-1} was ascribed to the saturated methyl (CH_{3sp}^3) attached to the imidazole ring at 3-position. Multiple bands (medium-weak) around 1628-1408 cm^{-1} were ascribed to the aromatic (-C=C- & -C=N-) of the imidazole ring and styrenic species. Other multiple vibrations in the region 1449-1333 cm^{-1} were attributed to the CH_2 and CH_3 bending vibrations in the fingerprint region. The absorption bands observed around 1159-1017 cm^{-1} were ascribed to (C-

N) bending vibration. However, after polymerization of the styrenic moiety only few characteristic absorption bands have emerged which indicated successful polymerization. In the FTIR spectrum of P[MVBIm-Cl], the medium to weak vibrational bands around 2928-2856 cm^{-1} were ascribed to the polymerized vinyl moiety on the styrene confirms polymerization and saturation of the vinyl moiety. Even though most of the vibrational bands were similar to those of the ILs-monomer beside the differences in relative intensity, the multiple bands (CH_2 and CH_3) observed shifted slightly after polymerization due to the absence of the vinyl cone-shielding in the resultant polymer materials. After anion-exchange of Cl^- with $TFSI^-$and PF_6^-, almost similar peaks were observed except the slightly shifting of the peaks due to the replacement of the halogen in both P[MVBIm-TFSI] and P[MVBIm-PF_6], respectively. Additionally, the peak at 819 cm^{-1} was ascribed P-F bond stretching vibration in P[MVBIm-PF_6] polymer confirming the successful anion-exchange with hexafluorophosphate [230].

4.3.4.2 Nuclear magnetic resonance (NMR) spectroscopy analysis of styrenic imidazolium-PILs

In the proton NMR of [MVBIm-Cl], protons feel different magnetic field strength owing to the location and the neighboring atoms directly attached. The protons attached directly to the aromatic rings and vinyl moieties were deshielded due to the less electron density caused by high electronegative atom, and the aromatic ring π-system. On the other hand, the high electron

density and weaker magnetic field environment of the third-position alkyl group resulted in the protons being shielded [220-221]. The proton NMR of P[MVBIm-Cl] showed similar chemical shifts except the protons on the vinyl portion of styrene which have been shifted upfield (shielded), owing to the absence of the vinyl π-systems due to polymerization of vinyl benzyl group [230]. The ^{13}C NMR spectra were obtained for ILs-monomer and polymerized ILs. As it was expected, carbon atoms on the aromatic rings and alkene moiety in the ILs-monomer appeared downfield due to the reduced electron density and $C{=}C_{sp^2}$-hybridization. However, the sp^3 hybridized carbon atoms at the first and third positions of the ILs-monomer appeared upfield owing to their $C\text{-}C_{sp^3}$ and $N\text{-}C_{sp^3}$ hybridizations. On the other hand, to corroborate the successful polymerization, the vinyl group carbon atoms in the polymerized system appeared upfield with $C\text{-}C_{sp^3}$ hybridizations [221, 230]. In addition, after anion-exchange of chloride with either $TFSI^-$ or PF_6^-, the ^1H NMR spectra of hydrophobic polymer materials showed relatively less deshielded chemical shifts due to the absence of chloride ion, respectively. The ^{31}P NMR spectrum of P[MVBIm-Cl] have multiplet (m) between -130 to -158 ppm confirming the presence of phosphorous atom coupled with six fluorine atoms. On the other hand, ^{19}F NMR spectrum was found to contain doublets (d) between -69 to -71.0 ppm which also confirmed the coupling of six fluorine atoms with one phosphorous atom with similar average coupling constant of $^1J_{P\text{-}F}$ = 704.43 Hz.

4.3.4.3 Thermogravimetric analysis of styrenic imidazolium-PILs

Styrenic imidazolium-based PILs showed relatively varied degradation profiles owing to both the cationic poly(styrenic) backbone and counter ions involved. In the chloride-containing PILs, weight loss (<5%) below 150 °C was due to the loss of moisture content from hygroscopic polyelectrolytes (Fig. 4.2). However, a continuous degradation from 150 °C and total (final) decomposition around 450 °C in all chloride-containing PILs was observed and due to low thermal stability and hygroscopic character of these PILs. In comparison, PF_6^- and $TFSI^-$-containing PILs showed no weight loss below 350 °C, which indicated their high thermal stability and hydrophobic character of the materials. The styrenic imidazolium-PILs with PF_6^- and $TFSI^-$ counter ions appeared more thermally stable and possibly decompose differently [227]. A two-steps (multimodal) degradation profile in PF_6^--containing PILs corresponded to the removal of counterion (PF_6^-) first (onset of decomposition ~350 °C), followed by the removal of poly(styrenic) backbone (second decomposition ~450 °C) [228]. However, the unimodal (one-step) decomposition of $TFSI^-$-containing PILs indicated that they are thermally stable which could be attributed to only the decomposition of poly(vinyl benzyl) backbone [227-228].

The nucleophilic character of Cl^- and the presence of *N*-alkylimidazole as a good leaving group seem to facilitate the S_N^2 displacement of the *N*-alkylimidazole via nucleophilic substitution

pathway [246]. Nucleophilic displacement of *N*-alkylimidazole by Cl^- nucleophilic attack revert back to poly(vinyl benzyl) chloride (PVBCl) and *N*-alkylimidazole, respectively. Thermal and glass transition temperatures are presented in Table 4.1. It showed that the glass transition temperatures (T_g) of polyelectrolytes studied were influenced by the type or size of counterion involved. For instance, the halide-containing PILs showed higher glass transition temperatures than their hydrophobic counter ion analogues, in the decreasing order $Cl^- \geq Br^- > PF_6^- > TFSI^-$ [228]. This therefore confirmed the general literature finding which suggestes that the larger the counterion size, the smaller the glass transition temperature [58, 228]. Generally, PILs anions act as plasticizers in plasticizing the PILs which normally depress the T_g [58].

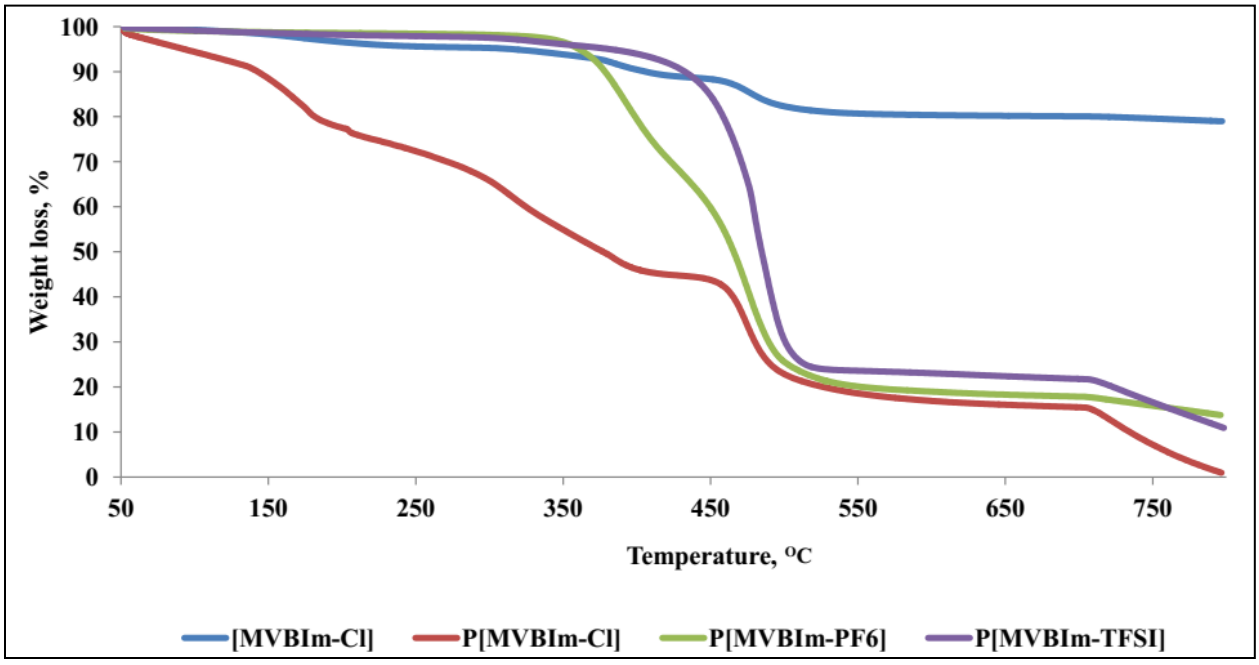

Figure 4.2 TGA profiles of styrenic imidazolium-based PILs

Table 4.1 Thermal and glass transition temperatures of vinyl and styrenic imidazolium PILs

Sample	T_{decomp} (°C)	T_g (°C)
P[3P-VImBr]	345	125
P[3Isop-VImBr]	320	138
P[3P-VImPF_6]	400	79
P[3Isop-VImPF_6]	350	57
[MVBIm-Cl]	355, 450	146
P[MVBIm-Cl]	270, 451	129
P[MVBIm-PF_6]	350, 450	53
P[MVBIm-TFSI]	451	15

4.3.4.4 Thermogravimetric analysis of vinyl imidazolium-PILs/MWCNT composites

TGA curves of some vinyl imidazolium-based PILs/MWCNT composites are shown in Fig. 4.3. Though the composites showed good thermal stability and hydrophobic character, a slight onset of decomposition around 250-350 °C can be seen and it was attributed to the degradation of organic PIL materials from the composites [240]. Another significant and common weight loss in polymer-functionalized derivatives above 700 °C can be attributed to the decomposition of carbon materials released during temperature scan under airflow condition. Based on percentage

weight loss, only <15% of the composites was decomposed and was probably attributed to the PIL moieties in all composites, respectively [240].

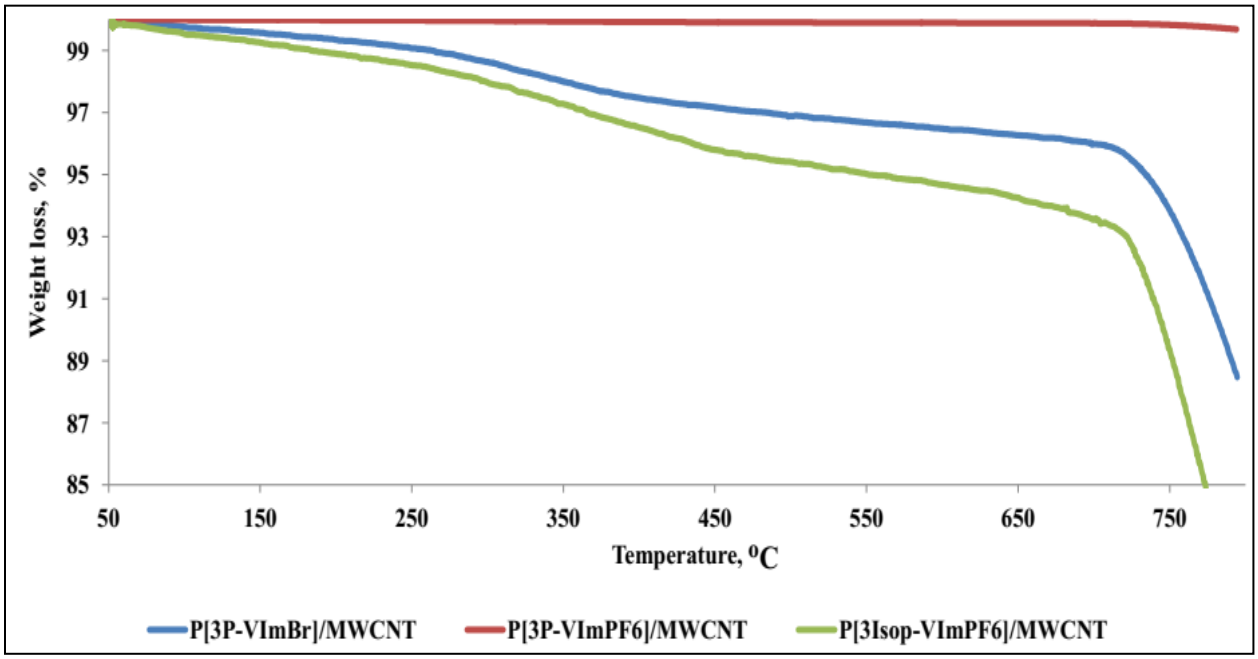

Figure 4.3 TGA profiles of some vinyl imidazolium-based PIL/MWCNT composites

4.3.4.5 FTIR spectroscopy of vinyl imidazolium-PIL/MWCNT composites

The weak absorption bands around 1239 cm^{-1} were assigned to the C-O and carboxylic/graphitic (C=C) domains in MWCNTs. The medium stretching band at 1751 cm^{-1} can be attributed to C=O on the surface of MWCNTs. However, in the [3Isop-$VIm^{+}PF_6^{-}$]/MWCNTs composite, the C=O stretching band was shifted to 1636 cm^{-1} suggesting the formation of amide bonds [232]. Beside in the corresponding ILs and [3Isop-$Vim^{+}PF_6^{-}$]/MWCNTs, the PILs-based MWCNTs composites showed completely different and new functionalities after functionalization. The

appearance or emerging of new absorption bands around 2324-2307 and 1240-1074 cm^{-1} ascribed to C-N and C=N is the complete evidence of the successful coating of polymer materials on the surface of MWCNTs.

4.3.4.6 Scanning electron microscopy/Energy-dispersible X-ray spectroscopy (SEM/EDS) analysis of vinyl imidazolium-PILs/MWCNT composites

In order to elucidate and study the surface morphology of the PILs/MWCNT composites, the samples were viewed under SEM using exceptionally low magnifications. It has been reported that MWCNTs usually showed tangled tubes with diameter range 100-200 nm (determined using TEM) [231]. However, some CNTs in this study revealed long and stripe-like nanostructures having the diameter of 17.23 nm with zigzag edges (Fig. 4.4). In addition, the MWCNTs produced were randomly mixed due to the synthetic method used, which makes their structural orientation different from those produced by growing them on a substrate by chemical vapor deposition (CVD) [232]. It can be observed from the SEM images that PILs were deposited on the surface of MWCNTs (Fig. 4.6A-B) [233]. Moreover, it was revealed that the surface functionalization of MWCNTs with PILs does not alter the surface morphology, but rather increased the diameter of the CNTs with cylindrical nanotubes were observed [234-235]. Due to the weak bond-formation between polymer materials and carbon nanotubes, the polymer/CNT

composites normally shows dispersion facilitated by weak *van der Waals* and electrostatic forces [235]. To elucidate the elemental composition of the composites, EDS spectra were obtained (Fig. 4.7). The EDS mappings showed that the samples are mainly composed of carbon and bromide. The intensity of the carbon peak in the EDS spectra confirmed the successful synthesis of carbon materials [234]. However, the presence of phosphorous and fluorine in P[3P-VIm^{+}PF$_6^{-}$], P[3Isop-VIm^{+}PF$_6^{-}$], and [3Isop-VIm^{+}PF$_6^{-}$] samples is as a results of counter-anion exchange.

4.3.4.7 Transmission electron microscopy (TEM) analysis of vinyl imidazolium-PIL/MWCNT composites

TEM micrographs of pure MWCNTs showed hollow tubular nanostructures [236]. However, some TEM micrographs (Fig. 4.8 and 4.9) showed PIL materials coated on the termini and insides of the elongated tubes. Complementary to the SEM results, the TEM micrographs showed that the surface of the MWCNTs was homogeneously covered by polymer materials, resulting in an increased surface (diameter) of the MWCNTs [236].

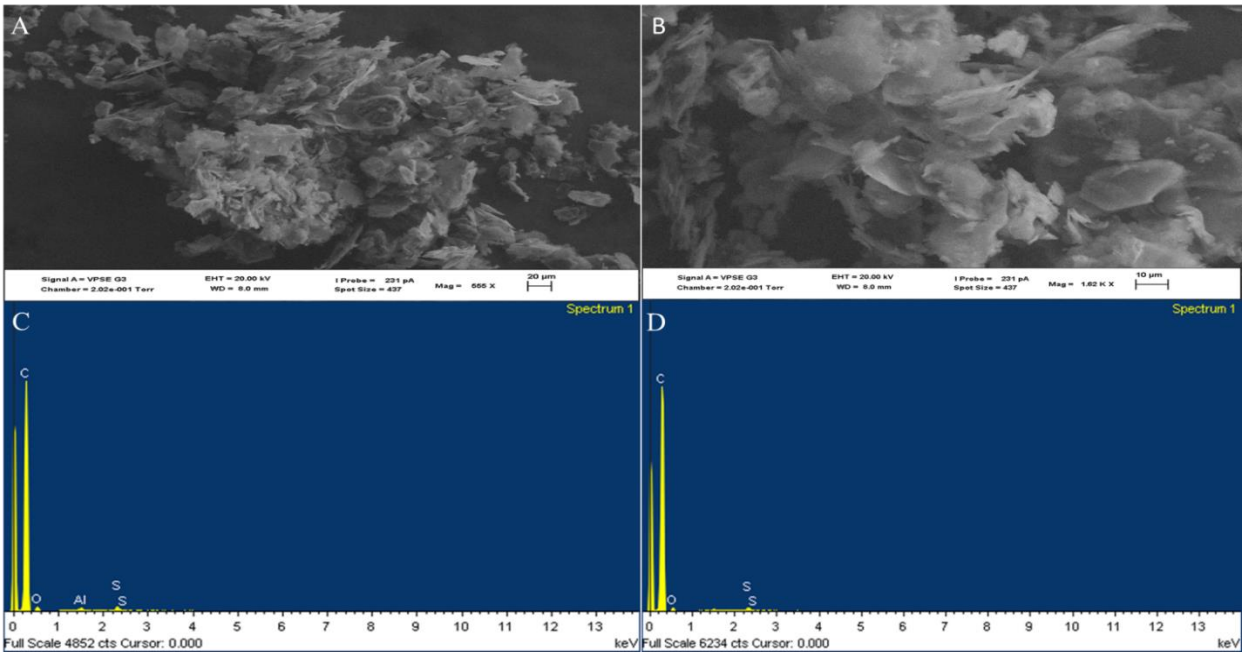

Figure 4.4 SEM (A & B) images and EDS (C & D) spectra of MWCNTs

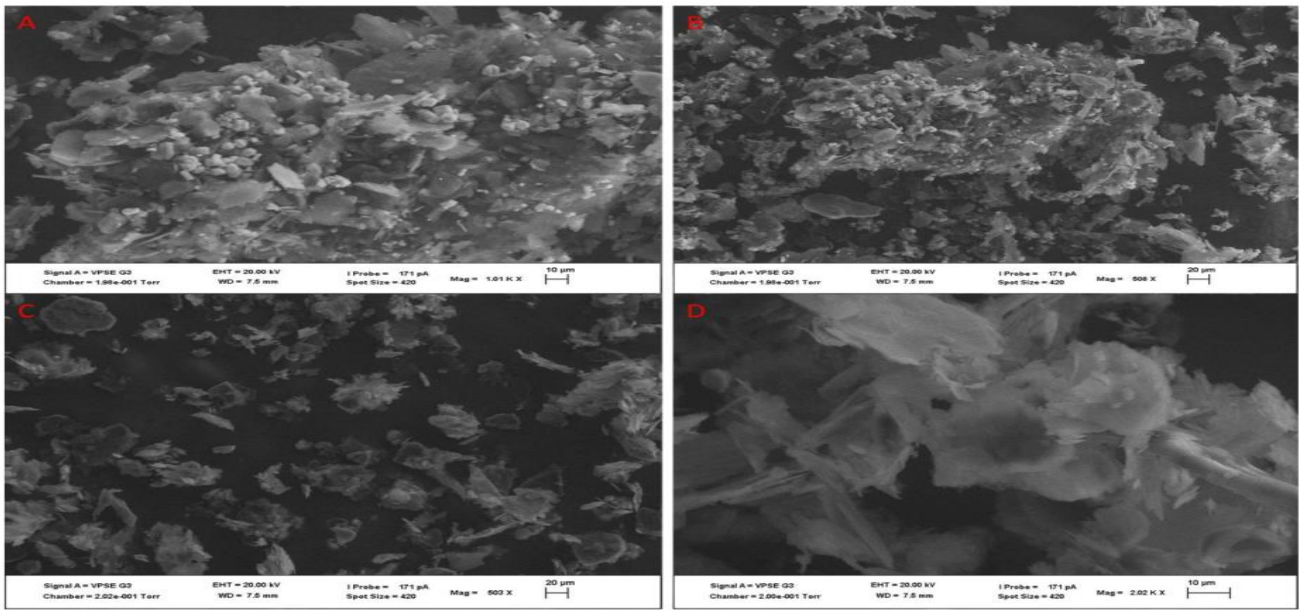

Figure 4.5 SEM images of P[3Isop-VImPF6]/MWCNT (A-B), and [3Isop-VImPF6]/MWCNT (C-D) composites

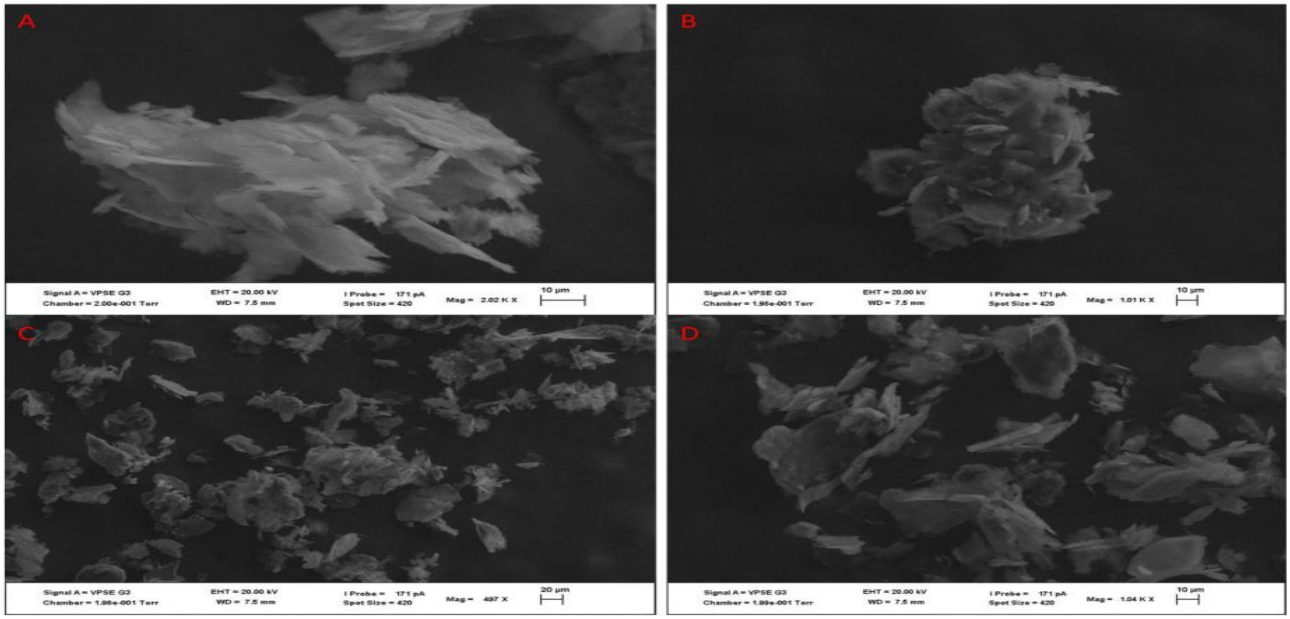

Figure 4.6 SEM images of P[3P-VImBr]/MWCNT (A-B), and P[3P-VImPF6]/MWCNT (C-D) composites

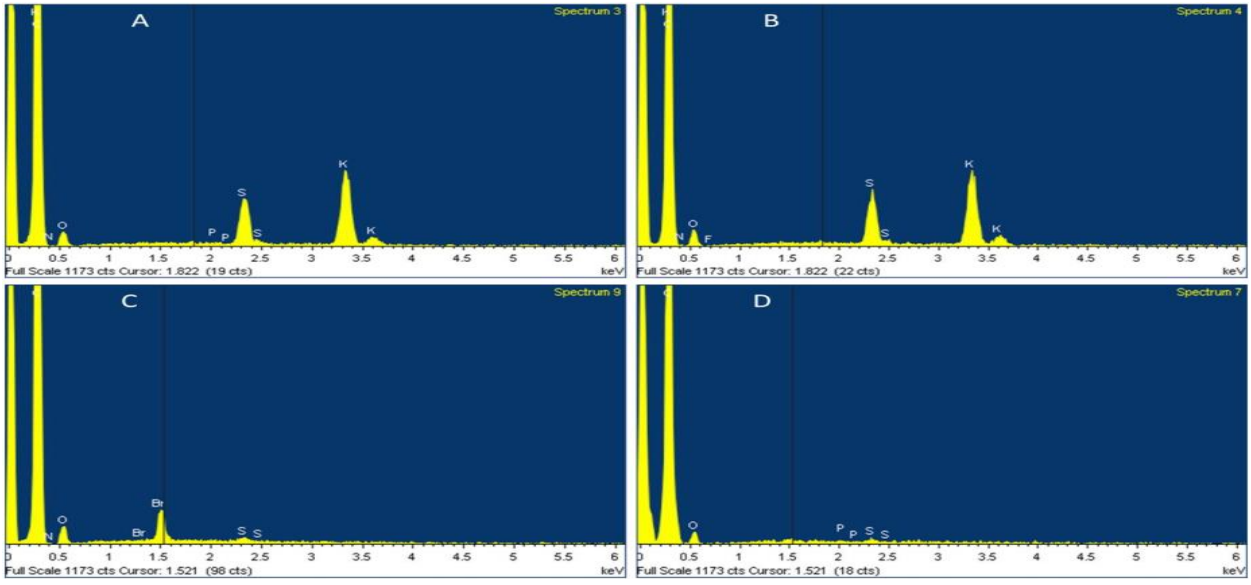

Figure 4.7 EDS spectra of P[3Isop-VImPF6]/MWCNT (A), [3Isop-VImPF6]/MWCNT (B), P[3P-VImBr]/MWCNT (C), and P[3P-VImPF6]/MWCNT (D) composites

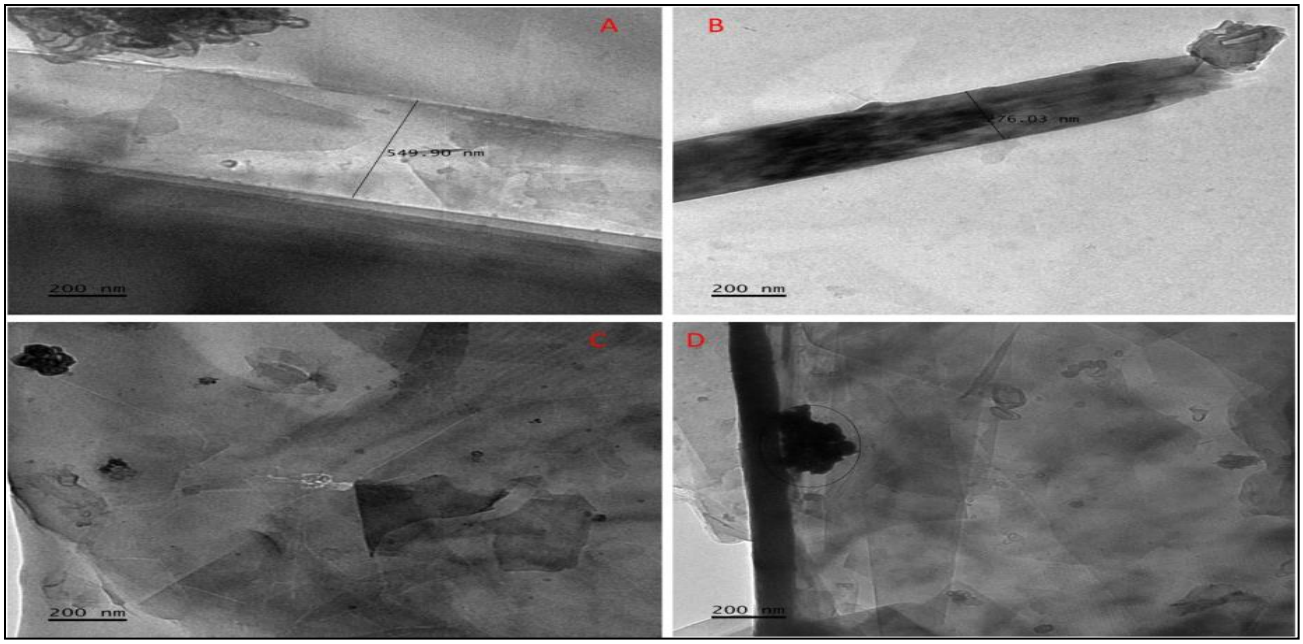

Figure 4.8 TEM micrographs of P[3P-VImBr]/MWCNT (A-B), and P[3P-VImPF6]/MWCNT (C-D) composites

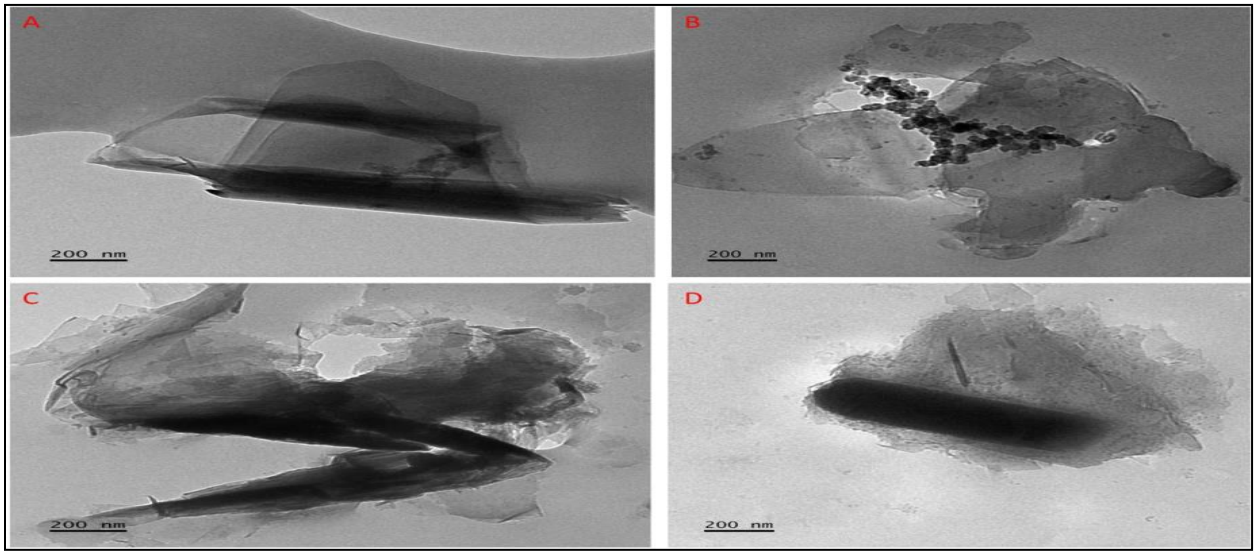

Figure 4.9 TEM micrographs of [3Isop-VImPF6]/MWCNT (A-B), and P[3Isop-VImPF6]/MWCNT (C-D) composites

4.3.5 Characterization of styrenic imidazolium-PILs/MWCNT composites

4.3.5.1 Thermogravimetric analysis of styrenic imidazolium-PILs/MWCNT composites

Styrenic imidazolium-PIL/MWCNT composites showed very good thermally stable character throughout heating (Fig. 4.10). However, a thermal decomposition between 250 and 450 °C, particularly in P[MVBIm-Cl]/MWCNT, was due to degradation of less thermally stable hydrophilic PILs moieties attached onto the surface of MWCNTs. Comparatively, the PIL/MWCNT composites containing hydrophobic counter ions showed relatively good thermal stability and only ~10% was lost. Strong ionic electrostatic interactions between oppositely charged ions, anion-π and/or cation-π interactions were believed to have played a crucial role in thermal stability of PIL/MWCNT composites.

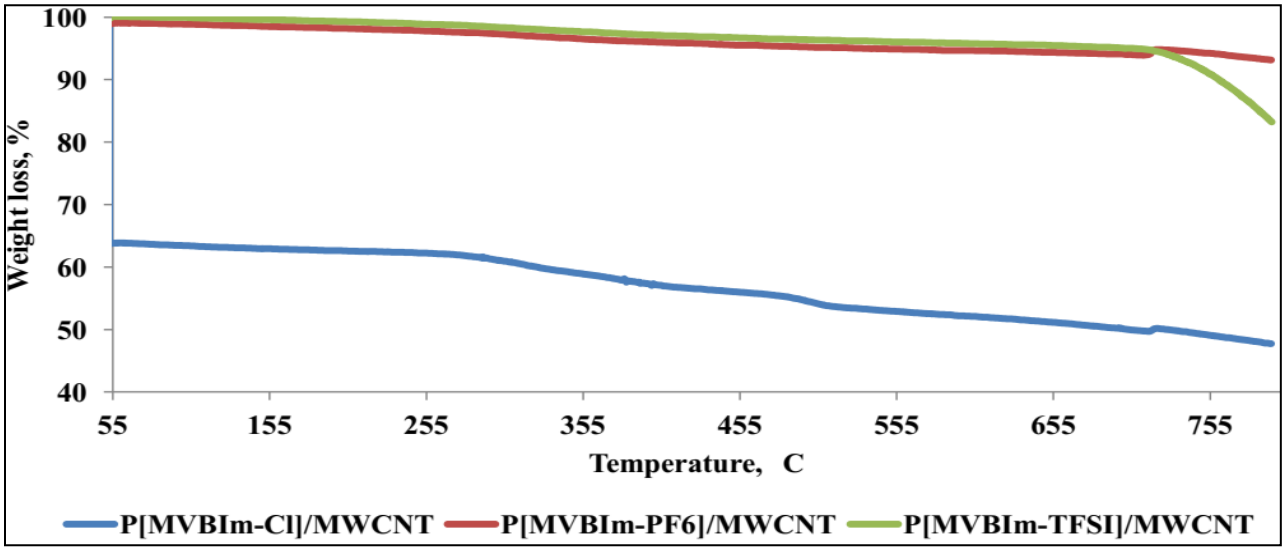

Figure 4.10 TGA profiles of some styrenic imidazolium-based PIL/MWCNT composites

4.3.5.2 FTIR spectra studies of styrenic imidazolium-PILs/MWCNT composites

Comparatively, the FTIR spectrum of MWCNTs showed absorption band around 1751 cm^{-1} which was ascribed to aromatic ring stretching vibration. Vibrational band around 1239 cm^{-1} was due to the presence of carboxylic group (-COOH) and graphitic moieties on the surface of MWCNT. The obtained FTIR absorption bands of MWCNTs agreed with those obtained in the literature [237]. Furthermore, the FTIR data of PIL/MWCNT composites showed completely different functional groups due to the chemical interactions between polymers and graphitic moieties of carbon nanotubes. For example, though the FTIR functional peaks of pure MWCNTs and PIL-functionalized carbon material derivatives oscillate around similar regions, minor frequency distortions or shifting due to the possible PIL-carbon material interactions were observed. Additionally, the appearance of vibrational bands around 1635 cm^{-1} in some PIL/MWCNT composites also confirmed the presence of aromatic rings within the composites.

4.3.5.3 SEM and EDS analysis of styrenic imidazolium-PILs/MWCNT composites

The surface morphologies of imidazolium-styrenic based PILs were obtained and are shown in Fig. 4.11. The SEM images of PILs showed relatively smooth-rough surface of hardy plastic materials. The hardening behaviour of polymer materials caused by cooling could be the ultimate reason for this latter surface morphology. It has been observed in this work that polymer

materials to behave elastic or behave like a plastic at high temperatures, while hardening at lower or room temperature. Additionally, the EDS data showed the elemental composition of each polymer material (Fig. 4.11). For instance, the presence of certain elements such as C, N, Cl, F, O, S, and P assertion or confirmed the successful coordination of imidazolium counter cation together with the Cl^-, $TFSI^-$ or PF_6^-, respectively. On the other hand, the surface modification of carbon materials with polymers was further investigated by utilizing SEM/EDS technique. As shown in Fig. 4.12, SEM images revealed well-dispersed CNT flakes with curved-like morphology. Comparatively, some PIL/MWCNT composites showed fairly clustered-together carbon nanotubes due to the hardening of PIL materials right on the surface of carbon materials. As it was expected, the EDS spectra of PIL/MWCNT composites feature the elements such as C, N, Cl, F, O, S, and P, which therefore confirmed the successful incorporation of PILs and carbon nanotubes. The carbon content in all EDS spectra also confirmed the presence of carbon nanotubes and imidazolium-styrenic PIL systems.

TEM micrographs of styrenic-imidazolium PIL/MWCNT composites are presented in Figs. 4. 13-4.15. TEM analysis revealed that the surface of the MWCNTs was modified by amorphous polymer materials into various tubular, elongated and spherical orientations with cavities and voids [236]. Although some agglomerated carbon nanotubes are observed (Fig. 4.13), some

polymer materials were seen to be coated and debundling the surface of carbon nanotubes [236]. However, in this work, the possible agglomeration of carbon nanomaterials was minimized by covering of the carbon nanotubes surface with PIL materials. The rough and porous structural morphology of these PIL/MWCNT composites helps to enhance and facilitate solid-liquid adsorption process.

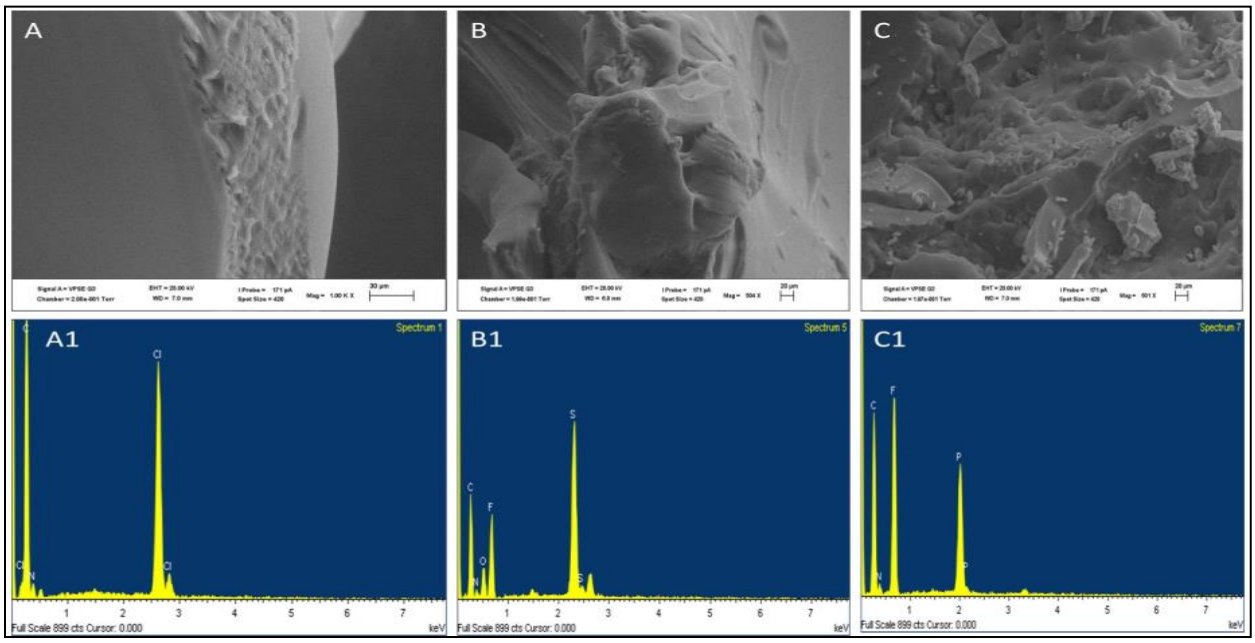

Figure 4.11 SEM images/EDS spectra of styrenic-imidazolium based PILs. P[MVBIm-Cl] (A-A1), P[MVBIm-TFSI] (B-B1), and P[MVBIm-PF6] (C-C1)

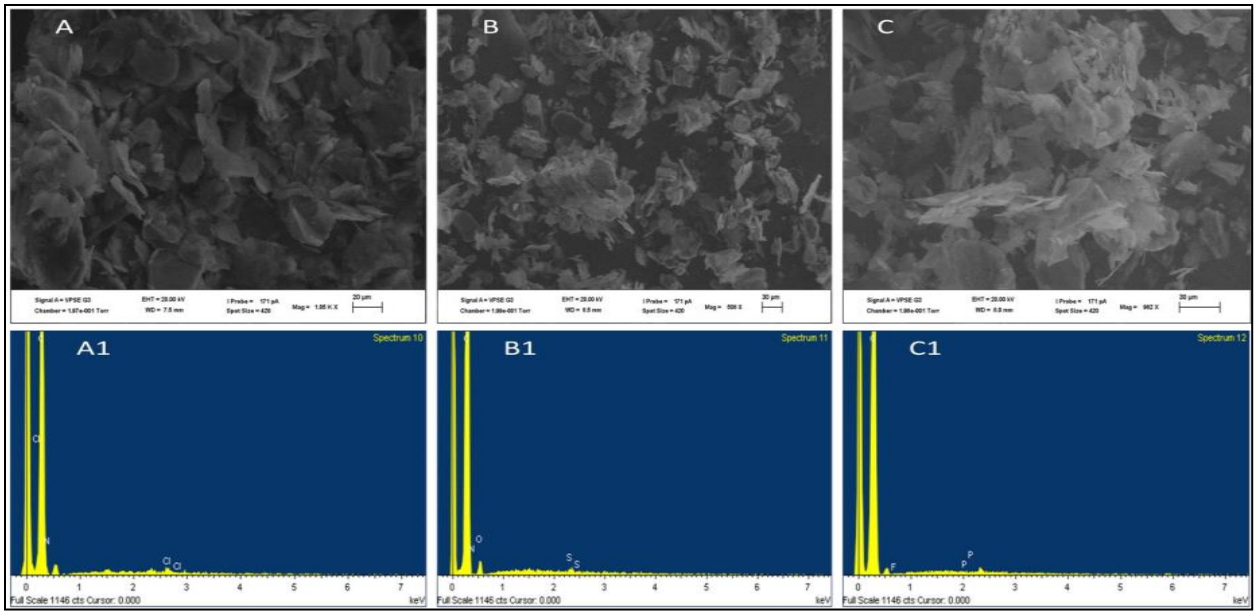

Figure 4.12 SEM images/EDS spectra of styrenic-imidazolium based PILs. P[MVBIm-Cl] (A-A1), P[MVBIm-TFSI] (B-B1), and P[MVBIm-PF6] (C-C1**)**

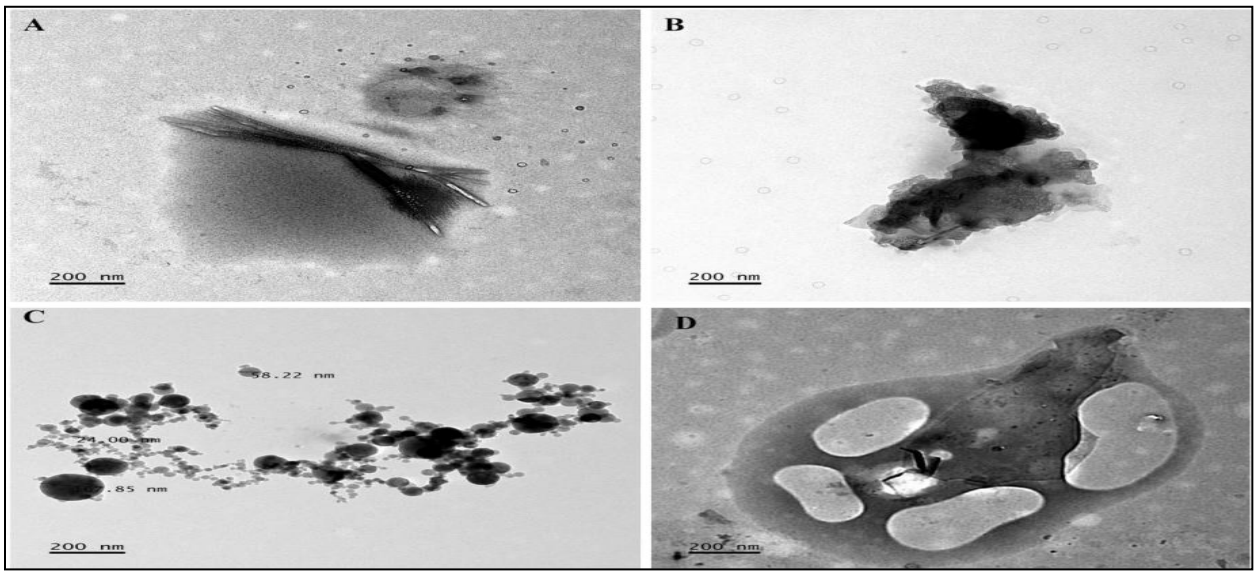

Figure 4.13 TEM micrographs of P[MVBIm-Cl]/MWCNT composites

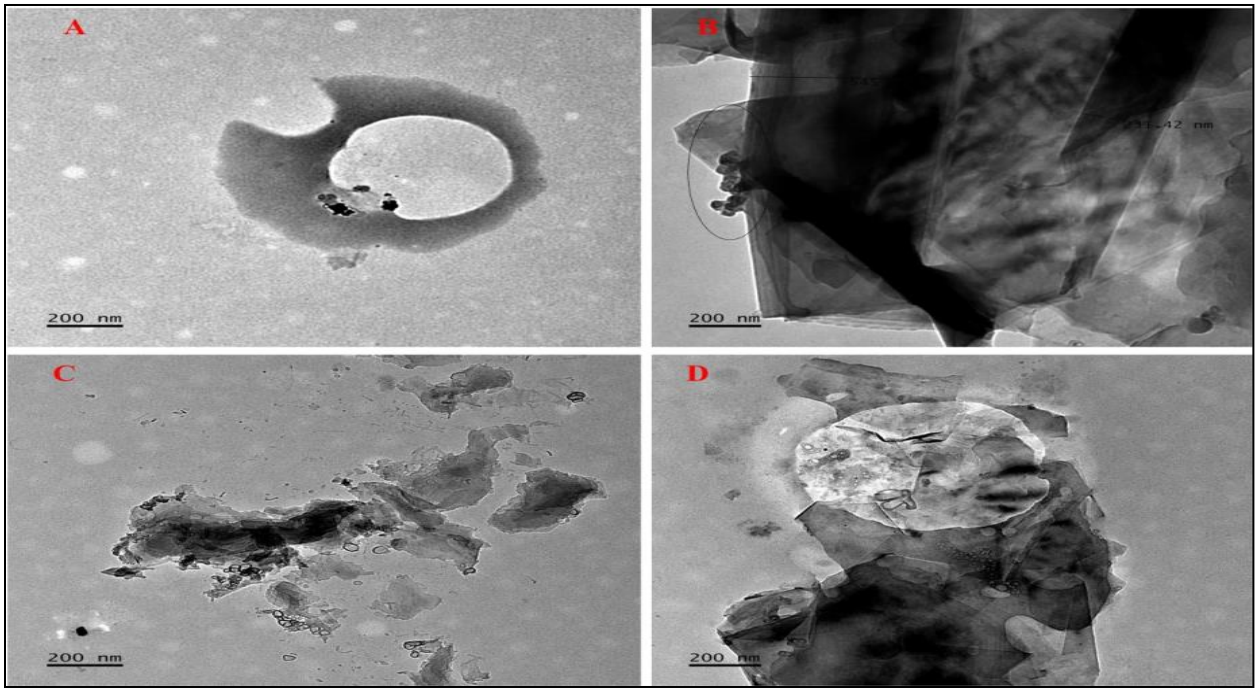

Figure 4.14 TEM micrographs of P[MVBIm-TFSI]/MWCNT composites

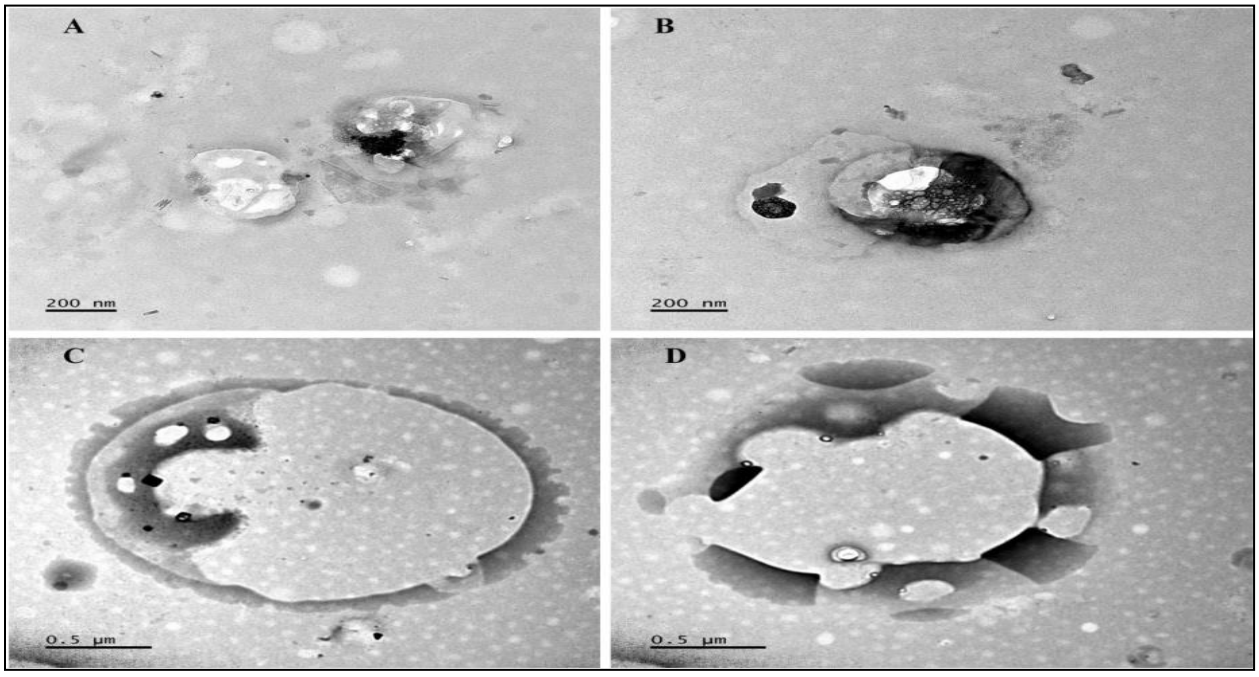

Figure 4.15 TEM micrographs of P[MVBIm-PF_6]/MWCNT composites

4.4 Chapter summary

In this chapter, imidazolium-containing PILs possessing vinyl and styrenic polymerizable moieties were synthesized and discussed. NMR and mass spectrometry were collected and the results obtained confirmed successful synthesis and purity of PILs materials. The FTIR spectra studies of all PILs containing hydrophobic anions showed that the characteristic vibrational bands appeared in low frequency region, confirming successful replacement of halide with bulky-hydrophobic anions. On the other hand, microscopic analyses revealed that modification of CNTs with amorphous polymer materials did not alter the surface morphology of carbon nanotubes. TEM images showed tubular and spherical elongated orientations of PILs/MWCNT composites. The structural cavities and voids noticed are very important for solid-liquid adsorption of metal ions.

CHAPTER FIVE

ADSORPTION STUDIES OF HEXAVALENT CHROMIUM SPECIES USING IONIC LIQUIDS AND POLYMER-FUNCTIONALIZED CARBON NANOTUBES AS ADSORBENTS

Chapter 5

5.1 Background on adsorption of Cr(VI) using ILs and PILs/MWCNT composites

Chromium exists in aqueous medium either as Cr(III) and/or as anionic Cr(VI) in the form of dichromate ($Cr_2O_7^{2-}$), hydrochromate ($HCrO_4^-$), or chromate (CrO_4^{2-}) depending on the pH and concentration of the solution [215, 253]. It has been reported that hexavalent chromium is 100-fold more toxic than the trivalent moiety (Cr (III)), especially in the oxidized forms [254]. Hexavalent chromium have been classified as carcinogenic towards humanity, and some worldwide organizations/countries including South Africa have recommended a maximum of 0.005 $mg \cdot L^{-1}$ level as the Cr(VI) limit in potable waters [255]. However, long term exposure of hexavalent chromium levels over 0.1 ppm can also cause cell disorder, respiratory problems, liver and kidney damage [256].

Several conventional methods such as coagulation and precipitation, membrane filtration have been developed and used to remove hexavalent chromium from industrial effluents [7, 257]. However, these methods possess several limitations such as high operation cost, chemical sludge, and low output which hinder their applicability so far. [7]. On the other hand, adsorption process has received considerable attention due to its effectiveness, ease of generation, and

economic viability [8]. Recently, the use of polymer materials as adsorbents to remove various metal ions from wastewater has been the subject of review. Kumar *et al*. [9-10] reported the use of polyaniline and aniline-formaldehyde condensation polymers to remove hexavalent Cr(VI) from wastewater. They observed that the removal of chromium species from wastewater was due to the electrostatic interactions between the chromate species and protonated polymer materials via the reduction of Cr(VI) to Cr(III). Based on the current literature, poly(4-vinylpyridine) N-alkyl quaternized polyelectrolyte materials with shorter alkyl chain length are water-soluble and inappropriate for removal of metal ions such as Cr(VI) from aqueous solution [216-217].

Functionalization with polymer materials helps to increase the surface area, dispersibility, reduces water solubility of CNTs and makes them more thermally stable [16, 220, 258]. The efficiency and feasibility of an adsorbent to be utilized in metal ions adsorption depends on the morphological structure and characteristics of the material, which provides ability to attract metal ions. However, the coating of ILs and PILs on the surface of CNTs offers more thermally stable and insoluble composites with completely new functionalities. Furthermore, the presence of asymmetrically coordinated counter-ions of imidazolium and pyridinium as part of carbon nanotubes is believed to be very crucial in Cr(VI) adsorption efficiency of the composites via electrostatic interactions. Owing to the properties of ILs, PILs, and their CNTs composites, in

this chapter, Cr(VI) was removed from aqueous solution using the as-synthesized ILs and PILs-CNTs composites.

5.2 Experimental procedure

The Cr(VI) adsorption experiments were performed according to the methods reported in the literature [240-241]. The parameters such as pH (2-10), contact time (10-120 mins), and initial Cr(VI) concentration (10-50 mg/L) were optimized. The optimization process was achieved by varying one parameter while keeping the others constant. In order to investigate the influence of these parameters on the retention of Cr(VI), the removal efficiency (R%) was determined using equation 5.1 [240-241].

$$R\% = \frac{C_0 - C_e}{C_0}\ x\ 100 \quad \text{.....5.1}$$

Where C_0 and C_e are the initial and final (equilibrium) concentrations of Cr(VI) (mg/L), respectively. Additionally, the adsorption capacity (metal uptake) q_e (mg/g), that is, the mass of the adsorbate adsorbed per gram of adsorbent at equilibrium time was determined using equation 5.2 [229-240]:

$$q_e = \frac{(C_0 - C_e)v}{100\ w} \quad \text{.....5.2}$$

Where *V* is the volume of the aqueous solution (mL) and *W* is the adsorbent weight (g). The stock solution (1000 mg/L) of Cr(VI) was prepared by dissolving 2.835 g of 99.5% potassium dichromate ($Cr_2O_7^{2-}$) in 1.0 L volumetric flask and filled to the mark. Then, appropriate dilutions or synthetic samples (10-50 mg/L) were prepared from the stock solution. The pH of aqueous solution was adjusted to the desired value by the addition of 0.1N HNO_3 or 0.1N NaOH solutions.

5.2.1 Batch Cr (VI) adsorption experiments

Briefly, 20 mg of each composite (adsorbent) was added to 50 mL of a solution of Cr(VI) of known concentration (10-50 mg/L) in 100 mL Erlenmeyer flask. The solution was stirred for 10-120 min at room temperature. Afterwards, the adsorbent was filtered and the residual concentration of Cr(VI) in solution was determined by the Varian 720-ES ICP Optical Emission Spectrometer at 267 nm. To complement the ICP-OES results retention of Cr(VI), SEM/EDS analysis was employed to analyse the adsorbent with adsorbed Cr(VI) post adsorption.

5.2.2 Sorption isotherm models

Langmuir and Freundlich adsorption isotherms are among the most commonly used isotherms to study adsorption processes [240-241]. The Langmuir adsorption isotherm describes the qualitative formation of a monolayer adsorbate on the surface of the adsorbent with relatively equivalent adsorption site, which suggests that the metal ions (adsorbate) are equally distributed between the solid and liquid phases [240-241]. However, it has been reported that the validity of Langmuir adsorption assumes the monolayer-type surface adsorption with forward adsorption process decreasing as the available vacant adsorption sites are filled by adsorbate [241]. Subsequently applied in liquid phase systems, Langmuir adsorption isotherm (eqn. 5.3) was initially derived for gas phase adsorption processes [241]. However, Azizian *et al*. [241] recently revised the century-old Langmuir isotherm and consequently reported the modified Langmuir isotherm (eqn. 5.4) and its linear form (eqn. 5.5) [241].

$$q_e = \frac{q_m K_L P}{1+K+P} \quad \text{.....5.3}$$

$$\theta_e = \frac{K_{ML} \cdot Ce}{C_s+(K_{ML}-1)C_e} \quad \text{.....5.4}$$

$$\frac{C_e}{q_e} = \frac{C_s}{q_m \cdot K_{ML}} + \frac{(K_{ML-1})C_e}{K_{ML} \cdot q_m} \quad \text{.....5.5}$$

Where θ_e is the maximum surface coverage at equilibrium, C_e is the solute concentration at equilibrium (mg/L), C_s is the saturated solute concentration, K_{ML} is the modified Langmuir equilibrium constant, and q_e is the amount of metal adsorbed per gram of the adsorbate at equilibrium (mg/g). The Langmuir plot of $\frac{1}{q_e}$ v $\frac{1}{C_e}$ was used to get the q_m and the Langmuir isotherm constant (K_{ML}) form the slope and the intercept of the graph. On the other hand, the Freundlich adsorption isotherm usually describes the adsorption in terms of multilayer interactions with heterogeneous surface adsorption [242]. The linear form of Freundlich isotherm is shown in equation 5.6.

$$\log q_e = \log K_f + {}^{1}/_{n} \log C_e \quad \text{.....5.6}$$

Where K_f is the approximate indicator of adsorption capacity (constant), ${}^{1}/_{n}$ is a function of the strength of adsorption [242-244]. The Freundlich plot $\log q_e \; v \; \log C_e$ was used to obtain the Freundlich constants and regression value (R^2).

5.3 Results and discussion

The pH optimization showed that the adsorption of Cr(VI) species occurred in the pH range 2-3 and all adsorption studies were performed at these pH. It has been clearly articulated in the literature that the pH of solution drastically influences the adsorption process of metal ions and

other species [259-260]. The influence of agitation time on Cr(VI) adsorption was also investigated. Some literature studies have reported that the effect of contact time is directly proportional to the adsorption of Cr(VI), while others have reported an opposite trend [242]. Furthermore, the effect of initial concentration of the metal ion solution was also studied.

5.3.1 Effect of pH solution

The influence of solution pH on Cr(VI) adsorption was investigated to verify the type of Cr(VI) species adsorbed and the possible mechanism behind the adsorption process (Fig. 5.1). The acidity/basicity of the solution greatly influences the metal species ionization and the concentration or availability of counter H^+ in the solution [261]. It has been reported that at low pH levels (≤3) Cr(VI) exist as dichromate ($Cr_2O_7^-$) and/or hydrochromate ($HCrO_4^-$), while at higher pH values it exist as chromate (CrO_4^{2-}) [9]. As shown in Fig. 5.1, the removal of Cr(VI) decreased with increasing pH due to either the reduction of Cr(VI) to Cr(III) and/or the ionic electrostatic interactions between Cr(VI) and positive-end of the composites [261]. The pH was optimized to the range 2-3 for all the adsorption studies. A maximum percentage removal of Cr(VI) was found to be 20% for (PIL3/MWCNT), 40% for (PIL5/MWCNT), and 25% for (PIL6/MWCNT) within two hours of agitation time. Species such as dichromate and hydrochromate were adsorbed (at low pH), thanks to the presence of the pool of H^+ ions in acidic

aqueous solution which acted to neutralize the negative-end of the adsorbent (composites) creating a conducive environment for electrostatic interactions between anionic $Cr_2O_7^-$ or $HCrO_4^-$ and the positive-end of the adsorbent(s) [262]. At pH<4, there were relatively strong electrostatic attractions between positively-charged composites and Cr(VI). On the other hand, upon increasing pH (≥4), the competition between the anionic chromate (CrO_4^{2-}) and hydroxyl (OH^-) to be adsorbed increases and consequently decrease the adsorption of Cr(VI) [261]. The surface-active sites of the composites were either protonated or deprotonated depending on the pH of the solution. The presence of poorly coordinated counter-ions of vinyl pyridinium or imidazolium PILs as part of carbon nanotubes have played a significant role in the adsorption capacity of the composites.

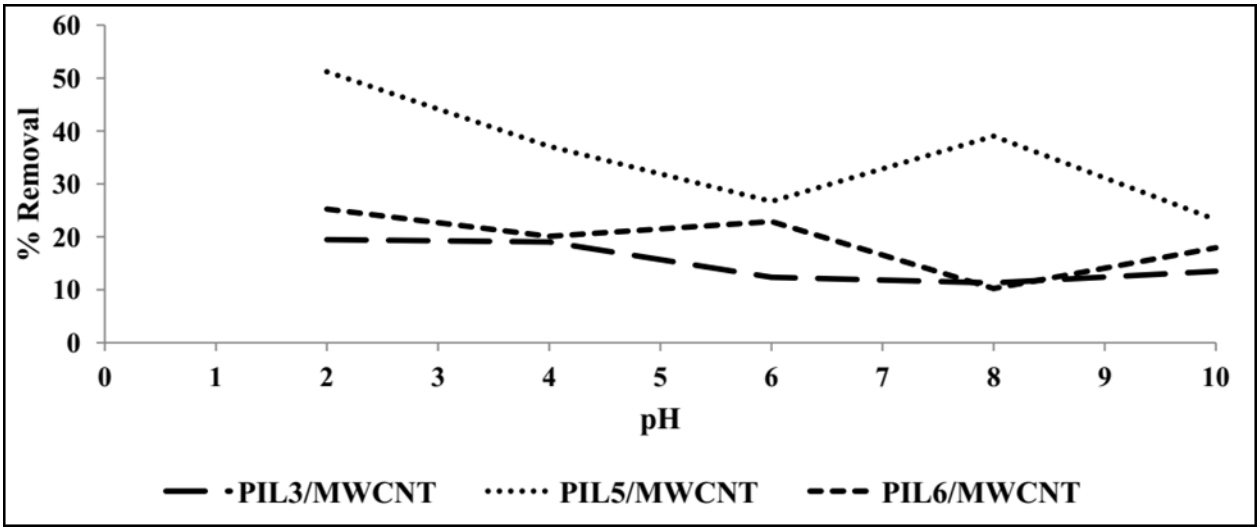

Figure 5.1 Effect of pH on the adsorption of Cr(VI)

5.3.2 Effect of contact time

As shown in Fig. 5.2, the adsorption of Cr(VI) fairly increased with contact time (1-2 h) and there was no adsorption observed below 60 minutes of contact time. However, continuous increase in Cr(VI) adsorption occurred after 1 h up to 2 h of agitation time with removal efficiency of 30% for (PIL3/MWCNT), 60% for (PIL5/MWCNT), and 35% for (PIL6/MWCNT). The increase in Cr(VI) adsorption as function of time can be attributed to the continuous availability of surface active sites on the composites with increasing contact time, which greatly interact with the Cr(VI) species. To further study the influence of contact time, the agitation time was increased to 5 and 12 h. The removal efficiency of 19% for (PIL3/MWCNT), 37% for (PIL5/MWCNT), and 19% for (PIL6/MWCNT) were observed after 12 h. As presented in Fig. 5.3, the increased agitation time have not exceptionally affected adsorption of Cr(VI). This is due to the early or quick oversaturation of the surface active sites of the adsorbents, indicating that the adsorbents could no longer adsorb an Cr(VI) beyond 2 h of agitation time. In addition, beyond 2 h of contact time, there is a limited number of available active sites and also increasing electrostatic repulsive forces among the Cr(VI) anions already adsorbed onto the composites. Long agitation time could also lead to the desorption of poorly coordinated Cr(VI) species to the solution. Previous studies have reported different agitation time equilibriums depending on the type of polymer materials used as adsorbent [164, 222]. For example, Mi *et al*.

[164] obtained 98% Cr(VI) adsorption within 24 h of equilibrium, while Briones *et al*. [222] obtained 72.2% Cr(VI) adsorption within 24 min of agitation time.

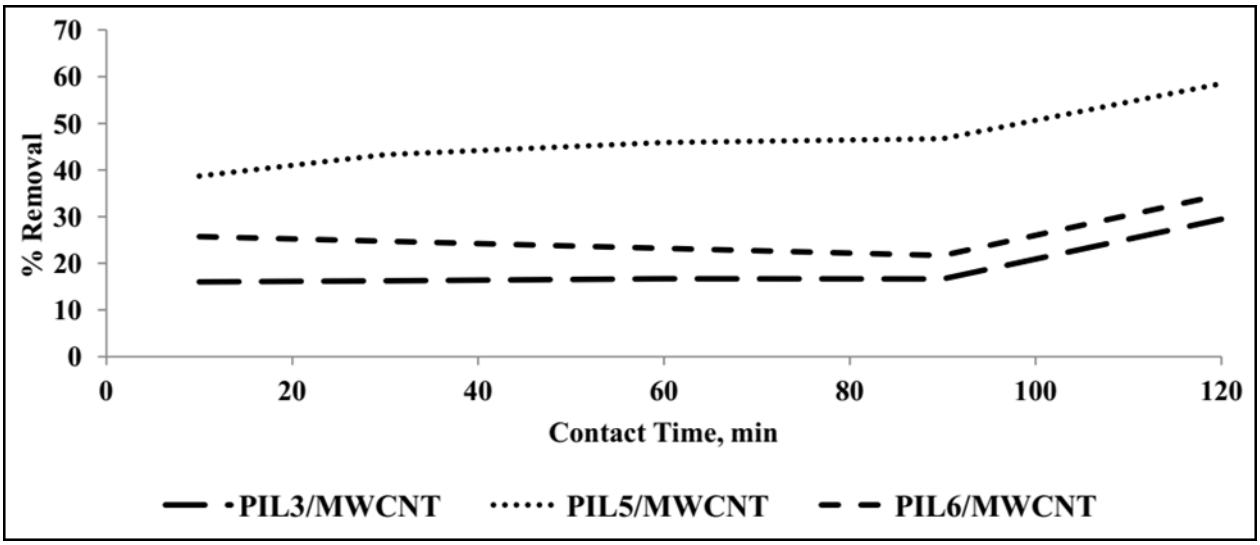

Figure 5.2 Effect of contact time on the adsorption of Cr(VI)

5.3.3 Effect of initial concentrations of the adsorption of Cr(VI)

Fig. 5.4 showed that the concentration of the metal solution does not significantly impact the adsorption of Cr(VI) onto PILs/MWCNT composites. At higher initial concentrations, the mounting number of Cr(VI) anions fiercely compete for the available adsorption sites and consequently cause electrostatic repulsions [262].

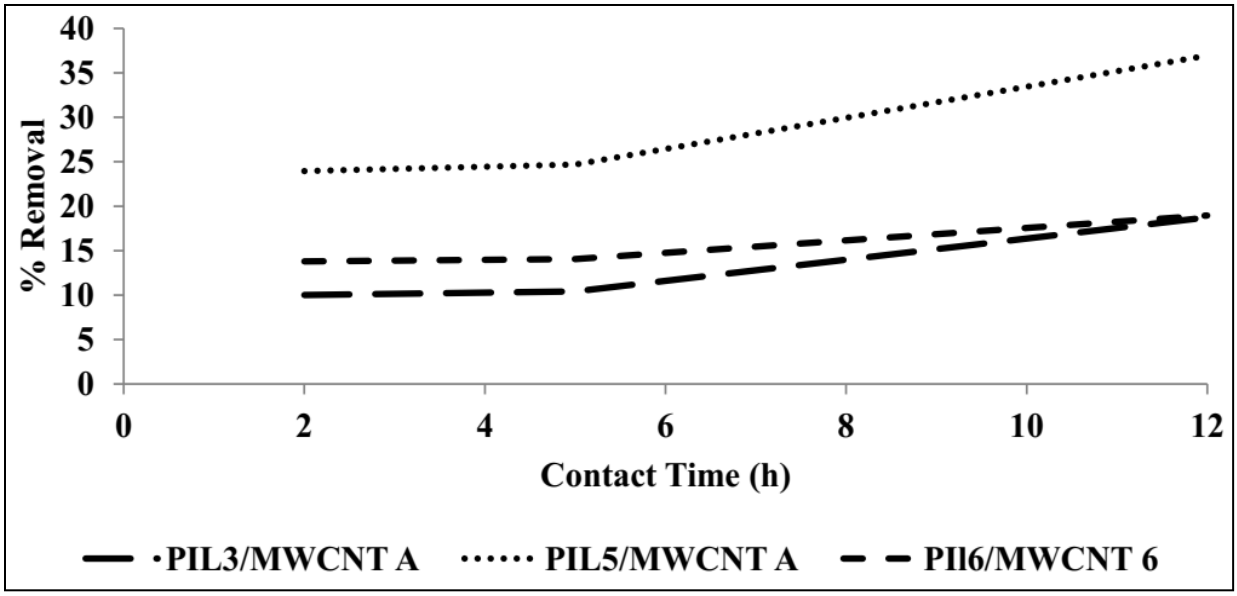

Figure 5.3 Removal of Cr(VI) at initial concentration (50 mg/L) and increased contact time (h)

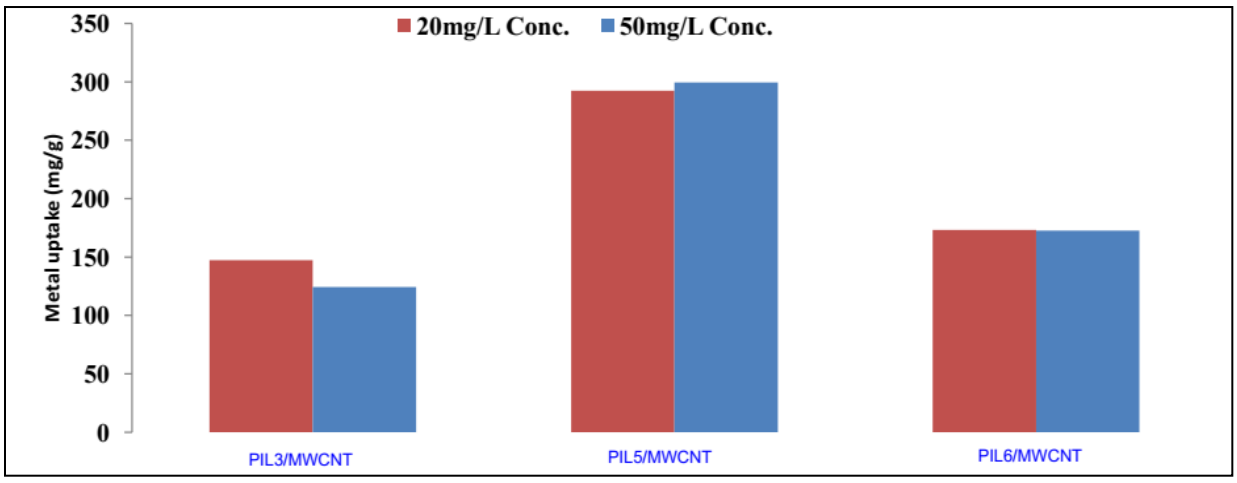

Figure 5.4 Effect of initial concentrations on the adsorption of Cr(VI) onto PILs/MWCNT composites

When using imidazolium-PILs containing vinyl and styrenic moieties, similar Cr(VI) adsorption trend was observed. As shown in Figs. 5.5-5.8, the adsorption of Cr(VI) as a function of time showed a maximum removal efficiency of 35% after 12 h and it could be seen that there was no significant adsorption beyond 2-4 h of agitation time. With most adsorbents, the adsorption reached equilibrium at ≤4 h and beyond that, the rate of adsorption decreases as the number of vacant sites were already filled and saturated by the adsorbate. Although the initial concentration could not primarily impact the rate or the amount of adsorbate to be adsorbed, high removal efficiency for Cr(VI) could be observed when 10 mg/L concentration was used and the following adsorption order in terms of initial concentration (mg/L) was observed: 10>30>50. The latter order can be attributed to a number of physicochemical factors such as the oversaturation of Cr(VI) species at higher concentrations versus limited vacant adsorption sites on the surface of solid adsorbent

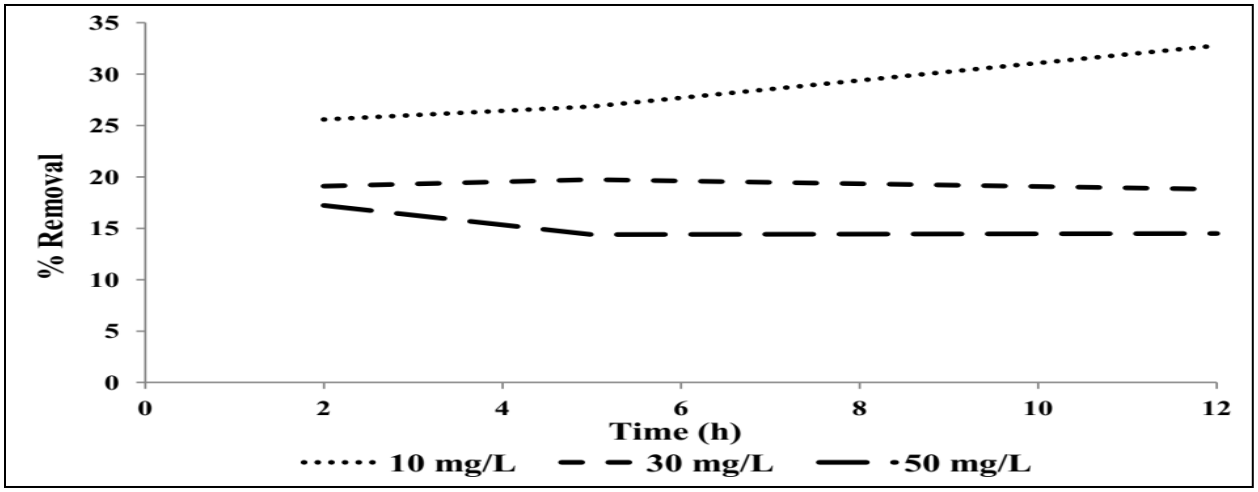

Figure 5.5 Adsorption of Cr(VI) onto P[3P-VImBr]/MWCNT composite

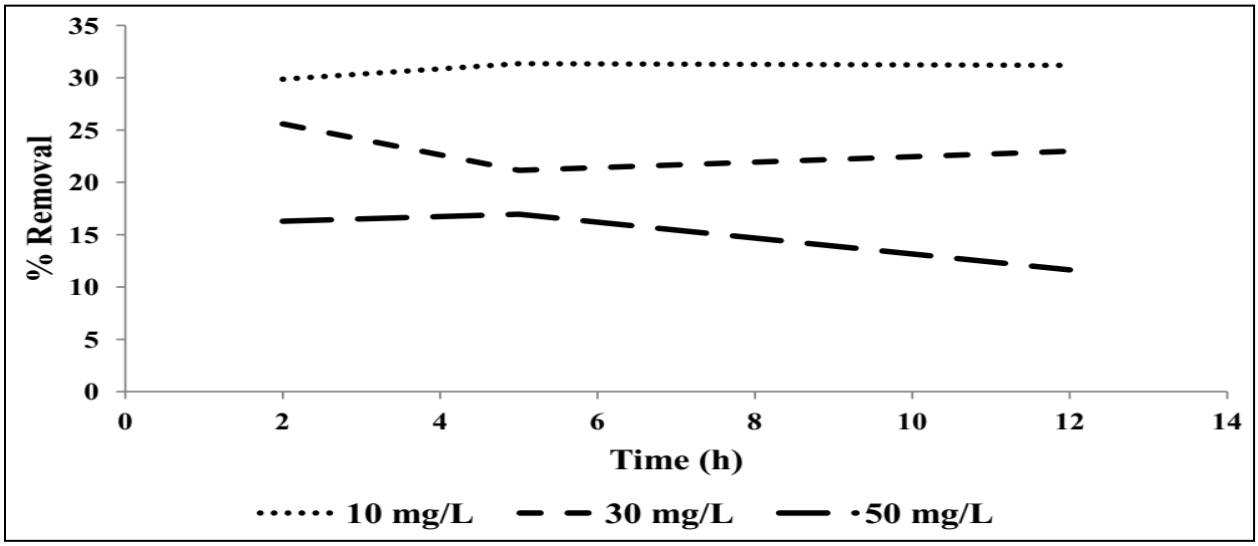

Figure 5.6 Adsorption of Cr(VI) onto P[3P-VImPF_6]/MWCNT composite

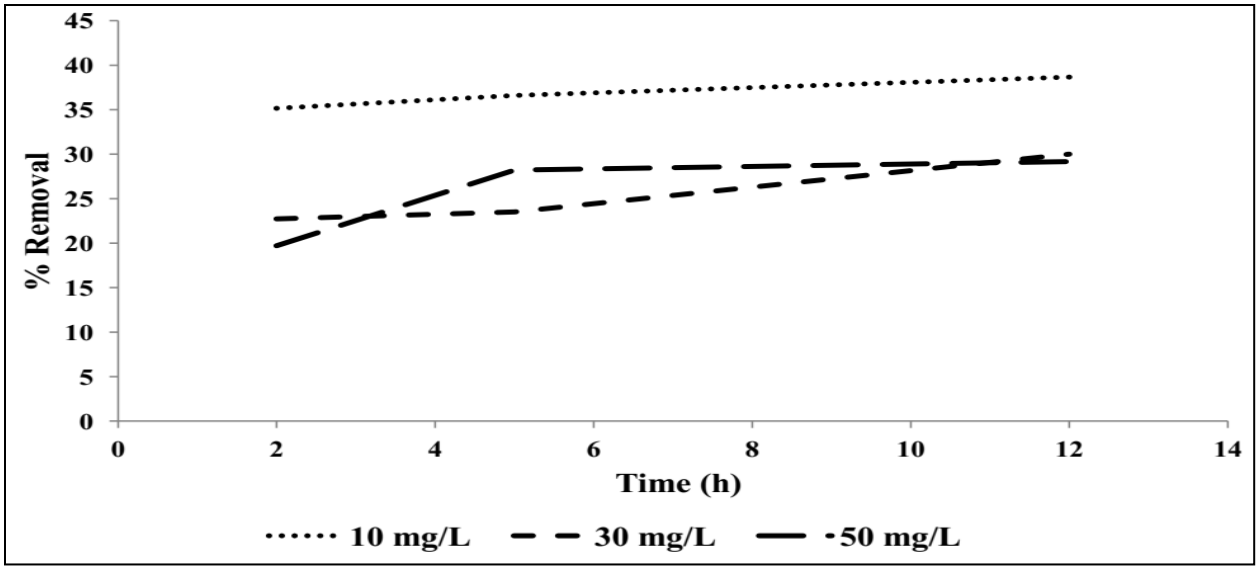

Figure 5.7 Adsorption of Cr(VI) onto [3Isop-VImPF_6]/MWCNT composite

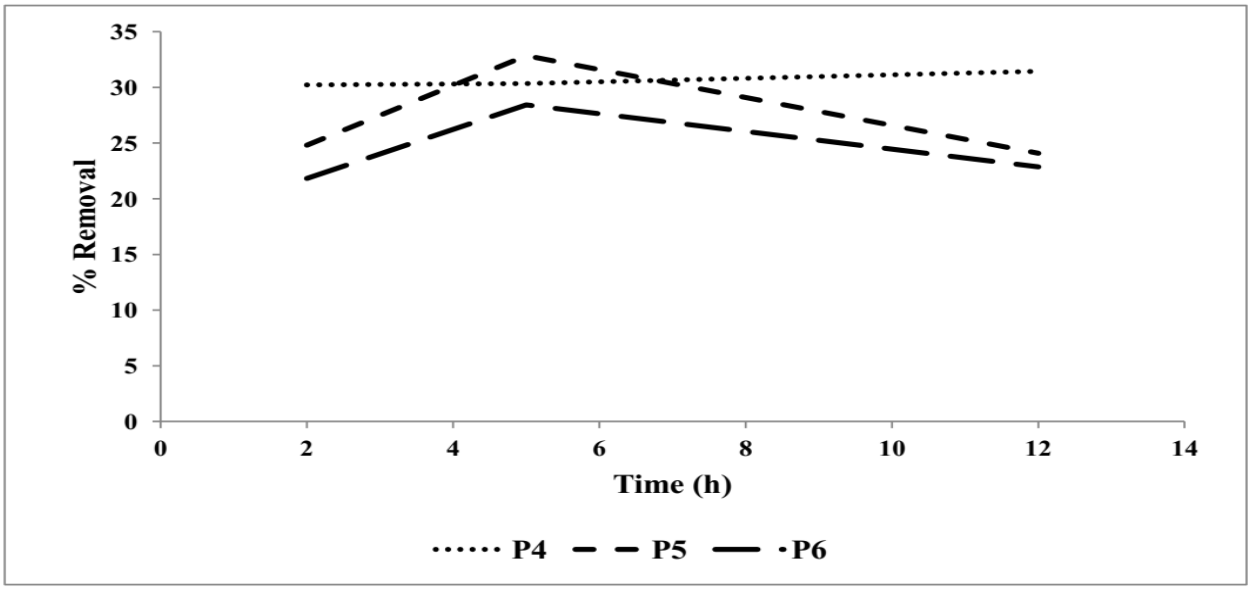

Figure 5.8 Adsorption of Cr(VI) onto P[MVBIm-Cl]/MWCNT (P4), P[MVBIm-PF6]/MWCNT (P5), and P[MVBIm-TFSI]/MWCNT (P6) composites

5.3.4 Adsorption and kinetic models

The adsorption data of Cr(VI) onto PILs/MWCNT composites also fitted well into both Langmuir and Freundlich isotherm models (Fig. 5.9). Interestingly, inasmuch as the data fitted well into Langmuir model with correlation co-efficient ($0.98 \leq R^2 < 1$) suggesting a monolayer adsorption process with equivalent adsorption sites, the multilayer adsorption process could not be ruled out. The latter appraise the heterogeneity contribution of PILs/MWCNT composites due to the nature of the composites such as the presence of bulky organic cations, some large counter anions and graphitic functional groups. To further understand the mechanism behind the adsorption of Cr(VI) onto PILs/MWCNT and ILs/MWCNT composites, the pseudo-second-order kinetic model was used to analyse the solid-liquid adsorption process. The pseudo-second-order kinetic model is expressed as follows [262]:

$$\frac{t}{q_t} = \frac{1}{q_e^2 K_2} + \frac{t}{q_e} \quad \text{.....5.7}$$

Where q_t(mg·g^{-1}) is the amount of Cr(VI) adsorbed per unit weight of the adsorbent (composite) at the time of t, q_e(mg·g^{-1}) is the maximum adsorption capacity, K_2 (g·mg^{-1}·min^{-1}) is the pseudo-second-order rate constant. The values of q_e and K_2 were obtained from both the intercepts and slope of the plot of t/q_t versus t, respectively. The parameters which include K_2, calculated

maximum adsorption capacities (q_{ecal}), experimental maximum adsorption capacities ($q_{e\cdot\exp}$), and correlation coefficients (R^2) obtained are listed in Table 5.1. As shown in both Fig. 5.9 (II) and Table 5.1, the plot of t/q_t versus t display straight lines with high correlation coefficients (R^2>0.99), confirming the applicability and feasibility of the pseudo-second-order kinetic model on the adsorption of Cr(VI) onto PILs/MWCNT composites [261]. However, comparing the (q_{ecal}) and ($q_{e\cdot\exp}$), it was observed that both values, particularly in most PILs/MWCNT composites showed close tolerance and therefore the kinetics of Cr(VI) adsorption onto PILs/MWCNT composites followed pseudo-second-order model.

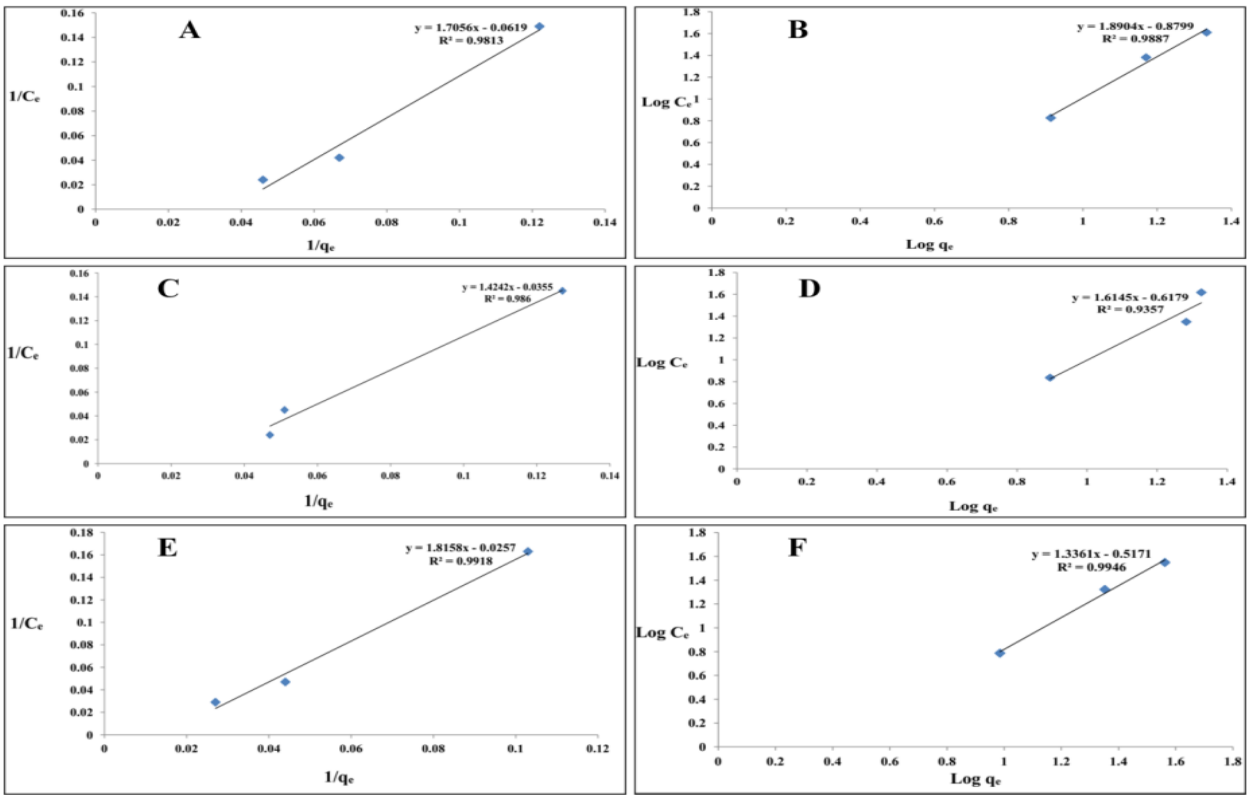

Figure 5.9 (I) Langmuir and Freundlich adsorption isotherms of P[3P-VImBr]/MWCNT (A-B), P[3P-VImPF_6]/MWCNT (C-D), and [3Isop-VImPF_6]/MWCNT (E-F) composites

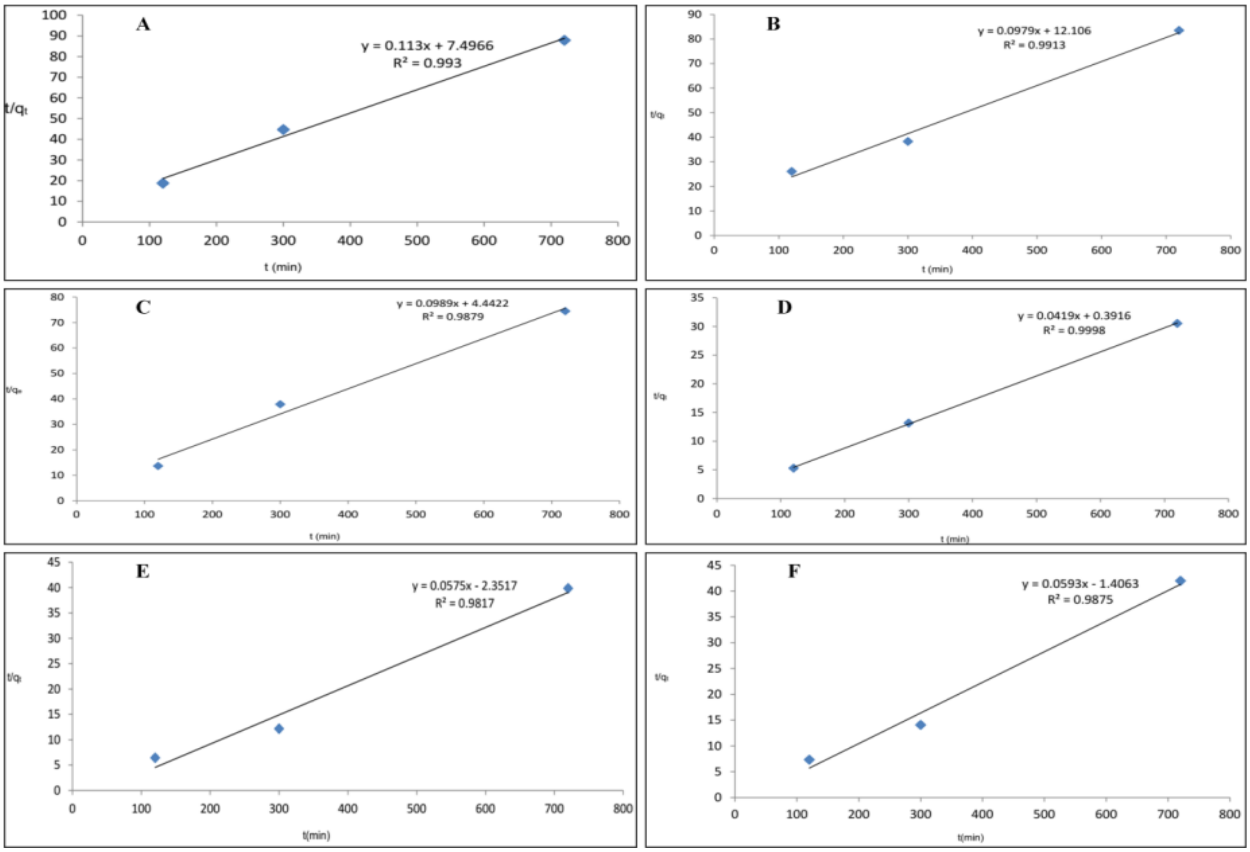

Figure 5.9 (II) Linear plots of t/qt vs t for the adsorption of Cr(VI) onto P[3P-VImBr]/MWCNT (A), P[3P-VImPF_6]/MWCNT (B), [3Isop-VImPF_6]/MWCNT (C), P[MVBIm-Cl]/MWCNT (D), P[MVBIm-PF_6]/MWCNT (E) and P[MVBIm-TFSI]/MWCNT (F) composites

Table 5.1 Pseudo-second-order kinetic model parameters for Cr(VI) adsorption onto PIL/MWCNT composites

PILs	$q_{e.\exp(\frac{mg}{g})}$	$q_{e.cal}(\frac{mg}{g})$	R^2	K_2 (g·mg·min)
PIL/MWCNT 1	8.193	8.849	0.993	0.0017
PIL/MWCNT 2	8.620	10.210	0.991	0.0012
PIL/MWCNT 3	9.665	10.121	0.987	0.0022
PIL/MWCNT 4	22.787	23.860	0.998	0.0045
PIL/MWCNT 5	18.063	17.540	0.982	0.0014
PIL 6/MWCNT	16.375	16.861	0.987	0.0025

Note: P[3P-VIm][Br]/MWCNT (PIL/MWCNT 1), P[3P-VIm][PF_6]/MWCNT (PIL/MWCNT 2), [3Isopropyl-VIm][PF_6]/MWCNT (PIL/MWCNT 3), P[MVBIm][Cl]/MWCNT (PIL/MWCNT 4), P[MVBIm][PF_6]/MWCNT (PIL/MWCNT 5), and P[MVBIm][TFSI]/MWCNT (PIL/MWCNT 6).

5.3.5 Adsorption of Cr(VI) onto ILs/MWCNT composites

The influence of solution pH on the adsorption of Cr(VI) on ILs/MWCNT composites was studied. As already indicated, the adsorption of Cr(VI) occurred under acidic medium due to the interactions of anionic Cr(VI) species such as dichromate ($Cr_2O_7^-$) and hydrochromate ($HCrO_4^-$) and the positively regions (pyridinium or imidazolium-cations) of the composites. For example, during the adsorption of Cr(VI) unto the pyridinium and imidazolium-based ILs/MWCNT composites, the availability of H^+ ions from the acidic solution normally neutralizes the negative-end of the adsorbent (which includes Br^- or PF_6^- counter anions) creating a favourable environment for electrostatic interactions between anionic $Cr_2O_7^-$ or $HCrO_4^-$ and the positive-end

of the adsorbent (pyridinium, imidazolium or graphitic groups) [261]. On the other hand, the minimal adsorption of Cr(VI) under basic conditions (pH≥4) can be attributed to the competition between the anionic chromate CrO_4^{2-} in Cr(VI) solution, hydroxyl (OH^-) group, and counter ions (Br^- and PF_6^- on the adsorbent) [261].

Figs. 5.10 to 5.13 shows the adsorption of Cr(VI) onto ILs/MWCNT composites as function of time, initial concentration and different adsorbent weight. In almost all the ILs-based composites, an increased agitation time beyond 3 h showed no significant effect on the adsorption of Cr(VI) due to early saturation of the active sites on the adsorbents. The active sites of the adsorbents were fully saturated or filled by Cr(VI) ions at early stages of agitation time, suggesting a very fast attraction of Cr(VI) in these adsorbents though there were limited active sites. In some cases, the adsorption of Cr(VI) onto ILs-based composites showed a decreasing adsorption order which suggested that after early stages (>2 h) of agitation time the adsorbate was probably released back to the solution. This was likely due to the physical and/or chemical parameters such as early saturation of active sites or the competition between poorly coordinated counter anions (Br^-, PF_6^-) and metal ions (dichromate/hydrochromate) to be attached on the pyridinium or imidazolium cations.

The dependence of Cr(VI) adsorption on the initial concentration was also studied and it was observed that the effect of increasing solute concentration was negligible and insignificant in this study, rather resulted in excessive competition between Cr(VI) species themselves (Figs. 5.10 to 5.13). Changing initial concentration from 10 mg/L to 50 mg/L did not affect the adsorption of Cr(VI) significantly. Additionally, the effect of adsorbent mass was also studied and two adsorbent dosages were compared (20 mg) [*N*-propylPyr$^+$][Br$^-$]/MWCNT and [*N*-IsopropylPyr$^+$][PF_6^-]/MWCNT composites and (50 mg) [MPIm$^+$][Br$^-$]/MWCNT and [IsopropylMIm$^+$][PF_6^-]/MWCNT composites. The results obtained showed that an increase in adsorbent weight did not affect the adsorption of Cr(VI), which therefore suggests that the lower adsorption of Cr(VI) in this study cannot be attributed to the limited adsorption active sites, but relatively to the competition between metal ions and ILs-counter anions in all the adsorbents.

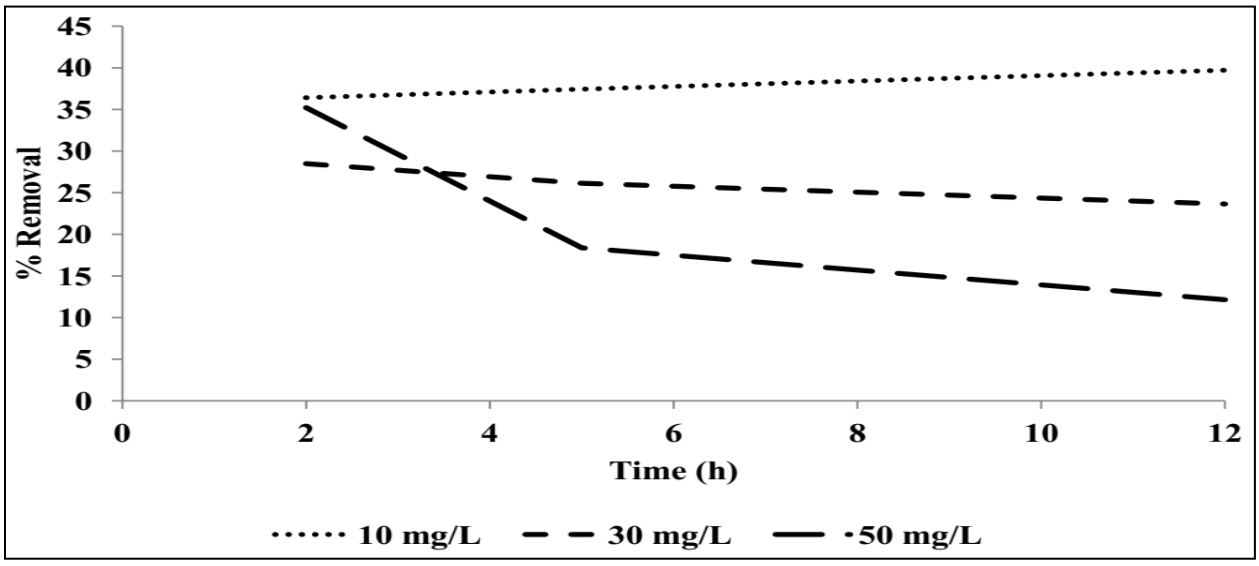

Figure 5.10 Adsorption of Cr(VI) onto [MPImBr]/MWCNT composite

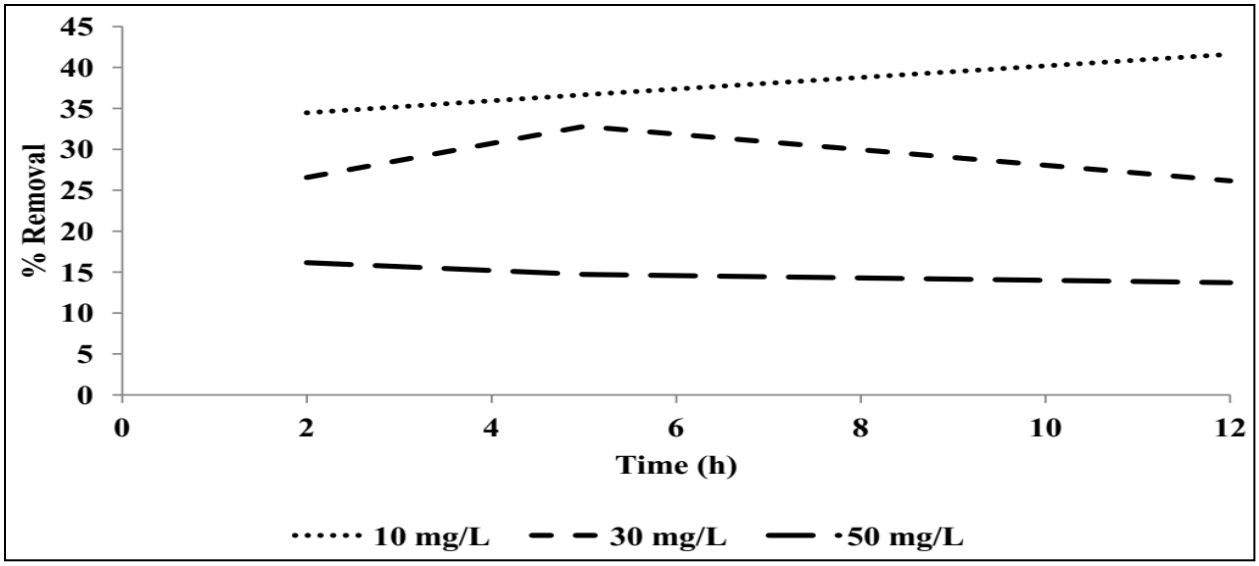

Figure 5.11 Adsorption of Cr(VI) onto [IsopMIm-PF6]/MWCNT composite

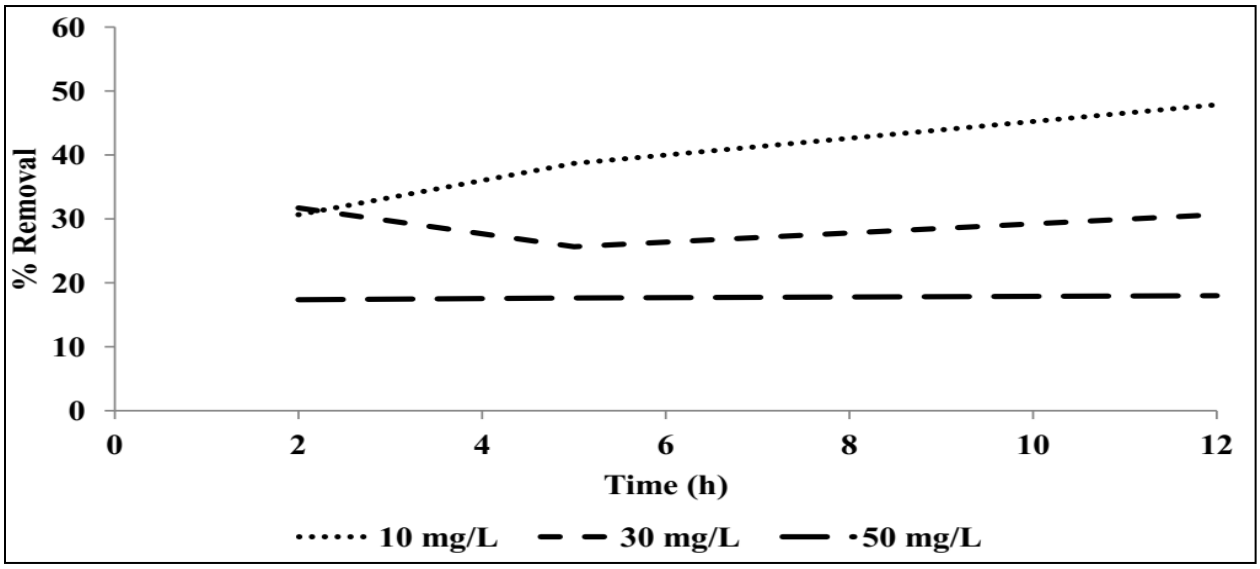

Figure 5.12 Adsorption of Cr(VI) onto [IsopMIm-PF6]/MWCNT composite

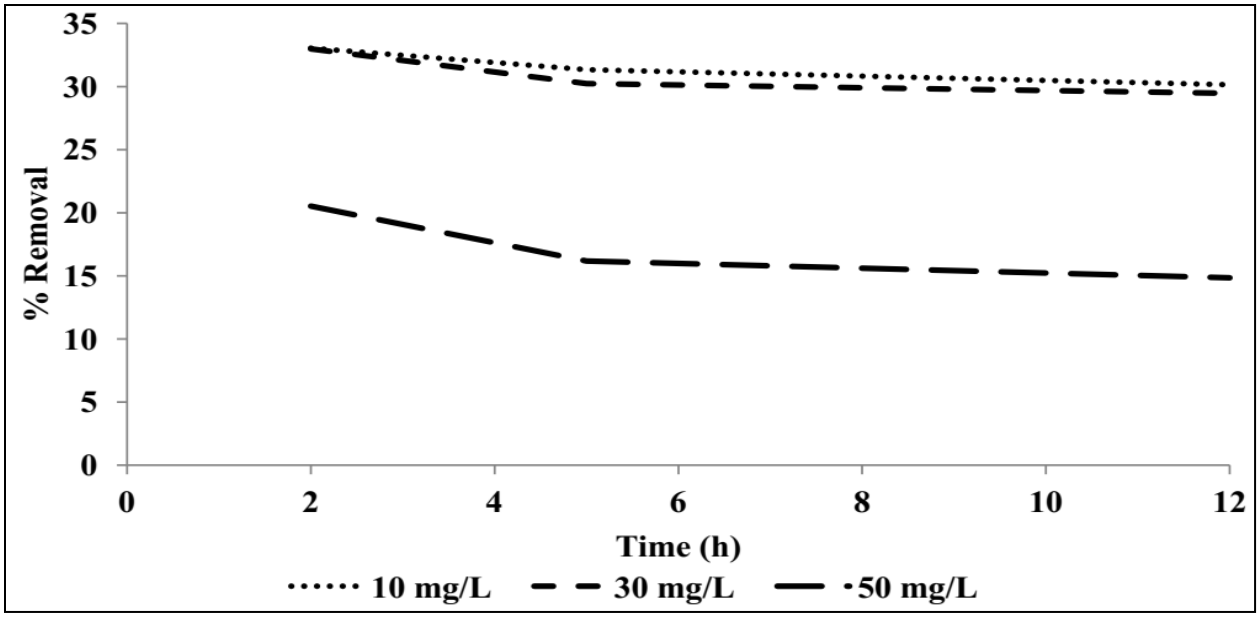

Figure 5.13 Adsorption of Cr(VI) onto [N-IsopPyrPF6]/MWCNT composite

5.3.6 Adsorption and kinetic models of Cr(VI) adsorption on ILs/MWCNTs

The sorption data fitted into both Langmuir (Fig. 5.14) and Freundlich (Fig. 5.15) isotherms and it was observed that the adsorption of Cr(VI) onto ILs/MWCNT composites best fitted well into Langmuir isotherm model, with highest correlation co-efficiencies ($0.98 \leq R2 < 1$). This therefore suggests that the adsorption of Cr(VI) onto ILs/MWCNT composites took place via monolayer adsorption process with equal number of uniform adsorption sites. However, based on the experimental data obtained (for example the amount of adsorbate on the surface of the adsorbent), the rate of adsorption as a function of agitation time and initial concentration observed, it can be concluded that the adsorption of Cr(VI) onto ILs/MWCNT composites is dependent on the number of available vacant sites and this also account to the decrease of Cr(VI)

adsorption with increasing agitation time. The available vacant sites are normally filled or saturated by Cr(VI) within early stages of contact time.

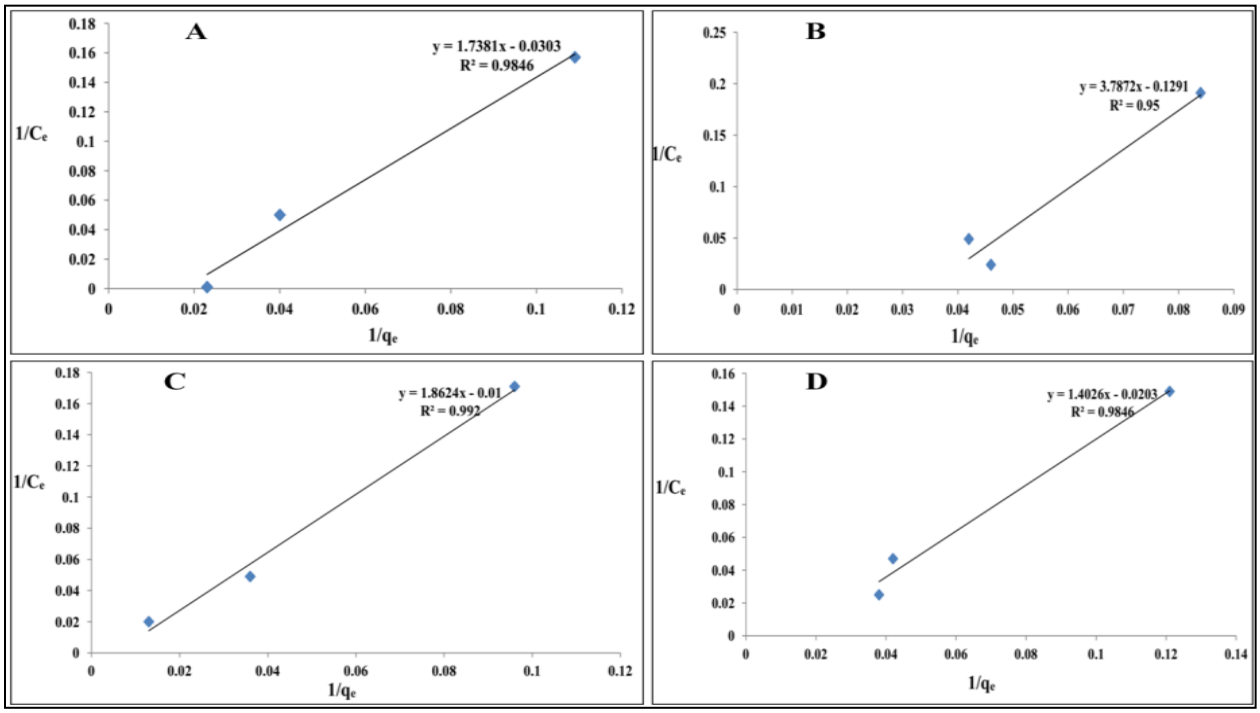

Figure 5.14 Langmuir adsorption isotherms of [MPIm-Br]/MWCNT (A), [IsopMIm-PF6]/MWCNT (B), [N-propylPyrBr]/MWCNT (C), and [N-IsopPyrPF6]/MWCNT (D) composites

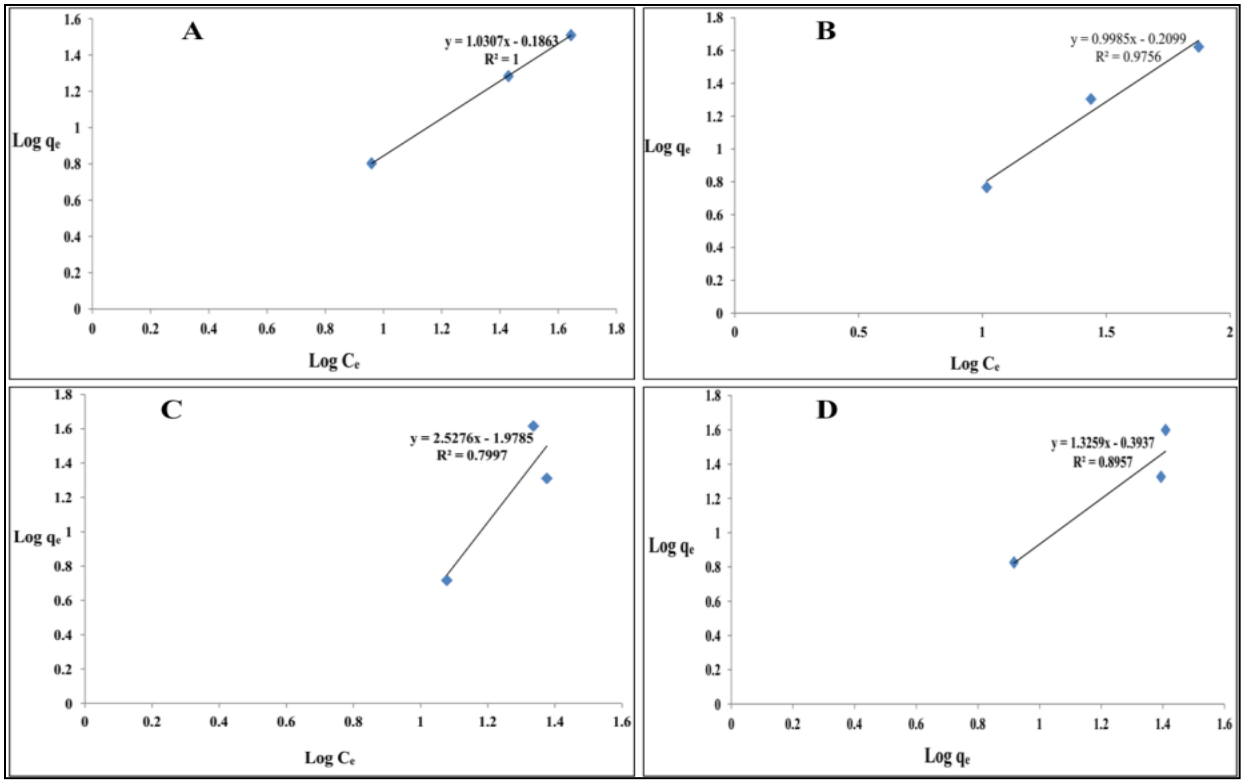

Figure 5.15 Freundlich adsorption isotherms of [MPIm-Br]/MWCNT (*A*), [IsopMIm-PF6]/MWCNT (*B*), [N-propylPyrBr]/MWCNT (*C*), and [N-IsopPyrPF6]/MWCNT (*D*) composites

5.3.7 FTIR spectroscopy and SEM/EDS analysis of composites after Cr(VI) adsorption

To further substantiate the results obtained from batch adsorption experiments, FTIR spectroscopic and SEM/EDS microscopic analysis were performed post adsorption. Generally, the infrared vibrational bands after Cr(VI) adsorption are always shifted either to higher or lower frequencies depending on the developed functional groups [262]. The FTIR spectra of some

PILs/MWCNT and ILs/MWCNT composites post adsorption were obtained and new changes in FTIR absorption bands were attributed to the interactions between the pyridinium/imidazolium cations or positive-end of the composites and the anionic chromium species at lower pH values [262].

SEM images of the PILs/MWCNT and ILs/MWCNT composites post adsorption showed that the surface morphology of the composites have drastically changed and the initial visible pores were filled or saturated by Cr(VI) species. The changes in surface morphology and the emerging of new attachments on the sidewalls and termini of carbon tubes confirmed successful coordination of chromium species with the functional groups of the composites. EDS spectra were also collected post-adsorption (Figs. 5.16-18). All the EDS spectra displayed the presence of elemental Cr around 0.6 and between 5-6 KeV. However, the microscopic and spectroscopic microanalysis results provided comprehensive evidence for the physical attachment of Cr(VI) species on the surface of PILs/MWCNT composites [222, 262]. The presence of bulky asymmetric pyridinium and imidazolium cations was believed to have played a pivotal role in the adsorption of anionic Cr(VI) species in this study via the electrostatic interactions. However, in almost all batch adsorption experiments, PILs/MWCNT and ILs/MWCNT composites containing halide-counter ions showed very low adsorption performance and this can be

attributed to the anionic competition triggered by bromide and hydroxyl anions for the H^+ ions in acidic medium, which led to possible electrostatic/steric repulsions inside the adsorption system.

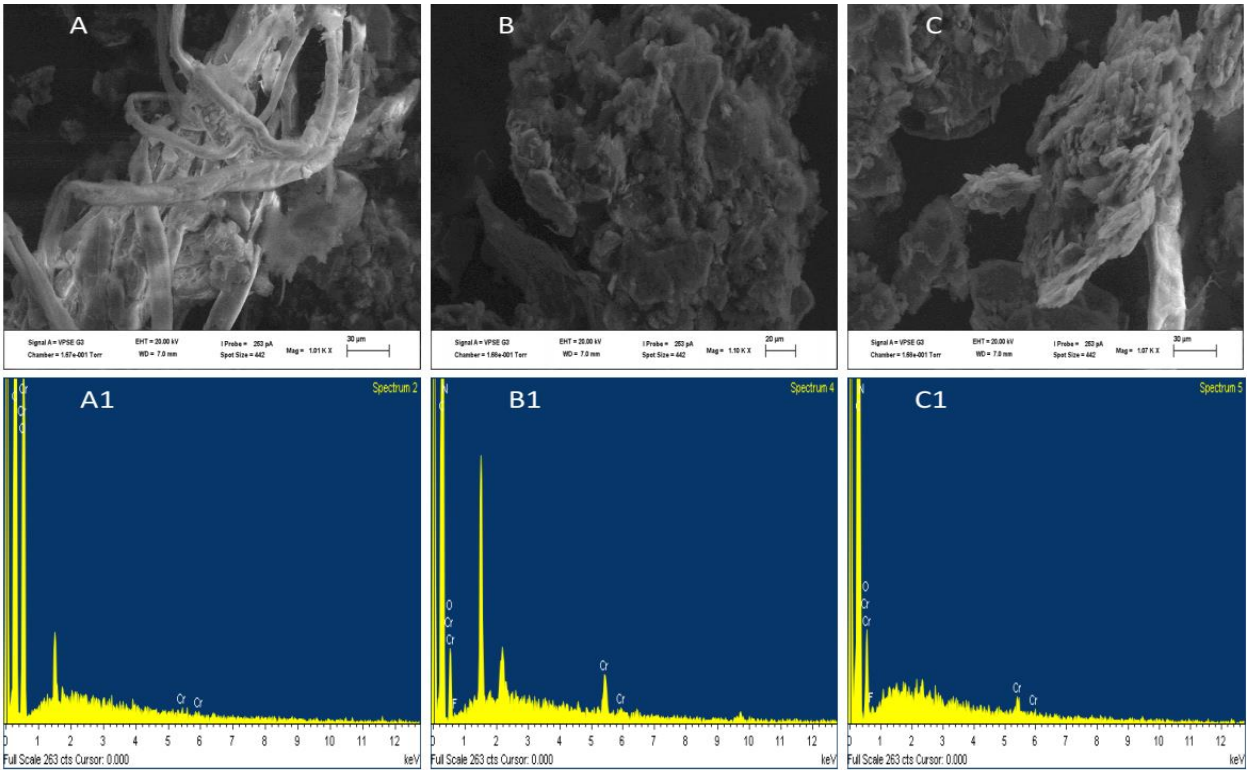

Figure 5.16 SEM images/EDS spectra of **PIL3/MWCNT** (*A-A1*), PIL5/MWCNT (*B-B1*), and **PIL6/MWCNT** (*C-C1*) composites after Cr(VI) adsorption

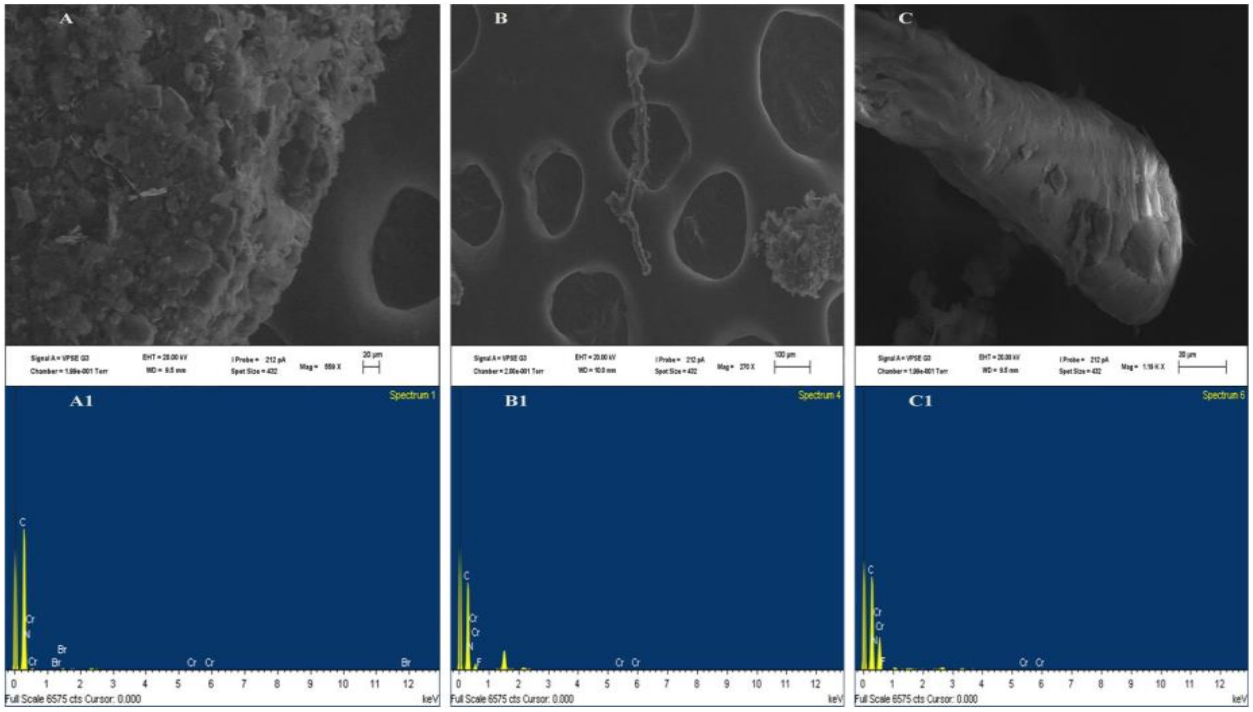

Figure 5.17 SEM images/EDS spectra of P[3P-VImBr]/MWCNT (A-A1), [3Isop-VImPF6]/MWCNT (B-B1), and P[3P-VImPF6]/MWCNT (C-C1) composites after Cr(VI) adsorption

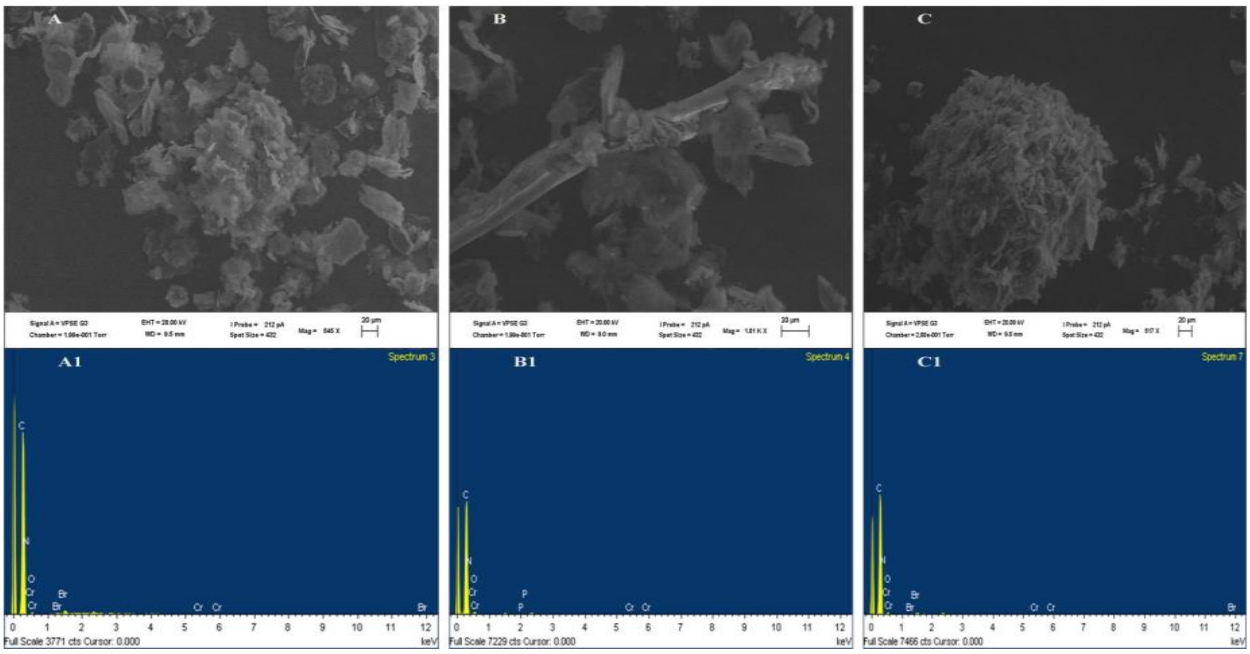

Figure 5.18 SEM images/EDS spectra of P[3P-VImBr]/MWCNT (A-A1), [3Isop-VImPF6]/MWCNT (B-B1), and P[3P-VImPF6]/MWCNT (C-C1) composites after Cr(VI) adsorption

5.4 Chapter summary

In summary, Cr(VI) was adsorbed onto ILs/MWCNT and PILs/MWCNT composites via solid-liquid adsorption process. Batch adsorption experiments showed that the adsorption of Cr(VI) was pH dependent and only took place under acidic conditions (optimized pH was 2-3). However, the cationic imidazolium and pyridinium-end functional groups of ILs and PIL/MWCNT composites are proposed to facilitate the possible Cr(VI) adsorption. The effect of contact time and initial concentrations were investigated, and it was revealed that contact time

and initial concentrations did not significantly influence the adsorption process. However, promising adsorptions were observed at 2 h of contact time and when the concentration of Cr(VI) solution was 10 mg•L^{-1}. The adsorption of Cr(VI) onto ILs/MWCNT and PILs/MWCNT composites followed Langmuir adsorption isotherm and fitted well into pseudo-second-order kinetic model, suggesting monolayer surface adsorption method which indicates one active site per species. Strong electrostatic interactions are believed to have facilitated the mechanism behind the adsorption of Cr(VI) onto PILs/MWCNT and ILs/MWCNT composites.

CHAPTER SIX

SUMMARY OF RESULTS, CONCLUSION AND FUTURE PROSPECT

6.1 Summary of results

In this study, imidazolium and pyridinium-based ionic liquids (ILs) were synthesized and characterized by FTIR, ^{1}H, ^{13}C, ^{19}F, and ^{31}P-NMR spectroscopy, thermal gravimetric analyses, solubility studies, and mass spectrometry. The influence of the propyl and isopropyl chain at the first and third positions of imidazolium and N-atom of pyridinium cations towards the thermal stability, conductivity, and solubility of the ionic liquids were investigated. It was observed that pyridinium-ILs decomposed at higher temperatures, displayed high melting points, and showed poor water solubility than the imidazolium counterparts and their conductivities are mainly influenced by mobility of ions.

Furthermore, multi-walled carbon nanotubes (MWCNTs) were synthesized by simple chemical method, and dispersed using imidazolium and pyridinium-based ionic liquids (ILs). ILs/MWCNT composites were characterized using FTIR spectroscopy, scanning electron microscopy (SEM), energy dispersive X-ray spectroscopy (EDS), thermogravimetric analysis (TGA) and solubility in different polar and non-polar solvents. Spectroscopic and microscopic studies showed graphitic and carboxylic groups in the pure MWCNTs. MWCNTs SEM images showed entangled bundles, while ILs/MWCNTs showed debundled composites with increased diameter and unaltered MWCNTs morphology. TGA analysis showed that the ILs/MWCNTs are

more thermally stable, owing to the *van der Waals* and non-covalent interactions within the composites matrices. Solubility studies indicate that ILs/MWCNT composites are hydrophobic and insoluble in water and other polar solvents.

Vinyl pyridinium PILs were synthesized via radical polymerization of ILs monomers using potassium persulfate. Highly elastic PILs materials and several PILs/MWCNT composites were synthesized and characterized with thermal, spectroscopic and microscopy techniques. FTIR spectra studies showed vibrational bands due to (C=N) at 1600 cm^{-1}, compared to 1640 and 1636 cm^{-1} in the literature [200]. Thermal studies revealed that pyridinium-PILs containing hydrophobic counter anions (PF_6^-) were stable above 350 °C than their halide-containing counterparts. The observed thermal stability of PILs can be attributed to strong electrostatic interactions between pyridinium cations and hexafluorophosphate anions. The delocalized charge in pyridinium cationic ring and the size of counter anions influenced the glass transition temperatures of PILs materials. Functionalization of the carbon nanotubes with vinyl pyridinium-PILs resulted in more thermally stable and relatively insoluble PILs/MWCNT composites. SEM/EDS and TEM microscopic analyses confirmed the coating of PILs materials on the surface of carbon nanotubes and it could be concluded that direct mixing-functionalization method did not alter the surface morphology of pristine carbon materials.

NMR and mass spectrometry results confirmed the synthesis of imidazolium-PILs materials. FTIR spectra of all imidazolium-PILs containing hydrophobic anions showed vibrational bands in low frequency region, confirming replacement of halide with bulky-hydrophobic anions. Interestingly, the microscopic analyses revealed that modification of CNTs with amorphous polymer materials did not alter the surface morphologies of carbon nanotubes. TEM micrographs showed tubular and spherical elongated orientations of PILs/MWCNT composites. The visible cavities and voids from the micrographs are very important for solid-liquid adsorption of metal ions.

The as-synthesized ILs and PILs/MWCNT composites were used as adsorbents for the removal of Cr(VI) ions in aqueous solution. Batch adsorption experiments showed that the adsorption of Cr(VI) was pH dependent and occurred under acidic conditions. Results from the studies indicated that the cationic imidazolium and pyridinium-end functional groups of ILs and PILs/MWCNT composites are the functionalities for possible Cr(VI) adsorption. The effect of contact time and initial concentrations were investigated, and it was revealed that the influence of time and initial concentration was insignificant in this study. This may be ascribed to the physic-chemical factors of the materials being used as adsorbent. The adsorption of Cr(VI) onto ILs/MWCNT and PILs/MWCNT composites followed Langmuir adsorption isotherm and fitted

well into pseudo-second-order kinetic model. This indicated monolayer surface adsorption method with one active site per species.

6.2 Conclusion

The current study presents the synthesis, characterization and evaluation of ionic liquids, polymeric ionic liquids and their carbon nanotubes-functionalized composites as potential adsorbents for metal ions. NMR, accurate mass analysis, FTIR, solubility test, and TGA were used to confirm the synthesis of imidazolium and pyridinium based ILs and PILs The presence of high electronegative halogen (Br^-) as counterion and the π-electron system in imidazolium and pyridinium counter cation rings resulted in deshielded ^1H and ^{13}C-NMR peaks. Single (accurate) mass analysis confirmed the purity of the as-synthesized ILs and PILs compounds based on CHN analysis.

FTIR analysis of all hydrophilic and hydrophobic ILs showed relatively similar vibrational bands with slight frequency shifts due to anion-exchange. Comparatively, the vibrational bands around 890-991 cm^{-1} corresponded to the P-F bonding in hydrophobic ILs. Thermal analysis showed that all ILs containing hydrophobic counter anion (PF_6^-) were more thermally stable than their corresponding hydrophilic counterparts. Pyridinium-based ILs with isopropyl isomer were more

thermally stable than those with propyl alkyl chain. The thermal stability trend for the pyridinium ILs was: [N-IsopropylPyrPF$_6$]>[N-propylPyrPF$_6$]>>[N-IsopropylPyrBr]>[N-propylPyrBr]. DSC showed that the glass transition temperatures of ILs were dependent on the counter anion. There bigger the counter anion, the smaller the glass transition temperature.

Vinyl pyridinium-based PILs/MWCNT composites were observed to be more times thermally stable and relatively insoluble in aqueous solution. This makes the compounds useful for solid-liquid adsorption processes. Structural studies of the PILs/MWCNTs showed unaltered surface morphologies and decreased crystalline size in pristine carbon nanotubes. The ILs/MWCNT and PILs/MWCNT composites used as adsorbents for Cr(VI) in aqueous solutions indicated that the adsorption occurred at pH 2-3. This only confirmed the adsorption of dichromate ($Cr_2O_7^-$) and hydrochromate ($HCrO_4^-$). At lower pH values, the ionic and π-anionic electrostatic interactions between the positively-end of the composites and Cr(VI) were believed to have facilitated the adsorption of anionic ($Cr_2O_7^-$) and ($HCrO_4^-$). Maximum removal efficiency of 60% was achieved.

The adsorption data obtained on the adsorption of Cr(VI) onto ILs/MWCNT and PILs/MWCNT composites fitted well into both Langmuir and Freundlich adsorption isotherms. The

homogeneity and heterogeneity character of the adsorbents probably came into play significantly and that can be attributed to the diversified nature of the composites which includes the bulky pyridinium and imidazolium organic cations with delocalized charges, some large counter anions and the graphitic functional carbon groups. In order to understand the mechanism behind the adsorption of Cr(VI) onto ILs/MWCNT and PILs/MWCNT composites, pseudo-second-order kinetic model was employed. The results showed that the calculated maximum adsorption capacities (q_{ecal}) and experimental maximum adsorption capacities ($q_{e.exp}$) were closely related, with higher correlation co-efficiencies (R^2>0.99) confirming the applicability and feasibility of pseudo-second-order model on the adsorption of Cr(VI) in this study. It could therefore be concluded that ILs/MWCNT and PILs/MWCNT composites of imidazolium and pyridinium are thermally stable, water insoluble, hydrophobic and are relatively good as adsorbents for Cr(VI) ions.

6.3 Future prospects

There is a need to study the physicochemical properties of the composites; particularly the ILs and PILs functionalized carbon materials. This is necessary in order to understand the processes and mechanisms behind the solid-liquid adsorption. The coordination and/or interaction protocols between ionic liquids derivatives and carbon nanotubes should also be investigated. Although, results from this study suggested that possible interactions between ionic liquids

derivatives and carbon nanotubes could be *van der Waals* forces, π-anion, π-cation, and/or electrostatic interactions, however, more must be done to investigate the possible impact of the molecular weight of polymeric ionic liquids on adsorption. In order to get more insights on the mechanisms and kinetics facilitating the solid-liquid adsorption process of metal ions, additional properties of the composites such as definite chemical composition and structural orientation should also be probed. On solid-liquid adsorption process, the effect of adsorbent weight and temperature variations is of importance in further studies. There is also a need to understand the nature and the chemical behaviour of ions participating in solid-liquid adsorption system of ILs and PILs-functionalized carbon nanotubes composites. Further studies should be conducted on the removal of other toxic metal ions and acid mine drainage. The reusability of the composites is another important parameters and in future studies, it should be further investigated.

REFERENCES

1. Obuseng, V.; Nareetsile, F.; Kwaambwa, H.M. A study of the removal of heavy metals from aqueous solutions by *Moringa oleifera* seeds and amine-based ligand 1,4- bis[N,N-bis(2-picoyl)amino]butane. *Anal. Chim. Acta*, **2012**, *730*, 87-92.

2. Nadeem, M.; Mahmooda, A.; Shahid, S.A.; Shah, S.S.; Khalid, A.M.; McKaye, G. Sorption of lead from aqueous solution by chemically modified carbon adsorbents. *J. Hazard. Mater*. **2006**, B*138*, 604-613.

3. Ren, L.; He, X.; Zhang , M.; Cai, H.C.; Liu, A.; Yang, D. Study on disaster controlling for water contamination of severe Cr-contaminated sites on Jialing River. *Proced. Environ. Sci*. **2016**, *31*, 295–302.

4. Pagnanelli, F.; Mainelli, S.; Veglio, F.; Toro, L. Heavy metal removal by olive pomace: Biosorbent characterization and equilibrium modeling. *Chem. Eng. Sci.* **2003**, *58*, 4709-4717.

5. Lakovleva, E.; Makila, E.; Salonene, J.; Sitarz, M.; Wang, S.; Sillanpaa, M.; Acid mine drainage treatment: Neutralization and toxic elements removal with unmodified and modified limestone. *Ecolog. Eng*. **2015**, *81*, 30-40.

6. Costello, C. Acid mine drainage innovative treatment technologies. *Nat. Net. Environ. Manag. Stud. USEPA*, Washington, D.C. **2003**.

7. Dai, J.; Ren, F.L.; Tao, C.Y. Adsorption of Cr(VI) and speciation of Cr(VI) and Cr(III) in aqueous solutions using chemically modified chitosan. *Int. J. Environ. Res. Public Health*. **2012**, *9*, 1757–1770.

8. Bhattacharya, A.K.; Naiya, T.K.; Mandal, S.N.; Das, S.K. Adsorption kinetics and equilibrium studies on removal of Cr(VI) from aqueous solutions using different low-cost adsorbents. *Chem*. *Eng*. *J*. **2008**, *137*, 529–541.

9. Kumar, P.A.; Chakraborty, S.; Ray, M. Removal and recovery of chromium from wastewater using short chain polyaniline synthesized on jute fiber. *Chem*. *Eng*. *J*. **2008**, *141*, 130–140.

10. Kumar, P.A.; Ray, M.; Chakraborty, S. Hexavalent chromium removal from wastewater using aniline formaldehyde condensate coated silica gel. *J*. *Hazard*. *Mater*. **2007**, *143*, 24–32.

11. Tavengwa, N.T.; Cukrowska, E.; Chimuka, L. Synthesis, adsorption and selectivity studies of N-propyl quaternized magnetic poly(4-vinylpyridine) for hexavalent chromium. *Talanta*, **2013**, *116*, 670–677.

12. Li, Y.; Li, G.; Wang, X.; Zhu, Z.; Ma, H.; Zhang, T.; Jin, J. Poly(ionic liquid)-wrapped single-walled carbon nanotubes for sub-ppb detection of CO_2. *Chem*. *Commun*. **2012**, *48*, 8222-8224.

13. Gargallo, L.; Miranda, B.; Ríos, H.; González-Nilo, F.; Radic, D. Surface characterization and study of Langmuir films of poly (4-vinylpyridine) quaternized with n-alkylbromide. *Polym*. *Int*. **2001**, *520*, 858–862.

14. Baughman, R.H.; Zakhidov, A.A.; de Heer, W.A. Carbon nanotubes-the route toward applications. *Science*. **2002**, *297*, 787-792.

15. Karousis, N.; Tagmatarchis, N.; Tasis, D. Current progress on the chemical modification of carbon nanotubes. *Chem*. *Rev*. **2010**, *110*, 5366-5397.

16. Le, C.M.Q.; Cao, X.T.; Jeong, Y.T.; Lim, K.T. Covalent functionalization of multi-walled carbon nanotubes with imidazolium-based poly(ionic liquid)s by Diels-Alder "click" reaction. *J. Ind. Eng. Chem.* **2018**, *450*, 122-129.

17. Zhao, L.; Yang, J.; Ye, H.; Zhao, F.; Zeng, B. Preparation of hydrophilic surface-imprinted ionic liquid polymer on multi-walled carbon nanotubes for the sensitive electrochemical determination of imidacloprid. *RSC Adv.* **2017**, *7*, 4704-4709.

18. Vicentini, F.C.; Ravanini, A.E.; Silva, T.A.; Janegitz, B.C.; Fatibello-Filho, V.Z.O. A novel architecture based upon multi-walled carbon nanotubes and ionic liquid to improve the electroanalytical detection of ciprofibrate. *Analyst*, **2014**, *139*, 3961-3967.

19. Lu, J.; Yan, F.; Texter, J. Advanced applications of ionic liquids in polymer science. *Prog. Polym. Sci.* **2009**, *34*, 431-448.

20. Wilkes, J.S. Properties of ionic liquid solvents for catalysis. *J. Mol. Catal. A*: *Chem.* **2014**, *214*, 11-17.

21. Lee, M.; Choi, U.H.; Colby, R.H.; Gibson, H.W. Ion conduction in imidazolium acrylate ionic liquids and their polymers. *Chem. Mater.* **2010**, *22*, 5814-5822.

22. Chanthad, C.; Masser, K.A.; Xu, K.; Runt, J.; Wang, Q. Synthesis of triblock copolymers composed of poly(vinylidene fluoride-co-hexafluoropropylene) and ionic liquids segments. *J. Mater. Chem.* **2012**, *22*, 341-344.

23. Willa, C.; Yuan, J.; Niederberger, M.; Koziej, D. When nanoparticles meet poly(Ionic Liquid)s: Chemoresistive CO_2 sensing at room remperature. *Adv. Funct. Mater.* **2015**, *25*, 2537–2542.

24. Vijakrishna, K.; Jewrajka, S.K.; Ruiz, A.; Marcilla, R.; Pomposo, J. A.; Mecerreyes, D.; Taton, D.; Gnanou, Y. Synthesis by RAFT and ionic responsiveness of double hydrophilic block copolymers based on ionic liquid monomers units. *Macromolecules*, **2008**, *41*, 6299-6308.

25. Sadeghpour, M.; Yusoff, R.B.; Aroua, M.K. Polymeric ionic liquids (PILs) for CO_2 capture. *Rev*. *Chem*. *Eng*. **2016**, *01*, 1-18.

26. Safavi, A.; Maleki, N.; Moradlou, O.; Sorouri, M. Direct electrochemistry of haemoglobin and its electrocatalytic effect based on its direct immobilization on carbon ionic liquid electrode. *Electrochem*. *Commun*. **2008**, *10*. 420-423.

27. Yuan, J.; Antoneitti, M. Poly(ionic liquid)s: Polymers expanding classical property profiles. *Polymer*, **2011**, *52*, 1469-1482.

28. Kadokawa, L. Polymerizable ionic liquids: Development to photo function poly(ionic liquid) materials. *Res*. *Art*. *TCIMAIL*. **2013**, *159*, 1-6.

29. Grygiel, K.; Wicklein, B.; Zhao, Q.; Eder, M.; Petterson, T.; Bergstrom, L.; Antoneitti, M.; Yuan, J. Omnidispersible poly(ionic liquid)-functionalized cellulose nanofibris: Surface grafting & polymer membrane reinforcement. *Chem*. *Commun*. **2014**, *50*, 12486-12489.

30. Bhavsar, R.S.; Kumbharkar, S.C.; Kharul, U.K. Polymeric ionic liquids (PILs): Effect of anion variation on their CO_2 sorption. *J*. *Membr*. *Sci*. **2012**, *389*, 305-315.

31. Kausar, A. Research progress in frontiers of poly(ionic liquid)s. *Rev*. *Polym*. *Plast*. *Technol*. *Eng*. **2017**, *57*, 1823-1838.

32. Nishimura, N.; Ohno, H. 15th anniversary of polymerized ionic liquids. *Polymer*, **2014**, *55*, 3289-3297.

33. Green, O.; Grubjesic, S.; Lee, S.; Firestone, M.A. The design of polymeric ionic liquids for the preparation of functional materials. *Polym*. *Rev*. **2009**, *49*, 339-360.

34. Yuan, J.; Antoneitti, M. Poly(ionic liquid) latexes prepared by dispersion polymerization of ionic liquid monomers. *Macromolecules,* **2011**, *44*, 744–750.

35. Manojkumar, K.; Mecerreyes, D.; Taton, D.; Gnanou, Y.; Vijayakrishna, K. Self-assembly of Poly(ionic liquid)s (PILs)-based amphiphilic homopolymers into vesicles and supramolecular structures with dye and silver nanoparticles. *Polym*. *Chem*. **2017**, *8*, 3497-3503.

36. Yuan, J.; Mecerreyes, D.; Antonietti, M. Poly(ionic liquid)s: An update. *Prog*. *Polym*. *Sci*. **2013**, *38*, 1009-1036.

37. Mecerreyes, D. Broadening the properties and applications of polyelectrolytes. *Prog*. *Polym*. *Sci*. **2011**, *36*, 1629-1648.

38. Qian, W.; Texter, J.; Yan, F. Frontiers in Poly(ionic liquid)s: Synthesis and applications. *Chem*. *Soc*. *Rev*. **2017**, *46*, 1124-1648.

39. Wu, B.; Zhang, Z.H.; Huang, M.H.; Peng, Y. Polymerizable ionic liquids and polymeric ionic liquids: facile synthesis of ionic liquids containing ethylene oxide repeating unit *via* methanesulfonate and their electrochemical properties. *RSC Adv*. **2017**, *7*, 5394-5401.

40. Eftekhari, A.; Saito, T. Synthesis and properties of polymerized ionic liquids. *Eur*. *Polym*. *J*. **2017**, *03*, 1-63.

41. Obadia, M.M.; Fagour, S.; Vygodskii, Y.S.; Vidal, F.; Serghei, A.; Shoplov, A. S.; Droekenmuller, E. Probing the effect of anion structure on the physical properties of cationic 1,2,4-triazolium-based poly(ionic liquid)s. *J. Polym. Sci. Part A*: *Polym. Chem*. **2016**, *54*, 2191-2199.

42. Kim, Y.; Song, M.; Kim, K.; Park, S.; Min, S.; Rhee, H. nafion/ZrSPP composite membrane for high temperature operation of PEMFCs. *Electrochem. Acta*, **2004**, *50*, 645-648.

43. Wood, T.J.; Schofield, W.C.E.; Lund, O.; Larsen, M. J.; Badyal, J.P.S. High ion-conducting poly(ionic liquid) layers. *Chem. Commun*. **2012**, *48*, 10201-10203.

44. Liu, Y.; Yuan, J.; Dong, Y.; Zhao, X.; Yin, J. Enhanced temperature effect electrorheological fluid based on cross-linked poly(ionic liquid) particles. *Soft. Matter*, **2017**, *13*, 1027-1039.

45. Jadhav, N.R.; Gaikwad, V.L.; Nair, K.J.; Kadam, H.M. Glass transition temperature: Basics and application in pharmaceutical sector. *Asian J. Pharmaceut*. **2009**, *3*, 82-89.

46. Hu, H.; Yuan, W.; Lu, L.; Zhao, H.; Jia, Z.; Bakerly, G.L. Low Glass transition temperature polymer electrolyte prepared from ionic liquid grafted polyethylene oxide. *J. Polym. Sci. Part A*: *Polym. Chem*. **2014**, *52*, 2104–2110.

47. Smith, T.W.; Zhao, M.; Yang, F.; Smith, D.; Cebe, P. Imidazole polymers derived from ionic liquid 4‑Vinylimidazolium monomers: Their synthesis and thermal and dielectric properties. *Macromolecules*, **2013**, *46*, 1133-1143.

48. Ediger, M.D.; Angell, C.A.; Nagel, S.R. Supercooled liquids and glasses. *J. Phys. Chem*. **1996**, *100*, 13200-13212.

49. Dudowicz, J.; Freed, K.F.; Douglas, J.F. The glass transition temperature of polymer melts. *J. Phys. Chem. B.,* **2005**, *109*, 21285–21292.

50. Jenkins M. Polymer science and materials case study. Level 2 (level I),N225, Lecture 3, Factors affecting the glass transition temperature. Available from: http:// www.eng.bham.ac.uk/metallurgy/people/Jenkinsfiles/L2%20PCS%202006.pdf. (Accessed: July **2017**).

51. Martin, A.; Swarbrick, J.; Cammarata, A. Physical Pharmacy: Physical Chemical Principles in the Pharmaceutical Sciences. *3rd ed*. Bombay:Varghese Publishing House. **1991**. 628-631.

52. The Glass transition in polymers, Doitpoms teaching and learning packages. University of Cambridge. Available from: http://www.doitpoms.ac.uk/tlplib/glass-transition/theory1.php. (Accessed: July **2017**).

53. Glass transition temperatures of sartomer products. Sartomer application bulletin. Available from: http://www.sartomereurope.com. (Accessed: June **2017**).

54. Forster, A.; Hempenstall, J.; Rades, T. Investigation of drug/polymer interaction in glass solutions prepared by melt extrusion. *Int. J. Vibrat. Spec*. **2001**, *5*, 1-15.

55. Smith, D.M. Synthesis and Characterization of poly(Ionic Liquids) derived from 1-ethyl-3-methyl-4-vinylimidazolium triflate. M.Sc Dissertation. Department of Chemistry Rochester Institute of Technology, Rochester, *NY 14623-5603*. **2011**. (Accessed: March **2017**).

56. Elabd, Y, A.; Ye, Y. Anion exchanged polymerized ionic liquids: High free volume single ion conductors. *Polymer*, **2011**, *52*, 1309−1317.

57. Huddleston, J.G.; Visser, A.E.; Reichert, W.M.; Willauer, H.D.; Broker, G.A.; Rogers, R.D. Characterization and comparison of hydrophilic and hydrophobic room temperature ionic liquids incorporating the imidazolium cation. *Green. Chem.* **2001**, *3*, 156-164.

58. Guo, J.; Zhou, Y.; Qiu, L.; Yuan, C.; Yan, F. Self-assembly of amphiphilic random co-poly(ionic liquid)s: The effect of anions, molecular weight, and molecular weight distribution. *Polym. Chem.* **2013**, *4*, 4004-4009.

59. Isik, M.; Fernandes, A.M.; Vijayakrishna, K.; Paulis, M.; Mecerreyes, D. Preparation of poly(ionic liquid) nanoparticles and their novel application as flocculants for water purification. *Polym. Chem.* **2016**, *7*, 1668-1674.

60. Mythri, J.; Arusha, B.S.; Reddy, M.S. Ionic liquids as green solvents-polymeric and catalytic applications. *Rev. J. Chem. Pharm. Sci.* **2014**, *3*, 80-81.

61. Marcilla, R.; Blazquez, J.A.; Fernandez, R.; Grande, H.; Pomposo, J.A.; Mecerreyes, D. Synthesis of novel polycations using the chemistry of ionic liquids. *Macromol. Chem. Phys.* **2005**, *206*, 299-304.

62. Zhang, W.; Yuan, J. Poly(1-vinyl-1,2,4-triazolium) poly(ionic liquids): Synthesis and unique behavior in loading metal ions. *Macromol. Rapid Commun.* **2016**, *37*, 1124-1129.

63. Weber, R.L.; Ye, Y.; Schmitt, A.L.; Banik, S.M.; Elabd, Y.A.; Mahanthappa, M.K. Effect of nanoscale morphologies on the conductivity of polymerized ionic liquid block copolymers. *Macromolecules*, **2011**, *44*, 5727-5735.

64. Vijakrishna, K.; Jewrajka, S.K.; Ruiz, A.; Marcilla, R.; Pomposo, J.A.; Mecerreyes, D.; Taton, D.; Gnanou, Y. Synthesis by RAFT and ionic responsiveness of double hydrophilic

block copolymers based on ionic liquid monomers units. *Macromolecules*, **2008**, *41*, 6299-6308.

65. Mori, H.; Yahagi, M.; Endo, T. RAFT polymerization of N-vinyimidazolium salts and synthesis of thermoresponsive ionic liquid block copolymers. *Macromolecules*, **2009**, *42*, 8082-8092.

66. Yuan, J.; Schlaad, H.; Giordano, C.; Antonietti, M. Designer polymers. *Eur*. *Polym*. *J*. **2011**, *47*, 401-826.

67. Chanthad, C.; Masser, K.A.; Xu, K.; Runt, J.; Wang, Q. Synthesis of triblock copolymers composed of poly(vinylidene fluoride-co-hexafluoropropylene) and ionic liquids segments. *J*. *Mater*. *Chem*. **2012**, *22*, 341-344.

68. Shi, Z.; Newell, B.S.; bailey, T.S.; Gin, D.L. Ordered microphase-separated, nanocharged-charged 187eblock copolymers via sequential ATRT of styrene and styrenic imidazolium monomers. *Polymer*, **2014**, *55*, 6664-6671.

69. Wiesenauer, E.F.; Nguyen, P.T.; Newell, B.S.; Noble, R.D.; Gin, D.L. imidazolium-containing hydrophobic ionic-hydrophilic ABC triblock copolymers. *Soft Matter*, **2013**, *9*, 7923-7927.

70. Obadia, M.M.; Mudraboyina, B.P.; Serghei, A.; Phan, T.N.T.; Gigmes, D.; Drockenmuller, E. Enhanced properties of anionic poly(ionic liquid)s with 1,2,3-triazolium counter cations. *ACS Macro Lett*. **2014**, *3*, 658-662.

71. Coupillaud, P.; Vignolle, J.; Mecerreyes, D.; Taton, D. Post-polymerization modification and organocatalysis using reactive statistical poly(ionic liquid)-based copolymers. *Polymer*, **2014**, *55*, 3404-3414.

72. Pourjavadi, A.; Hosseini, S. H.; Soleyman, R. Cross-linked poly(ionic liquid) as high loaded dual acidic organocatalyst. *J. Mol. Catal. A. Chem.* **2012**, *365*, 55-59.

73. Coupillaud, P.; Pinaud, J.; Guidolin, N.; Vignolle, J.; Fevre, M.; Veaudecrenne, E.; Mecerreyes, D.; Taton, D. Poly(ionic liquid)s –based on imidazolium hydrogen carbonate monomer units as recyclable polymer/supported-heterocyclic carbenes. *J. Polym. Sci., Part A*: *Polym. Chem.* **2013**, *51*, 4530-4540.

74. Grobeheilmann, J.; Bandomir, J.; Kragl, U. Preparation of poly(ionic liquid)s-supported recyclable organocatalyst for the asymmetric Nitroaldol (Henry) reaction. *Chem. Eur. J.* **2015**, *21*, 18951-18960.

75. Lambert, R.; Coupillaud, P.; Wirotius, A.; Vignolle, J.; Taton, D. Imidazolium-based Poly(ionic liquid)s featuring acetate counter anions. *Macromol. Rapid. Commun.* **2016**, *37*, 1143-1149

76. Bi, W.; Tian, M.; Row, K.H. Evaluation of molecular imprinted anion-functionalized poly(ionic liquid)s by multi-phase dispersive extraction of flavonoids from plant. *J. Chromatogr.* **2013**, *B913-914*, 61-68.

77. Kuzmicz, D.; Coupillaud, P.; Men, Y.; Vignolle, J.; Vendraminetto, G.; Ambrogi, M.; Taton, D.; Yuan, J. Functional mesoporous poly(ionic liquid) –based copolymer monoliths from synthesis to catalysis and microporous carbon production. *Polymer*, **2014**, *55*, 3423-3430.

78. Nakabayashi, K.; Umeda, A.; Sato, Y.; Mori, H. Synthesis of 1,2,4-triazolium based polymers and block copolymers by RAFT polymerization: Ion conductivity and assembled structures. *Polymer*, **2016**, *96*, 81-93.

79. Ding, S.; Tang, H.; Radosz, M.; Shen, Y. Atom transfer radical polymerization of ionic liquid 2-(1-butylimidazolium-3-yl)ethyl methacrylate tetrafluoroborate. *J. Polym. Part A. Polym. Chem*. **2004**, *42*, 5794-5801.

80. Tang, J.; Sun, W.; Tang, H.; Radosz, M.; Shen, Y. Enhanced CO_2 absorption of poly(ionic liquid)s. *Macromolecules*, **2005**, *38*, 2037–2039.

81. Sajida, M.; Nazala, M.K.; Ihsanullaha.; Baigb, N.; Osman, A.M. Removal of heavy metals and organic pollutants from water using dendritic polymers based adsorbents: A critical review. *Sep. Purif. Technol*. **2018**, *191*, 400–423.

82. Walcarius, A.; Mercier, L. Mesoporous organosilica adsorbents: Nanoengineered materials for removal of organic and inorganic pollutants. *J. Mater. Chem*. **2010**, *20*, 4478–4511.

83. Abbas, I.A.; Al-Amer, A.M.; Laoui, T.; Al-Marri, MJ.; Nasser, M.S. Heavy metal removal from aqueous solution by advanced carbon nanotubes: critical review of adsorption applications. *Sep. Purif. Technol*. **2016**, *157*, 141–161.

84. Gao, P.; Liu, Z.H.; Xue, G.; Han, B.; Zhou, M.H. Preparation and characterization of activated carbon produced from rice straw by $(NH_4)HPO_4$ activation. *Bioresour Technol.* **2010**, *102*, 3645-3648.

85. Lin, S.H.; Juang, R.S. Adsorption of phenol and its derivatives from water using synthetic resins and low-cost natural adsorbents: A review. *J. Environ. Manag.* **2009**, *90*, 1336–1349.

86. Sajid, M.; Basheer, C.; Alsharaa, A.; Narasimhan, K.; Buhmeida, A.; AlQahtani, M. Development of natural sorbent based micro-solid-phase extraction for determination of phthalate esters in milk samples. *Anal. Chim. Acta*. **2016**, *924*, 35–44.

87. Matandabuzo, M.; Ajibade, P.A. Removal of metal ions from aqueous solutions using activated carbon prepared from *Zea mays* stem. *Chem. Eng. Biotechnol. Food industry (St.Cerc.St. CICBIA)*. **2018**, *19*, 117-132.

88. Pan, B.; Pan, B.; Zhang, W.; Lv, L.; Zhang, Q.; Zheng, S. Development of polymeric and polymer-based hybrid adsorbents for pollutants removal from waters. *Chem. Eng. J.* **2009**, *151*, 19–29.

89. Lofrano, G.; Carotenuto, M.; Libralato, G.; Domingos, R.F.; Markus, A.; Dini, L.; Gautam, R.K.; Baldantoni, D.; Rossi, M.; Sharma, S.K.; Chattopadhyaya, M.C.; Giugni, M.G.; Meric, S. Polymer functionalized nanocomposites for metals removal from water and wastewater: An overview. *Water Res.* **2016**, *92*, 22-37.

90. Jiang, Y.; Li, F.; Ding, G.; Chen, Y.; Liu, Y.; Hong, Y.; Liu, P.; Qi, X.; Ni, L. Synthesis of a novel ionic liquid modified copolymer hydrogel and its rapid removal of Cr(VI) from aqueous solution. *J. Colloid. Interf. Sci.* **2015**, *455*, 125–133.

91. Hu, C.; Gao, Q.; Liu, S.; Chang, L.; Xia, K.; Han, B.; Zhou, C. Crosslinked poly(ionic liquid) anchored with organic probe as a new promising platform for organic solvent-free recognition, quantification, and selective removal of heavy metal ion. *Chem. Eng. J.* **2018**.

92. Shen, L.C.; Nguyen, X.T.; Hankins, N.P. Removal of heavy metal ions from dilute aqueous solutions by polymer–surfactant aggregates: A novel effluent treatment process. *Sep. Purif. Technol*. **2015**, *152*, 101–107.

93. Iliaa, R.; Liatsoub, I.; Savvaa, I.; Vasilec, E.; Vekasd, L.; Marinicae, O.; Mpekrisa, F.; Pashalidisb, I.; Krasia-Christoforou, T. Magnetoresponsive polymer networks as adsorbents for the removal of U(VI) ions from aqueous media. *Euro. Polym. J.* **2017**, *97*, 138–146.

94. Akl, Z.F.; El-Saeed, S.M.; Atta, A.M. In-situ synthesis of magnetite acrylamide aminoamidoxime 191anocomposites adsorbent for highly efficient sorption of U(VI) ions. *J. Ind. Eng. Chem*. **2016**, *34*, 105–116.

95. Ozay, O.; Ekici, S.; Aktas, N.; Sahiner, N. P(4-vinyl pyridine) hydrogel use for the removal of UO_2^{2+} and Th^{4+} from aqueous environments, *J. Environ. Manag*. **2011**, *92*, 3121–3129.

96. Al Hamouz, O.C.S.; Estatie, M.K.; Morsy, M.A.; Saleh. T.A. Lead ion removal by novel highly cross-linked Mannich based polymers. *J. Taiwan Institute Chem. Eng*. **2017**, *70*, 345–351.

97. Zhou, Z.; Kong, D.; Zhu, Z.; Wang, N.; Wang, Z.; Wang, Q.; Liu, W.; Li, Q.; Zhang, W.; Ren, Z. Preparation and adsorption characteristics of an ion-imprinted polymer for fast removal of Ni(II) ions from aqueous solution. *J. Hazard. Mater*. **2018**, *341*, 355–364.

98. Chen, L.; Huang, X. Preparation of an adsorbent based on polymeric ionic liquid for the simultaneous extraction of acidic, basic and neutral pollutants. *J. Chromat. A.* **2016**, *1466*, 42–49.

99. Lam, B.; Deon, S.; Morin-Crini, N.; Crini, G.; Fievet, P. Polymer-enhanced ultrafiltration for heavy metal removal: Influence of chitosan and carboxymethyl cellulose on filtration performances. *J. Cleaner Prod*. **2018**, *171*, 927-933.

100. Huang, Y.; Wu, D.; Wang, X.; Huang, W.; Lawless, D.; Feng, X. Removal of heavy metals from water using polyvinylamine by polymer-enhanced ultrafiltration and flocculation. *Sep. Purif. Technol*. **2016**, *158*, 124–136

101. Siahkamari, M.; Jamali, A.; Sabzevari, A.; Shakeri, A. Removal of Lead(II) ions from aqueous solutions using biocompatible polymeric nano-adsorbents: A comparative study. *Carbohyd. Polym*. **2017**, *157*, 1180–1189.

102. Cao, Y.L.; Pan, Z.H.; Shi, Q.X.; Yu, J.Y. Modification of chitin with high adsorption capacity for methylene blue removal. *Int. J. Biol. Macromol*. **2018**, *114*, 392–399.

103. Cegłowski, M.; Schroeder, G. Removal of heavy metal ions with the use of chelating polymers obtained by grafting pyridine–pyrazole ligands onto polymethylhydrosiloxane. *Chem. Eng. J*. **2015**, *259*, 885–893.

104. El-Saida, W.A.; El-Khoulyb, M.E.; Alia, M.H.; Rashadc, R.T.; Elshehyd, E.A.; Al-Bogami, A.S. Synthesis of mesoporous silica-polymer composite for the chloridazon pesticide removal from aqueous media. *J. Environ. Chem. Eng*. **2018**, *6*, 2214–2221.

105. Hosseini, S.; Mahmud, N.H.M.E.; Yahya, R.B.; Ibrahim, F.; Djordjevic, I. Polypyrrole conducting polymer and its application in removal of copper ions from aqueous solution. *Mater*. *Lett*. **2015**, *149*, 77–80.

106. García-Fernández, M. J.; Sancho-Querol, S.; M. Pastor-Blas, M.; Sepúlveda-Escribano, A. Surfactant-assisted synthesis of conducting polymers. Application to the removal of nitrates from water. *J*. *Colloid*. *Interf*. *Sci*. **2017**, *494*, 98–106.

107. Ko, D.; Mines, P.D.; Jakobsen, M.H.; Yavuz, C.T.; Hansen, H.C.B.; Andersen, H.R. Disulfide polymer grafted porous carbon composites for heavy metal removal from stormwater runoff. *Chem. Eng. J.* **2018**, *384*, 685-692.

108. Yuan, G.; Tu, H.; Liu, J.; Zhao, C.; Liao, J.; Yang, Y.; Yang, J.; Liu, N. A novel ion-imprinted polymer induced by the glycylglycine modified metalorganic framework for the selective removal of Co(II) from aqueous solutions. *Chem*. *Eng*. *J*. **2018**, *333*, 280–288.

109. Liang, Q.; Geng, J.; Luo, H.; Fang, W.; Yin, Y. Fast and selective removal of Cr(VI) from aqueous solutions by a novel magnetic Cr(VI) ion-imprinted polymer. *J*. *Mol*. *Liq*. **2017**, *248*, 767–774.

110. Xi, Y.; Luo, Y.T.; Luo, J.M.; Luo, X.B. Removal of cadmium(II) from wastewater using novel cadmium ion-imprinted polymers. *J*. *Chem*. *Eng*. *Data*, **2015**, *60*, 3253–3261.

111. So, J.; Pang, C.; Dong, H.; Jang, P.; U,J.; Ri, K.; Yun, C. Adsorption of 1-naphthyl methyl carbamate in water by utilizing a surface molecularly imprinted polymer. *Chem*. *Phys*. *Lett*. **2018**, *699*, 199–207.

112. He, J.; Li, Y.; Wang, C.; Zhang, K.; Lin, D.; Kong, L.; Liu, J. Rapid adsorption of Pb, Cu and Cd from aqueous solutions by β-cyclodextrin polymers. *Appl. Surf. Sci*. **2017**, *426*, 29–39.

113. Fallah, N.; Taghizadeh, M.; Hassanpour, S. Selective adsorption of Mo(VI) ions from aqueous solution using a surface-grafted Mo(VI) ion imprinted polymer. *Polymer*, **2018**, *144*, 80-91.

114. Xu, X.; Wang, M.; Wu, Q.; Xu, Z.; Tian, X. Synthesis and application of novel magnetic ion-imprinted polymers for selective solid phase extraction of cadmium(II). *Polymers*, **2017**, *9*, 1-12.

115. Alizadeh, T. An imprinted polymer for removal of Cd^{2+} from water samples: Optimization of adsorption and recovery steps by experimental design. *Chin. J. Polym. Sci*. **2011**, *29*, 658–669.

116. Li, W.M.; He, R.; Tan, L.; Xu, S.Y.; Kang, C.C.; Wei, C.H.; Tang,Y.W. One-step synthesis of periodic ion imprinted mesoporous silica particles for highly specific removal of Cd^{2+} from mine wastewater. *J. Sol-Gel Sci. Technol*. **2016**, *78*, 632–640.

117. Li, L.; Zhu, F.; Lu, Y.; Guan, J. Synthesis, adsorption and selectivity of inverse emulsion Cd(II) imprinted polymers. *Chin. J. Chem. Eng*. **2018**, *26*, 494–500.

118. Luo, X.; Liu, L.; Deng, F.; Luo, S. Novel ion-imprinted polymer using crown ether as a functional monomer for selective removal of Pb(II) ions in real environmental water samples. *J. Mater. Chem. A*. **2013**, *1*, 8280-8286.

119. Younis, M.R.; Bajwa, S.Z.; Lieberzeit, P.A.; Khan, W.S.; Mujahid, A.; Ihsan, A.; Rehman, A. Molecularly imprinted porous beads for the selective removal of copper ions. *J. Sep. Sci*. **2016**, *39*, 793–798.

120. Wen, X.; Sun, N.; Yan, C.; Zhou, S.; Pang, T. Rapid removal of Cr(VI) ions by densely grafted corn stalk fibers: High adsorption capacity and excellent recyclable property. *J. Taiwan Institute Chem. Eng*. **2018**, *000*, 1–10.

121. Rashid, S.; Shen, C.; Yang, J.; Liu, J.; Li, J. Preparation and properties of chitosan–metal complex: Some factors influencing the adsorption capacity for dyes in aqueous solution. *J. Environ. Sci*. **20118**, *66*, 301–309.

122. Say, R.; Birlik, E.; ErsÖz, A.; Yılmaz, F.; Gedikbey, T.; Denizli, A. Preconcentration of copper on ion-selective imprinted polymer microbeads. *Anal. Chim. Acta*. **2003**, *480*, 251–258.

123. Liu, H.; Kong, D.; Sun, W.; Li, Q.; Zhou, Z.; Ren, Z. Effect of anions on the polymerization and adsorption processes of Cu(II) ion-imprinted polymers. *Chem. Eng. J*. **2016**, *303*, 348–358.

124. Abbasi, S.; Roushani, M.; Khani, H.; Sahraei, R.; Mansouri, G. Synthesis and application of ion-imprinted polymer nanoparticles for the determination of nickel ions. *Spectrochim Acta Part A*. **2015**, *140*, 534–543

125. Branger, C.; Meouche, W.; Margaillan, A. Recent advances on ion-imprinted polymers. *React. Funct. Polym*. **2013**, *73*, 859–875.

126. He, J.; Shang, H.; Zhang, X.; Sun, X. Synthesis and application of ion imprinting polymer coated magnetic multi-walled carbon nanotubes for selective adsorption of nickel ion. *Appl*. *Surf*. *Sci*. **2018**, *428*, 110–117.

127. Zhu, F.; Li, L.; Xing, J. Selective adsorption behavior of Cd(II) ion imprinted polymers synthesized by microwave-assisted inverse emulsion polymerization: Adsorption performance and mechanism. *J*. *Hazard*. *Mater*. **2017**, *321*, 103–110.

128. Kang, R.; Qiu, L.; Fang, L.; Yu, R.; Chen, Y.; Lu, X.; Luo, X. A novel magnetic and hydrophilic ion-imprinted polymer as a selective sorbent for the removal of cobalt ions from industrial wastewater. *J*. *Environ*. *Chem*. *Eng*. **2016**, *4*, 2268–2277.

129. Xu , D.; Wu, W.D.; Qi, H. J.;Yang, R. X.; Deng, W. Q. Sulfur rich microporous polymer enables rapid and efficient removal of mercury(II) from water. *Chemosphere*, **2018**, *196*, 174-181.

130. Sáncheza, J.; Espinosaa, C.; Poochb, F.; Tenhub, H.; Pizarroc, G.P.;Oyarzún, D.P. Poly(N,N-dimethylaminoethyl methacrylate) for removing chromium (VI) through polymer-enhanced ultrafiltration technique. *React*. *Funct Polym*. **2018**, *127*, 67–73.

131. Dautoo, U.K.; Shandil, Y.; Chauhan, G.S. New crosslinked hydrazide–based polymers as Cr(VI) ions adsorbents. *J*. *Environ*. *Chem*. *Eng*. **2017**, *5*, 5815–5826.

132. Thakur, S.S.; Chauhan, G.S. Gelatin–silica–based hybrid materials as efficient candidates for removal of chromium (VI) from aqueous solutions. *Ind*. *Eng*. *Chem*. *Res*. **2014**, *53*, 4838–4849.

133. Abdel-halim, E.S.; Al-deyab, S.S. Hydrogel from crosslinked polyacrylamide/guargum graft copolymer for sorption of hexavalent chromium ion. *Carbohyd. Polymer*, **2011**, *86*, 1306–1312.

134. Ozer, C.; Boysan, F. Imamoglu, M.; Yildiz, S.Z. Enhanced adsorption of hexavalent chromium ions on polyamine polyurea polymer: isotherm, kinetic, thermodynamic studies and batch processing design. *J. Disper. Sci. Technol.* **2016**, *37*, 860–865.

135. Modrzejewska, Z.; Kaminski, W. Separation of Cr(VI) on chitosan membranes, *Ind. Eng. Chem. Res.* **1999**, *38*, 4946–4950.

136. Anirudhan, T.S.; Rijith, S.; Suchithra, P. S.Preparation and characterization of iron(III) complex of an amino-functionalized polyacrylamide-grafted lignocellulosics and its application as adsorbent for chromium(VI) removal from aqueous media. *J Appl. Polym. Sci.* **2010**, *115*, 2069–2083.

137. Attia, A.A.; Khedr, S.A.; Elkholy, S.A. Adsorption of chromium ion (VI) by acid activated carbon. *Braz. J. Chem. Eng.* **2010**, *27*, 183–193.

138. Ren, Z.; Zhu, X.; Du, J.; Kong, D.; Wang, N.; Wang, Z.; Wang, Q.; Liu, W.; Li, Q.; Zhou, Z. Facile and green preparation of novel adsorption materials by combining sol-gel with ion imprinting technology for selective removal of Cu(II) ions from aqueous solution. *Appl. Surf. Sci.* **2018**, *435*, 574–584.

139. Mishra, S.; Verma, N. Surface ion imprinting-mediated carbon nanofiber-grafted highly porous polymeric beads: Synthesis and application towards selective removal of aqueous Pb(II). *Chem. Eng. J.* **2017**, *313*, 1142–1151.

140. Samadi, N.; Ansari, R.; Khodavirdilo, B. Removal of Copper ions from aqueous solutions using polymer derivations of poly (styrene-altmaleic anhydride). *Egyptian J. Petroleum*, **2017**, *26*, 375–389.

141. Wang, X.; Wang, C. Chitosan-poly(vinyl alcohol)/attapulgite nanocomposites for copper(II) ions removal: pH dependence and adsorption mechanisms. *Colloids Surf A*. **2016**, *500*, 186–194.

142. Zahria, N.A.M.; Jamilb, S.N.A.; Abdullaha, L.C.; Hueyd, S.J.; Yawa, T.C.S.; Mobarekehe, M.N.; Rapeia, N.S.M. Equilibrium and kinetic behavior on cadmium and lead removal by using synthetic polymer. *J. Water Proc. Eng*. **2017**, *17*, 277–289.

143. Allafchian, A.R.; Shiasi, A.; Amiri, R. Preparing of poly(acrylonitrile co maleic acid) nanofiber mats for removal of Ni(II) and Cr(VI) ions from water. *J. Taiwan Institute Chem. Eng*. **2017**, *80*, 563–569.

144. Yusoff, M.M.; Mostapa, N.R.N.; Sarkar, S.; Biswas, T.K.; Rahman, L.; Arshad, S.E.; Sarjadi, M.S.; Kulkarni, A.D. Synthesis of ion imprinted polymers for selective recognition and separation of rare earth metals. *J. Rare Earths*. **2017**, *35*, p. 177.

145. Sikder, M.T.; Kurasaki, M.; Tanaka, S.; Saito, T. Application of zerovalent iron impregnated chitosan-caboxymethyl-bcyclodextrin composite beads as arsenic sorbent. *J. Environ. Chem. Eng*. **2014**, *2*, 370–376.

146. Zhoua, Y.; Hua, Y.; Huanga, W.; Chenga, G.; Cuic, C.; Lu, J. A novel amphoteric β-cyclodextrin-based adsorbent for simultaneous removal of cationic/anionic dyes and bisphenol A. *Chem. Eng. J*. **2018**, *341*, 47–57.

147. Tolessaa, T.; Zhoua, X.X.; Amdea, M.; Liu. J.F. Development of reusable magnetic chitosan microspheres adsorbent for selective extraction of trace level silver nanoparticles in environmental waters prior to ICP-MS analysis. *Talanta*, **2017**, *169*, 91–97.

148. Huo, Y.; Wu, H.; Wang, Z.; Wang, F.; Liu, Y.; Feng, Y.; Zhao, Y. Preparation of core/shell nanocomposites adsorbents based on amine polymer-modified magnetic materials for the efficient adsorption of anionic dyes. *Colloid. Surf. A*. **2018**, *549*, 174–183.

149. Sikdera, T.; Jakariyac, M.D.; Rahmana, M.; Fujitaa, S.; Saitoc, T.; Kurasaki, M. Facile synthesis, characterization, and adsorption properties of Cd(II) from aqueous solution using *β*-cyclodextrin polymer impregnated in functionalized chitosan beads as a novel adsorbent. *J*. *Environ*. *Chem*. *Eng*. **2017**, *5*, 3395–3404.

150. Maity, A.; Ray, S.K. Chitosan based nanocomposite adsorbent—Synthesis, characterization and application for adsorption of binary mixtures of Pb(II) and Cd(II) from water. *Carbohyd. Polym*. **2018**, *182*, 159–171.

151. Srivastava, V.C.; Mall, I.D.; Mishra, I.M. Equilibrium modelling of single and binary adsorption of cadmium and nickel onto bagasse fly ash. *Chem*. *Eng*. *J*. **2006**, *117*, 79–91.

152. Heidari, A.; Younesi, H.; Mehraban, Z.; Heikkinen, H. Selective adsorption of Pb(II), Cd(II), and Ni(II) ions from aqueous solution using chitosan–MAA nanoparticles. *Int*. *J*. *Biol*. *Macromol*. **2013**, *61*, 251–263.

153. Ravi, S.; Ahn, W.S. Facile synthesis of a mesoporous organic polymer grafted with 2-aminoethanethiol for Hg^{2+} removal. *Micropor*. *Mesopor*. *Mater*. **2018**. *271*, 59-67.

154. Taghizadeh, M.; Hassanpour, S. Selective adsorption of Cr(VI) ions from aqueous solutions using a Cr(VI)-imprinted polymer supported by magnetic multiwall carbon nanotubes. *Polymer*, **2017**, *132*, 1-11.

155. Lessa, E.F.; Nunes, M.L.; Fajardo, A.R. Chitosan/waste coffee-grounds composite: An efficient and eco-friendly adsorbent for removal of pharmaceutical contaminants from water. *Carbohyd. Polym*. **2018**, *189*, 257–266.

156. Wen, Q.; Wang, Y.; Xu, K.; Li, N.; Zhang, H.;Yang, Q. A novel polymeric ionic liquid-coated magnetic multiwalled carbon nanotubes for the solid-phase extraction of Cu, Zn-superoxide dismutase. *Anal. Chim. Acta*. **2016**, *939*, 54-63.

157. Zhanga, T.; Yuea, X.; Zhangb, K.; Zhaoa, F.; Wanga, Y.; Zhang, K. Synthesis of Cu(II) ion-imprinted polymers as solid phase adsorbents for deep removal of copper from concentrated zinc sulfate solution. *Hydrometallurgy*, **2017**, *169*, 599–606.

158. Maatar, W.; Boufi, S. Poly(methacylic acid-co-maleic acid) grafted nanofibrillated cellulose as a reusable novel heavy metal ions adsorbent. *Carbohyd. Polym*. **2015**, *126*, 199–207.

159. He, Y.; Liu, Q.; Liu, F.; Huang, C.; Peng, C.; Yang, Q.; Wang, H.; Hu, J.; Liu, H. Porous organic polymer bifunctionalized with triazine and thiophene groups as a novel adsorbent for removing Cu(II). *Micropor. Mesopor. Mater*. **2016**, *233*, 10-15.

160. Zhu, Y.; Zhang, H.; Hui, A.; Ye, X.; Wang, A. Fabrication of porous adsorbent via eco-friendly Pickering-MIPEs polymerization for rapid removal of Rb^+ and Cs^+. *J. Environ. Chem. Eng*. **2018**, *6*, 849–857.

161. Zhou, G.; Luo, J.; Liu, C.; Chu, L.; Crittenden, J. Efficient heavy metal removal from industrial melting effluent using fixed-bed process based on porous hydrogel adsorbents. *Water Res*. **2018**, *131*, 246-254.

162. Mythri, J.; Anusha, B.S.; Reddy, M.S. Ionic liquids as green solvents: Polymeric and catalytic applications. *J. Chem. Pharm. Sci*. **2004**, *3*, 80-82.

163. Romero, A.; Santos, A.; Tojo, T.; Rodriguez, A. Toxicity and biodegradability of imidazolium ionic liquids. *J. Hazard. Mater*. **2008**, *151*, 268-273.

164. Mi, H.; Jiang, Z.; Kong, J. Hydrophobic poly(ionic liquid) for highly effective separation of methyl blue and chromium ions from water. *Polymers*, **2013**, *5*, 1203-1214.

165. Antonietti, M.; Kuang, D.; Smarsly, B.; Zhou, Y. Ionic liquids for the convenient synthesis of functional nanoparticles and other inorganic nanostructures. *Angew. Chem. Int. Ed.* **2004**, *43*, 4988–4992.

166. Kubisa, P. Application of ionic liquids as solvents for polymerization process. *Prog. Polym. Sci*. **2004**, *29*, 3-12.

167. Olivier-Bourbigou, H.; Myona, L.; Morvan, D. Ionic liquids and catalysis. *Appl. Catal. A. Gen*. **2010**, *373*, 1-56.

168. Wasserscheid, P.; Keim, W. Ionic liquids-New solutions for transition metal catalysis. *Angew. Chem. Int. Ed*. **2000**, *39*, 3772-3789.

169. Mantz, R.A.; Trulove, P.C. Viscosity and density of ionic liquids: Wassercheid, P.; Welton, T., Eds.; Wiley-Verlag GmbH & Co. **2002**, *3*, 56-68.

170. Vekariya, R.L.; Dhar, A.; Lunagariya, *J. Comp. Interface*. **2017**, *24*, 801-916.

171. Dyzuba, S.V.; Bartsch, R.A. New room-temperature ionic liquids with C2-symmetrical imidazolium cations. *Chem. Commun*. **2001**, *16*, 1466-1467.

172. Kowsari, E. Advanced applications of ionic liquids in polymer science. *Polym. Sci*. **2011**, *1*, 3-28.

173. Siedlecka, E.M.; Czerwicka, M.; Neumann, J.; Stepnowski, P.; Fernandez, J.F.; Thoming, J. Ionic liquids-methods of degradation and recovery. Kokorin, A (Ed). **2011**, *28*, 701-723.

174. Shariati, A.; Peters, C.J. High pressure phase equilibria of systems with ionic liquids. *J. Supercrit. Fluids*. **2005**, *34*, 171-176.

175. Keskin, S.; Kayrak-Talay, D.; Akman, U. A review of ionic liquids towards supercritical fluid 202anocomposit. *J. Supercrit. Fluids*, **2007**, *43*, 150-180.

176. Lunagariya, J.; Dhar, A.; Vekariya, R.L. Efficient esterification of n-butanol with acetic acid catalyzed by the Bronsted acidic ionic liquids: influence of acidity. *RSC Adv*. **2017**, *7*, 5412-5420.

177. Vekariya, R.L. A review of ionic liquids: Applications towards catalytic organic transformations. *J. Mol. Liq*. **2017**, *227*, 44-60.

178. Davis, J.H. Task-specific ionic liquids. *Chem. Lett*. **2004**, *33*, 1072-1077.

179. Zhang, S.; Sun, N, He, X.; Lu, X.; Zhang, X. Physical properties of ionic liquids: Database and evaluation. *Green Chem. Technol. Inst. Pro. Eng. Sci*. Beijing, 100080, China.

180. Vekariya, R.L. Reduction of micellar size of PEO-PPO-PEO triblock copolymer in the presence of ionic liquid in aqueous solutions: A SANS study. *J. Dispers. Sci. Technol*. **2018**, *39*, 517-521.

181. Lunagariya, L.; Kumar, N.S.; Asif, M.; Dhar, A.; Vekariya, R.L. Dependency of anion and chain length of imidazolium based ionic liquids on micellization of the block copolymer F127 in aqueous solution. *Polymers*, **2017**, *9*, 1-10.

182. Hallett, J.P.; Welton, T. Room-temperature ionic liquids: Solvents for synthesis and catalysis. *Chem. Rev.* **2011**, *111*, 3508–3576.

183. Yang, Y.K.; Xie, X.L.; Cui, W. Functionalization of carbon nanotubes with ionic liquids. In *Green Solvents II: Properties and Applications in Chemistry*; Mohammad, A., Inamuddin, Ed.; Springer Dordrecht Heidelberg: New York, London, **2012**; 399–434.

184. Papaiconomou, N.; Yakelis, N.; Salminen, J.; Bergman, R.; Prausinitz, J.M. Synthesis and properties of seven ionic liquids containing 1-methyl-3-octylimidazolium or 1-butyl-4-methylpyridinium cations. *J. Chem. Eng. Data*, **2006**, *51*, 1389- 1393.

185. Khupse, N.D.; Kumar, A. Ionic liquids: New materials with wide applications. *Ind. J. Chem*. **2010**, *49A*, 635- 648.

186. Dzyuba, S.V. Synthesis, properties, and applications of ionic liquids. *Ph. D Thesis*, Texas Tech University, USA. **2002**.

187. Alamdari, R.F.; Zamani, F.G.; Shekarriz, M. Synthesis and thermal characterization of mono and dicationic imidazolium pyridinium based ionic liquids. *Orient. J. Chem*. **2015**, *31*, 1127- 1132.

188. Liu, Q.S.; Li, P.P.; Biermann, U.W.; Chen, J.; Liu, X.X. Density, dynamic viscosity, and electrical conductivity of pyridinium- based hydrophobic ionic liquids. *J. Chem. Thermod*. **2013**, *66*, 88-94.

189. Benito, J.; Garcia- Mardones, M.; Perez- Gregorio, V.; Gascon, I.; Lafuente, C. Physicochemical study of n-Ethylpyridinium bis(trifluoromethylsulfonyl)imide ionic liquid. *J. Sol. Chem*. **2014**, *43*, 676-710.

190. Dharaskar, S.A.; Wasewar, K.L.; Varma, M.N.; Shende, D.Z.; Yoo, C.K. Synthesis, characterization and application of 1-butyl-3-methylimidazolium tetrafluoroborate for extractive desulfurization of liquid fuel. *Arab. J. Chem*. **2013**, *9*, 578-587.

191. Eftakhari, A.; Saito, T. Synthesis and properties of polymerized ionic liquids. *European. Polym. J*. **2017**, *90*, 245-272.

192. He, L.; Xu, Q.; Hua, C.; Song, R. Effect of multi-walled carbon nanotubes on crystallization, thermal, and mechanical properties of poly(vinylidene fluoride). *Polym. Compos*. **2010**, 921-927.

193. Fukushima, T.; Kosaka, A.; Ishimura, Y.; Yamamoto, T.; Takigawa, T.; Ishii, N.; Aida, T. Molecular ordering of organic molten salts triggered by single-walled carbon nanotubes. *Science*, **2003**, *300*, 2072-2074.

194. França, J.P.M.; Nieto de Castro, C.A.; Pádua, A.A.H. Molecular Interactions and Thermal Transport in Ionic Liquids with Carbon Nanomaterials. *Physi. Chem. Chem. Phy.* **2017**, *19*, 17075-17087.

195. Asaka, K. Development of human-friendly polymeric actuators based on nano-carbon electrodes. *Synthesiology*, **2016**, *9*, 117-123.

196. Sugino, T.; Kiyohara, K.; Takeuchi, I.; Mukai, K.; Asaka, K. Actuator properties of the complexes composed by carbon nanotube and ionic liquid: The effects of additives. *Sens.Actuators B.* **2009**, *141*, 179–186.

197. Espejo, C.; Carri, F.J.; Martınez, D.; Berm udez, M.D. Multiwalled carbon nanotube-imidazolium tosylate ionic liquid lubricant. *Tribol. Lett*. **2013**, *50*, 127–136.

198. Yang, Y.K.; Yu, L.J.; Peng, R.G.; Huang, Y.L.; He, C.E.; Liu, H.Y.; Wang, X.B.; Xie, X.L.; Mai, Y.W. Incorporation of liquid-like multiwalled carbon nanotubes into an epoxy matrix by solvent-free processing. *Nanotechnology*, **2012**, *23*, e225701.

199. Salam, M.A.; Burk, R. Synthesis and characterisation of multi-walled carbon nanotubes modified with octadecylamine and polyethylene glycol. *Arab. J. Chem*. **2013**, *10*, 921-927.

200. Pereira, E.L.M.; Batista, A.S.M.; Ribeiro, F.A.S.; Asantos, A.P.; Furtado, C.A.; Faria, L.O. Preliminary studies of MWCNT/PVDF polymer composites. *Int. J. Chem. Mol. Eng*. **2016**, *10*, 144-147.

201. Ohba, T.; Chaban, V.V. A highly viscous imidazolium ionic liquid inside carbon nanotubes. *J. Phys. Chem. B.* **2014**, *118*, 6234-6240.

202. Chaban, V.V.; Prezhdo, O.V. Nanoscale carbon greatly enhances mobility of a highly viscous ionic liquid. *ACS Nano*, **2014**, *8*, 8190-8197.

203. Taherkhani, F.; Minofar, B. The effect of nitrogen doping on glass transition and electrical conductivity of [EMIM][PF6] ionic liquid encapsulated in zigzag carbon Nanotube. *J. Phys. Chem. C*., **2017**, *121*, 15493-15508.

204. Chen, S.; Guozhong, W.; Sha, M.; Huang, S. Transition of ionic liquid [bmim][PF6] from liquid to high-melting-point crystal when confined in multiwalled carbon nanotubes. *J. Am. Chem. Soc*. **2007**, *129*, 2416-2417.

205. Ohba, T.; Hata, K.; Chaban, V.V. Nanocrystallization of imidazolium ionic liquid in carbon nanotubes. *J. Phys. Chem. C*. **2015**, *119*, 28424–28429.

206. Subramanian, K.; Das, A.; Heinrich, G. Development of conducting polychloroprene rubber using imidazolium based ionic liquid modified multi-walled carbon nanotubes. *Compos. Sci. Technol*. **2011**, *71*, 1441–1449.

207. Bellayer, S.; Gilman, J.W.; Eidelman, N.; Bourbigot, S.; Flambard, X.; Fox, D.M.; De Long, H.C.; Trulove, P.C. Preparation of homogeneously dispersed multiwalled carbon nanotube/polystyrene 206 anocomposites via melt extrusion using trialkyl imidazolium compatibilizer. *Adv. Funct. Mater*. **2005**, *15*, 910–916.

208. Wang, J.; Chu, H.; Li, Y. Why single-walled carbon nanotubes can be dispersed in imidazolium based ionic liquids. *ACS Nano*, **2008**, *2*, 2540–2546.

209. Dyke, C.A.; Tour, J.M. Solvent-free functionalization of carbon nanotubes. *J. Phys. Chem. A*. **2003**, *125*, 1156-1157.

210. Pinkert, A.; Marsh, K.N.; Pang, S.S.; Staiger, M.P. Ionic liquids and their interaction with cellulose. *Chem. Rev.* **2009**, *109*, 6712–6728.

211. Fileti, E.E.; Chaban, V.V. Imidazolium ionic liquid helps to disperse fullerenes in water. *J. Phys. Chem* Lett. **2014**, *5*, 1795-1800.

212. Lee, D.W.; Seo, J.W. Preparation of carbon nanotubes from graphite powder at room temperature. *Mater. Sci*. **2011**, *4*, 1-10.

213. Liu, X.; Guo, J.; Chen, J.; Zhang, J.; Zhang, J. Synergistic effect of ionic liquid intercalation and multiwalled carbon nanotube spacers with improved supercapacitor performance. *J. Power Sources*. **2017**, *363*, 54-60.

214. Toral, M.I.; Navarrete, J.G.; Leiva, A.; Ríos, H.E.; Urzúa, M.D. Chromium retention properties of N-alkyl quaternized poly(4-vinylpyridine). *Euro. Polym. J*. **2009**, *45*, 730–737.

215. Namasivayam, C.; Sureshkumar, M.V. Removal of chromium (VI) from water and wastewater using surfactant modified coconut coir pith as a biosorbent. *Bioresour. Technol*. **2008**, *99*, 2218–2225.

216. Hara, M. (editor). Polyelectrolytes science and technology. New York: Marcel Dekker; **1993**. *Chapter 3*.

217. Gargallo, L.; Miranda, B.; Ríos, H.; González-Nilo, F.; Radic, D. Surface characterization and study of Langmuir films of poly (4-vinylpyridine) quaternized with n alkylbromide. *Polym. Int*. **2001**, *50*, 858–62.

218. Shaplov, A.S.; Ponkratov*a*, D.O.; Vlasov*b*, P.S.; Lozinskaya, E.I.; Komarova*a*, L.I.; Malyshkina, I.A.; Vidal, F.; Nguyen, G.T.M.; Armand, M.; Wandrey, C.; Vygodskii, Y. S. Synthesis and properties of polymeric analogs of ionic liquids. *Polym. Sci. Series B*, **2013,** *55*, 3–4.

219. Shaplov, A.S.; Vlasov, P.S.; Armand, M.; Lozinskaya, E.I.; Ponkratov, D.O.; Malyshkina, I.A.; Vidal, F.; Okatova, O.V.; Pavlov, G.M.; Wandrey, C.; Godovikova, I.A.; Vygodskii, Y.S. Design and synthesis of new anionic ‘‘polymeric ionic liquids’’ with high charge delocalization. *Polym. Chem.*, **2011**, *2*, 2609–2618.

220. Matandabuzo, M.; Ajibade, P.A. Synthesis and surface functionalization of multi-walled carbon nanotubes with imidazolium and pyridinium based ionic liquids: Thermal stability, dispersibility and hydrophobicity characteristics. *J. Mol. Liq.* **2018**, *286*, 248-293.

221. Esma, C.B.; Zoulikha, D.; Ali, M. Molecular weight effect on the quaternization of poly(4-vinylpyridine) with alkylbromide. *J. Macromol. Sci., Part A: Pure and Appl. Chem.* **2012**, *49*, 1084–1091.

222. Briones, X.O.; Tapiab, R.A.; Campodónicoa,P.R.; Urzúac, M.; Leivad, A.; Contrerasc, R.; González-Navarrete, J. Synthesis and characterization of poly (ionic liquid) derivatives of N-alkyl quaternized poly(4-vinylpyridine). *React. Funct. Polym.* **2018**, *124*, 64–71.

223. Le, V. T.; Ngo, C.L.; Le, Q.T.; Ngo, T.T.; Nguyen, D.N.; Vu, M.T. Surface modification and functionalization of carbon nanotube with some organic compounds. *Adv. Nat. Sci.*: *Nanosci. Nanotechnol.* **2013**, *4*, 1-5.

224. Hong, C.Y.; You, Y.Z.; Pan, C.Y. Functionalized multi-walled carbon nanotubes with poly(N-(2-hydroxypropyl)methacrylamide) by RAFT polymerization. *J. Polym. Sci., Part A*: *Polym. Chem.* **2006**, *44*, 2419-2427.

225. Sun, J.T.; Hong, C.Y.; Pan, C.Y. Surface modification of carbon nanotubes with dendrimers or hyperbranched polymers. *Polym. Chem.* **2011**, *2*, 998-1007.

226. Green, M.D.; la Cruz, D.S.; Ye, Y.; Layman, J.M.; Elabd, Y.A.; Winey, K.I.; Long, T.E. Alkyl-substituted *N*-vinylimidazolium polymerized ionic liquids: Thermal properties and ionic conductivities. *Macromol. Chem. Phys.* **2011**, *212*, 2522-2528.

227. Hemp, S.T.; Zhang, M.; Allen, M.H Jr.; Cheng, S.; Moore, R.B.; Long T.E. Comparing ammonium and phosphonium polymerized ionic liquids: Thermal analysis, conductivity, and morphology. *Macromol. Chem. Phys.* **2013**, *214*, 2099-2107.

228. Weber, R.L.; Ye, Y.; Banik, S.M.; Elabd, Y.A.; Hickner, M.A.; Mahanthappa M.K. Thermal and ion transport properties of hydrophilic and hydrophobic polymerized styrenic imidazolium ionic liquids. *J*. *Polym*. *Sci*: *Part B*: *Polym*. *Phys*. **2011**, *49*, 1287–1296.

229. Tunckol, M.; Hernandez, Z.H.; Sarasua, J.R.; Durand, J.; Serp, P. Polymerized ionic liquid functionalized multi-walled carbon nanotubes/polyetherimide composites. *Eur*. *Polym*. *J*. **2013**, *49*, 3770–3777.

230. Zhang, Y.; Shen, Y.; Yuan, J; Han, D.; Wang, Z.; Zhang, Q.; Niu, L. Design and synthesis of multifunctional materials based on an ionic-liquid backbone. *Angew*. *Chem*. *Int*. *Ed*. **2006**, *45*, 5867 –5870.

231. Haldera, K.; Khana, M.M.; Grünauera, J.; Shishatskiya, S.; Abetza, C.; Filiza, V.; Abetz, V. Blend membranes of ionic liquid and polymers of intrinsic microporosity with improved gas separation characteristics. *J*. *Membr*. *Sci*. **2017**, *539*, 368–382.

232. Dworaka, C.; Ligona, S.C.; Tiefenthallera, R.; Lagref, J.J.; Frantzb, R.; Cherkaouib, Z.M.; Liska, R. Imidazole-based ionic liquids for free radical photopolymerization. Designed Monomers. Polymer, **2015**, *18*, 262–270.

233. Yang, F. Synthesis and characterization of ionic liquids monomers and polymers derived from 2-subtituted-1,3-diakyl-4(5)-vinylimidazolium salts. *M.Sc Thesis*, Rochester Institute of Technology, Rochester, NY 14623-5603, **2012**.

234. Olorunyomi, J.F.; Chan, K.Y.; Gao, L.; Voskanyan, A.A.; Li, C.Y.V. Direct synthesis of anion exchange polymer threaded in a metalorganic framework through in situ polymerization of an ionic liquid. *Micropor*. *Mesopor*. *Mater*. **2018**, *259*, 255-263.

235. Jiang, Y.; Li, F.; Ding, G.; Chen, Y.; Liu, Y.; Hong, Y.; Liu, P.; Qi, X.; Ni, L. Synthesis of a novel ionic liquid modified copolymer hydrogel and its rapid removal of Cr(VI) from aqueous solution. *J*. *Colloid*. *Interface Sci*. **2015**, *455*, 125–133.

236. Garaga, M.N.; Nayeri, M.; Martinelli, A. Effect of the alkyl chain length in 1-alkyl-3-methylimidazolium ionic liquids on inter-molecular interactions and rotational dynamics: A combined vibrational and NMR spectroscopic study. *J*. *Mol*. *Liq*. **2015**, *210*, 169–177.

237. Chen, F.; Song, Z.; Nie, J.; Yu, G.; Li, Z.; Lee, M. Ionic liquid-based carbon nanotube coated magnetic nanoparticles as adsorbent for the magnetic solid phase extraction of triazole fungicides from environmental water. *RSC Adv*. **2016**, *6*, 81877–81885.

238. Dikio, Z.D.; Shooto, N.D.; Thema, F.T.; Farah, A.M. Raman and TGA study of carbon nanotubes synthesized over Mo/Fe catalyst on aluminum oxide, calcium carbonate and magnesium oxide support. *Chem*. *Sci*. *Trans*. **2013**, *2*, 1160-1173.

239. Hall, K.R.; Eagleton, L.C.; Acrivos, A.; Vermeulen, T. Pore-and solid-diffusion kinetics in fixed-bed adsorption under constant-pattern conditions. *Ind. Eng. Chem. Fundamen.*, **1966**, *5*, 212-223.

240. Dada, A.O.; Olalekan, A.P.; Olatunya, A.M.; DADA, O. Langmuir, Freundlich, Temkin and Dubinin–Radushkevich isotherms studies of equilibrium sorption of Zn^{2+} unto phosphoric acid modified rice husk. *J. Appl. Chem*. **2012**, *3*, 38-45.

241. Azizian, S.; Eris, S.; Wilson, L.D. Re-evaluation of the century-old Langmuir isotherm for modeling adsorption phenomena in solution. *J. Chem. Phys*. **2018**, *513*, 99-104.

242. Voudrias, E.; Fytianos, F.; Bozani, E. Sorption description isotherms of dyes from aqueous solutions and waste waters with different sorbent materials. *Global Nest, Int. J.* **2002**, *4*, 75-83.

243. Salamone, J.C.; Israel, S.C.; Taylor, P.; Snider, B. Synthesis and homopolymerization studies of vinylimidazolium salts. *Polymer*, **1973**, *14*, 639–644.

244. Ohno, H.; Ito, K. Room-temperature molten salt polymers as a matrix for fast ion conduction. *Chem. Lett.* **1998**, *27*, 751–752.

245. Bacon, S.; Ross, R.J.; Daugulis, A.; Parent, J.S. Imidazolium-based poly ionic liquid absorbents for bioproduct recovery. *Green Chem.*, **2017**, *19*, 5203-5213.

246. Andrzejewska, E. Photoinitiated polymerization in ionic liquids and its application. *Polym. Int*. **2017**, *66*, 366-381.

247. Peng, R.; Wang, Y.; Tang, W.; Yang, Y.; Xie, X. Progress in imidazolium ionic liquids assisted fabrication of carbon nanotube and graphene polymer composites. *Polymers,* **2013**, *5*, 847-872.

248. Zhang, R.H.; Yang, Y.K.; Xie, X.L.; Li, R.K.Y. Dispersion and crystallization studies of hyper-branched poly(urea-urethane)s-grafted carbon nanotubes filled polyamide-6 nanocomposites. *Composites. A.*, **2010**, *41*, 670–677.

249. Cui, W.; Du, F.P.; Zhao, J.C.; Zhang, W.; Yang, Y.K.; Xie, X.L.; Mai, Y.W. Improving thermal conductivity while retaining high electrical resistivity of epoxy composites by incorporating silica-coated multi-walled carbon nanotubes. *Carbon,* **2011**, *49*, 495–500.

250. Zhou, X.S.; Wu, T.B.; Ding, K.L.; Hu, B.J.; Hou, M.Q.; Han, B.X. Dispersion of graphene sheets in ionic liquid Bmim PF_6 stabilized by an ionic liquid polymer. *Chem. Commun.* **2010**, *46*, 386–388.

251. Xiao, C.H.; Chu, X.C.; Wu, B.H.; Pang, H.L.; Zhang, X.H.; Chen, J.H. Polymerized ionic liquid-wrapped carbon nanotubes: The promising composites for direct electrochemistry and biosensing of redox protein. *Talanta,* **2010**, *80*, 1719–1724.

252. Meyer, F.; Raquez, J.M.; Coulembier, O.; de Winter, J.; Gerbaux, P.; Dubois, P. Imidazolium end-functionalized poly(L-lactide) for efficient carbon nanotube dispersion. *Chem. Commun.* **2010**, *46*, 5527–5529.

253. Zhao, D.; Gupta, A.K.S.; Stewart, L. Selective removal of Cr(VI) oxyanions with a new anion exchanger. *Ind. Eng. Chem. Res.* **1998**, *37*, 4383–4387.

254. Cespón-Romero, R.M.; Yebra-Biurruny, M.C.; Bermejo-Barrera, M.P. Pre-concentration and speciation of chromium by the determination of total chromium and chromium(III) in natural waters by flame atomic absorption spectrometry with a chelating ion-exchange flow injection system. *Anal*. *Chim*. *Acta*. **1996**, *327*, 37–45.

255. Imanaka, S.; Hayashi, H. Behavior of hexavalent chromium in water supply system by IC-ICP-MS method. *Water Sci*. *Technol*. *Water Supply*. **2012**, *13*. DOI:10.2166/ws.2012.086.

256. Liu, C.; Qiao, S.; Luo, W.; Liu, Y.; Liu, D.; Li, X.; Liu, M. Thermodynamics, kinetics and regeneration studies for adsorption of Cr(VI) from aqueous solution using modified cellulose as adsorbent. *Bioresources*, **2014**, *9*, 6998-7017.

257. Li, C.; Zhang, Y.; Peng, J.; Wu, H.; Zhai, M. Adsorption of Cr(VI) using cellulose microsphere-based adsorbent prepared by radiation-induced grafting. *Radiation Phy*. *Chem*. **2012**, *81*, 967-970.

258. Le, C.M.Q.; Cao, X.T.; Lim, K.T. Ultrasound-promoted direct functionalization of multi-walled carbon nanotubes in water via Diels-Alder "click chemistry. *Ultrason*. *Sonochem*. **2017**, *39*, 321-329.

259. Li, K.; Li, P.; Cai, J.; Xiao, S.; Yang, H.; Li, A. Efficient adsorption of both methyl orange and chromium from their aqueous mixtures using a quaternary ammonium salt modified chitosan magnetic composite adsorbent. *Chemosphere*, **2016**, *154*, 310–318.

260. Anah, L.; Astrini, N. Influence of pH on Cr(VI) ions removal from aqueous solutions using carboxymethyl cellulosebased hydrogel as adsorbent. *IOP Conf*. *Serbia*: *Earth Environ*. *Sci*. **2017**, *60*, 012010.

261. Mack, C.; Wilhelmi, B.; Duncan, J.R.; Burgess, J.E. Biosorption of precious metals. *Biotechnol*. *Adv*. **2007**, *25*, 264-271.

262. Robati, D. Pseudo-second-order kinetic equations for modeling adsorption systems for removal of lead ions using multi-walled carbon nanotube. *J. Nanostruct. Chem*. **2013,** *3*, 1-6.

APPENDICES

Appendix 1

APX1-1 Nomenclature of Ionic liquids synthesized.

Name of compound	**Code/formulae**
N-propylpyridinium bromide	$[N\text{-propylPyr}]^+[Br]^-$
N-isopropylpyridinium bromide	$[N\text{-isopropylPyr}]^+[Br]^-$
N-propylpyridinium hexafluorophosphate	$[N\text{-propylPyr}]^+[PF_6]^-$
N-isopropylpyridinium hexafluorophosphate	$[N\text{-isopropylPyr}]^+[PF_6]^-$
3-methyl-1-propylimidazolium bromide	$[MPIm]^+[Br]^-$
1-isopropyl-3-methylimidazolium bromide	$[IsopropylMIm]^+[Br]^-$
1-isopropyl-3-methylimidazolium hexafluorophosphate	$[IsopropylMIm]^+[PF_6]^-$
3-methyl-1-propylimidazolium hexafluorophosphate	$[MPIm]^+[PF_6]^-$
3-ethyl-1-isopropylimidazolium bromide	$[EisopropylIm]^+[Br]^-$

APX 1-2 Nomenclature of ILs monomers and polymeric ionic liquids synthesized.

Name of compound	**Code/formulae**
Poly[4-vinylpyridine]	P4-VP
Poly[*N*-ethyl-4-vinylpyridinium bromide]	PIL1
Poly[*N*-propyl-4-vinylpyridinium bromide]	PIL2
Poly[*N*-isopropyl-4-vinylpyridinium bromide]	PIL3
Poly[*N*-ethyl-4-vinylpyridinium hexafluorophosphate]	PIL4
Poly[*N*-propyl-4-vinylpyridinium hexafluorophosphate]	PIL5
Poly[*N*-isopropyl-4-vinylpyridinium hexafluorophosphate]	PIL6
1-vinylimidazole	1-VIm
3-propyl-1-vinylimidazolium bromide	[3P-VImBr]
3-isopropyl-1-vinylimidazolium bromide	[3Isop-VImBr]
Poly[3-propyl-1-vinylimidazolium bromide]	P[3P-VImBr]
Poly[3-isopropyl-1-vinylimidazolium bromide]	P[3Isop-VImBr]
Poly[3-propyl-1-vinylimidazolium hexafluorophosphate]	$P[3P\text{-}VImPF_6]$
Poly[3-isopropyl-1-vinylimidazolium hexafluorophosphate]	$P[3Isop\text{-}VImPF_6]$
3-methyl-1-(4-vinyl benzyl)imidazolium chloride	[MVBIm-Cl]

Poly[3-methyl-1-(4-vinyl benzyl)imidazolium chloride]	P[MVBIm-Cl]
Poly[3-methyl-1-(4-vinyl benzyl)imidazolium hexafluorophosphate]	P[MVBIm-PF_6]
Poly[3-methyl-1-(4-vinyl benzyl)imidazolium bis(trifluoromethanesulfonyl)imide]	P[MVBIm-TFSI]

Appendix 2

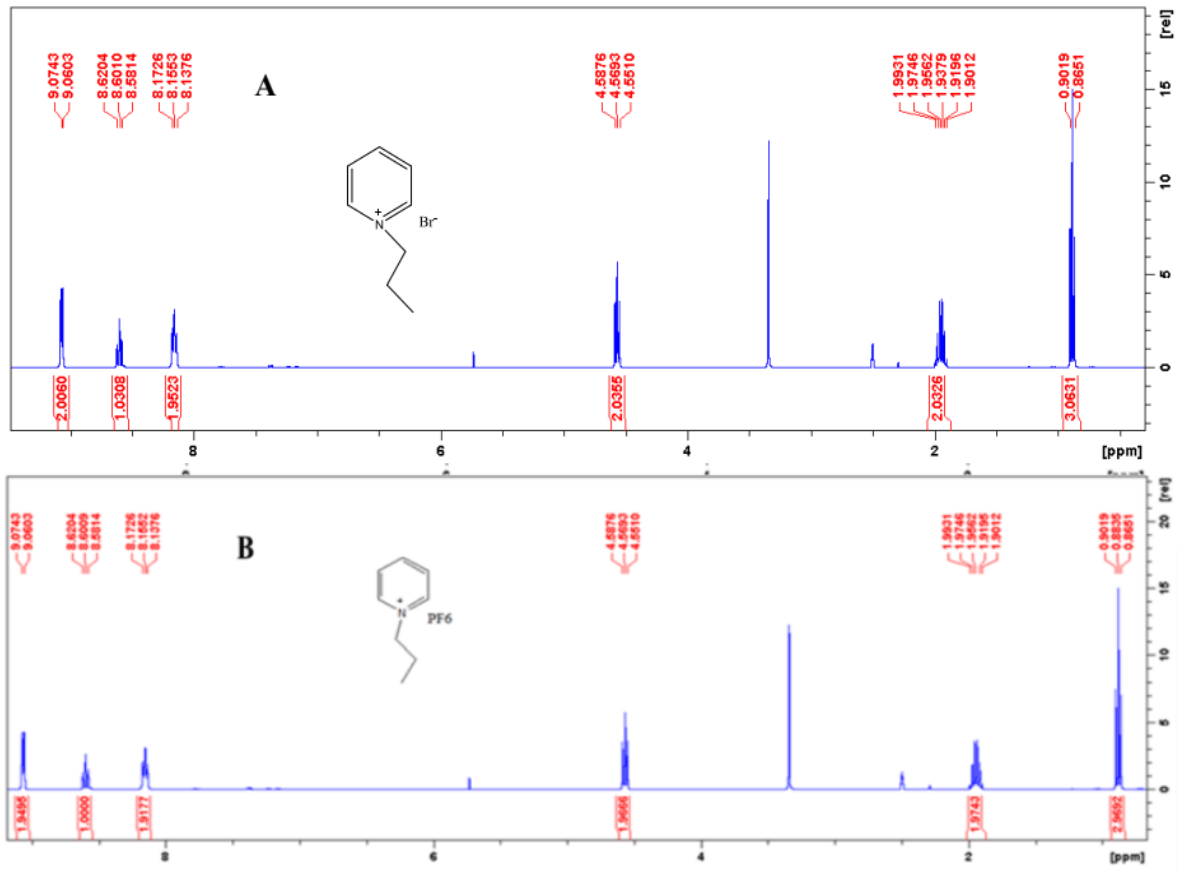

APX 2-1 ^{1}H NMR of [*N*-propylPyr]$^{+}$[Br]$^{-}$ (A), and [*N*-propylPyr]$^{+}$[PF_6]$^{-}$ (B)

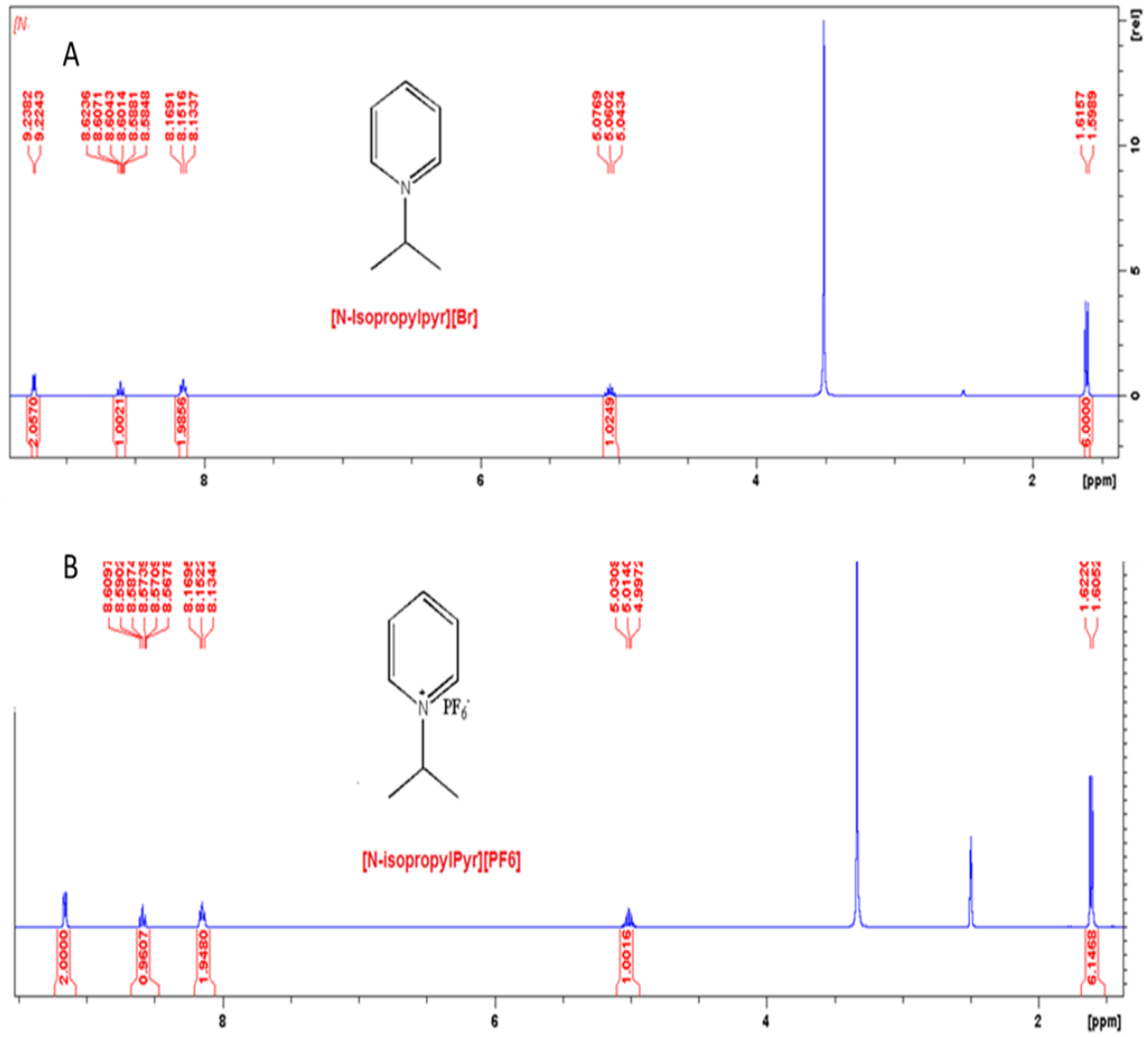

APX 2-2 ^{1}H NMR of [*N*-isopropylPyr]$^{+}$[Br]$^{-}$ (A), and [*N*-isopropylPyr]$^{+}$[PF_6]$^{-}$ (B)

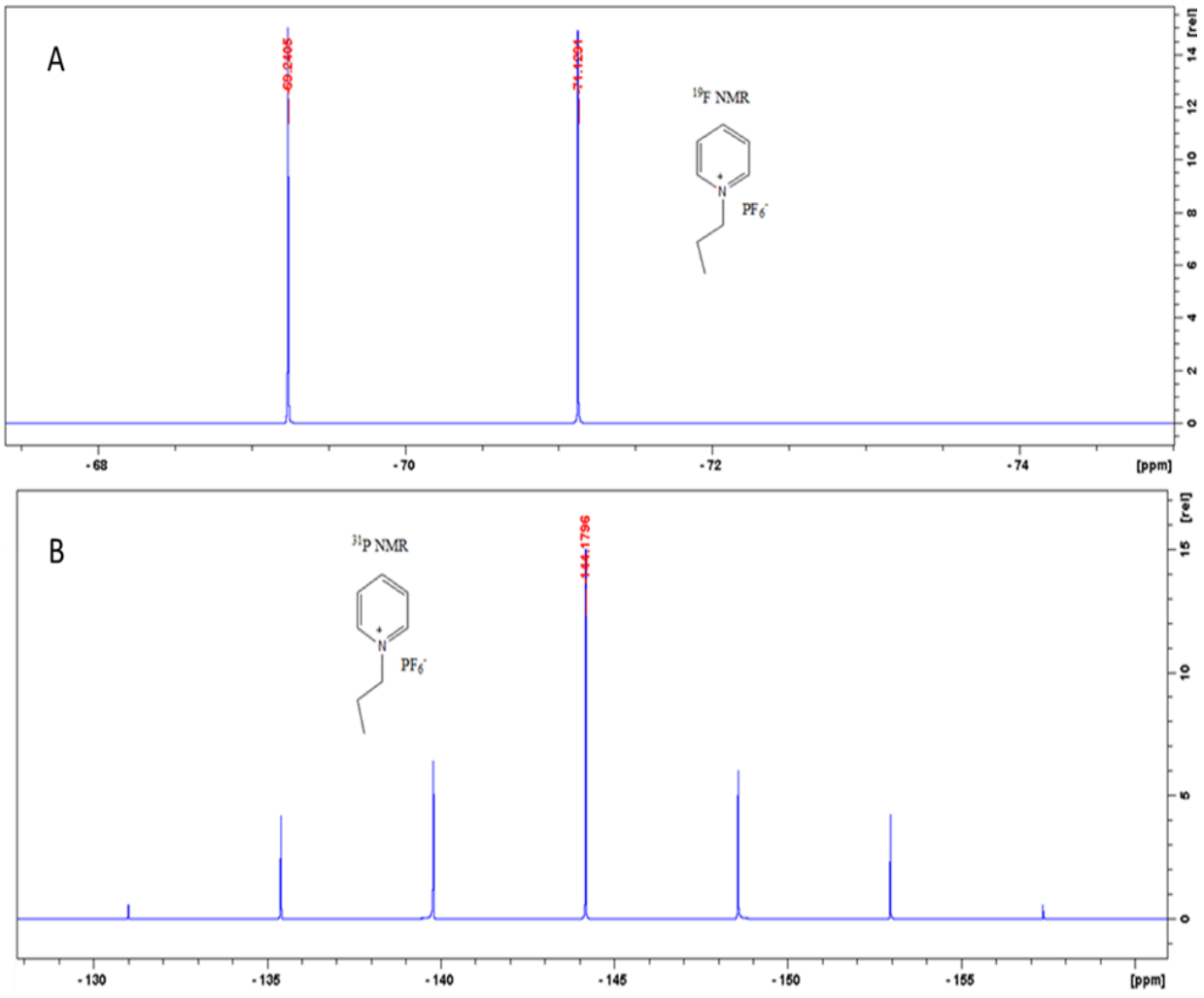

APX 2-3 ^{19}F NMR (A) and ^{31}P NMR (B) for [*N*-propylPyr]$^+$[PF_6]$^-$

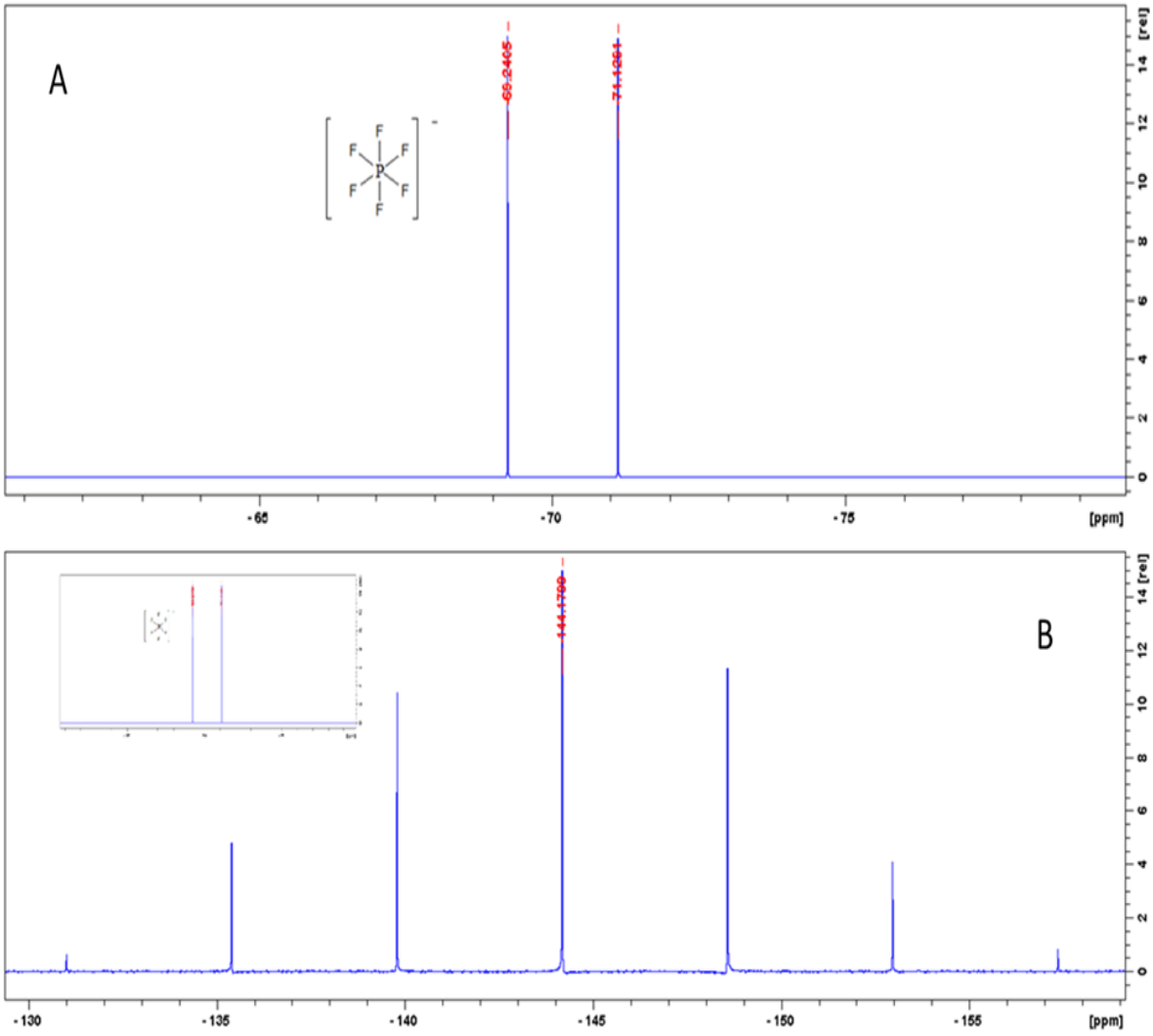

APX 2-4 ^{19}F NMR (A) and ^{31}P NMR (B) of [*N*-isopropylPyr]$^{+}$[PF_6]$^{-}$

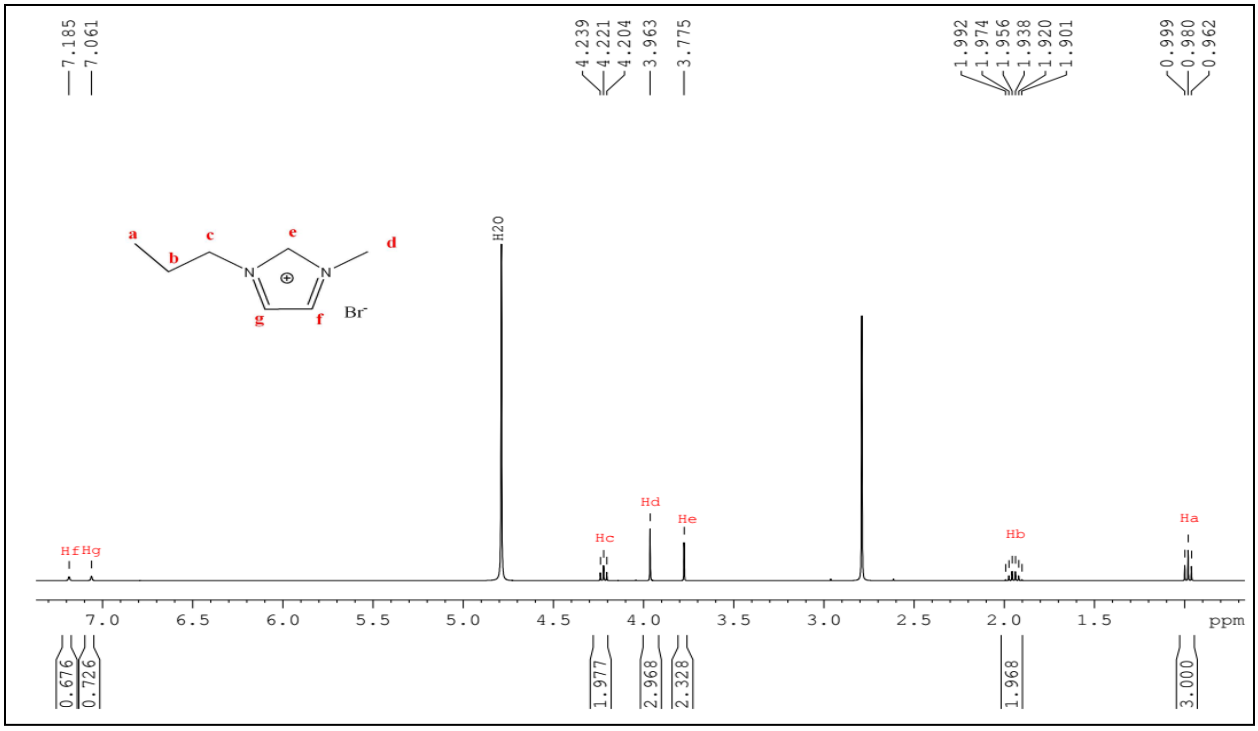

APX 2-5 ^{1}H NMR of [MPIm^{+}][Br^{-}], dissolved in H_2O

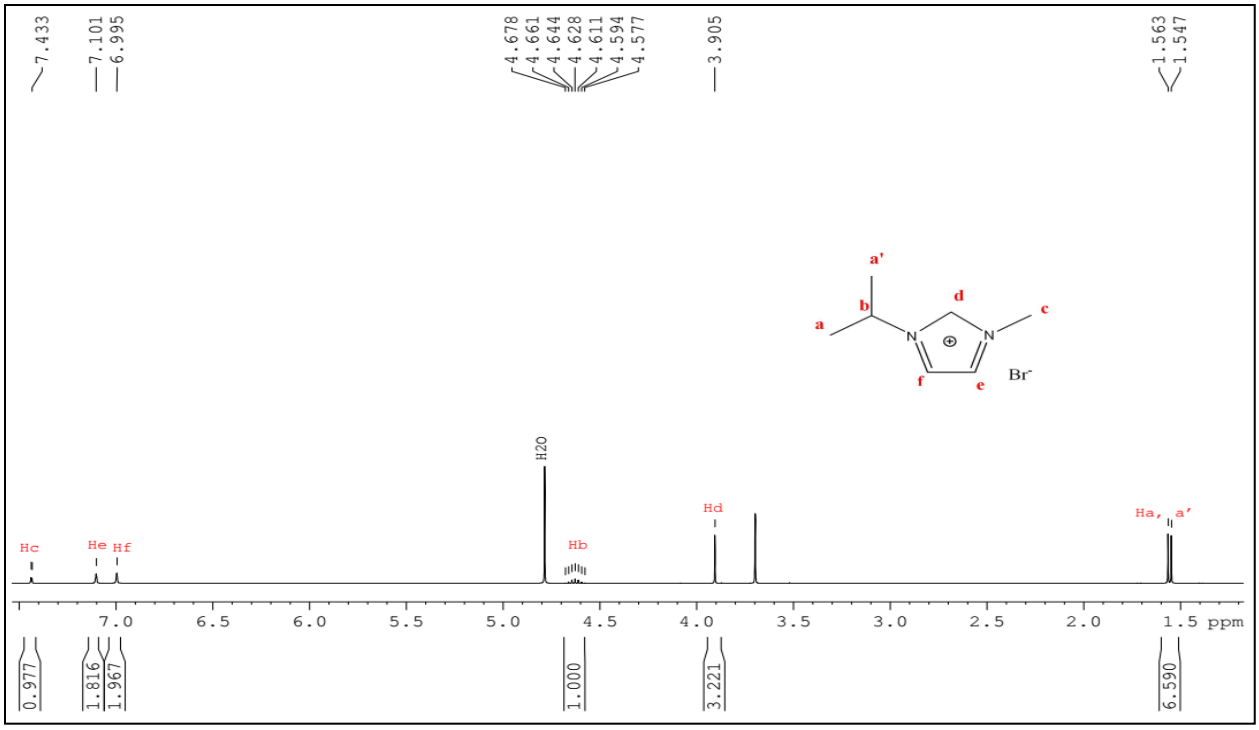

APX 2-6 ^{1}H NMR of [isopropylMIm^{+}][Br^{-}], dissolved in H_2O

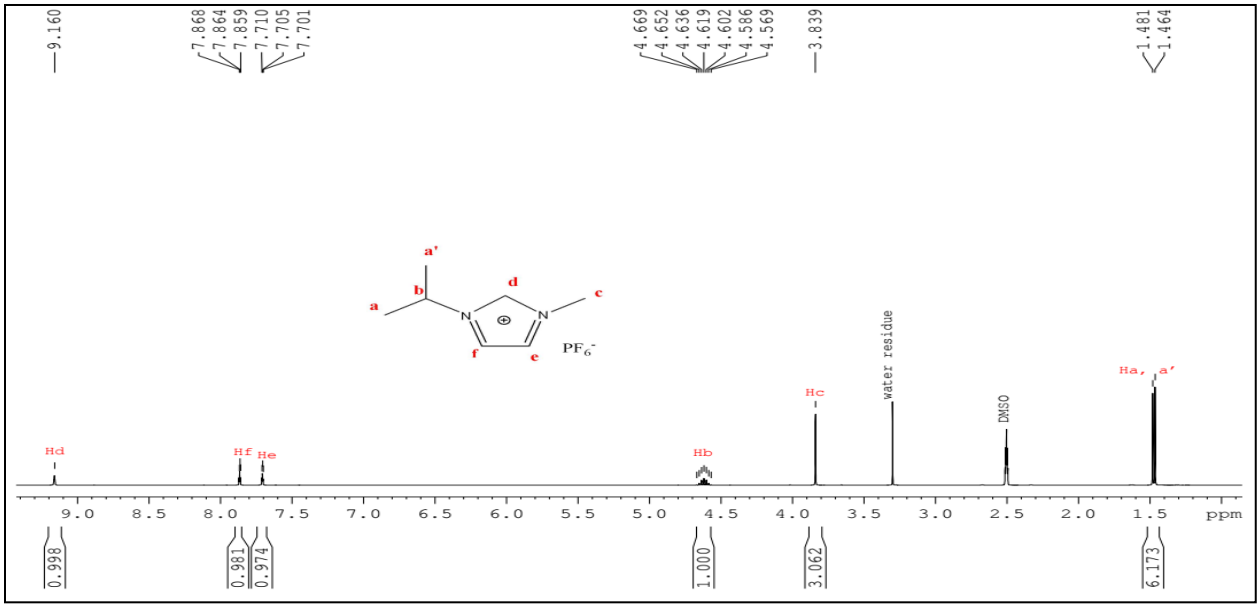

APX 2-7 ^{1}H NMR of [IsopropylMIm^{+}][PF_6^{-}], dissolved in DMSO

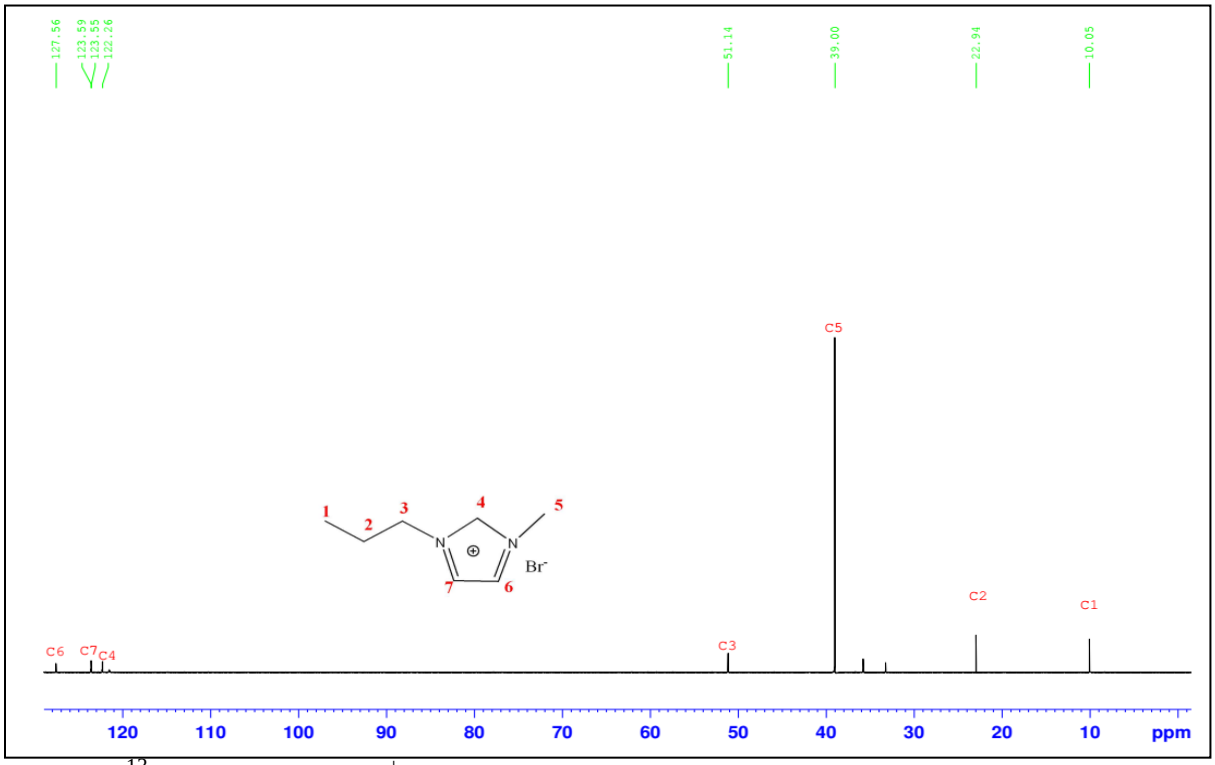

APX 2-8 ^{13}C-NMR of [MPIm^{+}][Br^{-}], dissolved in H_2O

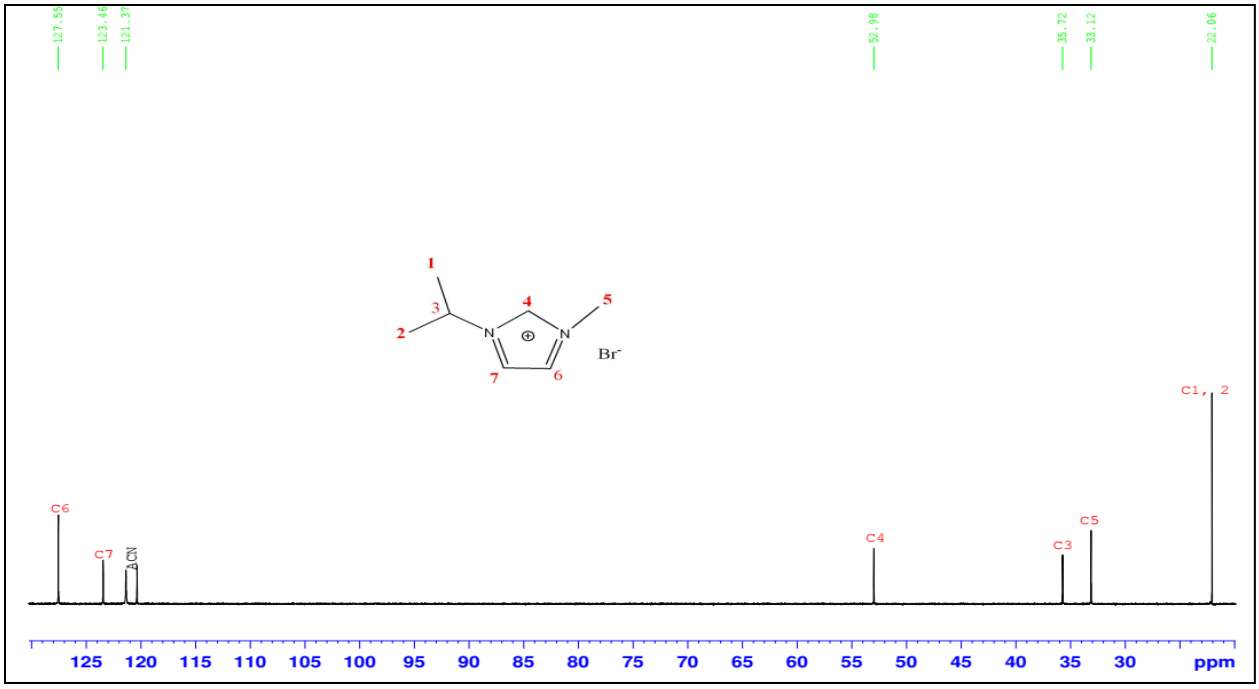

APX 2-9 ^{13}C-NMR of [isopropylMIm^{+}][Br^{-}], dissolved in H_2O

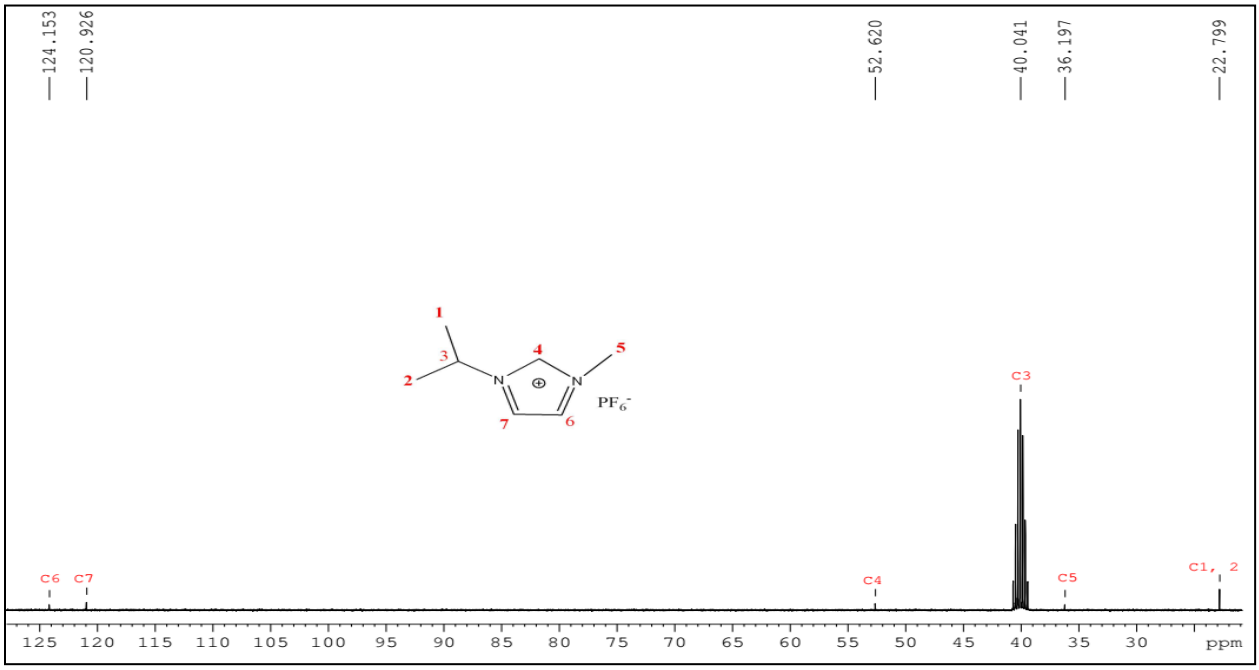

APX 2-10 ^{13}C-NMR of [IsopropylMIm^{+}][PF_6^{-}], dissolved in DMSO

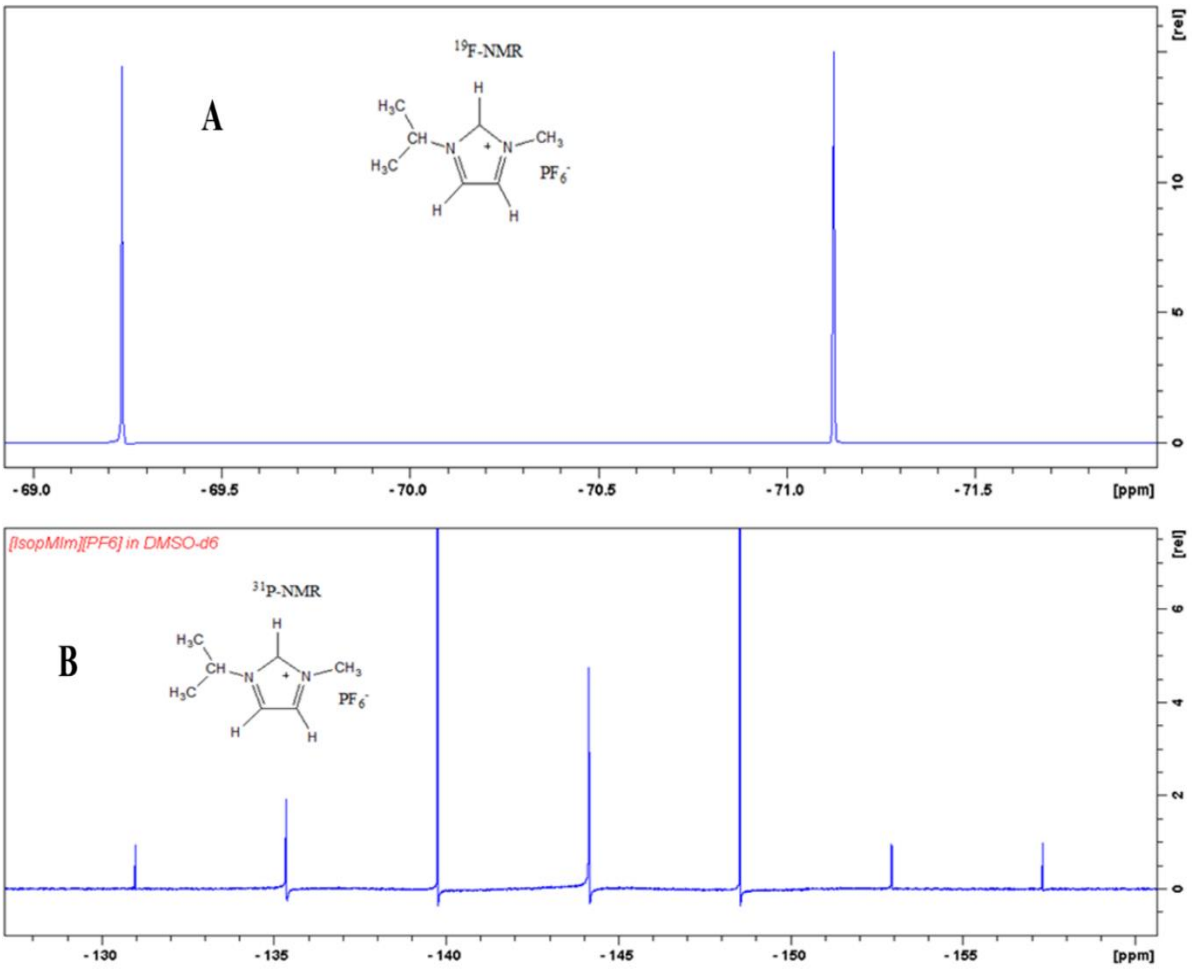

APX 2-11 ^{19}F NMR (A) and ^{31}P NMR (B) of [*N*-isopropylMIm^{+}][PF_6^{-}]

Elemental Composition Report **Page 1**

Single Mass Analysis
Tolerance = 50.0 PPM / DBE: min = -1.5, max = 500.0
Element prediction: Off
Number of isotope peaks used for i-FIT = 2

Monoisotopic Mass, Even Electron Ions
3 formula(e) evaluated with 1 results within limits (up to 20 closest results for each mass)
Elements Used:
C: 5-10 H: 10-15 N: 0-5
[MPIm+Br-] 2 (0.034) Cm (1:61)
TOF MS ES+

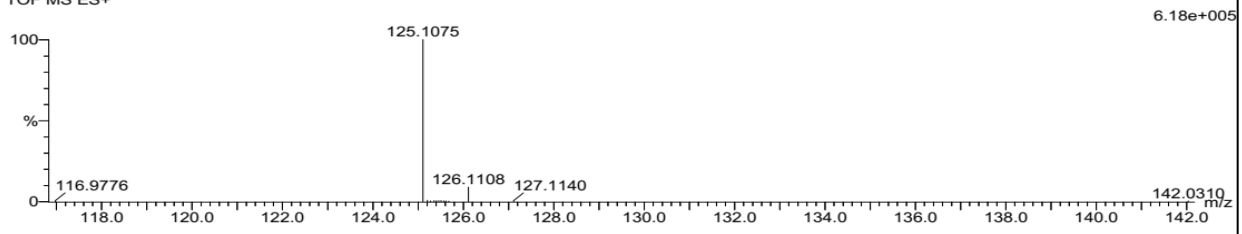

Minimum:				-1.5			
Maximum:		5.0	50.0	500.0			
Mass	Calc. Mass	mDa	PPM	DBE	i-FIT	i-FIT (Norm)	Formula
125.1075	125.1079	-0.4	-3.2	2.5	154.3	0.0	C7 H13 N2

APX 2-12 Accurate mass (Single Mass) Analysis of [*MPIm*$^+$], $C_7H_{14}N_2^+$. Single mass analysis based on CHN

Elemental Composition Report **Page 1**

Single Mass Analysis
Tolerance = 50.0 PPM / DBE: min = -1.5, max = 500.0
Element prediction: Off
Number of isotope peaks used for i-FIT = 2

Monoisotopic Mass, Even Electron Ions
3 formula(e) evaluated with 1 results within limits (up to 20 closest results for each mass)
Elements Used:
C: 5-10 H: 10-15 N: 0-5
[IsopMIm+PF6-] 49 (1.619) Cm (1:61)
TOF MS ES+

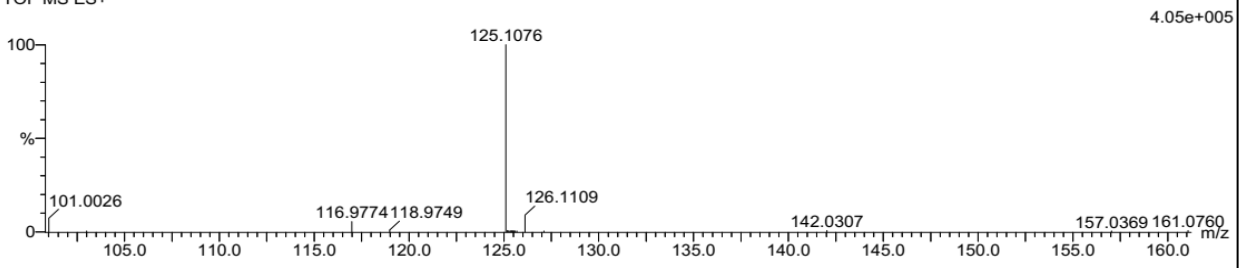

Minimum:				-1.5			
Maximum:		5.0	50.0	500.0			
Mass	Calc. Mass	mDa	PPM	DBE	i-FIT	i-FIT (Norm)	Formula
125.1076	125.1079	-0.3	-2.4	2.5	158.9	0.0	C7 H13 N2

APX 2-13 Accurate mass (Single Mass) Analysis of [IsopropylM*Im*$^+$], $C_7H_{14}N_2^+$. Single mass analysis based on CHN

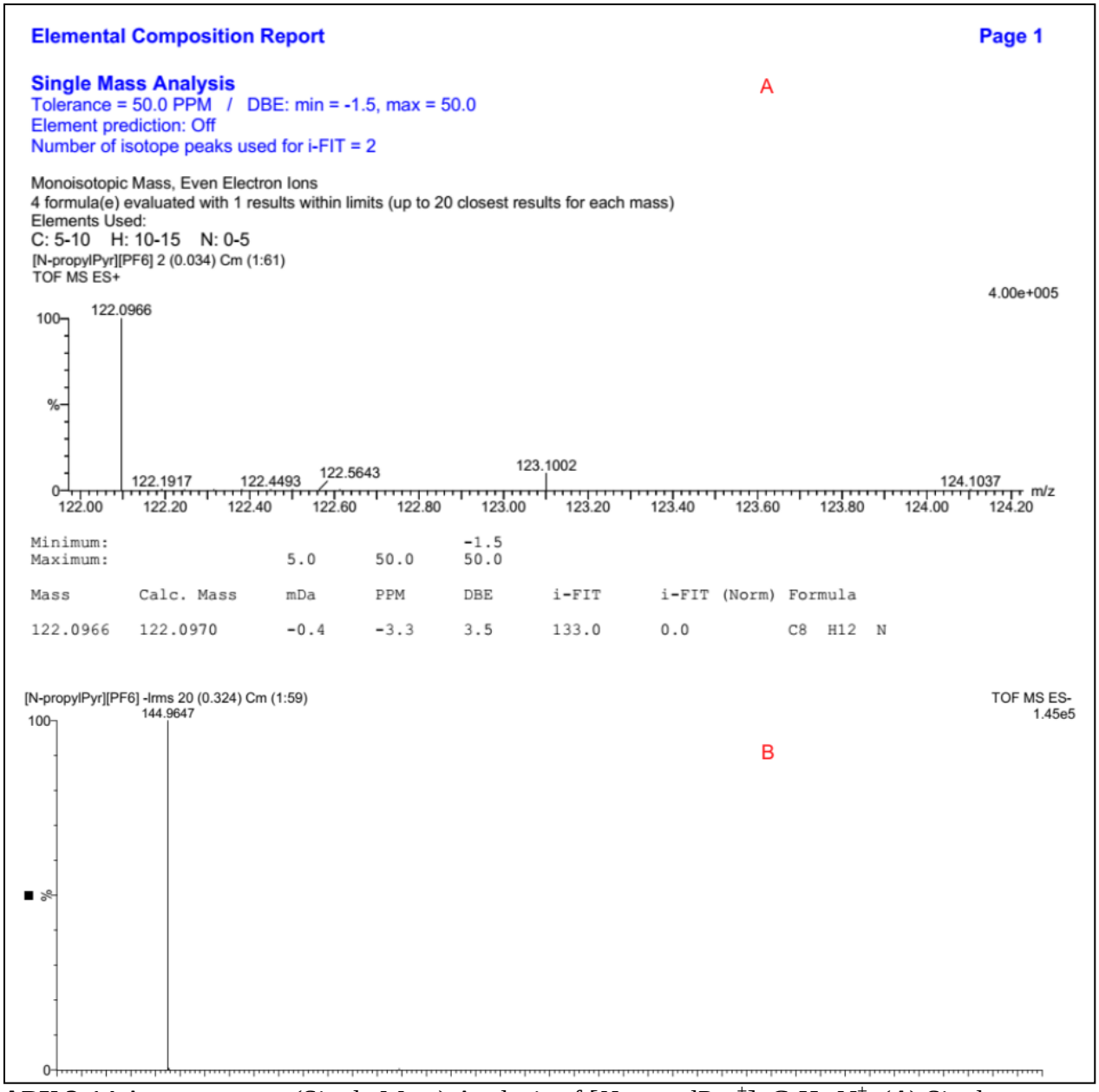

APX 2-14 Accurate mass (Single Mass) Analysis of [*N*-propylPyr^{+}], $C_8H_{12}N^{+}$. (***A***) Single mass analysis based on CHN, (***B***) TOF mass spectrometry ES of PF_6

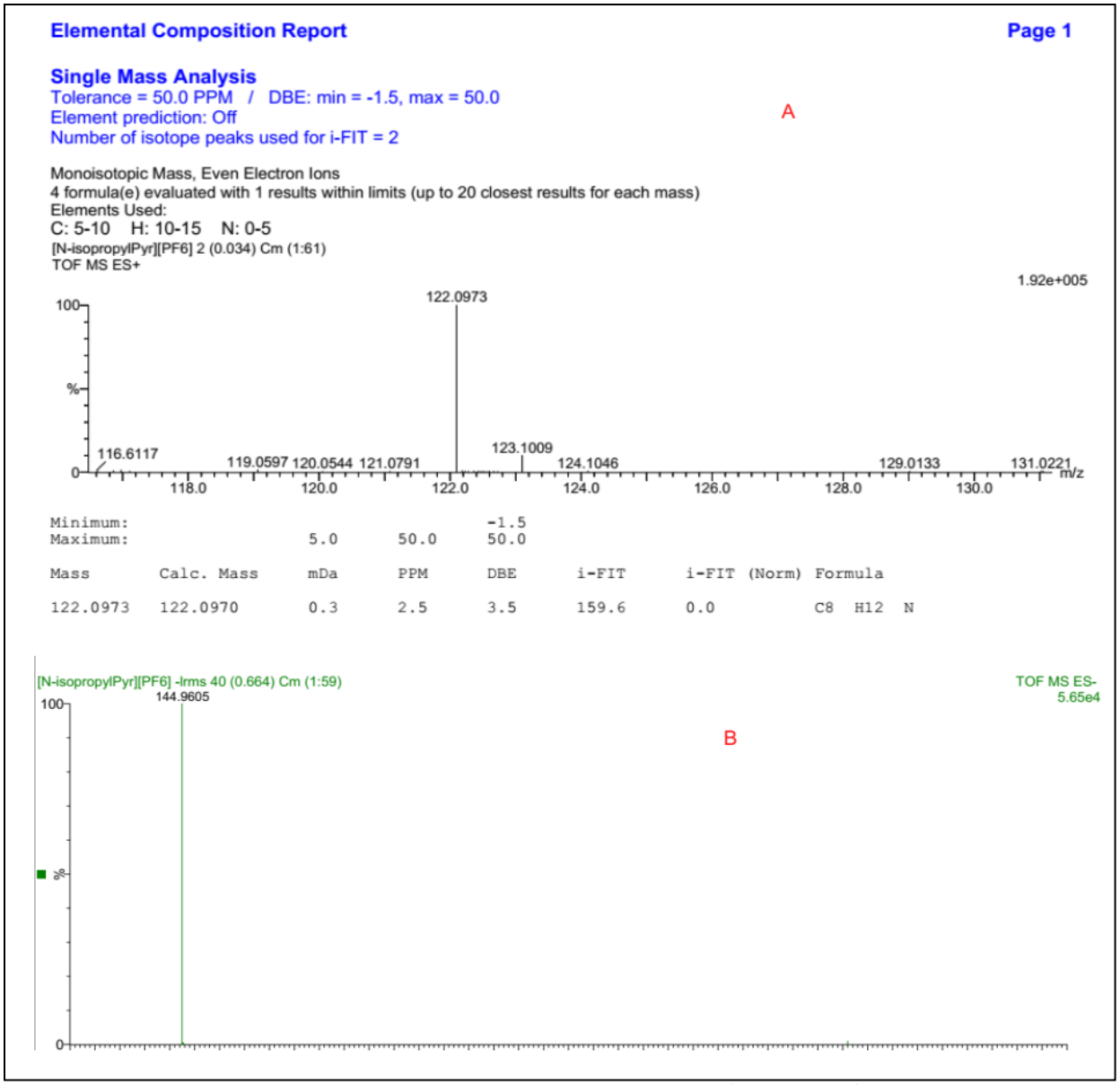

APX 2-15 Accurate (single Mass) Analysis of [*N*-isopropylPyr$^+$], $C_8H_{12}N^+$. (***A***) Single mass analysis based on CHN, (***B***) TOF mass spectrometry ES of PF_6

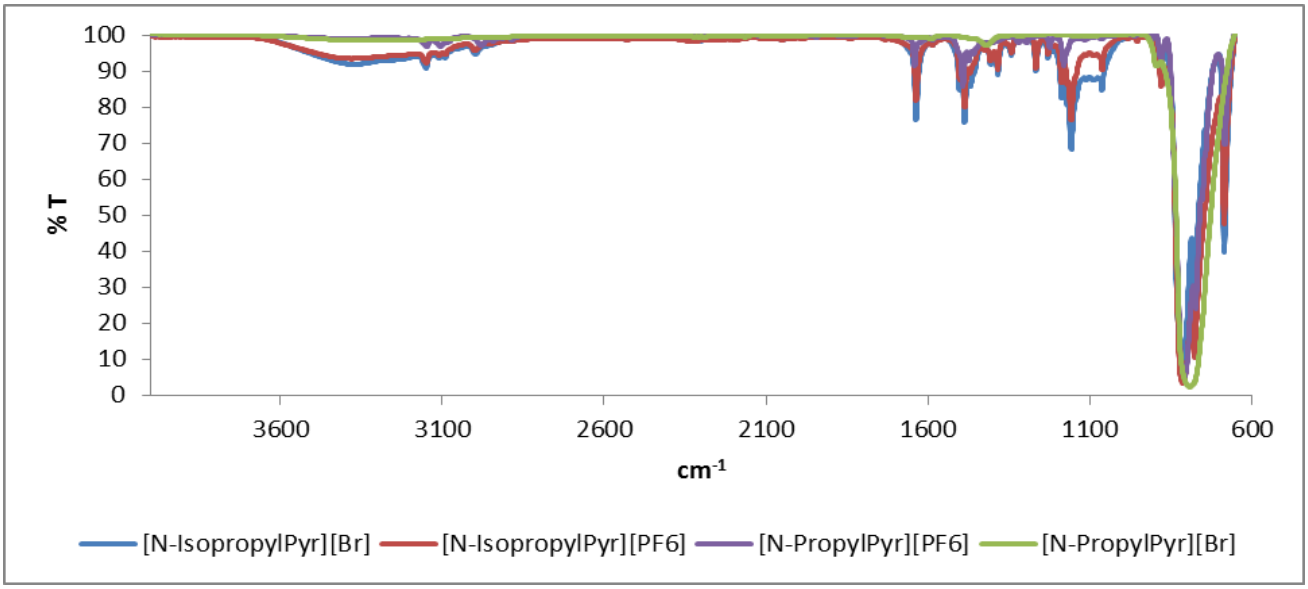

APX 2-16 FTIR spectra of pyridinium-based ionic liquids

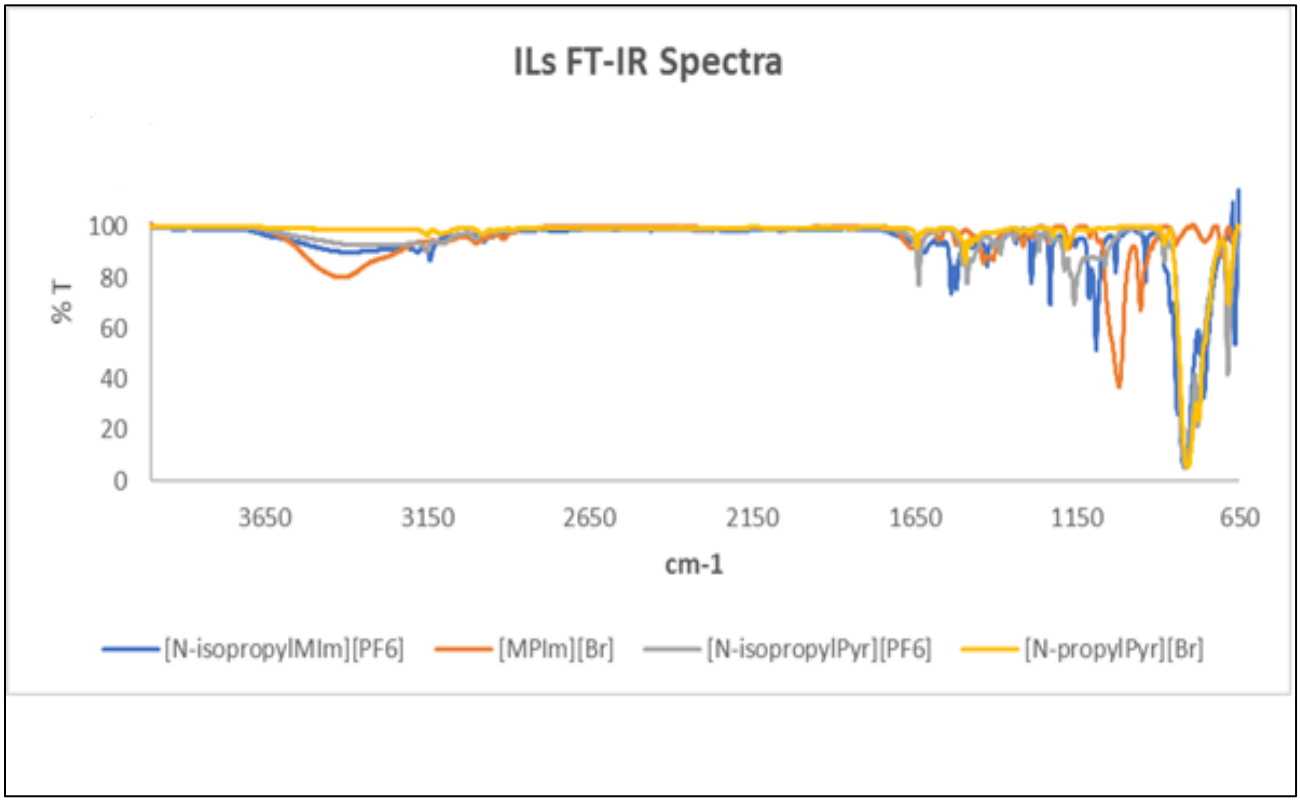

APX 2-17 FTIR spectra of some imidazolium and pyridinium-based ILs

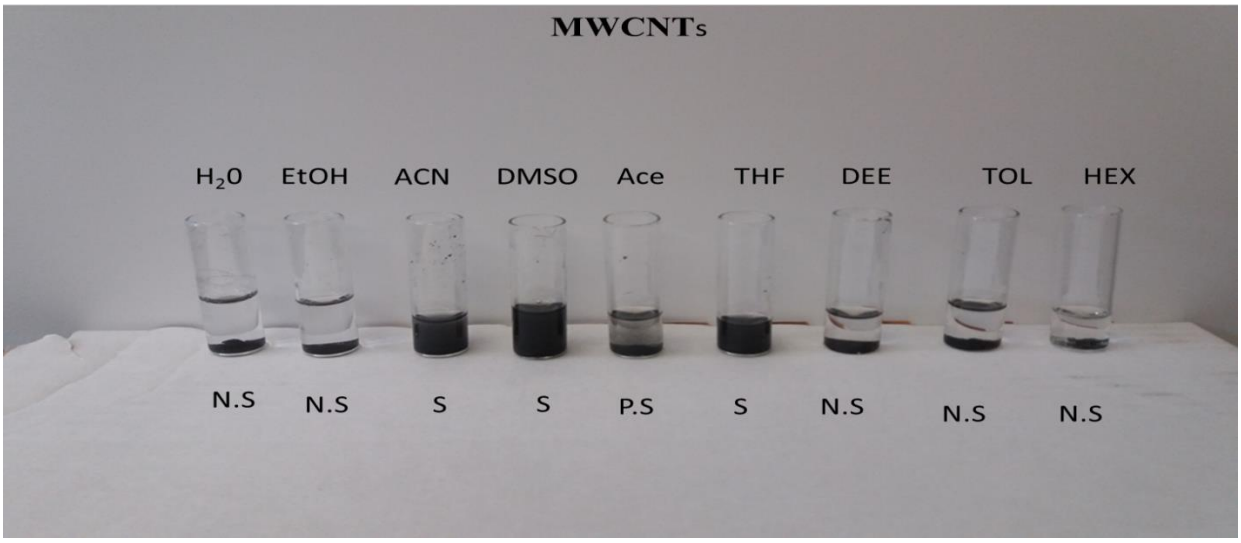

APX 2-18 Solubility of MWCNTs in different solvents

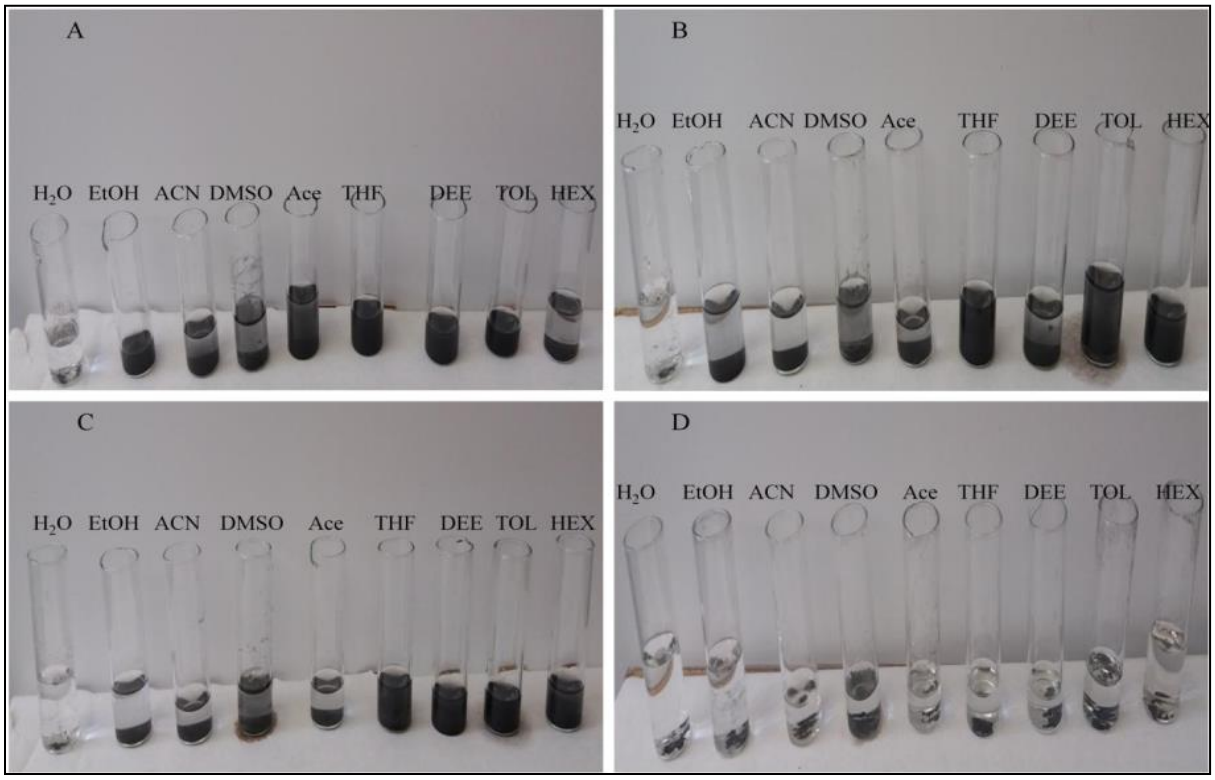

APX 2-19 Solubility of some ILs/MWCNT composites; [$MPIm^+$][Br^-]/MWCNT(***A***), [N-propylPyr^+][Br^-]/MWCNT (***B***), [isopropylMIm^+][PF_6^-]/ MWCNT (***C***), and [N-isopropylPyr^+][PF_6^+]/MWCNT (***D***): Where (S, N.S, and P.S) stands for soluble, non-soluble, and partial soluble, respectively

Appendix 3

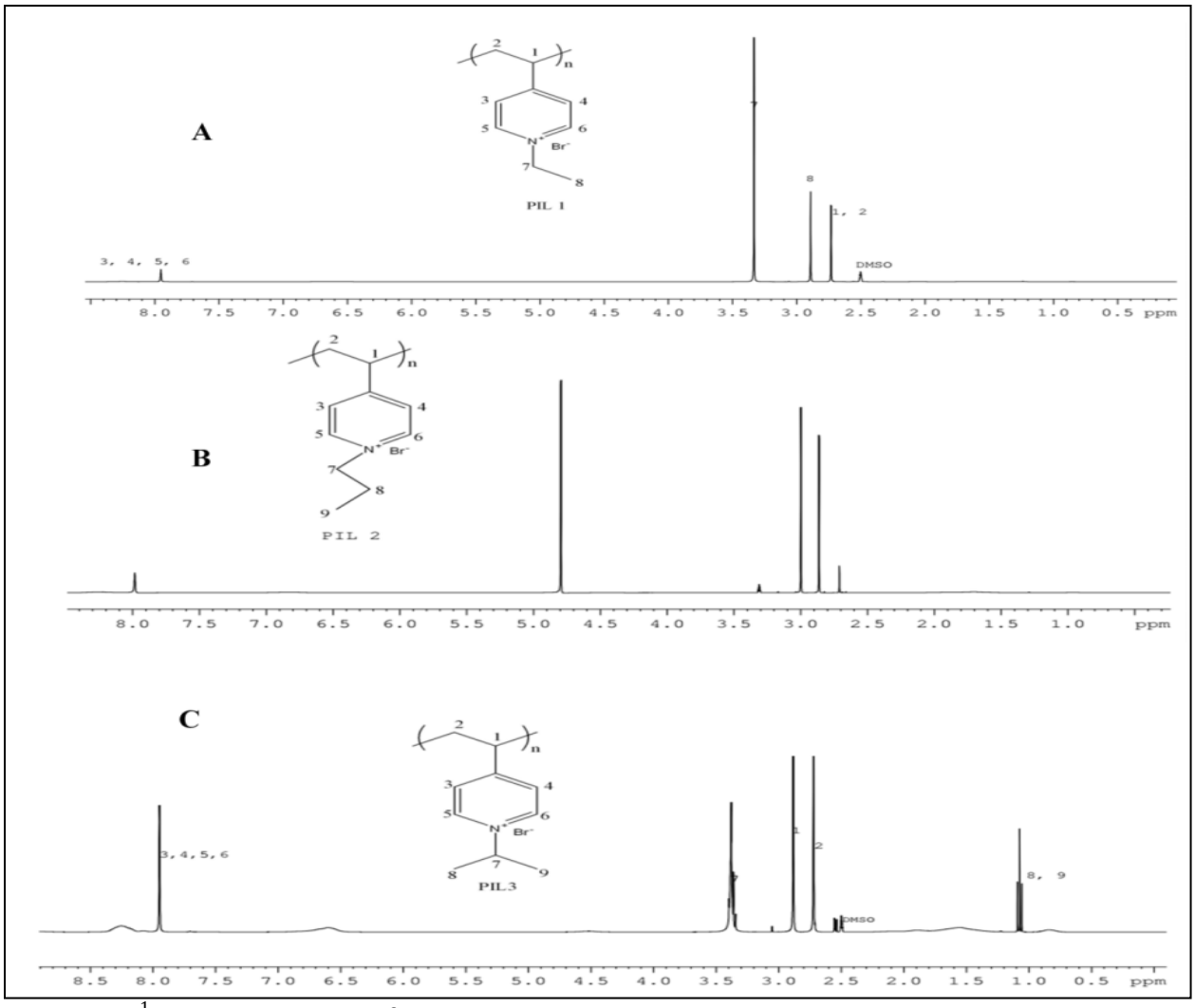

APX 3-1 ^{1}H-NMR spectra of poly(*N*-ethyl-4-vinylpyridinium bromide) PIL1 **(A)**, poly(*N*-propyl-4-vinylpyrinium bromide) PIL2 **(B)**, and poly(*N*-isopropyl-4-vinylpyrinium bromide) PIL3 **(C)**

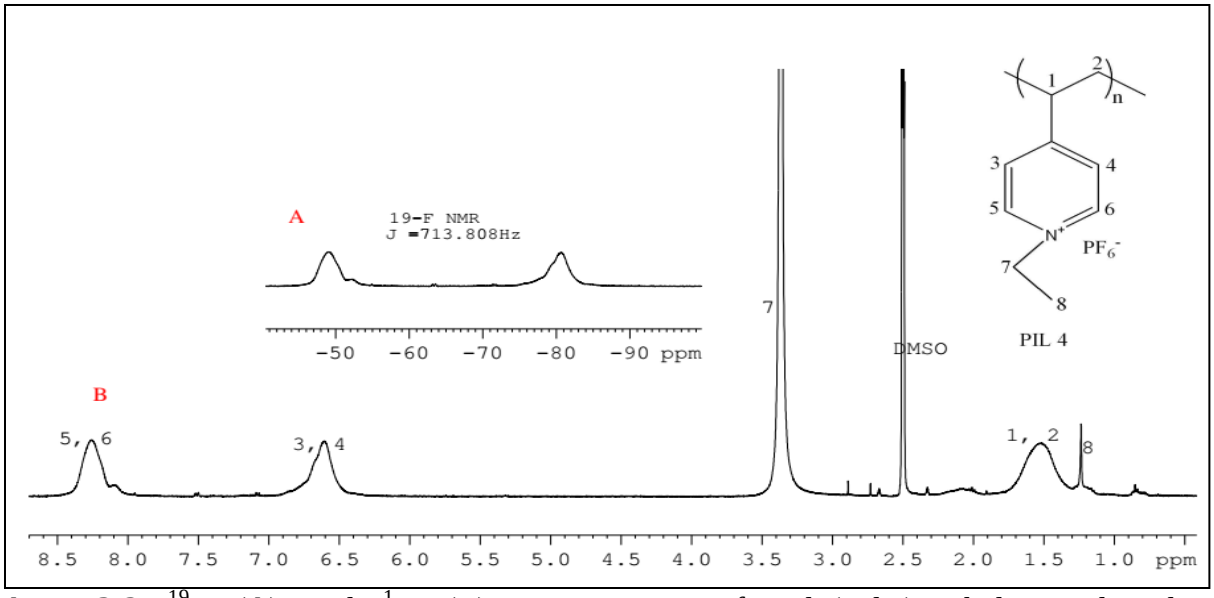

APX 3-2 ^{19}F (**A**) and ^{1}H (**B**)-NMR spectra of poly(poly(*N*-ethyl-4-vinylpyridinium hexafluorophosphate) PIL 4

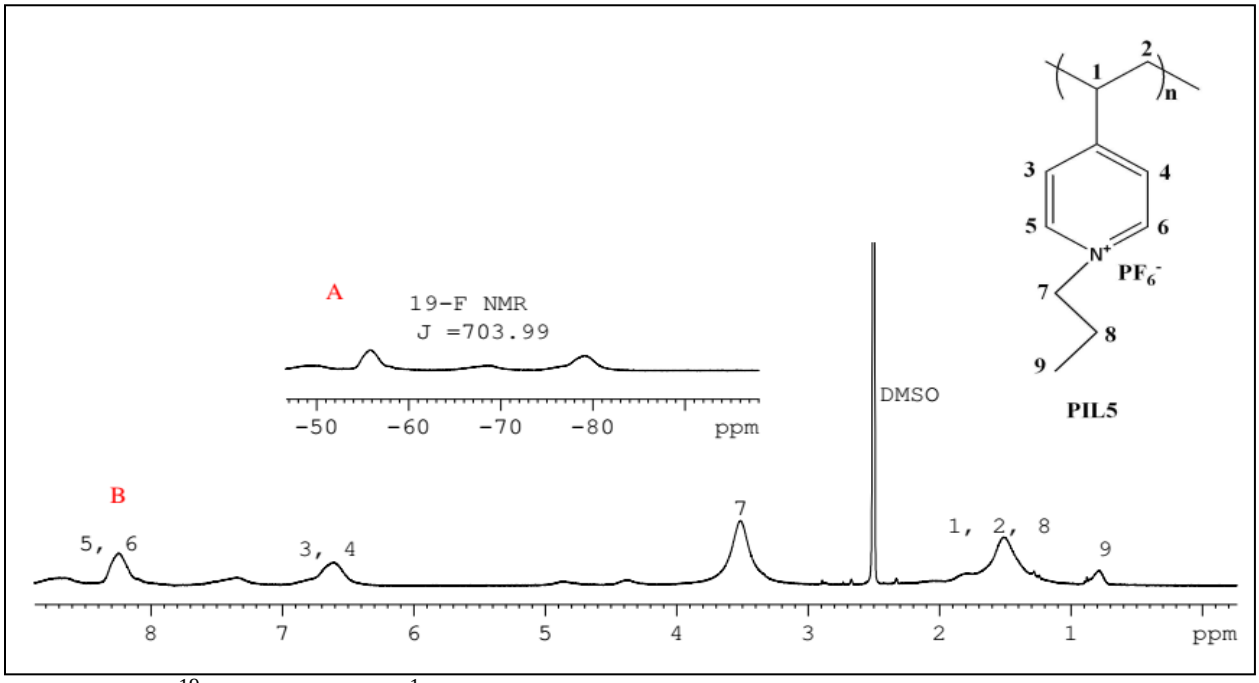

APX 3-3 ^{19}F (**A**) and ^{1}H (**B**)-NMR spectra of poly(*N*-propyl-4-vinylpyridinium hexafluorophosphate) PIL 5

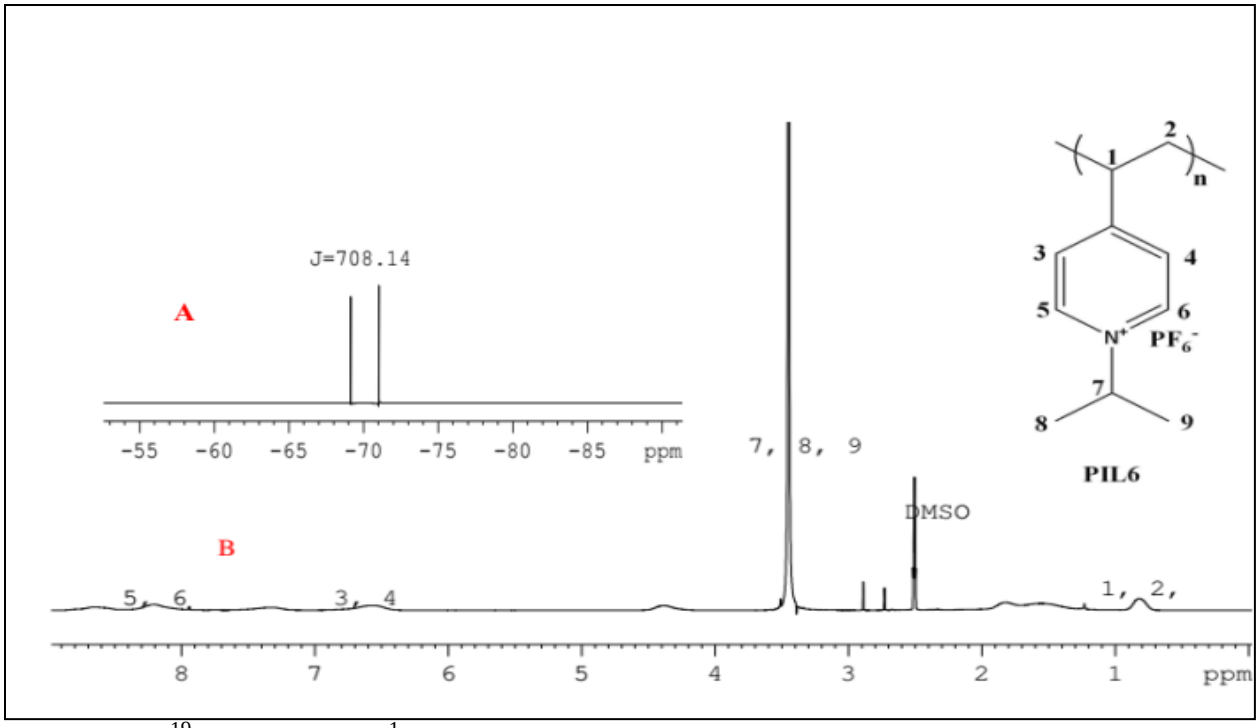

APX 3-4 ^{19}F (**A**) and ^{1}H (**B**)-NMR spectra of poly(*N*-isopropyl-4-vinylpyridinium hexafluorophosphate) PIL 6

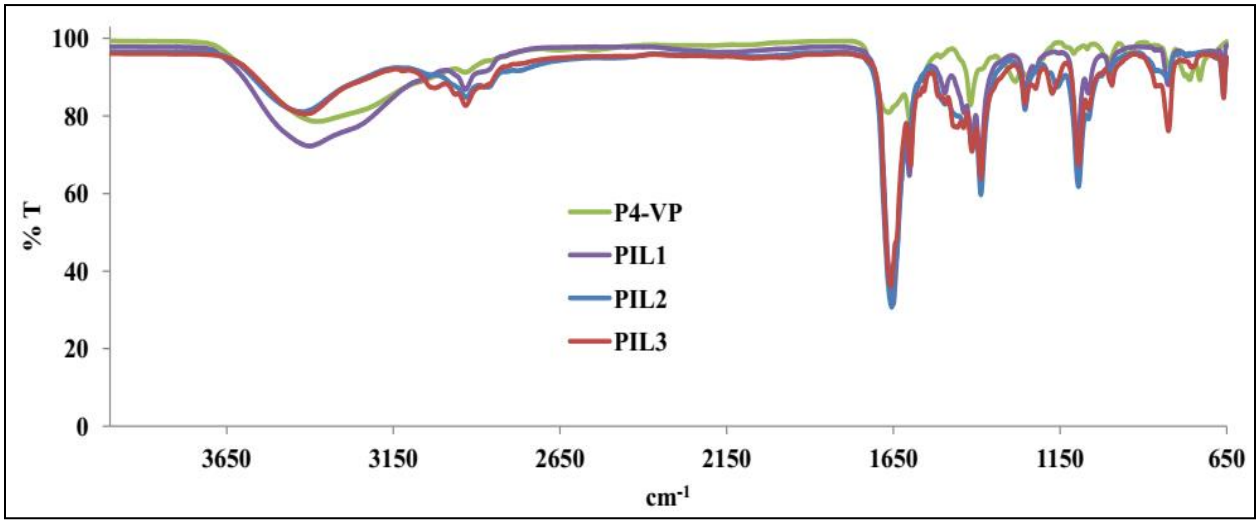

APX 3-5 FTIR spectra of poly(4-vinylpyridine) **P4-VP**, poly(*N*-ethyl-4-vinylpyrinium bromide) **PIL1,** poly(*N*-propyl-4-vinylpyrinium bromide) **PIL2**, and poly(*N*-isopropyl-4-vinylpyrinium bromide) **PIL3**.

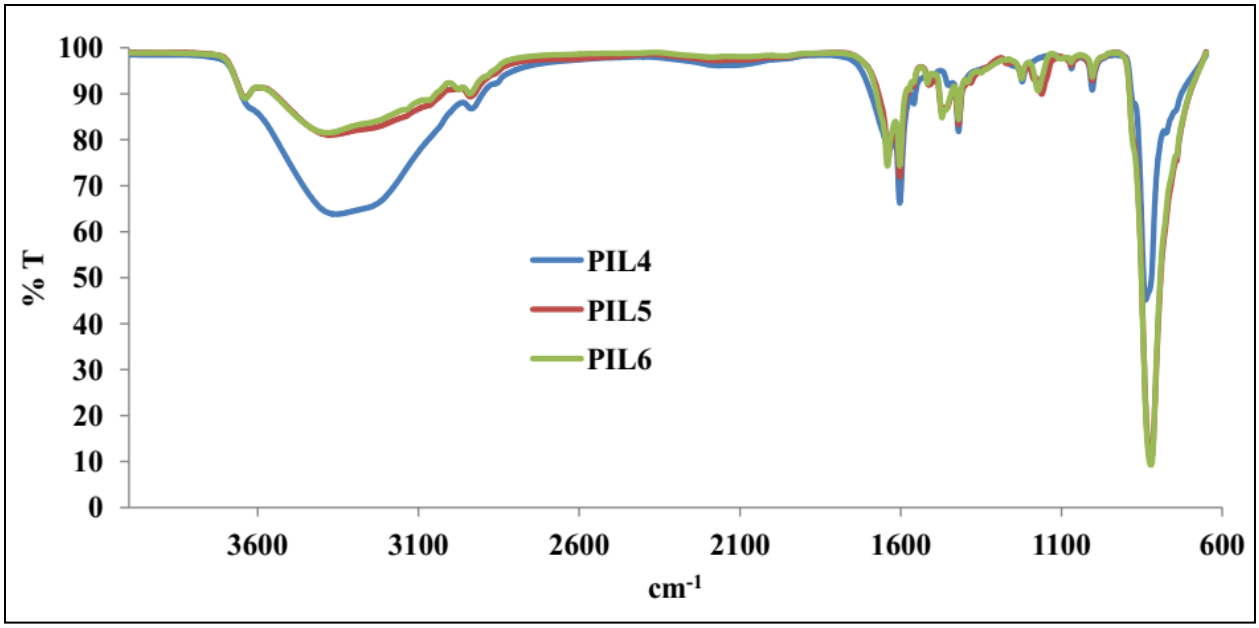

APX 3-6 FTIR spectra of poly(*N*-ethyl-4-vinylpyrinium hexafluorophosphate) **PIL4,** poly(*N*-propyl-4-vinylpyrinium hexafluorophosphate) **PIL5**, poly(*N*-isopropyl-4-vinylpyrinium hexafluorophosphate) **PIL6**

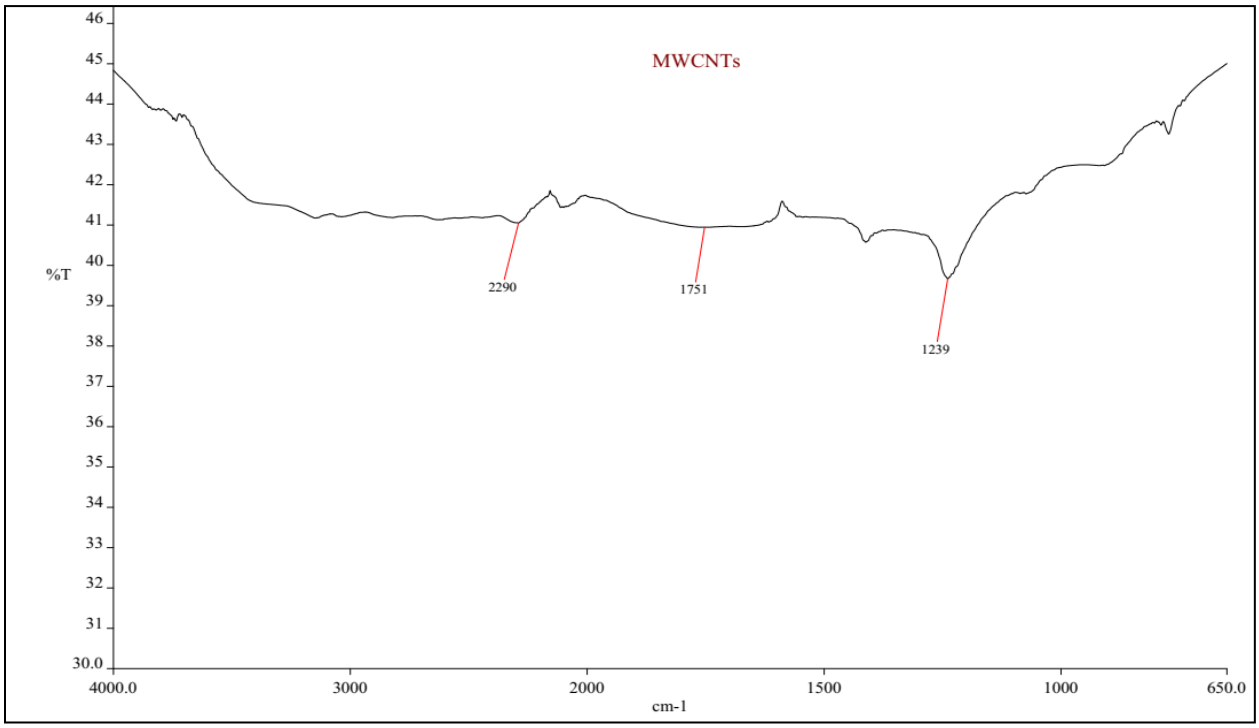

APX 3-7 FTIR spectrum of pristine MWCNTs

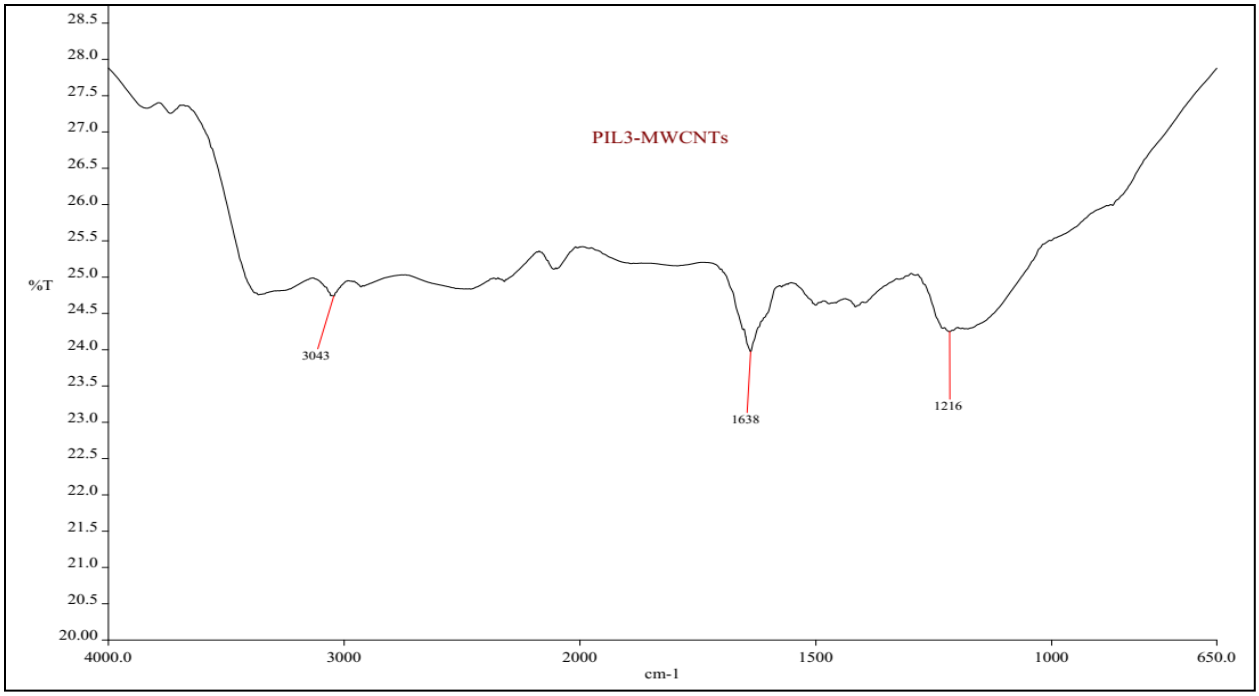

APX 3-8 FTIR spectrum of pure PIL3/MWCNT composites

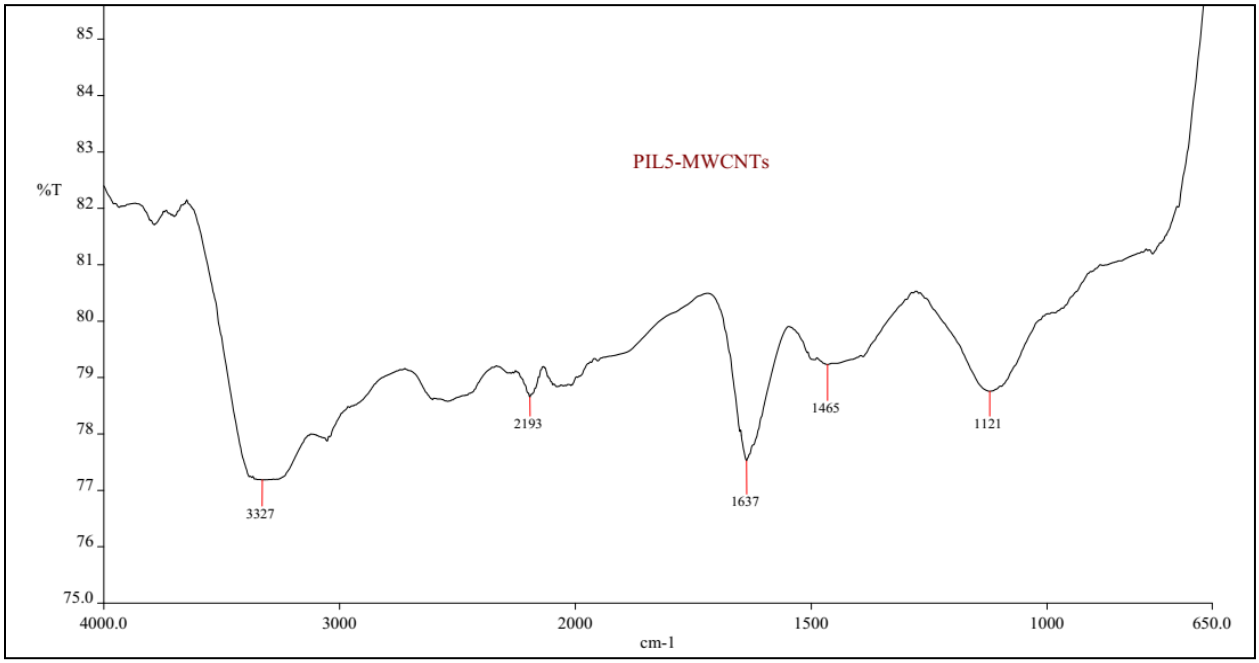

APX 3-9 FTIR spectrum of pure PIL5/MWCNT composites

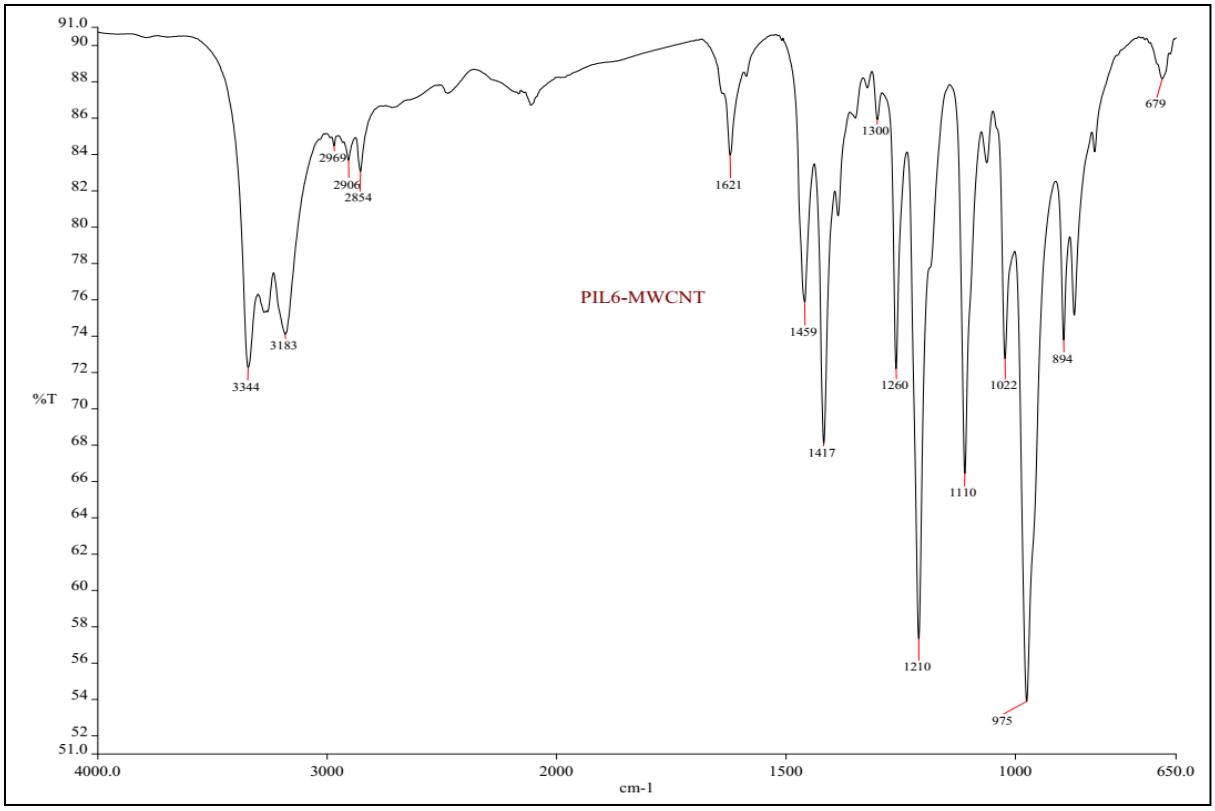

APX 3-10 FTIR spectrum of pure PIL6/MWCNT composites

Appendix 4

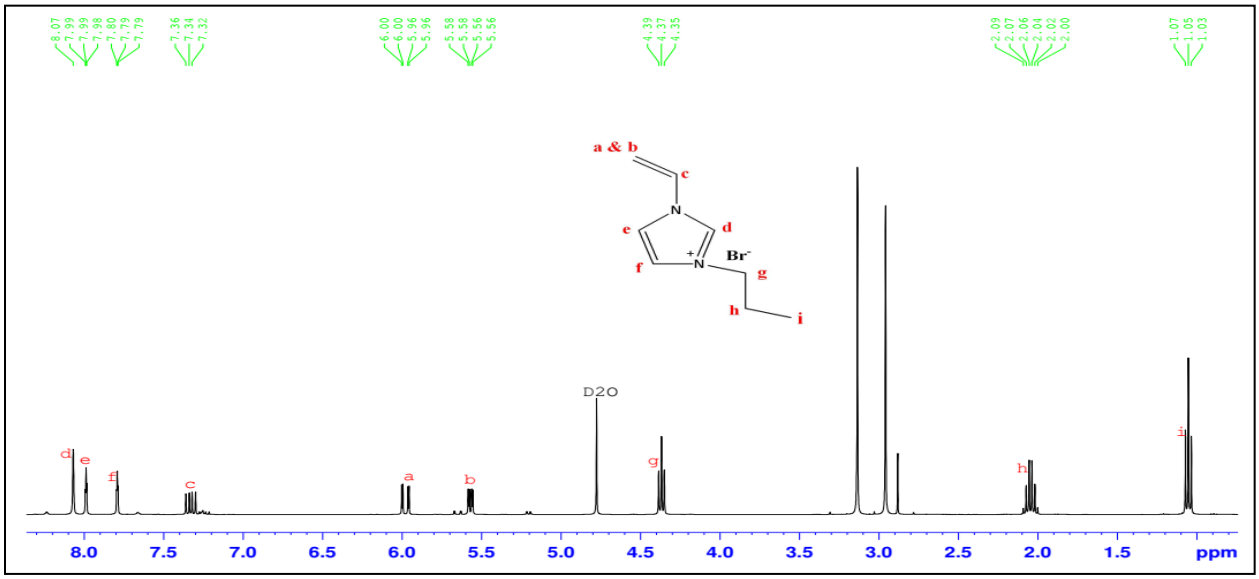

APX 4-1 ^{1}H-NMR of 3-propyl-1-vinylimidazolium bromide

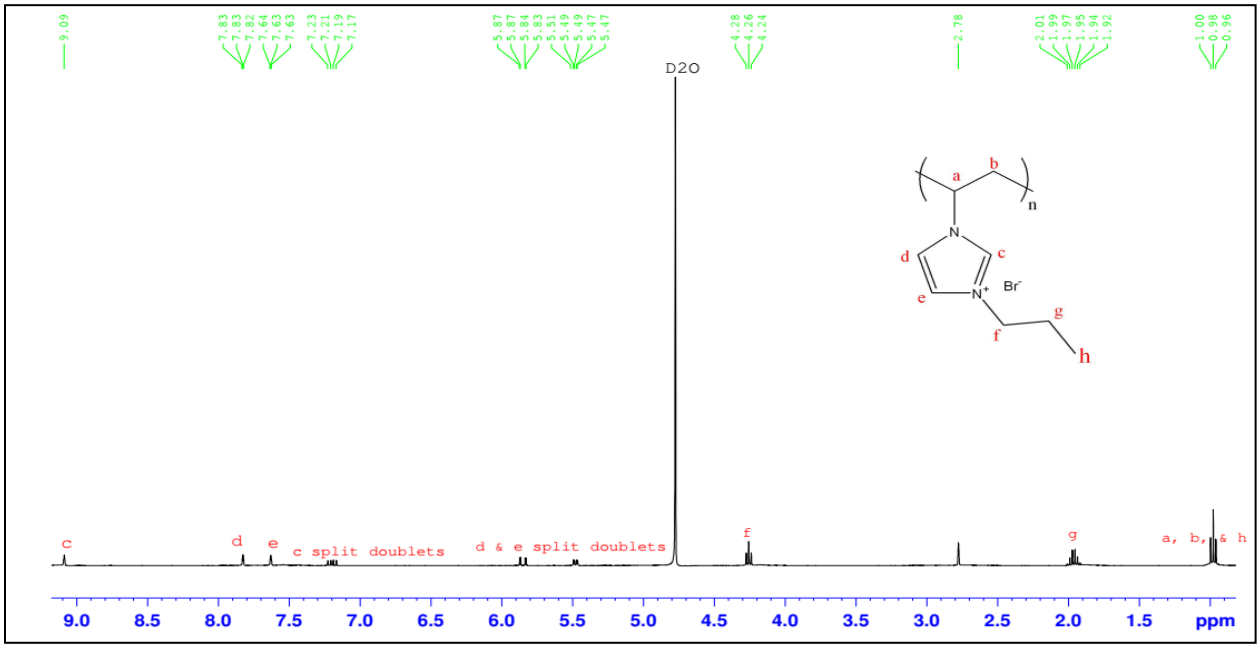

APX 4-2 ^{1}H NMR of poly(3-propyl-1-vinylimidazolium bromide).

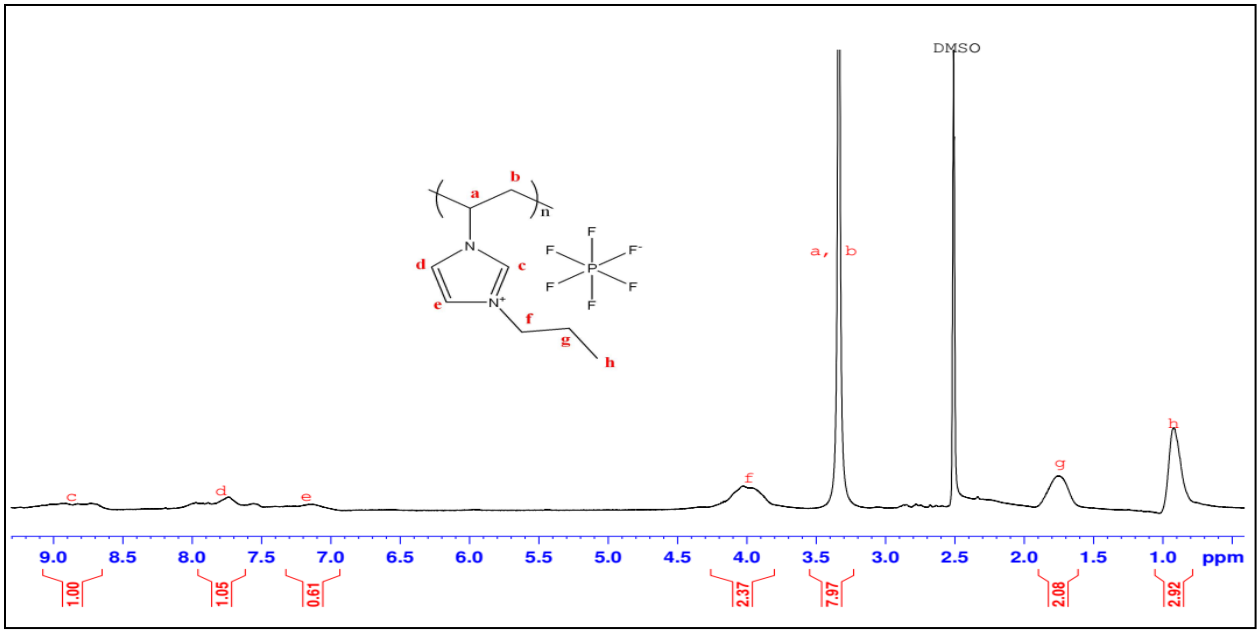

APX 4-3 ^{1}H NMR of poly(3-propyl-1-vinylimidazolium hexafluorophosphate)

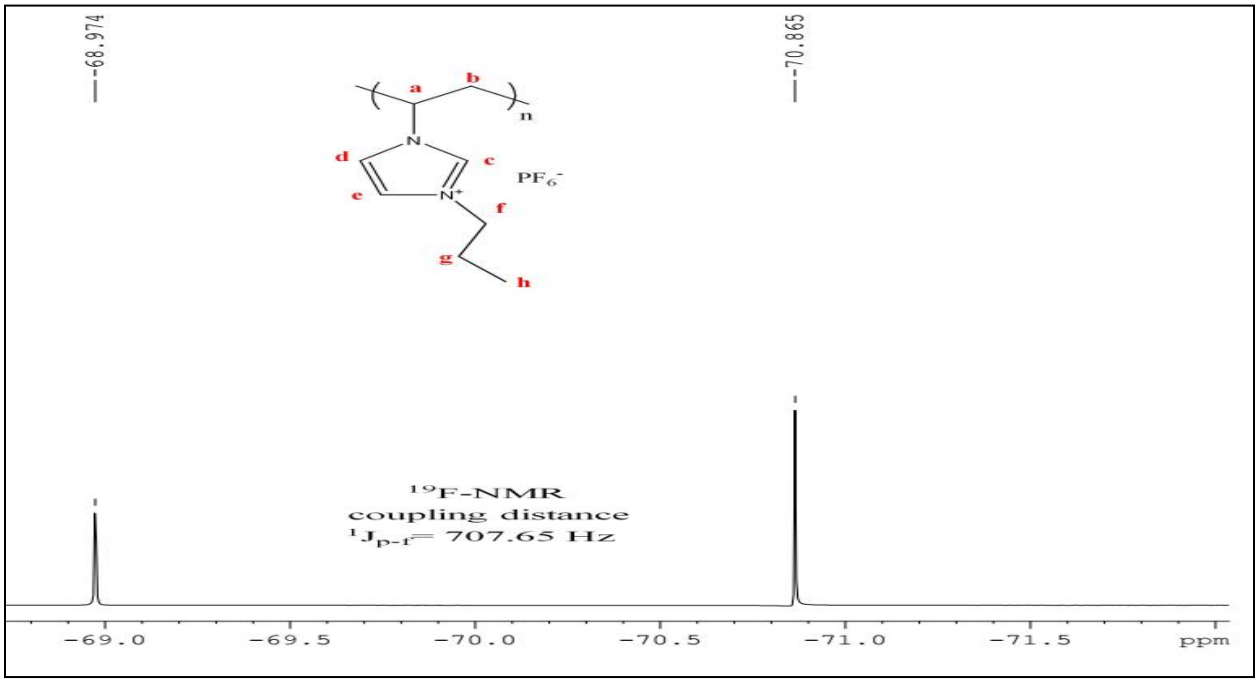

APX 4-4 ^{19}F NMR of poly(3-propyl-1-vinylimidazolium hexafluorophosphate)

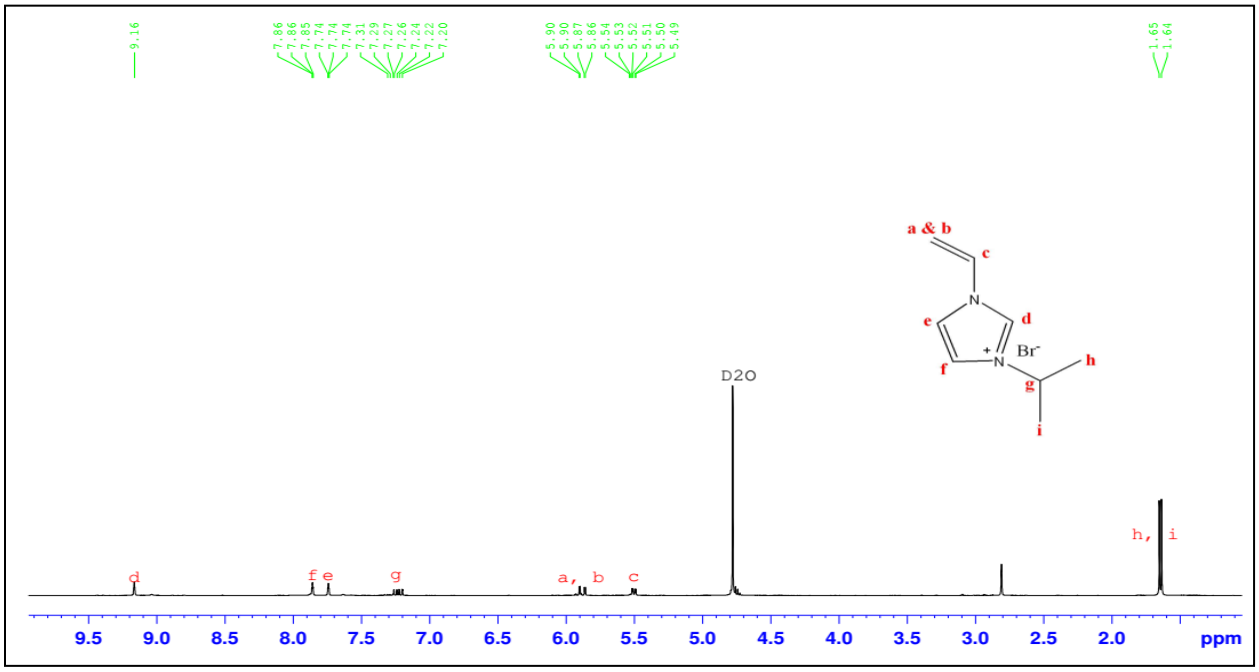

APX 4-5 ^{1}H NMR of 3-isopropyl-1-vinylimidazolium bromide

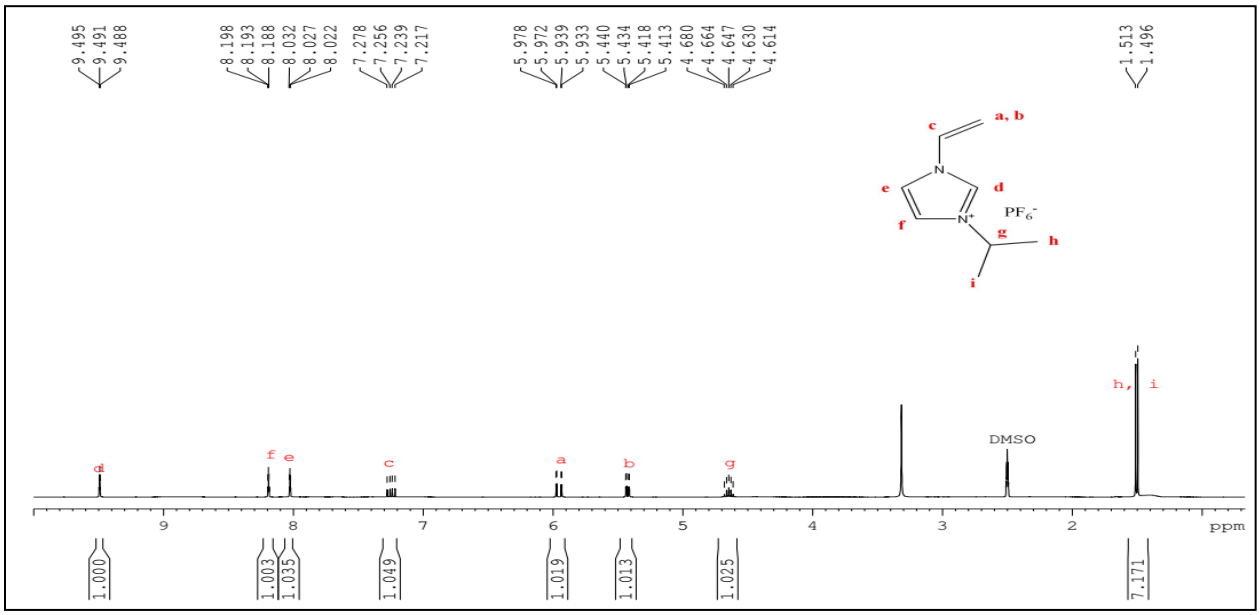

APX 4-6 ^{1}H NMR of 3-isopropyl-1-vinylimidazolium hexafluorophosphate

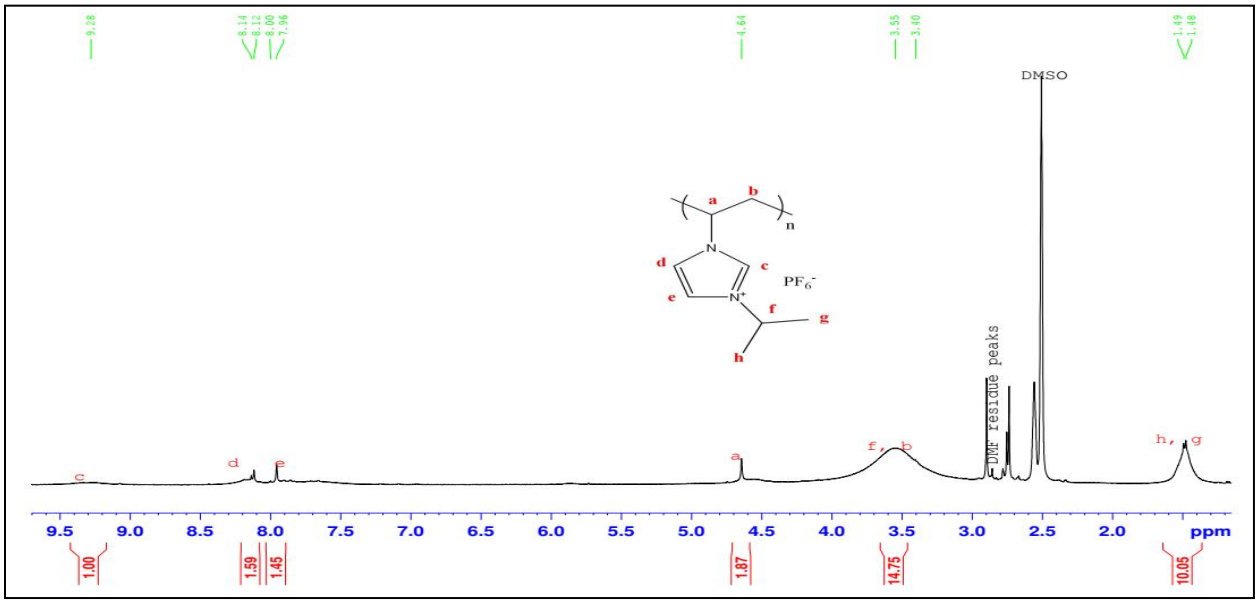

APX 4-7 ^{1}H NMR of poly(3-isopropyl-1-vinylimidazolium hexafluorophosphate)

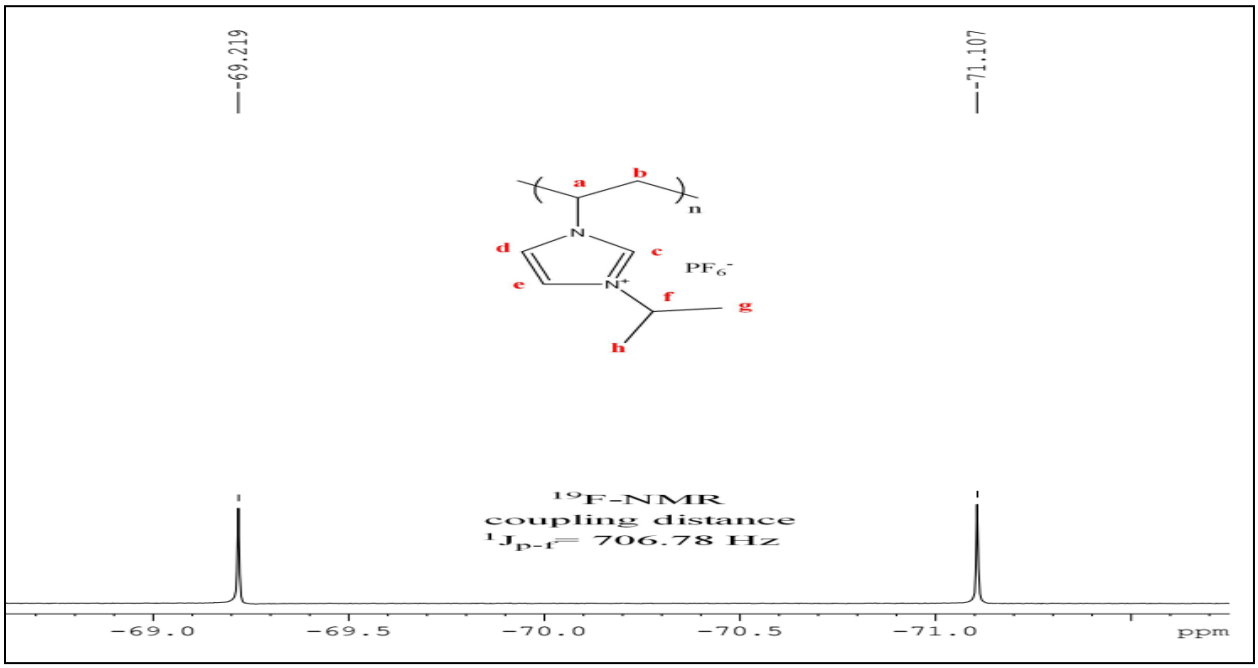

APX4-8 ^{19}F NMR of poly(3-isopropyl-1-vinylimidazolium hexafluorophosphate)

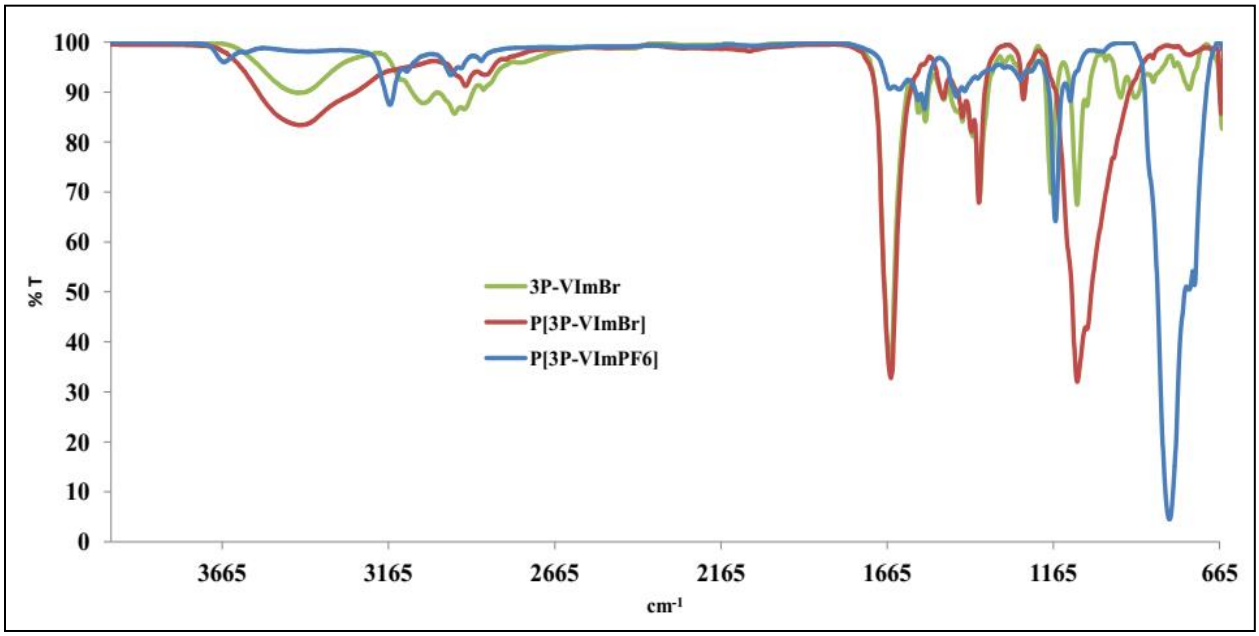

APX 4-9 FTIR of 3-propyl-1-vinylimidazolium bromide (3P-VImBr), poly[3-propyl-1-vinylimidazolium bromide] P[3P-VImBr], and poly[3-propyl-1-vinylimidazolium hexafluorophosphate] P[3P-VImPF_6]

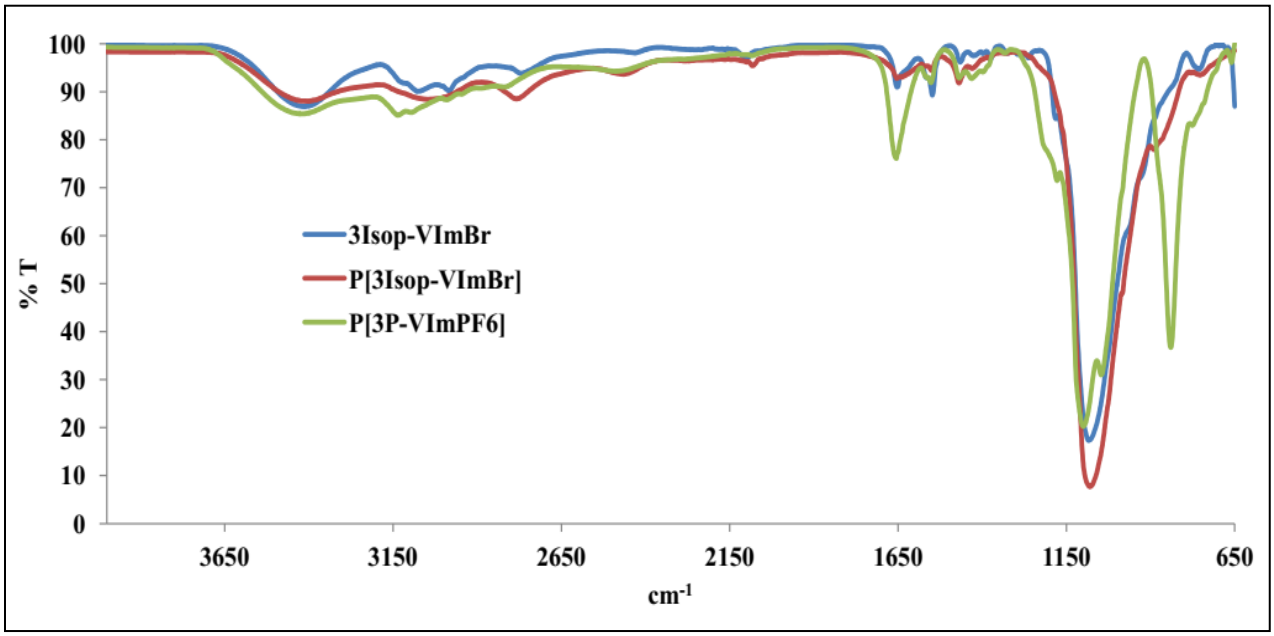

APX 4-10 FTIR of 3-isopropyl-1-vinylimidazolium bromide [3Isop-VImBr], poly[3-isopropyl-

1-vinylimidazolium bromide] P[3Isop-VImBr], and poly[3-isopropyl-1-vinylimidazolium hexafluorophosphate] P[3Isop-VImPF_6]

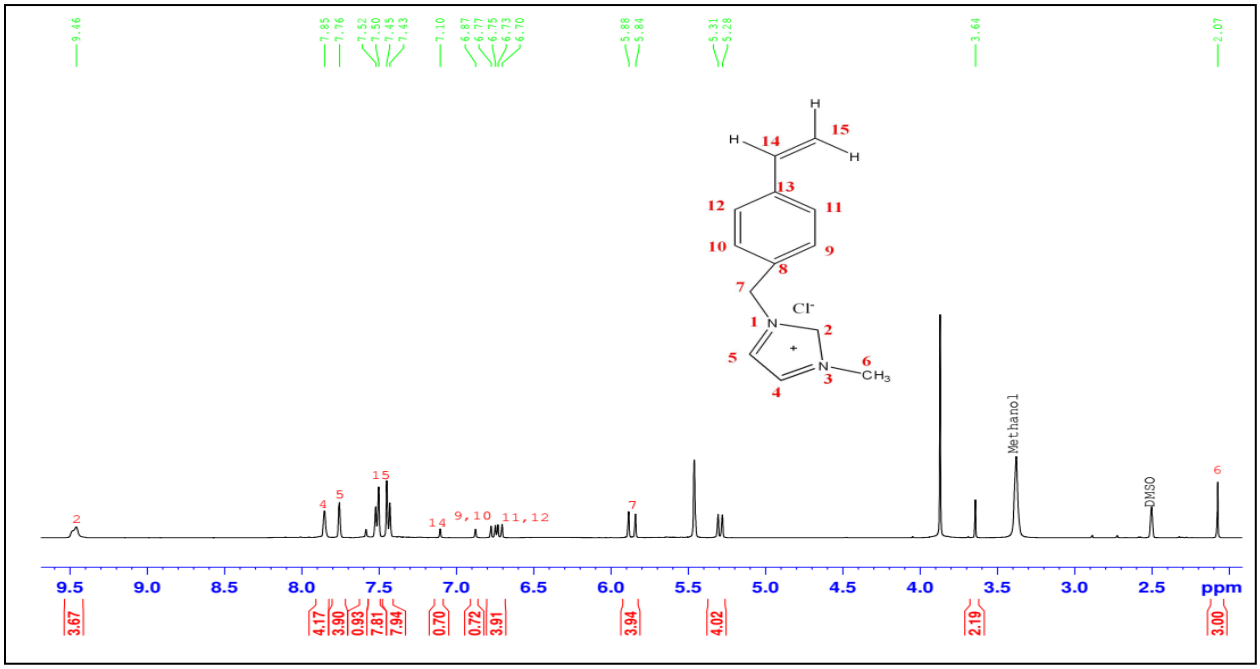

APX 4-11 ^{1}H NMR of [MVBIm-Cl]

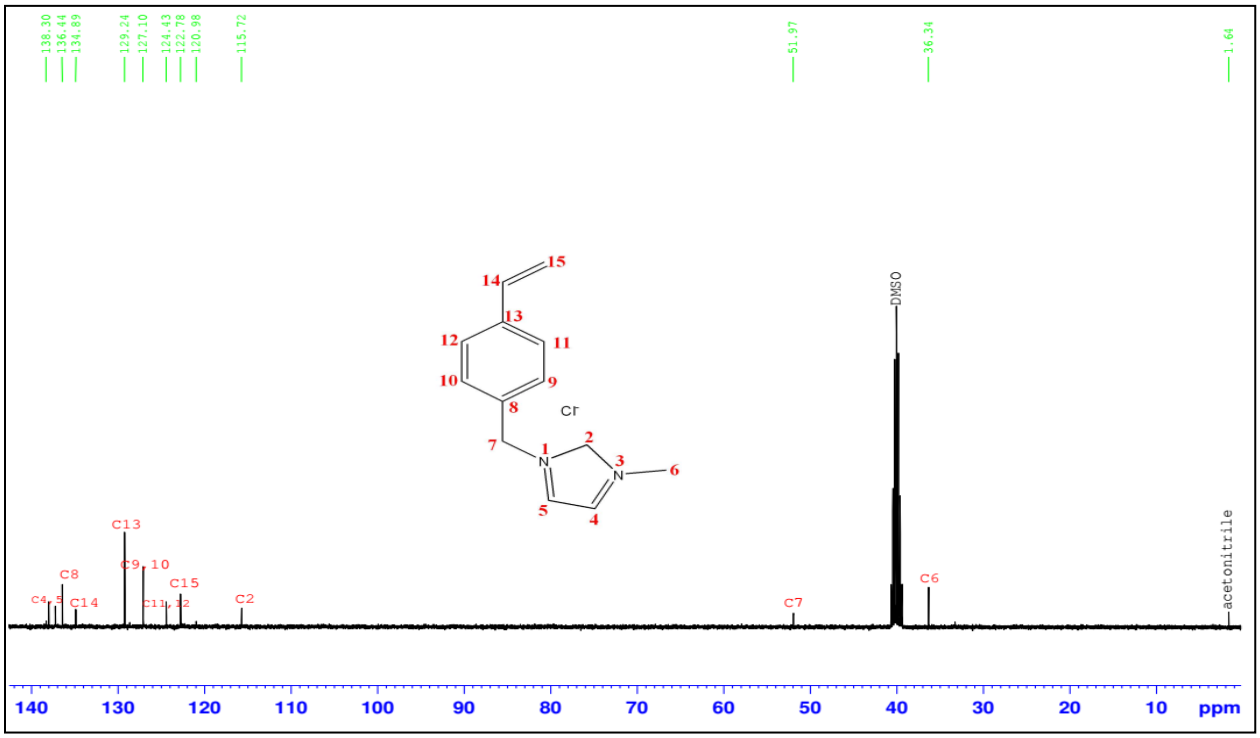

APX 4-12 ^{13}C NMR of [MVBIm-Cl]

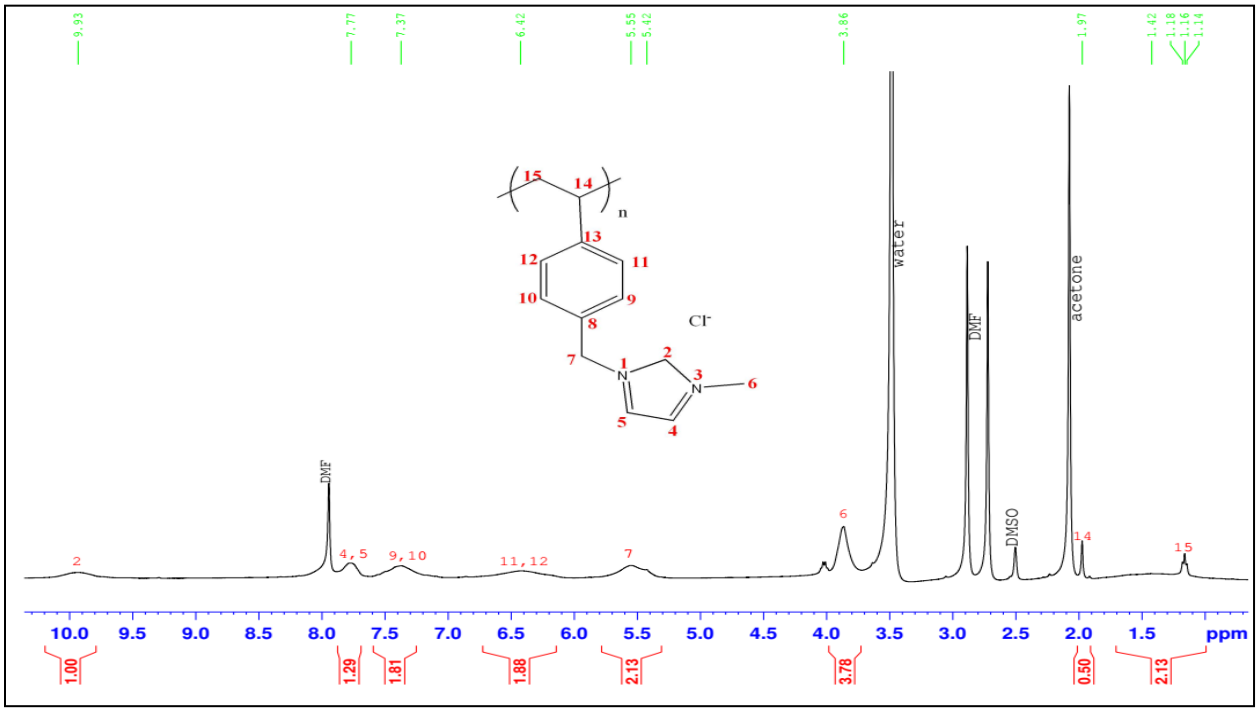

APX 4-13 ^{1}H NMR of P[MVBIm-Cl]

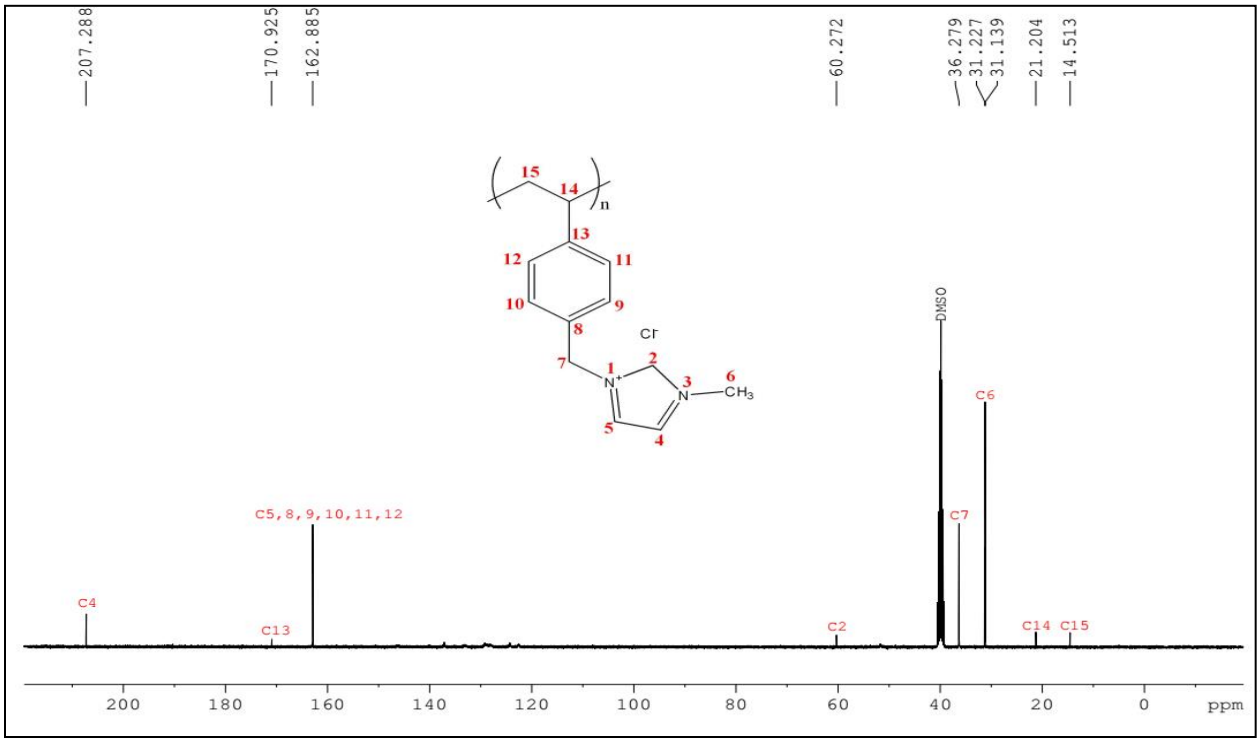

APX 4-14 ^{13}C NMR of P[MVBIm-Cl]

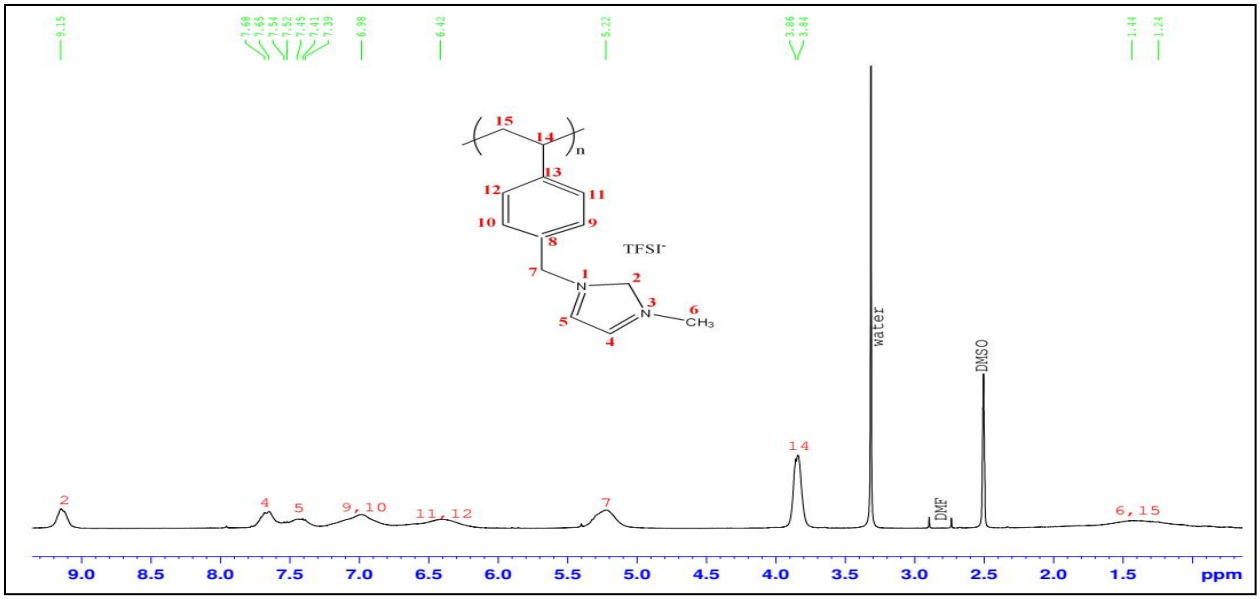

APX 4-15 ^{1}H NMR of P[MVBIm-TFSI]

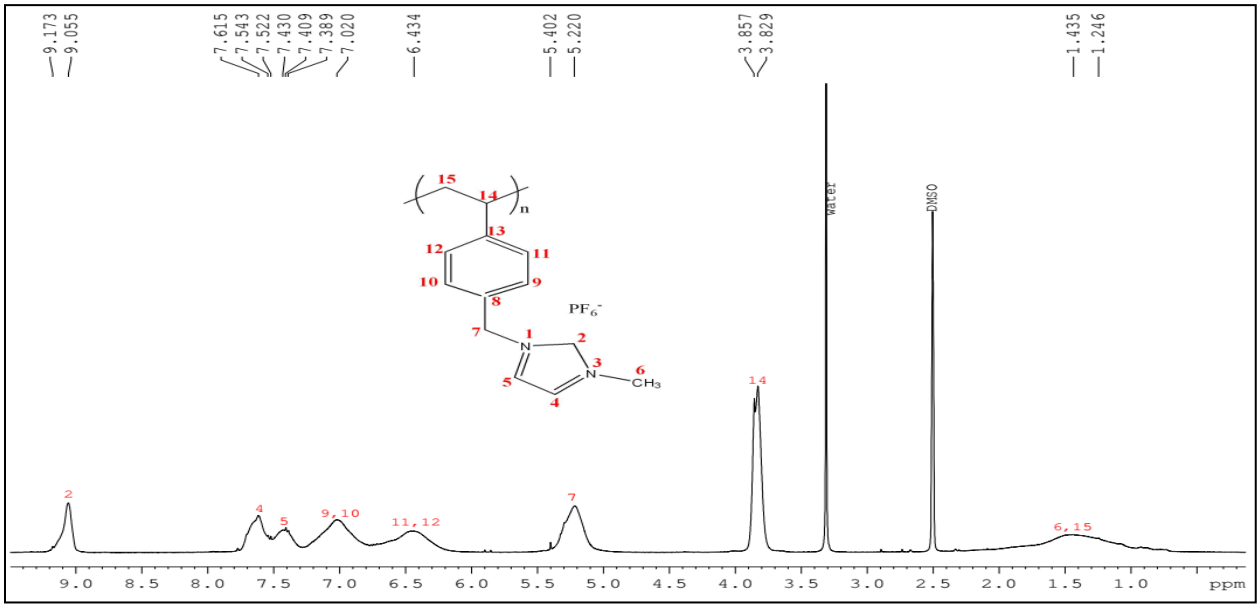

APX 4-16 ^{1}H NMR of P[MVBIm-PF_6]

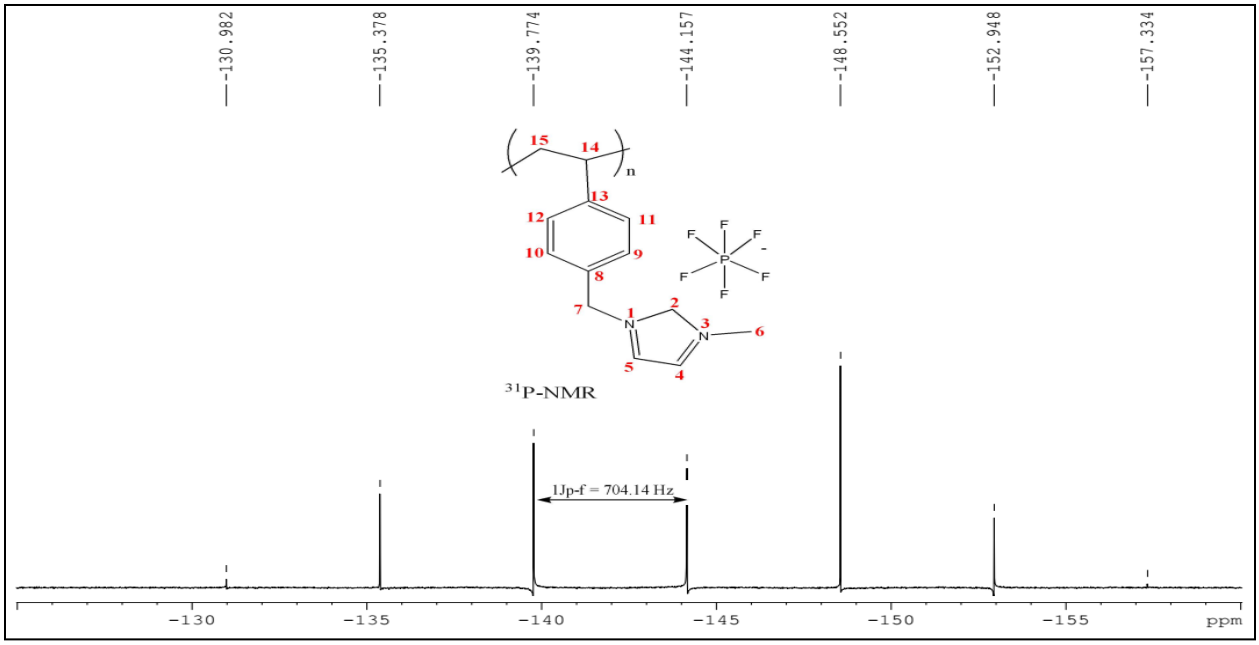

APX 4-17 ^{31}P NMR of P[MVBIm-PF_6]

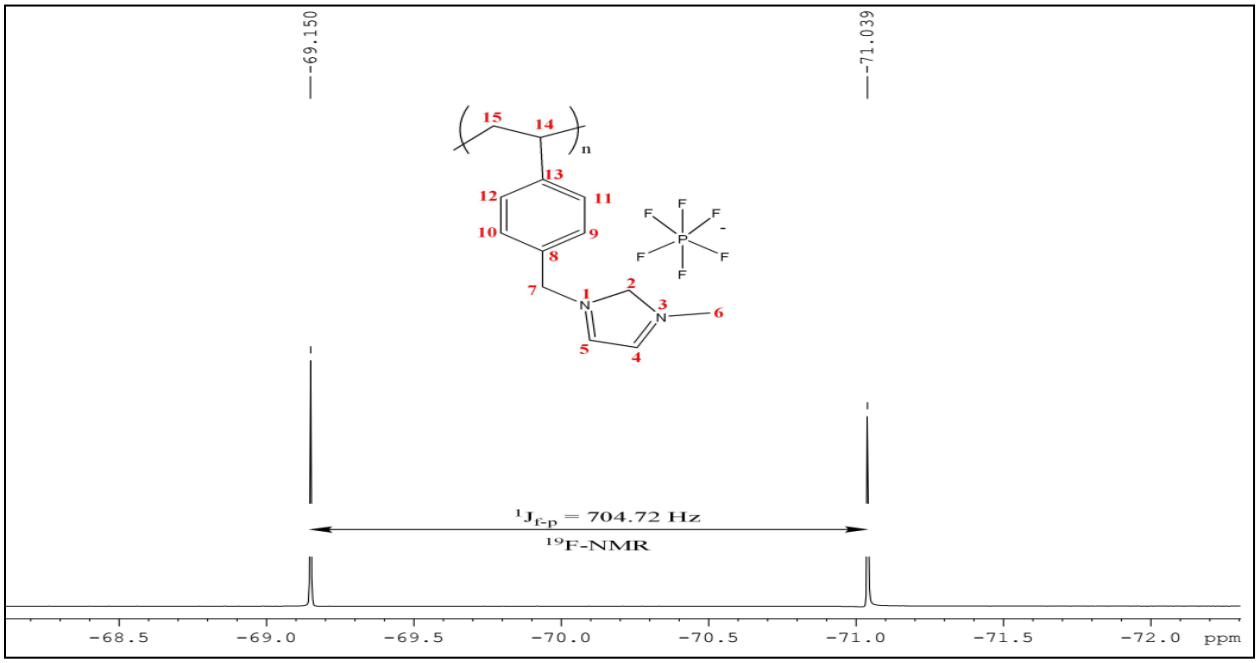

APX4-18 ^{19}F NMR of P[MVBIm-PF_6]

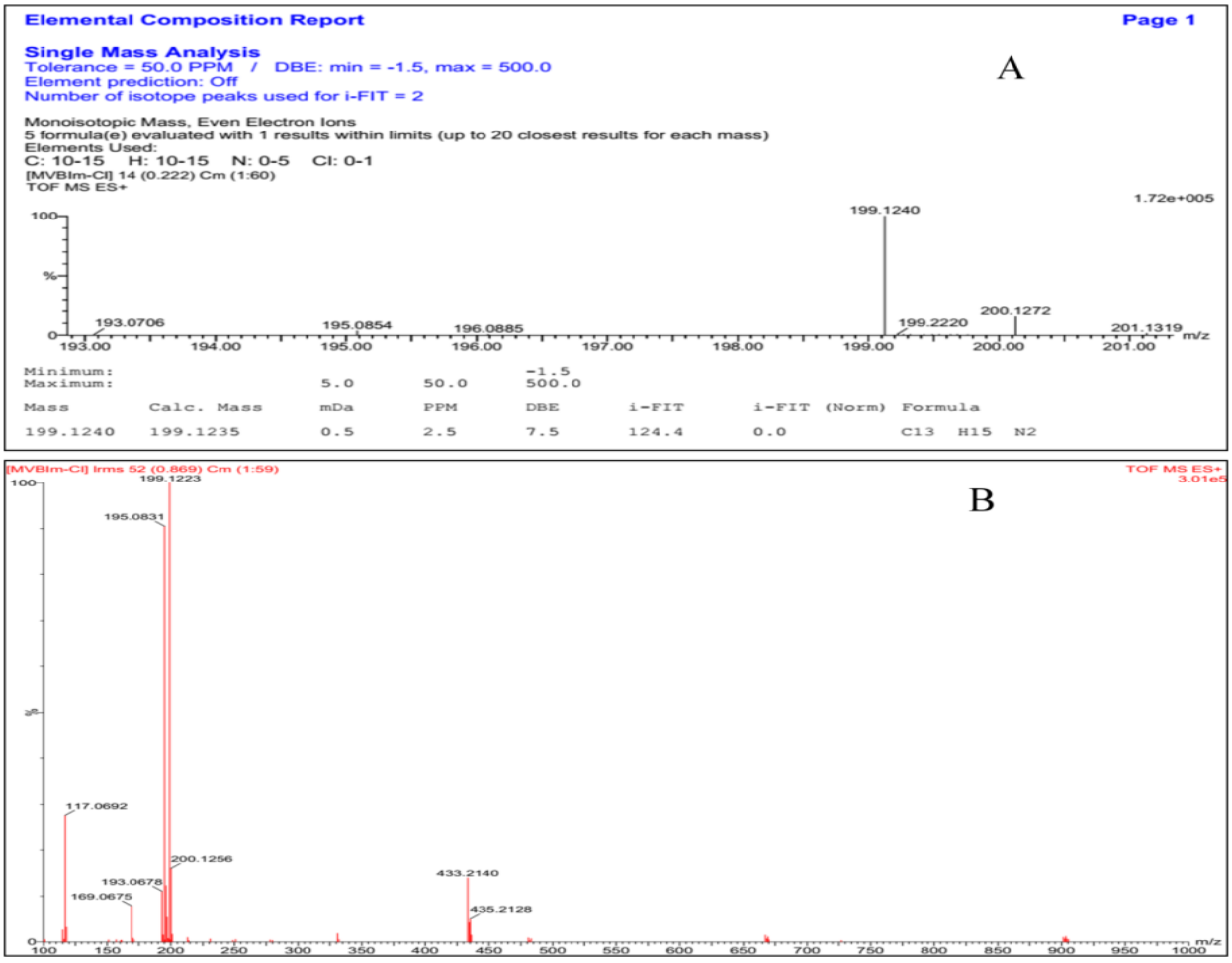

APX 4-19 Accurate (single Mass) Analysis of [MVBIm^{+}], $C_{13}H_{16}N_2^{+}$ based on CHN and TOF mass spectrometry ES

APX 4-20 TOF mass spectrometry ES of P[MVBIm-Cl]

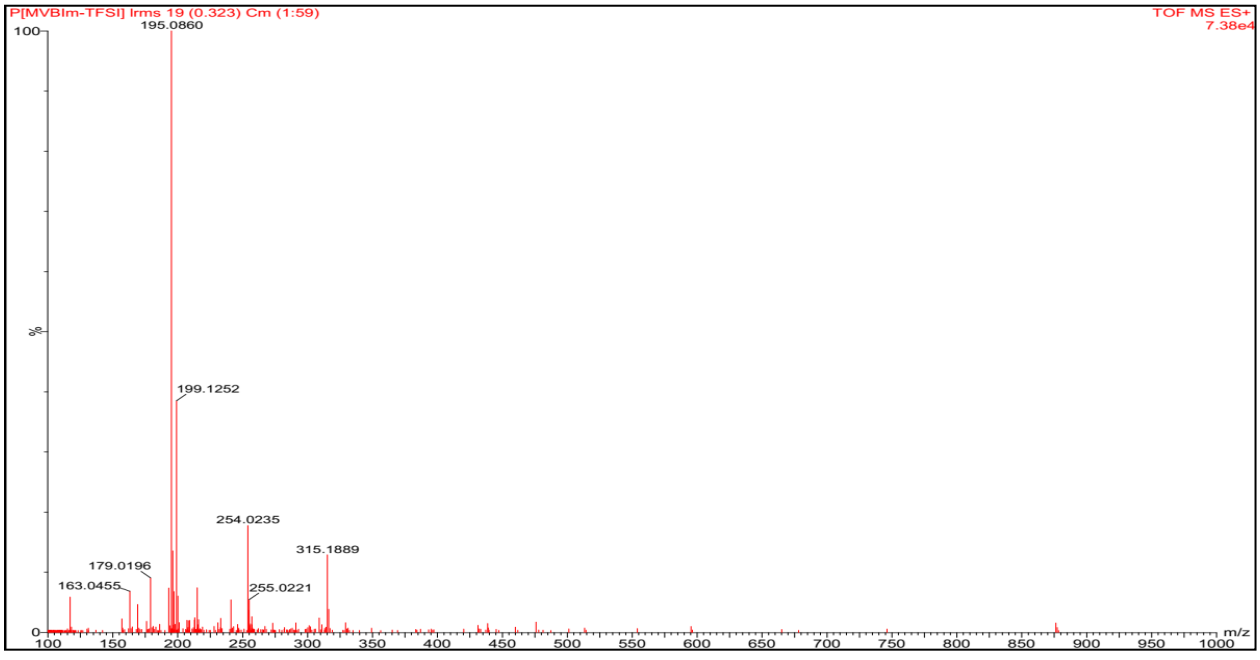

APX 4-21 TOF mass spectrometry ES of P[MVBIm-TFSI]

APX 4-22 TOF mass spectrometry ES of P[MVBIm-PF_6]

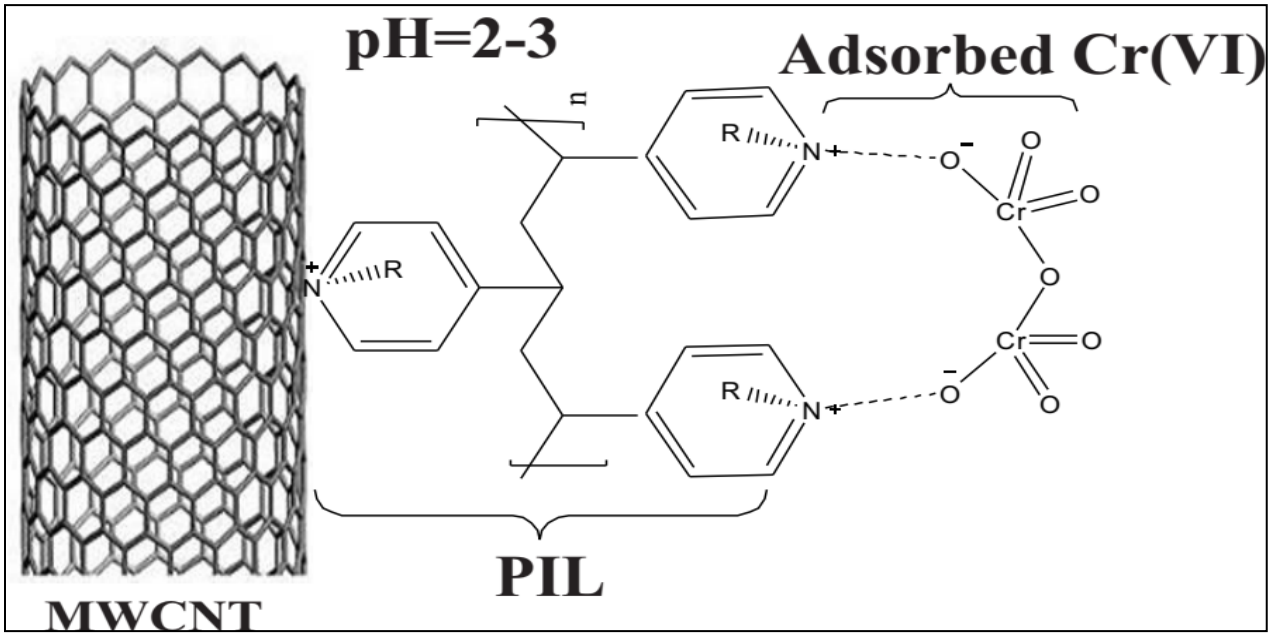

APX 4-23 Possible interactions (electrostatic) between PIL/MWCNT composites and Cr(VI)